(2)

DNA-TR-89-14

THE AIR TRANSPORT OF RADIATION (ATR) CODE

Development and Testing of ATR5

F. Dolatshahi, et al.
Science Applications International Corporation
10260 Campus Point Drive
San Diego, CA 92121

January 1990

Technical Report

CONTRACT No. DNA 001-85-C-0255

THIS WORK WAS SPONSORED BY THE DEFENSE NUCLEAR AGENCY
UNDER RDT&E RMC CODES B3500854662 RM RK 00113 25904D
AND B3500854662 RN RA 00017 25904D.

Prepared for
Defense Nuclear Agency
6801 Telegraph Road
Alexandria, VA 22310-3398

DISTRIBUTION LIST UPDATE

This mailer is provided to enable DNA to maintain current distribution lists for reports. We would appreciate your providing the requested information.

☐ Add the individual listed to your distribution list.

☐ Delete the cited organization/individual.

☐ Change of address.

NAME: _____

ORGANIZATION _____

OLD ADDRESS	CURRENT ADDRESS

TELEPHONE NUMBER ( ) _____

SUBJECT AREA(s) OF INTEREST

DNA OR OTHER GOVERNMENT CONTRACT NUMBER

CERTIFICATION OF NEED TO KNOW BY GOVERNMENT SPONSOR (if other than DNA)

SPONSORING ORGANIZATION

CONTRACTING OFFICER OR REPRESENTATIVE

SIGNATURE

CUT HERE AND RETURN

Director
Defense Nuclear Agency
ATTN: TITL
Washington, DC 20305-1000

Director
Defense Nuclear Agency
ATTN: TITL
Washington, DC 20305-1000

UNCLASSIFIED
SECURITY CLASSIFICATION OF THIS PAGE

REPORT DOCUMENTATION PAGE

1a. REPORT SECURITY CLASSIFICATION UNCLASSIFIED	1b. RESTRICTIVE MARKINGS
2a. SECURITY CLASSIFICATION AUTHORITY N/A since Unclassified	3. DISTRIBUTION/AVAILABILITY OF REPORT Approved for public release; distribution is unlimited.
2b. DECLASSIFICATION/DOWNGRADING SCHEDULE N/A since Unclassified	
4. PERFORMING ORGANIZATION REPORT NUMBER(S) SAIC-88/3009	5. MONITORING ORGANIZATION REPORT NUMBER(S) DNA-TR-89-14
6a. NAME OF PERFORMING ORGANIZATION Science Applications International Corporation 6b. OFFICE SYMBOL (If applicable)	7a. NAME OF MONITORING ORGANIZATION Defense Nuclear Agency
6c. ADDRESS (City, State, and ZIP Code) 10260 Campus Point Drive San Diego, CA 92121	7b. ADDRESS (City, State, and ZIP Code) 6801 Telegraph Road Alexandria, VA 22310-3398
8a. NAME OF FUNDING/SPONSORING ORGANIZATION 8b. OFFICE SYMBOL (If applicable) RARP/Kehlet	9. PROCUREMENT INSTRUMENT IDENTIFICATION NUMBER DNA 001-85-C-0255
8c. ADDRESS (City, State, and ZIP Code)	10. SOURCE OF FUNDING NUMBERS PROGRAM ELEMENT NO: 62715H; PROJECT NO: RN RM; TASK NO: RA RK; WORK UNIT ACCESSION NO: DH008005

11. TITLE (Include Security Classification)
THE AIR TRANSPORT OF RADIATION (ATR) CODE
Development and Testing of ATR5

12. PERSONAL AUTHOR(S)
Dolatshahi, F.; Kaul, D. C.; Phillips, L.; Roberts, J. A.

13a. TYPE OF REPORT	13b. TIME COVERED	14. DATE OF REPORT (Year, Month, Day)	15. PAGE COUNT
Technical	FROM 850405 TO 880330	900102	160

16. SUPPLEMENTARY NOTATION
This work was sponsored by the Defense Nuclear Agency under RDT&E RMC Codes B3500854662 RM RK 00113 2590AD and B3500854662 RN RA 00017 2590AD

17. COSATI CODES			18. SUBJECT TERMS (continue on reverse if necessary and identify by block number)		
FIELD	GROUP	SUB-GROUP	Radiation Transport	Kerma	Fission Products
12	5		Nuclear Weapons	Neutrons	ATR Code
18	4		Dose	Gamma Rays	

19. ABSTRACT (continue on reverse if necessary and identify by block number)

The Air Transport of Radiation (ATR) code is the standard ~~DNA~~ model for initial radiation dose (kerma free-in air) from nuclear weapons in uniform air and air over ground geometries. ATR predicts free field dose from neutron, gamma ray, X-ray, and secondary gamma rays, from a parameterized data base.

This report describes modifications made to the code to provide for improved uniform air and air over ground dose distributions. Effects of atmospheric moisture are now accounted for. The fission product radiation model has been modified to include contributions from individual fissile isotopes and has been provided with empirical corrections to allow it to better replicate observed dose values. The resulting version of the code is ATR5.

20. DISTRIBUTION/AVAILABILITY OF ABSTRACT	21. ABSTRACT SECURITY CLASSIFICATION
☐ UNCLASSIFIED/UNLIMITED ■ SAME AS RPT ☐ DTIC USERS	UNCLASSIFIED

22a. NAME OF RESPONSIBLE INDIVIDUAL	22b. TELEPHONE (Include Area Code)	22c. OFFICE SYMBOL
Bennie F. Maddox	(703) 325-7042	DNA/CSTI

DD Form 1473, JUN 86 — Previous editions are obsolete

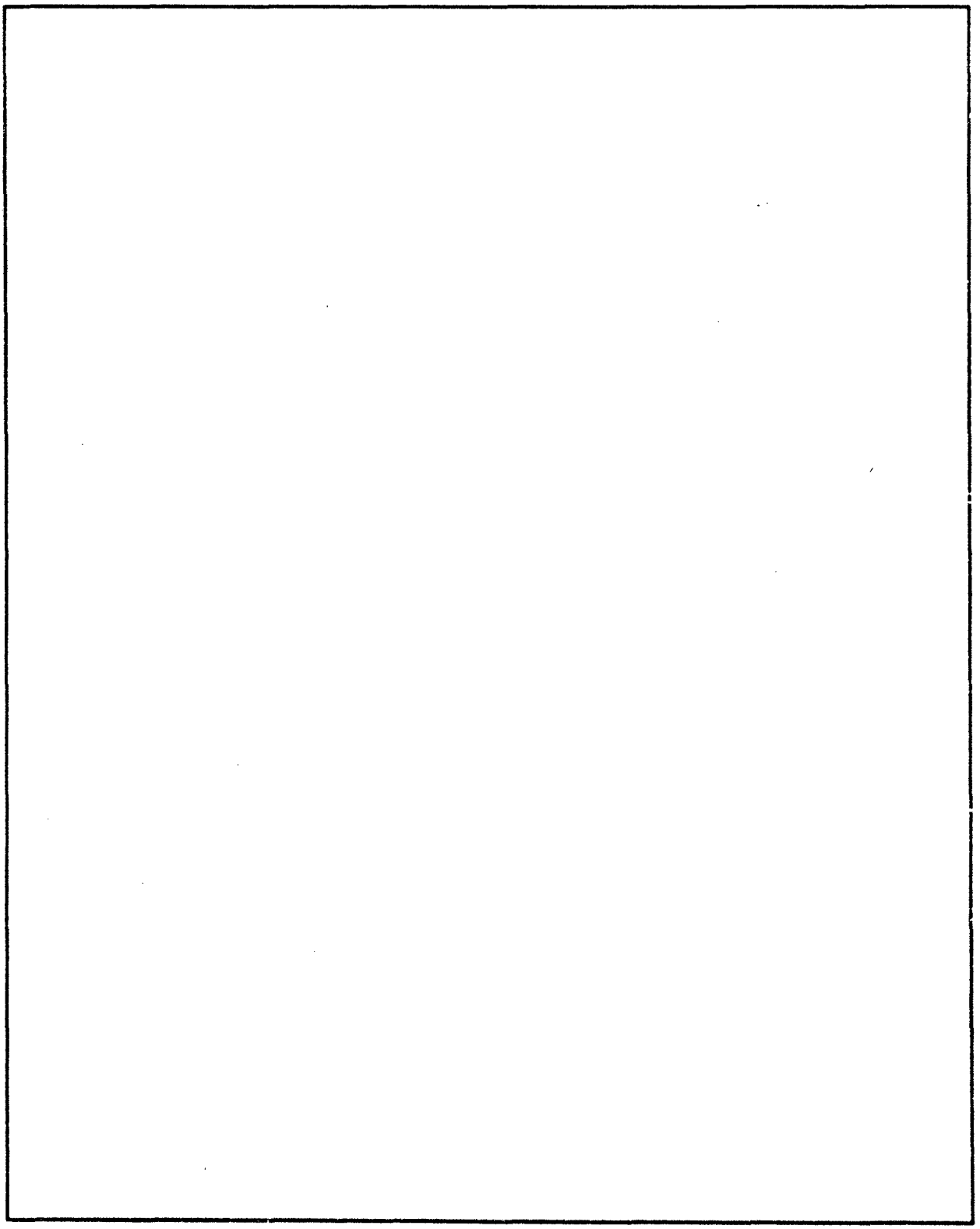

PREFACE

The authors would like to thank Mr. Jess Marcum, Research and Development Associates (RDA) for his continued interest and helpful suggestions during the progress of the work reported herein.

TABLE OF CONTENTS

FIGURES

FIGURES (Continued)

FIGURES (Concluded)

TABLES

TABLES (Concluded)

SECTION 1

INTRODUCTION

The Air Transport of Radiation (ATR) Code has been developed under the sponsorship of the Defense Nuclear Agency (DNA) as its standard model of initial radiation free field dose (kerma free-in-air) from nuclear weapons in uniform air and air-over-ground geometries. The ATR code is capable of predicting free field dose from x-ray, prompt gamma-ray, neutron, neutron-induced (secondary) gamma-ray and fission product gamma-ray components of initial radiation. It makes such predictions with a minimum of user input, thus making it ideal for use by weapon effects analysts who are unfamiliar with the details of radiation transport methodology. As such, it has been used to aid in the establishment of targeting doctrine and troop safety exclusion radii. Portions of the code have been extracted for use as modules in larger codes. The code has also been used to supply radiation environment data sets for use in a variety of applications, such as systems analysis and engagement codes, the DNA Effects Manual One (EM-1) and the DNA Electronic Handbook Series.

The development of ATR was begun in 1970 and continued over the next seven years. A bibliography of ATR-related reports is provided in Table 1. In its initial form ATR was intended to provide transport data for prompt radiation components for sources in uniform air and in the vicinity of the air-ground interface. By the time version 4 was released in 1976, the basic code had been expanded to include delayed gamma rays and to treat sources near the top of the atmosphere, among other, additional capabilities.

This period of ATR development coincided with major improvements in the state-of-the-art in radiation transport codes and cross sections and the capabilities of computers to cope with large computational tasks. Thus, in 1975 the entire ATR data base was replaced with results calculated using new DNA-sponsored evaluations of nitrogen and oxygen cross sections (ATR3). At that time new corrections to the uniform air data for the proximity of the source to the ground were also incorporated. These were derived from DNA-sponsored calculations of fission and 14 MeV neutron sources at heights to 300 meters and ranges to 1500 meters, such problems being the largest which could be run at that time.

In 1977, ATR underwent another modification. The effort, sponsored not by DNA but by Ballistic Research Laboratory (BRL), accomplished the installation of source energy-dependent air-over-ground correction factors for neutron and gamma radiation. The data from which those correction factors were derived were calculated under DNA sponsorship and were the results of the first effort to apply DOT in the adjoint mode for such a problem, i.e., long ranges in air-over-ground geometry. That version of the ATR code is known as ATR4.1. Subsequent to the production of ATR4.1 it was found that the two-dimensional transport calculations on which its air-over-ground correction factors were based were performed using a ground moisture level significantly below normal levels. This caused ATR4.1 to overestimate the neutron dose and overestimate the secondary gamma ray dose in the vicinity of the ground. As a result of this finding, the most accurate application of ATR, using version 4.1 and those previous, may be obtained by using ATR4 for neutron and secondary gamma ray dose data and ATR4.1 for prompt and delayed gamma ray dose data.

The above paragraphs provide a very brief summary of the complex development process of the ATR code. A more comprehensive history of that development up to 1977 is contained in Appendix A of this report. From 1977 to the present ATR has been used by many agencies in its various versions and has been examined for internal consistency and tested against independent data. This report describes the results of a program begun in 1985 to revise ATR based on insights gained from that collective experience. The program includes revision or replacement of the following portions of ATR:

- o Uniform Air Transport Data Base
  - Neutron
  - Gamma Ray
  - Secondary Gamma Ray
  - Humidity Correction
- o Air-Ground Interface Transport Correction

Table 1. ATR documentation summary.

REPORT	CONTENT
SAI-71-565-LJ November 1971	Paper given at RSIC Workshop on Radiation Transport in Air. Describes logic of code and some data base development.
DNA2803I May 1972	First report describing basic concepts of ATR and the first distributed version of the code; describes neutron and secondary gamma-ray data base generation. Includes air/ground and exponential air correction factors.
DNA3144A April 1973	Users manual for ATR-2 version of the code; does not describe data base generation.
DNA3279T August 1974	Describes data base generation for photons (prompt gamma rays and x-rays) and the prompt gamma-ray air/ground correction factors.
DNA3362Z August 1974	Summary of the capabilities of the ATR code with updates to ATR-2.
DNA3819F July 1975	Describes ATR-3 including new data base using DNA cross section library, new air/ground correction factors, low energy x-rays, and new REGROUP routine.
DNA4061 January 1976	Describes TDATR, the time-dependent prompt photon and secondary gamma-ray version of ATR.
DNA3395F January 1976	Describes fission product model and summarizes total capability of the ATR-4 code.
BRL CR 343 August 1977	Describes ATR-4.1 with energy-dependent air/ground correction factors. Work supported by BRL.

o Delayed Gamma Ray Model

- Source
- Transport

o User Features

- Air density/humidity Input
- Fluence-to-dose conversion factors

In addition the revised version of ATR, which should be referred to as ATR5, has been extensively tested against dose measurements made on a number of atmospheric tests carried out in Nevada and the Pacific.

1.1 UNIFORM AIR TRANSPORT DATA.

The models of neutron and gamma-ray transport in uniform, dry air, implemented in ATR, through version 4.1, are based on calculations using one-dimensional discrete ordinates methodology with S_{16} quadrature and multigroup coupled cross sections composed of 22 neutron and 18 gamma-ray groups with a P_3 Legendre polynominal scattering approximation. Such calculational limitations are typical of those necessitated by available computer and data resources at the outset of ATR development. Now, more than a decade later, modern evaluated cross sections can be used in one-dimensional calculations having an S_{40} quadrature, a 174 neutron - 38 gamma ray group cross section set and a Legendre scattering approximation as high as P_8. Data calculated using such methodology are coplotted with those from ATR4/4.1 for neutron, secondary gamma ray and prompt gamma ray kerma from a fission weapon source in Figures 1, 2 and 3, respectively. The data for transport through dry air vary between ATR4 and newer methods differ by twenty percent or more, depending on distance. More importantly, significant variations occur when moisture is added to the atmosphere, particularly for neutron kerma. Therefore, the first task in the program described herein is to produce a new uniform air data set for transport from neutron and gamma-ray sources and to parameterize those data for inclusion in ATR. The second task is to develop a data set of radiation transport in air of various moisture contents on which to base a model of air humidity effects on free field dose and to implement that model in ATR.

1.2 AIR-GROUND INTERFACE TRANSPORT CORRECTION.

ATR versions 3 and 4 contain models for the perturbation of spatial dose distributions near the air-ground interface based on two-dimensional discrete ordinate calculations using fission and fusion sources having heights extending to 300 meters. The useful horizontal distance limit of those data is 1500 m. The simple four-element ground used in those calculations lacks the trace elements necessary to accurately depict the secondary gamma-ray environment, particularly at short distances, as shown in Figure 4.

ATR4.1 contains an air/ground perturbation model based on adjoint two-dimensional discrete ordinates calculations, which provide the importance of each source particle energy group (dose per source neutron or gamma ray) for producing free field dose one meter above the ground. The useful limits of these calculations are approximately 1000 meters source height and 1200 meters horizontal distance. These calculations were performed for a mean Western European soil containing virtually all trace elements of interest, but with an abnormally low moisture content. The result was a set of fully source energy-differential air-ground correction factors for ATR4.1, but ones which resulted in the overprediction of neutron dose and under prediction of secondary gamma-ray dose, as shown in Figures 5 and 6, respectively.

The third task in the present program is to develop and implement a set of air-ground interface dose correction factors based on a contemporary adjoint, two-dimensional discrete ordinates calculation which incorporates a 240 angle quadrature, a 37 neutron - 21 gamma-ray group cross section set with P_3 Legendre scattering, extended spatial limits (1000 m vertical 2000 m horizontal) and mean, moist Western European soil.

1.3 DELAYED GAMMA-RAY TRANSPORT.

The delayed (fission product) gamma-ray model implemented in ATR4/4.1 is an appendage having its own transport data set, rather than being fully integrated into ATR, using the same transport data sets as the prompt radiation component. Thus, ATR4/4.1 does not display a total initial gamma-ray dose, but rather a total comprised of prompt and secondary gamma rays and a separate tabulation of delayed gamma-ray dose, which must be combined by hand to obtain the true total. In addition to this inconvenience, the dose calculated using the ATR4/4.1 delayed gamma-ray model does not agree well with test

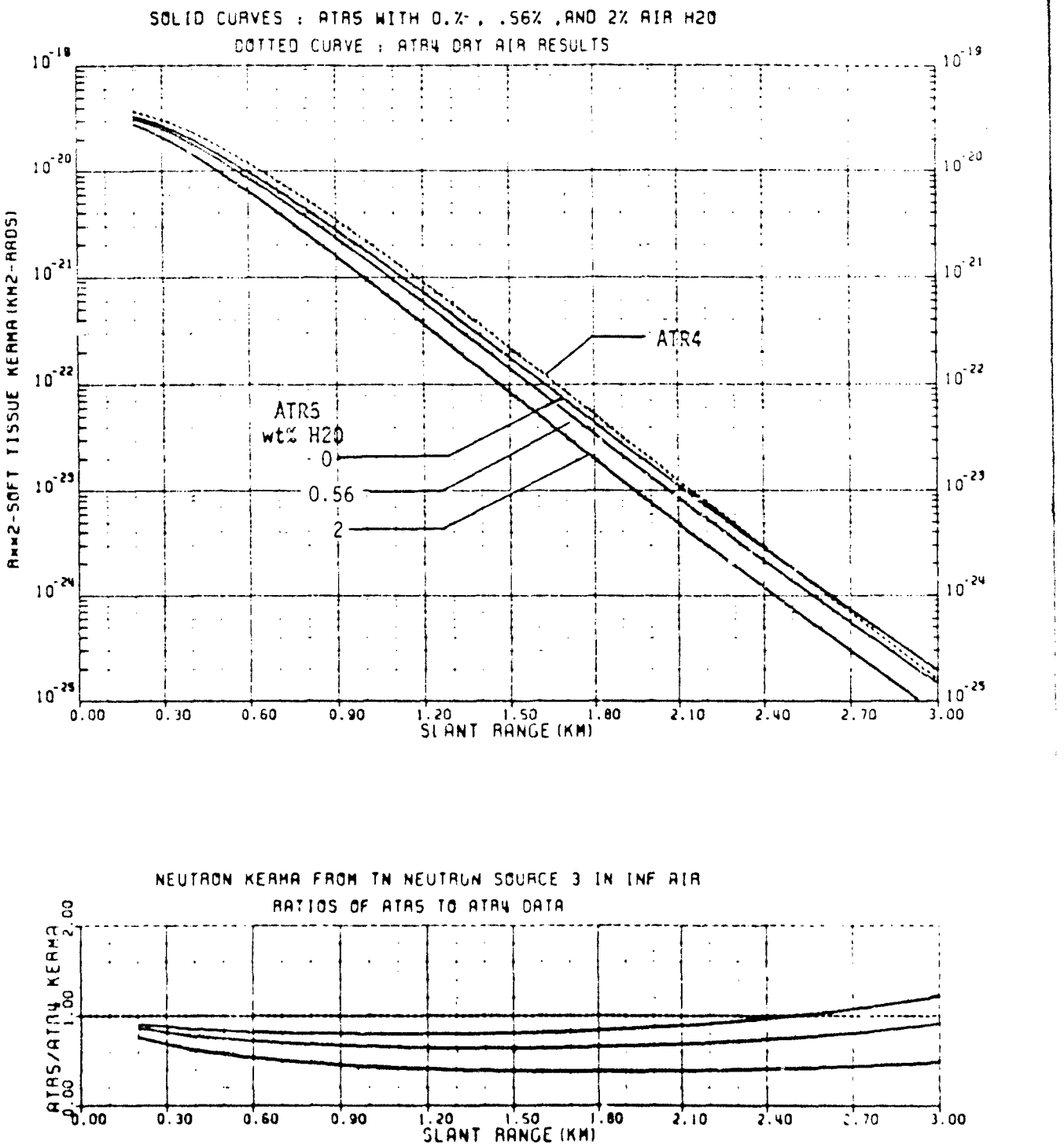

Figure 1. Neutron kerma from a boosted fission source in uniform dry and moist air, ATR4 and ATR5 calculations.

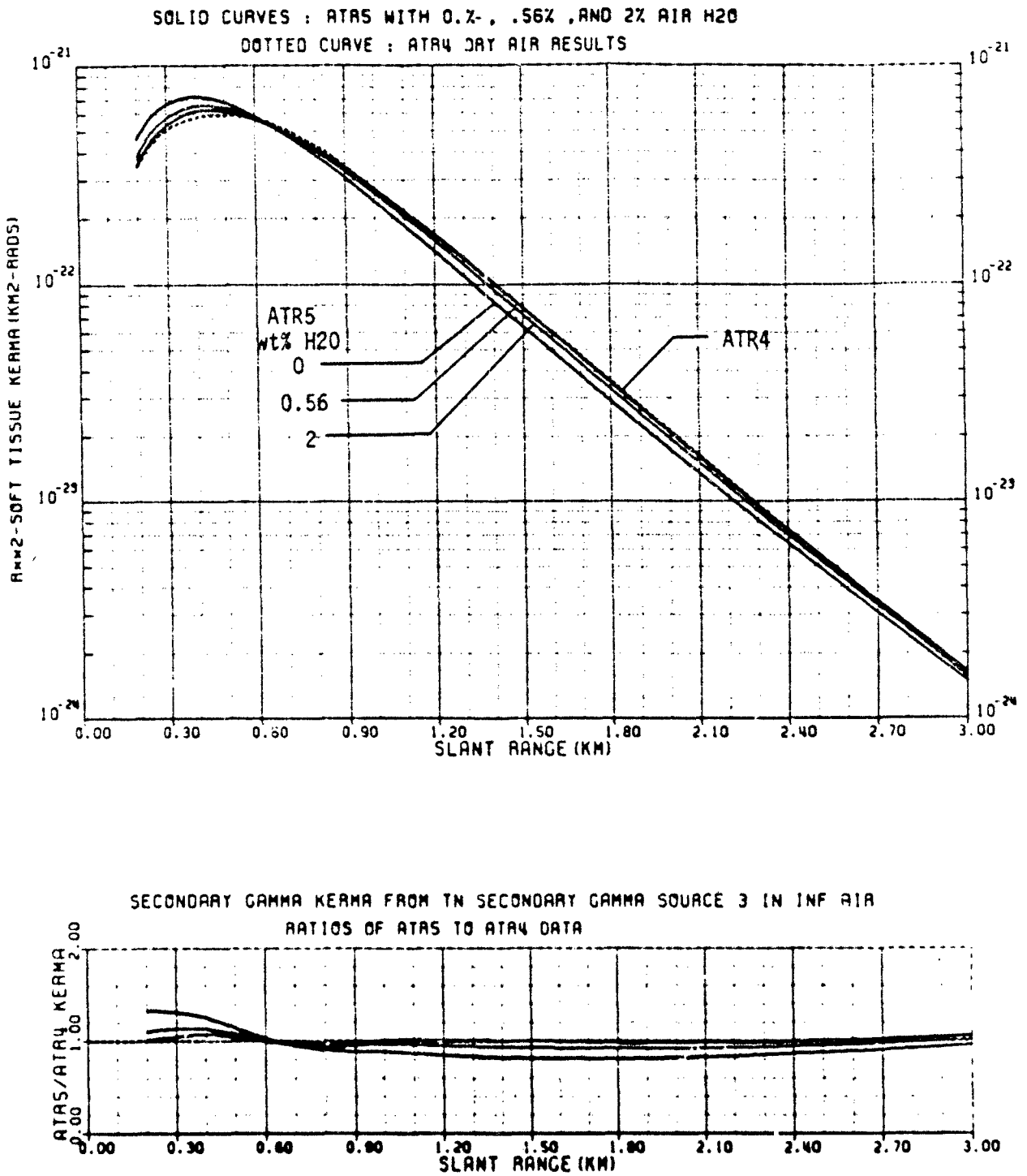

Figure 2. Secondary gamma ray kerma from a boosted fission source in uniform dry and moist air, ATR4 and ATR5 calculations.

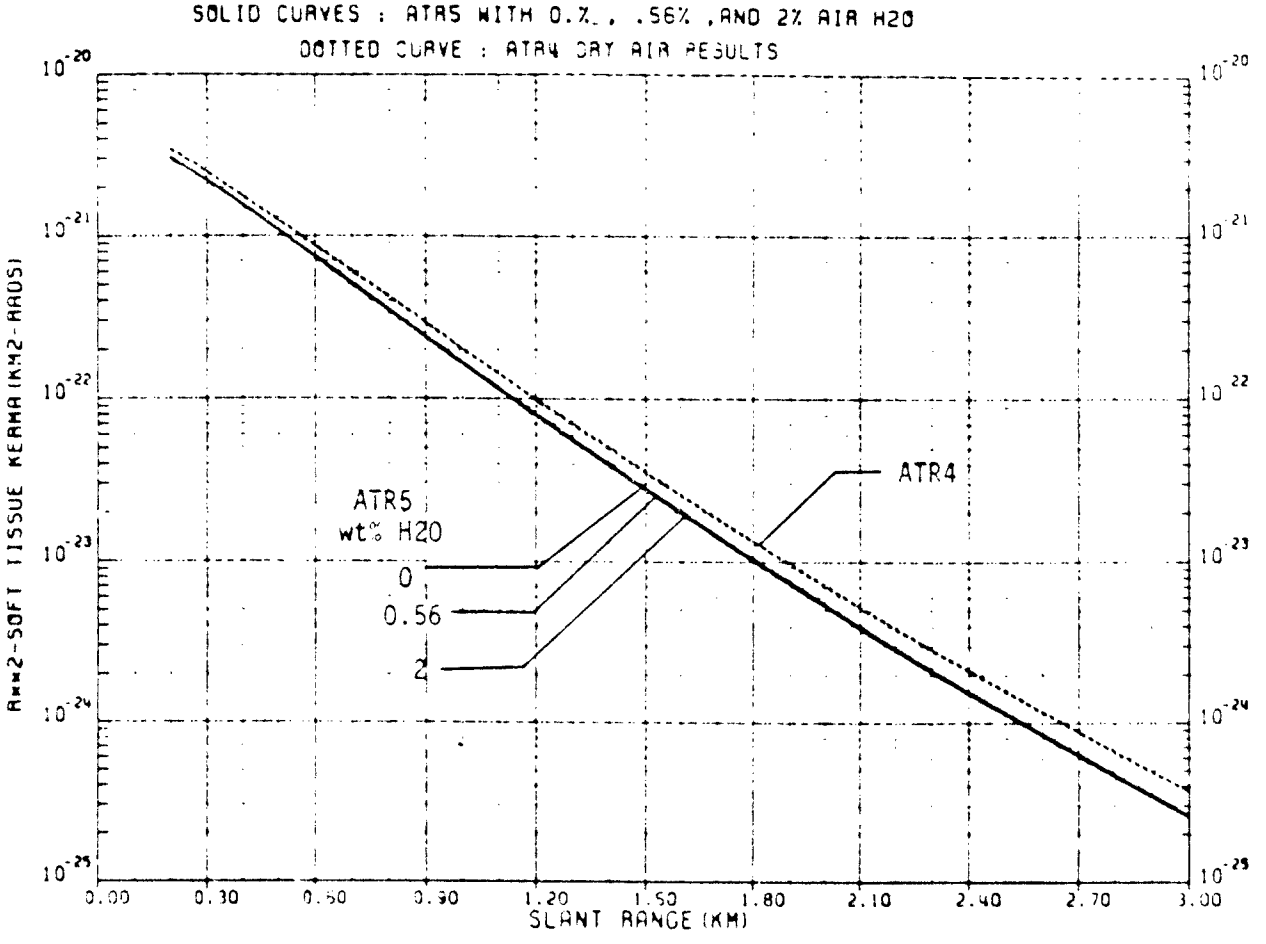

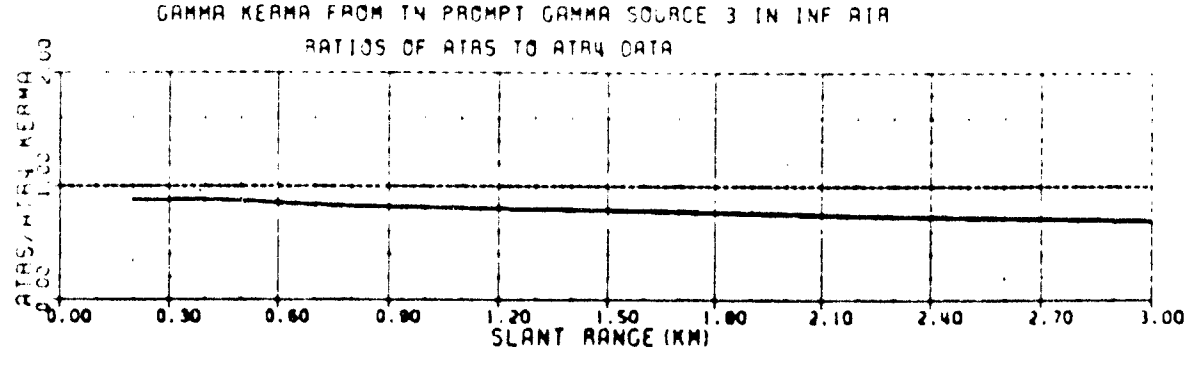

Figure 3. Gamma ray kerma from a boosted fission gamma ray source in uniform dry and moist air, ATR4 and ATR5 caluclations.

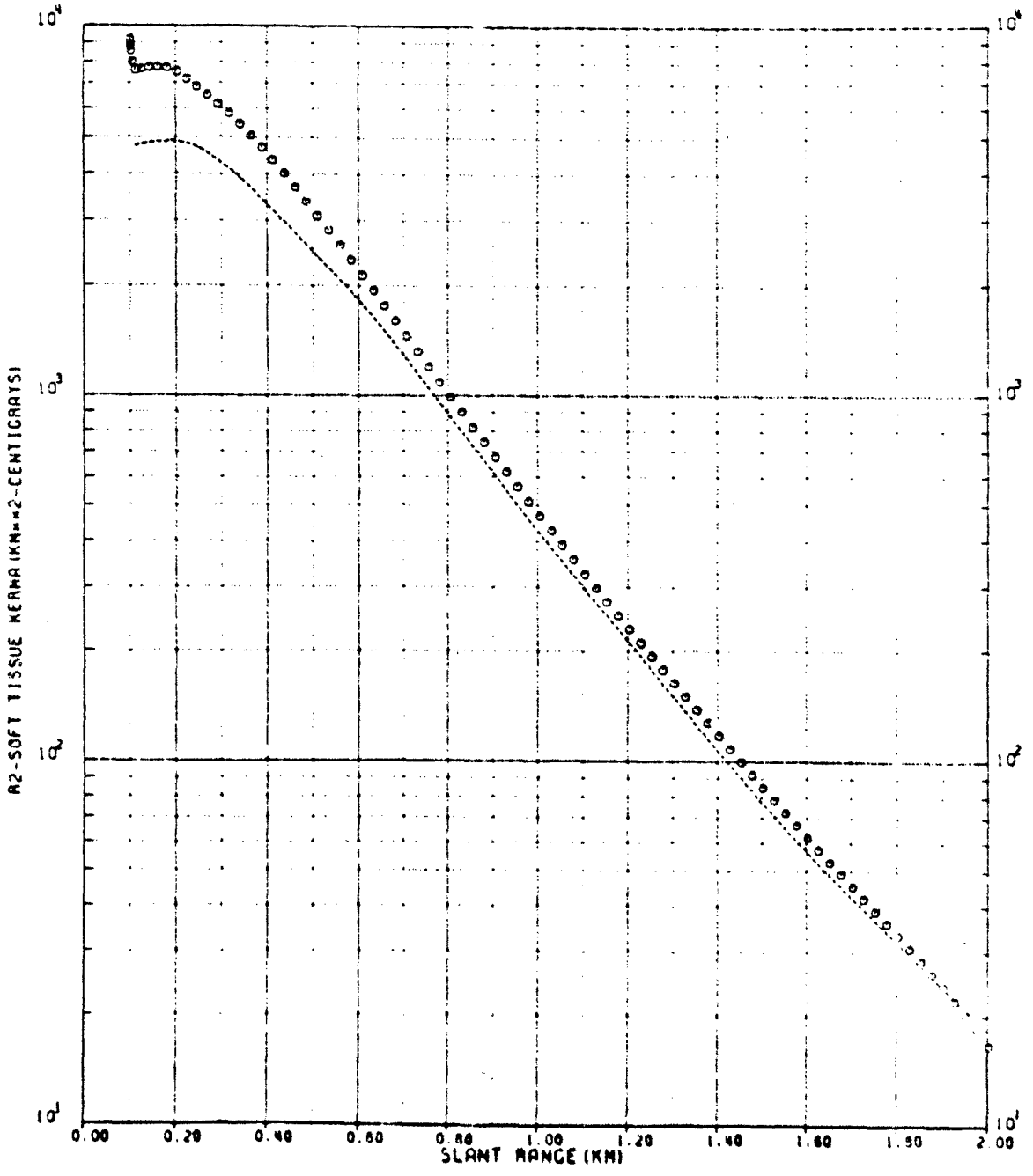

Figure 4. Secondary gamma ray kerma at the ground from a boosted fission source (HOB = 100 meters) calculated using ATR5 (ooo) and ATR4 (---).

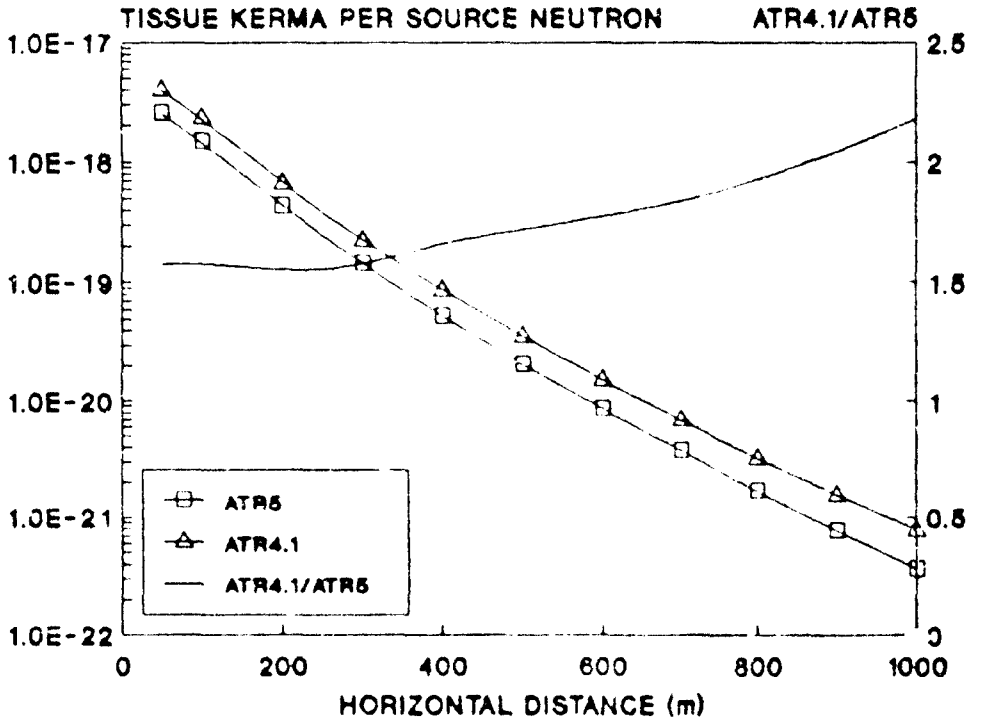

Figure 5. Neutron kerma from a fission source at 100 meters burst height, ATR4.1 and ATR5.

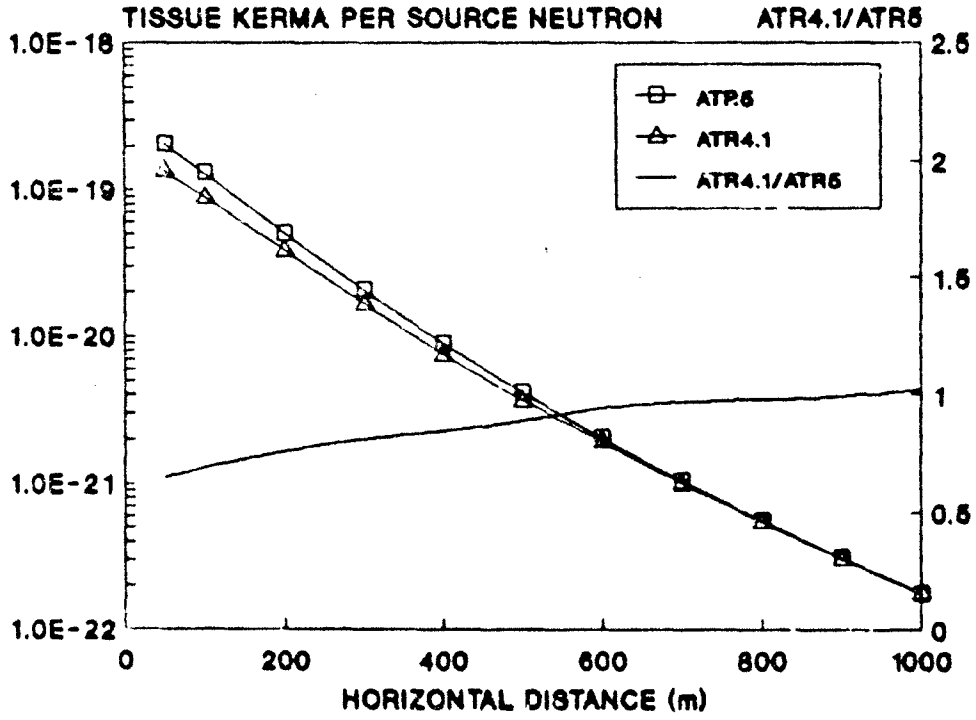

Figure 6. Secondary gamma ray kerma from a fission source at 100 meters burst height, ATR4.1 and ATR5.

measurements, as will be described later.

Task four of the present effort is to revise the delayed radiation model, fully integrating it into the ATR structure, to enable it to calculate dose from fission products of the three main fissile elements, U-235, U-238, and Pu-239, and to test the resulting model against relevant weapon test data and results of other calculational models.

1.4 USER FEATURES.

In addition to the obvious need to include provision for input of atmospheric moisture content and weapon fissile components associated with each weapon yield fraction, as required by the ATR modifications described above, a fifth task of this program is to improve input commands and other user features of the code, such as the fluence-to-dose conversion factor library. Specifically, the input commands are to be modified to include direct specifications of mean air density between source and detector location.

1.5 TECHNICAL APPROACH.

The approach to accomplishing previous revisions of ATR was to maintain a complete history of the evolution of ATR imbedded in the code itself, i.e., to make the code capable of reproducing results from all previous versions of the code as well as that from the current version for a given problem. That was achieved either by overlaying correction factors upon existing models or by simply retaining both the new and old models or data sets within the code. The overlay or additive modification approach was used primarily because it was found to be easier to parameterize corrections to the existing data base than to parameterize a data base starting from scratch. Further, maintenance of previous versions of the code, considered necessary for the sake of consistency and historical perspective, was implicit in that approach.

After three overlaid revisions to ATR it was decided that the previous approach had reached a point of diminishing returns, both in terms of simplicity and precision. The present modifications to ATR are based on calculational results derived from much higher quality cross section representations and sophisticated application of radiation transport calculation methods than those available in the past. In addition, parameterization of the new data can be accomplished using approaches not tried in the original model. Therefore, the philosophy of retention of historical data in ATR has been abandoned in favor of simply replacing the present data sets with new ones. The command structure of ATR has been retained with a minimum of modifications in order to make ATR revision as transparent to the user as possible. The programming style has been kept to a level common to most computers, retaining the machine-independent quality of the code. The release of the revised version of the code, known as ATR5, is being held in abeyance pending an additional modification to provide realistic energy- and angle-differential fluence at the air-ground interface and final testing. Release is expected during calendar year 1988.

The remainder of this report describes (Section 2) the superficial modifications to ATR, including revised input commands, energy group architecture, internal source spectra, and fluence-to-dose conversion factors, (Section 3) the revised ATR uniform air transport data base, (Section 4) the revised ATR air-ground interface perturbation model, and (Section 5) the revised ATR delayed gamma-ray model, including tests of that model against relevant weapon test data.

SECTION 2

ATR INPUT FORMAT AND DEFAULT MODIFICATIONS

This section describes the major superficial changes made to the ATR code as a result of the present program. These include

- o Input Commands
  - Meteorological Data
  - Fissile Material Specification
- o Energy Group Architecture
- o Internal Source Spectrum
- o Fluence-to-Dose Conversion Factors

2.1 METEOROLOGICAL DATA INPUT.

The specification of atmospheric conditions in ATR has been modified to provide for direct input of the mean density between source and detector and for the input of atmospheric moisture content. Previously, the air density used in ATR calculations was specified by locating the source and detector within an atmospheric density profile based on the U.S. Standard Atmosphere (dry air). That was accomplished by specifying ground elevation relative to sea level and source and detector height relative to the ground. In principle, an ATR user could obtain the desired average air density by trial and error through the variation of the ground elevation, but the procedure was cumbersome. To alleviate this problem and to make ATR more flexible in application, two modifications have been made to the code. First, while the standard atmospheric density profile has been retained within ATR, allowing atmospheric conditions to be completely specified by the input of source height, detector height and ground elevation, those atmospheric specifications can be overridden through the use of a new command card, *MET. Second, the specification of atmospheric conditions thought the use of the *MET command can now include moisture content. The objective of this modification is to permit the ATR user tospecify a set of meteorological parameters to obtain a mean air density and moisture content which exactly corresponds to a problem of interest.

The format of the input command is:

*MET(i) Values

where the index i determines the meaning of the sequence of values following the parenthesis, as follows:

Index i	Value 1	Value 2	Value 3
1	Temperature	Pressure	%Relative Humidity
2	Temperature	Pressure	Dew Point Temperature
3	Density of Moist Air	Wt % of Water	Not Used
4	Density of Moist Air	Density of Water Vapor	Not Used
5	Density of Dry Air	Wt % of Water	Not Used
6	Density of Dry Air	Density of Water Vapor	Not Used

As with past ATR commands, the values may be entered in free format separated only by a space. Units of input values are restricted to:

Temperature: Degrees Centigrade (°C)

Pressure: Millibars (mb)

Relative Humidity: Percent (%)

Density: Grams per cubic centimeter (g/cc)

If a *MET command is not used, ATR automatically determines the average air density between source and detector locations as in previous versions of ATR. Also, the moisture content of the air is set to a *default value of 0.0 percent density (dry air)*.

Examples of *MET input commands are as follows:

Example 1. *MET(1) 10.0 970.0 80.0
Represents atmosphere having a temperature 10 C, a barometric pressure of 970 mb and a relative humidity of 80%.

Example 2. *MET(4) 1.1889E-3 7.507E-6
Represents an atmosphere having a total (moist) air density of $1.889 * 10^{-3}$ g/cc and a water vapor density of $7.507 * 10^{-6}$ g/cc and is the equivalent of that atmosphere specified in Example 1.

Some useful relationships between the various atmospheric parameters are provided below and may be considered typical of a range of conditions to be found at an elevation of 1 km above sea level.

T(C)	P(mb)	RH(%)	Moist Air Density g/cm^3	Wt% Water
30	899	50	1.024E-3	1.47
25	899	50	1.044E-4	1.10
20	899	50	1.060E-3	0.812
15	899	50	1.083E-3	0.593
10	899	50	1.103E-3	0.427
5	899	50	1.124E-3	0.303
0	899	50	1.145E-3	0.212

The equations incorporated in ATR for the calculation of atmospheric density components are provided in Appendix B of this report.

When a *MET command is encountered in ATR, the code calculates a new ground elevation and overrides any other specified through the *GROUND command. This new ground elevation is selected such that the mean air density corresponds to that midway between source and detector. This is done to insure that a realistic atmospheric density profile exists between source and detector. The existence of such a profile is important, because the density at the source location is used in ATR to calculate the fireball radius, which is pertinent to delayed radiation intensity.

The revised ground elevation is calculated using the expression:

$$Z_g = (-13800 \times \ln (\rho / \rho_o))^{1.1.04} - (Z_s + Z_d)/2 \qquad (1)$$

where

Z_g is the ground elevation above sea level in meters

ρ is the mean air density (g/cc)

ρ_o is the sea level air density (1.225E-03 g/cc)

Z_s is the source height above the *ground* in meters

Z_d is the detector height above the *ground* in meters

Ground levels calculated using this expression correspond to appropriate elevations, as specified by the U.S. Standard Atmosphere, within a few percent for source-detector mean elevations above sea level to 5000 meters. Input combinations of source and detector heights and mean air densities which result in ground elevations below sea level are not allowed. Beyond 10,000 meters the accuracy of this expression is worse than a few percent, but that is not significant in relation to its use in ATR, which is to determine whether the fireball touches the ground.

2.2 FISSILE MATERIAL SPECIFICATION.

Section 5 of this report describes revisions made in the ATR delayed radiation model. Formerly, all

fission product radiation was based on photon emission from the fission products of a single fissile material, U-235. However, as will be described later in this report, the model has been revised to accommodate delayed photon emission from the fission products of three fissile materials, U-235, U-238, and Pu-239. The inclusion of such detail is important because, over much of the time regime of interest to initial radiation, the photon energy emission rate of U-238 is double that of U-235, which in turn is twenty-five percent more than that of Pu-239.

The quantity required for specifying the contribution of each nuclide to the delayed gamma-ray free field is the yield or the fraction of the total yield due to the fission of each nuclide. The command used to accomplish the input of these quantities is the *FP command. Formerly, specification of the fission product source require up to two input statements:

*FP-Y value,

which specified the *total yield* value, in kilotons, and

*FP-F value,

which specified the *fraction of the total yield due to fission*. In the event the *FP-F command was omitted a value of 1.0 was adopted as the default value.

As revised, a third *FP input command has been included, as follows:

*FP-I values,

which specifies the respective *fractions of the fission yield* due to U-235, U-238 and Pu-239 fission, *IN THAT ORDER*. Omission of the *FP-I command results in U-235 fission by default. Examples of revised fission product source input commands are as follows:

Example 1. *FP-Y 21
*FP-F 1.00
*FP-I 0 0 0 2 0 8
Represents a total weapon yield of 21 kt, 100% of which results from fission, 20% U-238 and 80% Pu-239.

Example 2. *FP-Y 1000
*FP-F 0.70
*FP-I 0.05 0.95 0 0
Represents a total weapon yield of 1000 kt (one megaton) of which 70% is produced by fission, 5% from U-235 and 95% from U-238.

As stated earlier, this revision of ATR has integrated the delayed radiation computation into the code. Thus, delayed radiation dose is now included automatically as all or part of the output resulting from the following commands:

*DOSE/FP/

which specifies the fission product dose versus running geometry coordinate

*DOSE/GG/

which specifies the total gamma ray dose versus running geometry coordinate.

*DOSE/T/

which specifies the total neutron plus gamma-ray dose versus running geometry coordinate.

However, as of this time the *PRINT and *WRITE command have not been modified to include fission product gamma ray output. The primary reason for this is that full incorporation of that component would require calculation of time-integral, angle-differential flux. This cannot be readily accomplished in the one-dimensional format common to the other radiation components because the fission product source does not remain fixed at the original burst location but rather rises with the ascending fireball. Incorporation of fission product gamma rays into the *PRINT and *WRITE commands is expected to occur when ATR is modified to produce fluence data in a two-dimensional format. That modification is part of the ongoing program to modify ATR to account for energy- and angle-differential fluence perturbations at the air-ground interface, as mentioned previously.

2.3 ENERGY GROUP ARCHITECTURE.

The energy boundaries of the multigroup neutron and gamma-ray fluence modeled in ATR have been changed, although the 22 neutron - 18 gamma-ray group format has been retained. The new group structure is the compatible with all major cross section sets sponsored by the Defense Nuclear Agency. Those includes the DNA Few-Group

Cross Section Set (DLC-31) (Ref.4), the revised DNA Few-Group set now being tested (DLC-130) (Ref.51), and Vitamin E (Ref. 60). The new ATR energy bounds for neutrons and gamma rays are provided in Tables 2 and 3, respectively, along with those of DLC-31 and DLC-130. Note that the top most gamma ray energy group boundary in the revised ATR is 12 MeV, where as that of DLC-31 is 14 MeV. That change was made to provide a more realistic differential spectrum (photons/MeV) in the highest energy gamma ray group, since the highest energy gamma ray to be encountered in air-ground transport is that of 10.8 MeV, produced by neutron capture in nitrogen.

2.4 INTERNAL SOURCE SPECTRA.

The source spectra traditionally contained in ATR, unclassified fission and thermonuclear weapon neutron spectra originally developed by W. Biggers of Los Alamos National Laboratory, and the generic prompt gamma-ray source spectrum have been regrouped into the new energy bounds described above. Those sources, accessible in ATR through the *Z-SOURCE command, are provided in Tables 4 and 5 for neutrons and gamma rays, respectively.

2.5 FLUENCE-TO-DOSE CONVERSION FACTORS.

The most frequently used portion of the output from an ATR calculation is that which provides total dose, kerma, or a similar integral quantity as a function of range. New fluence-to-dose conversion factors have been incorporated in ATR in an effort to more completely satisfy diverse user needs.

Tables 6 and 7 list the revised ATR fluence-to-dose conversion factors for neutrons and gamma rays respectively, by energy group. Those conversion factors and their origin are described in detail in Appendices C and D of this report, brief summaries of which are provided below.

- ANSI Standard Dose - For the Calculation of Human Dose Equivalent, i.e., quality factor-weighted dose. These values are relevant to radiation protection and risk of long term illness, such as cancer, from radiation exposure. Dose equivalent has no known relevance to early effects, such as prodromal syndrome or early mortality.

- Soft Tissue Kerma - Kinetic energy of charged particles released in soft tissue by ionizing radiation. This quantity is used to calculate free field tissue dose and replaces both the soft tissue Kerma and Henderson dose conversion factors in previous versions of ATR. The Henderson dose conversion factor was simply that for a four element tissue model now considered obsolete.

- Mid-head and Mid-phantom Dose - Fluence-to-soft tissue dose conversion factors which include the effect of transmission into the mid-head and mid-torso locations in a 70 kg anthropomorphic phantom.

- Concrete Kerma - Kinetic energy of charged particles released in concrete by ionizing radiation.

- Dry Air Kerma - Kinetic energy of charged particles released in dry air by ionizing radiation. Dry Air Kerma in units of rads may be converted to units of roentgens by dividing the rad values by 0.87.

- Non-Ionizing Silicon Kerma - Kinetic energy released in silicon crystal by neutrons which is associated with crystaline structure changes rather than creation of free electrons.

- 1 MeV Equivalent Damage Fluence - The fluence of 1 MeV neutron (fast reactor leakage neutrons, having a mean energy of approximately 1 MeV) required to produce the same amount of non-ionizing silicon Kerma-related damage.

- Ionizing Silicon Kerma - Kinetic energy released in silicon crystal by neutrons and gamma rays in the form of electron hole pairs.

The *DOSE command will cause ATR to calculate and display values for all the above dose quantities. In addition the *FLUXWT Command allows the user to provide up to 5 sets of additional fluence to dose conversion factors as input to ATR. The first set of fluence-to-dose factors entered in the revised ATR via the *FLUXWT command will produce integral values displayed as part of

Table 2. ATR detector energy group boundaries for neutrons (MeV) with DLC-31 and DLC-130 group boundaries for comparison.

ATR5			DLC-31			DLC-130		
Group	Lower Energy	Upper Energy	Group	Lower Energy	Upper Energy	Group	Lower Energy	Upper Energy
1.	1.00(-11)	4.14(-07)	1.	1.00(-11)	4.14(-07)	1.	1.00(-11)	4.14(-07)
2.	4.14(-07)	1.13(-06)	2.	4.14(-07)	1.13(-06)	2.	4.14(-07)	1.13(-06)
3.	1.13(-06)	3.06(-06)	3.	1.13(-06)	3.06(-06)	3.	1.13(-06)	3.06(-06)
4.	3.06(-06)	1.07(-05)	4.	3.06(-06)	1.07(-05)	4.	3.06(-06)	1.07(-05)
5.	1.07(-05)	2.90(-05)	5.	1.07(-05)	2.90(-05)	5.	1.07(-05)	2.90(-05)
6.	2.90(-05)	1.01(-04)	6.	2.90(-05)	1.01(-04)	6.	2.90(-05)	1.01(-04)
7.	1.01(-04)	1.23(-03)	7.	1.01(-04)	5.83(-03)	7.	1.01(-04)	2.75(-03)
						8.	2.75(-03)	5.83(-03)
			8.	5.83(-03)	1.23(-03)	9.	5.83(-03)	1.23(-03)
8.	1.23(-03)	2.19(-02)	9.	1.23(-03)	3.35(-03)	10.	1.23(-03)	3.35(-03)
			10.	3.35(-03)	1.03(-02)	11.	3.35(-03)	1.03(-02)
			11.	1.03(-02)	2.19(-02)	12.	1.03(-02)	2.19(-02)
9.	2.19(-02)	1.11(-01)	12.	2.19(-02)	2.48(-02)	13.	2.19(-02)	2.48(-02)
			13.	2.48(-02)	5.25(-02)	14.	2.48(-02)	3.43(-02)
						15.	3.43(-02)	5.25(-02)
			14.	5.25(-02)	1.11(-01)	16.	5.25(-02)	1.11(-01)
10.	1.11(-01)	1.58(-01)	15.	1.11(-01)	1.58(-01)	17.	1.11(-01)	1.58(-01)
11.	1.58(-01)	5.50(-01)	16.	1.58(-01)	5.50(-01)	18.	1.58(-01)	2.47(-01)
						19.	2.47(-01)	3.68(-01)
						20.	3.68(-01)	5.50(-01)
12.	5.50(-01)	1.11(+00)	17.	5.50(-01)	1.11(+00)	21.	5.50(-01)	6.39(-01)
						22.	6.39(-01)	7.43(-01)
						23.	7.43(-01)	8.21(-01)
						24.	8.21(-01)	9.62(-01)
						25.	9.62(-01)	1.11(+00)
13.	1.11(+00)	1.83(+00)	18.	1.11(+00)	1.83(+00)	26.	1.11(+00)	1.42(+00)
						27.	1.42(+00)	1.83(+00)
14.	1.83(+00)	2.31(+00)	19.	1.83(+00)	2.31(+00)	28.	1.83(+00)	2.31(+00)
15.	2.31(+00)	3.01(+00)	20.	2.31(+00)	2.39(+00)	30.	2.31(+00)	2.39(+00)
			21.	2.39(+00)	3.01(+00)	31.	2.39(+00)	3.01(+00)
16.	3.01(+00)	4.07(+00)	22.	3.01(+00)	4.07(+00)	32.	3.01(+00)	4.07(+00)
17.	4.07(+00)	4.97(+00)	23.	4.07(+00)	4.72(+00)	33.	4.07(+00)	4.72(+00)
			24.	4.72(+00)	4.97(+00)	34.	4.72(+00)	4.97(+00)
18.	4.97(+00)	6.38(+00)	25.	4.97(+00)	6.38(+00)	35.	4.97(+00)	6.38(+00)
19.	6.38(+00)	8.19(+00)	26.	6.38(+00)	7.41(+00)	36.	6.38(+00)	7.41(+00)
			27.	7.41(+00)	8.19(+00)	37.	7.41(+00)	8.19(+00)
20.	8.19(+00)	1.00(+01)	28.	8.19(+00)	9.05(+00)	37.	8.19(+00)	9.05(+00)
			29.	9.05(+00)	1.00(+01)	38.	9.05(+00)	1.00(+01)
21.	1.00(+01)	1.22(+01)	30.	1.00(+01)	1.11(+01)	39.	1.00(+01)	1.11(+01)
			31.	1.11(+01)	1.22(+01)	40.	1.11(+01)	1.22(+01)
22.	1.22(+01)	1.49(+01)	32.	1.22(+01)	1.28(+01)	41.	1.22(+01)	1.25(+01)
			33.	1.28(+01)	1.38(+01)	42.	1.25(+01)	1.38(+01)
			34.	1.38(+01)	1.42(+01)	43.	1.38(+01)	1.42(+01)
			35.	1.42(+01)	1.49(+01)	44.	1.42(+01)	1.49(+01)
			36.	1.49(+01)	1.69(+01)	45.	1.49(+01)	1.69(+01)
			37.	1.69(+01)	1.96(+01)	46.	1.69(+01)	1.96(+01)

Table 3. ATR source and detector energy group boundaries for prompt gamma rays, and detector energy group boundaries for secondary gamma rays (MeV) with DLC-31 and DLC-130 group boundaries for comparison.

ATR			DLC-31			DLC-130		
Group	Lower Energy	Upper Energy	Group	Lower Energy	Upper Energy	Group	Lower Energy	Upper Energy
1.	1.00(-02)	4.50(-02)	1.	1.00(-02)	2.00(-02)	1.	1.00(-02)	2.00(-02)
			2.	2.00(-02)	3.00(-02)	2.	2.00(-02)	3.00(-02)
			3.	3.00(-02)	4.50(-02)	3.	3.00(-02)	4.50(-02)
2.	4.50(-02)	1.00(-01)	4.	4.50(-02)	7.00(-02)	4.	4.50(-02)	7.00(-02)
			5.	7.00(-02)	1.00(-01)	5.	7.00(-02)	1.00(-01)
3.	1.00(-01)	1.50(-01)	6.	1.00(-01)	1.50(-01)	6.	1.00(-01)	1.50(-01)
4.	1.50(-01)	3.00(-01)	7.	1.50(-01)	3.00(-01)	7.	1.50(-01)	3.00(-01)
5.	3.00(-01)	4.50(-01)	8.	3.00(-01)	4.50(-01)	8.	3.00(-01)	4.50(-01)
6.	4.50(-01)	7.00(-01)	9.	4.50(-01)	7.00(-01)	9.	4.50(-01)	7.00(-01)
7.	7.00(-01)	1.00(+00)	10.	7.00(-01)	1.00(+00)	10.	7.00(-01)	1.00(+00)
8.	1.00(+00)	1.50(+00)	11.	1.00(+00)	1.50(+00)	11.	1.00(+00)	1.50(+00)
9.	1.50(+00)	2.00(+00)	12.	1.50(+00)	2.00(+00)	12.	1.50(+00)	2.00(+00)
10.	2.00(+00)	2.50(+00)	13.	2.00(+00)	2.50(+00)	13.	2.00(+00)	2.50(+00)
11.	2.50(+00)	3.00(+00)	14.	2.50(+00)	3.00(+00)	14.	2.50(+00)	3.00(+00)
12.	3.00(+00)	4.00(+00)	15.	3.00(+00)	4.00(+00)	15.	3.00(+00)	4.00(+00)
13.	4.00(+00)	5.00(+00)	16.	4.00(+00)	5.00(+00)	16.	4.00(+00)	5.00(+00)
14.	5.00(+00)	6.00(+00)	17.	5.00(+00)	6.00(+00)	17.	5.00(+00)	6.00(+00)
15.	6.00(+00)	7.00(+00)	18.	6.00(+00)	7.00(+00)	18.	6.00(+00)	7.00(+00)
16.	7.00(+00)	8.00(+00)	19.	7.00(+00)	8.00(+00)	19.	7.00(+00)	8.00(+00)
17.	8.00(+00)	1.00(+01)	20.	8.00(+00)	1.00(+01)	20.	8.00(+00)	1.00(+01)
18.	1.00(+01)	1.20(+01)	21.	1.00(+01)	1.40(+01)	21.	1.00(+01)	1.20(+01)
						22.	1.20(+01)	1.40(+01)
						23.	1.40(+01)	2.00(+01)

Table 4. Energy distributions for ATR5 neutron sources.

Group	Energy Boundaries (MeV)	Fission Weapon *N-SOURCE(1) (Fraction in Group)	Thermonuclear *N-SOURCE(2) (Fraction in Group)
1	1.07(-5) - 2.90(-5)	0.0	0.0
2	2.90(-5) - 1.01(-4)	0.0	0.00200
3	1.01(-4) - 1.23(-3)	0.0	0.05719
4	1.23(-3) - 2.19(-2)	0.01649	0.34417
5	2.19(-2) - 1.11(-1)	0.20617	0.10964
6	0.111 - 0.158	0.01799	0.01142
7	0.158 - 0.550	0.15129	0.09058
8	0.550 - 1.11	0.21587	0.08500
9	1.11 - 1.83	0.14678	0.06200
10	1.83 - 2.31	0.10173	0.02592
11	2.31 - 3.01	0.03871	0.02608
12	3.01 - 4.07	0.05480	0.02600
13	4.07 - 4.97	0.01177	0.01700
14	4.97 - 6.36	0.01832	0.01800
15	6.36 - 8.19	0.01274	0.01470
16	8.19 - 10.0	0.00734	0.01410
17	10.0 - 12.2	0.0	0.02560
18	12.2 - 15.0	0.0	0.07060

Table 5. Energy distribution for the ATR5 prompt fission gamma-ray source.

Group	Energy Boundaries (MeV)	Prompt Fission *G-SOURCE(1) (Fraction in Group)
1	0.01 - 0.045	0.03259
2	0.045 - 0.10	0.01644
3	0.10 - 0.15	0.04881
4	0.15 - 0.30	0.10321
5	0.30 - 0.45	0.13571
6	0.45 - 0.70	0.20256
7	0.70 - 1.00	0.16332
8	1.0 - 1.5	0.14073
9	1.5 - 2.0	0.06429
10	2.0 - 2.5	0.03743
11	2.5 - 3.0	0.02225
12	3.0 - 4.0	0.02109
13	4.0 - 5.0	0.00746
14	5.0 - 6.0	0.00265
15	6.0 - 7.0	0.00092
16	7.0 - 8.0	0.00038
17	8.0 - 10.0	0.00016
18	10.0 - 12.0	0.0

Table 6. Fluence-to-dose conversion factors for neutrons (rad/(n/cm^2)).

Group	Upper Energy (MeV)	ANS Standard (rem)	Soft Tissue	Mid-Phantom	Concrete	Dry Air	Non-Ionizing Silicon	Ionizing Silicon	Mid-Head	1MeV Equivalent Fluence
1	4.14(-07)	8.7195(-10)	1.4969(-11)	6.2660(-11)	2.1222(-13)	4.7503(-10)	5.2272(-14)	1.4942(-14)	6.9450(-11)	1.5817(-03)
2	1.13(-06)	1.2200(-09)	3.7144(-12)	5.0530(-11)	1.2093(-13)	1.1531(-10)	1.3947(-14)	3.9798(-15)	1.3660(-10)	4.2203(-04)
3	3.06(-06)	1.3387(-09)	2.5611(-12)	1.0850(-10)	1.0927(-13)	6.9943(-11)	8.0791(-15)	2.2895(-15)	9.0210(-11)	2.4446(-04)
4	1.07(-05)	1.2270(-09)	1.4750(-12)	1.4340(-10)	1.0395(-13)	4.0089(-11)	4.6701(-15)	1.2754(-15)	1.5210(-10)	1.4131(-04)
5	2.90(-05)	1.3328(-09)	1.0006(-12)	2.0310(-10)	1.0770(-13)	2.2720(-11)	3.3388(-15)	7.8905(-16)	1.7700(-10)	1.0103(-04)
6	1.01(-04)	1.1995(-09)	1.0808(-12)	9.8400(-11)	1.3253(-13)	1.3056(-11)	2.9450(-15)	6.8608(-16)	1.8000(-10)	8.9113(-05)
7	1.23(-03)	1.1344(-09)	4.9812(-12)	9.3644(-11)	4.0494(-13)	5.6482(-12)	2.0002(-14)	3.2015(-15)	1.3690(-10)	6.0524(-04)
8	2.19(-02)	1.1325(-09)	7.1195(-11)	1.4412(-10)	4.8449(-12)	5.3517(-12)	2.4580(-13)	6.1825(-14)	1.6217(-10)	7.4376(-03)
9	1.11(-01)	3.7130(-09)	4.2273(-10)	1.4576(-10)	3.0032(-11)	2.2691(-11)	1.4132(-12)	5.1437(-13)	1.8633(-10)	4.2761(-02)
10	1.58(-01)	7.8414(-09)	8.0649(-10)	1.6600(-10)	6.0427(-11)	4.4365(-11)	1.3610(-12)	5.9340(-13)	2.2880(-10)	4.1182(-02)
11	5.50(-01)	1.6810(-08)	1.3089(-09)	2.1850(-10)	1.3142(-10)	9.2396(-11)	2.1730(-11)	1.1842(-11)	2.3740(-10)	6.5751(-01)
12	1.11(+00)	3.2305(-08)	2.1072(-09)	3.0200(-10)	2.2466(-10)	1.6766(-10)	2.9483(-11)	2.0337(-11)	4.8710(-10)	8.9212(-01)
13	1.83(+00)	3.5994(-08)	2.7753(-09)	5.7360(-10)	2.8763(-10)	2.9132(-10)	2.9197(-11)	2.5495(-11)	9.7680(-10)	8.8346(-01)
14	2.31(+00)	3.5183(-08)	3.2121(-09)	8.4300(-10)	3.1423(-10)	3.4383(-10)	5.1396(-11)	5.0890(-11)	1.2580(-09)	1.5552(+00)
15	3.01(+00)	3.5554(-08)	3.5462(-09)	1.0590(-09)	3.1704(-10)	5.1820(-10)	6.1673(-11)	6.6914(-11)	1.5571(-09)	1.8662(+00)
16	4.07(+00)	3.8713(-08)	4.2223(-09)	1.1920(-09)	5.4502(-10)	1.0885(-09)	4.6307(-11)	5.8964(-11)	2.0400(-09)	1.4102(+00)
17	4.97(+00)	4.2000(-08)	4.4767(-09)	1.7262(-09)	5.9644(-10)	1.1795(-09)	5.8074(-11)	8.5471(-11)	2.5168(-09)	1.7573(+00)
18	6.38(+00)	4.2561(-08)	4.7306(-09)	2.3250(-09)	7.0865(-10)	9.4466(-10)	6.7542(-11)	1.4966(-10)	3.0170(-09)	2.0437(+00)
19	8.19(+00)	4.1013(-08)	5.2725(-09)	2.5558(-09)	1.0007(-09)	9.7582(-10)	6.6396(-11)	4.0598(-10)	3.5304(-09)	2.0091(+00)
20	1.00(+01)	4.0885(-08)	5.6470(-09)	2.8410(-09)	1.2579(-09)	1.1271(-09)	6.5379(-11)	7.1390(-10)	4.0200(-09)	1.9783(+00)
21	1.22(+01)	4.5402(-08)	6.1563(-09)	3.5854(-09)	1.6656(-09)	1.6126(-09)	7.0073(-11)	9.1268(-10)	4.4495(-09)	2.1203(+00)
22	1.49(+01)	5.5367(-08)	6.6327(-09)	3.7868(-09)	2.0211(-09)	2.2471(-09)	7.3445(-11)	1.0103(-09)	4.8170(-09)	2.2224(+00)

Table 7. Fluence-to-dose conversion factors for gamma rays (rad/(γ/cm^2)).

Group	Upper Energy (MeV)	ANS Standard (rem)	Soft Tissue	Mid-Phantom	Concrete	Dry Air	Ionizing Silicon	Mid-Head
1	4.50(-02)	1.3701(-10)	6.0114(-11)	7.1336(-12)	3.7236(-10)	6.2508(-11)	4.5330(-10)	8.4308(-12)
2	1.00(-01)	7.4882(-11)	3.2540(-11)	1.7080(-11)	1.1325(-10)	3.1457(-11)	1.3010(-10)	2.1849(-11)
3	1.50(-01)	9.1322(-11)	5.1977(-11)	3.2772(-11)	7.1064(-11)	4.7534(-11)	7.4778(-11)	3.7991(-11)
4	3.00(-01)	1.5431(-10)	1.0378(-10)	6.0709(-11)	1.0142(-10)	9.3913(-11)	1.0207(-10)	8.1868(-11)
5	4.50(-01)	2.5263(-10)	1.9196(-10)	1.1335(-10)	1.7583(-10)	1.7342(-10)	1.7533(-10)	1.3505(-10)
6	7.00(-01)	3.5816(-10)	2.9573(-10)	1.6867(-10)	2.6854(-10)	2.6674(-10)	2.6695(-10)	2.1511(-10)
7	1.00(+00)	4.8429(-10)	4.2645(-10)	2.6638(-10)	3.8568(-10)	3.8570(-10)	3.8465(-10)	3.0557(-10)
8	1.50(+00)	6.3631(-10)	5.8513(-10)	3.8948(-10)	5.2693(-10)	5.2670(-10)	5.2419(-10)	4.1010(-10)
9	2.00(+00)	8.1131(-10)	7.5648(-10)	4.5963(-10)	6.8109(-10)	6.8038(-10)	6.7815(-10)	5.5478(-10)
10	2.50(+00)	9.5976(-10)	9.0414(-10)	5.4096(-10)	8.1798(-10)	7.8903(-10)	7.9609(-10)	6.6096(-10)
11	3.00(+00)	1.0997(-09)	1.0412(-09)	7.2340(-10)	9.4730(-10)	9.6569(-10)	9.7433(-10)	7.9649(-10)
12	4.00(+00)	1.2784(-09)	1.2152(-09)	9.6853(-10)	1.1181(-09)	1.0916(-09)	1.1278(-09)	9.3139(-10)
13	5.00(+00)	1.5007(-09)	1.4352(-09)	1.0765(-09)	1.3485(-09)	1.2933(-09)	1.3741(-09)	1.0706(-09)
14	6.00(+00)	1.7142(-09)	1.6445(-09)	1.1518(-09)	1.5763(-09)	1.4851(-09)	1.6230(-09)	1.3972(-09)
15	7.00(+00)	1.9219(-09)	1.8496(-09)	1.3693(-09)	1.8057(-09)	1.6444(-09)	1.8657(-09)	1.5120(-09)
16	8.00(+00)	2.1266(-09)	2.0616(-09)	1.5307(-09)	2.0428(-09)	1.8983(-09)	2.1538(-09)	1.5717(-09)
17	1.00(+01)	2.4293(-09)	2.3471(-09)	1.7258(-09)	2.3829(-09)	2.1301(-09)	2.5247(-09)	1.8254(-09)
18	1.20(+01)	2.8449(-09)	2.7272(-09)	2.1086(-09)	2.8566(-09)	2.4563(-09)	3.0656(-09)	2.2349(-09)

the *DOSE output. Previously, the ATR user could only obtain access to the results of *FLUXWT entries through the use of summary tables which are part of the *PRINT command output.

SECTION 3

UNIFORM AIR TRANSPORT DATA BASE

Modification of ATR has included the replacement of the source detector energy-differential transport data modules for neutrons secondary gamma rays and prompt gamma rays. Angular fluence data have also been modified to be consistent with the scalar fluence information.

3.1 DATA BASE CALCULATION.

The transport data base for the ATR model is comprised of downscatter spectra in 22 neutron and 18 gamma-ray fluence energy groups from 18 neutron and 18 gamma-ray source groups. These data have been produced using the ANISN, one-dimensional, discrete ordinates transport code (Ref.20). Calculations have been performed using an S_{40} Gaussian quadrature and cross sections from the VITAMIN-E coupled neutron-gamma-ray Library having a P_5 Legendre scattering approximation for neutrons and P_8 for gamma rays.

The VITAMIN-E cross section library has a format consisting of coupled neutron-gamma-ray multigroup data in 174 neutron and 38 gamma-ray energy groups. The energy structure of VITAMIN-E neutron cross sections is comprised of nearly equal lethargy increments from 20 MeV to 0.1 eV with one additional group below 0.1 eV. The conversion to ATR 22 neutron - 18 gamma-ray group format was accomplished by collapsing source values for all VITAMIN-E groups constituent to a specified ATR source group, such that the sum of the sources was one particle, performing the transport calculation in uniform air using the full VITAMIN-E group structure and summing fluence data within ATR energy bounds. The in-group source weighting for gamma-ray source groups was based on a 1/E source shape. The in-group source weighting for neutrons was based on the ATR internal thermonuclear source spectrum in DLC-31 format (37 neutron groups).

The calculations were carried out in spherical geometry to an optical depth of 550 grams/cm^2 of moist air as specified in Table 8, having a density of:

$1.115 * 10^{-3}$ g/cc dry air

$6.330 * 10^{-6}$ g/cc water vapor

$1.121 * 10^{-3}$ g/cc total moist air

Table 8. Data base moist air element specifications.

Element - Medium	Weight%	Number Density(atoms/b-cm)
H - Water	6.317E-02	4.235E-07
O - Water	5.012E-01	2.117E-07
O - Air	2.302E+01	9.722E-06
N - Air	7.514E+01	3.625E-05
Ar - Air	1.283E+00	2.170E-07

Thus, the calculations extended to a radius of approximately 5 km. Only the data to 500 gram/cc (approximately 4.5 km) were used to establish the data base for ATR, in order to allow for perturbations caused by the vacuum at the outer boundary of the calculation.

3.2 DATA BASE PARAMETERIZATION.

It would be possible to create an air transport model simply by saving and performing interpolation operations on a complete set of differential fluence data from one-dimensional discrete ordinate calculations. However, such a system would be very large and unwieldy. Similarly, those data could be fit with high order polynomial functions. Again, the size of the coefficient data array would be very large.

The modeling approach used in ATR is to use efficient functional forms to fit the data base and to separate variable relationships so that a minimum number of computations have to be performed to reconstruct the required fluence data. Previous versions of ATR have incorporated separate functional fits of total fluence, energy-differential fluence, and angle-differential fluence data. This approach was taken because the total fluence was easily fit with few coefficients, while the differential fluence models could be based on data normalized to total fluence. That approach allowed energy- and angle-differential models to be constructed at specific distances, with interpolation to intermediate distances, rather than as continuous functions of energy.

The functional form used in previous versions of ATR to fit the data as described above is a polynomial series comprised of half-integer and logarithmic terms, known as Webster Functions. Even though these functions provided great flexibility in fitting complex data, it was found that the differential data could not be adequately fit with one polynomial series. However, it was discovered that the ratios between the first order functional fit and the data itself were more amenable to the fitting procedure. Thus,previous versions of ATR contain one or two iterative correction routines to improve the quality of the fit. Likewise, when revisions have been made to the code, additional corrective layers have been applied rather than refitting the data base from scratch.

There has been one previous major revision to the ATR data base, at which time the original data were modified to reproduce a set computed using improved cross sections. It was decided that adding still another layer of modifications would increase the running time of the code, further complicate its already complicated internal structure, and possibly provide an unreliable fit to the data. Thus, it was decided to fit the one-dimensional transport data base starting from scratch in the current revision of ATR.

The approach to data parameterization in the current revision of ATR is changed from that used in previous versions. Because the primary quantity used in ATR for calculation of range-dependent dose or kerma is energy-differential fluence, there was no particular reason to fit the total fluence separately, except for the sake of convenience. Thus, the approach was taken to directly parameterize energy-differential fluence as a function of distance.

As revised, ATR computes energy-differential fluence using two models. First, the code calculates the uncollided, energy-differential fluence using the total cross section applicable to each source energy group. Second, the code computes the scattered fluence contribution. The model used to fit scattered fluence data, including in-source group scatter, is based on the fact that the function

$$\text{Function} = F(\mu r) \times (e^{-\mu r}) / r^2 \qquad (2)$$

where r is distance,

μ is the inverse relaxation length, and

$F(\mu r)$ is a polynomial,

which is often used to approximate the variation of kerma or fluence with distance, takes the form of a Taylor series on r with powers in half-integer steps.

It was found that a series truncated at powers of ± 3, including twelve functional terms and a constant, could reproduce the energy- differential fluence data with great accuracy within one or two percent at each location. Through multiple trials a subset of six terms of the original thirteen was found which could reproduce the data nearly as well, certainly within the ± 5 percent limits which were the target criteria. Thus, a software system was devised which performed a least squares fit to all possible combinations of six of the available thirteen terms, and provided the results, in terms of the resulting coefficients, in order of descending coefficient of determination value. Top combinations of coefficients were tentatively chosen for inclusion in the system. In

those cases where several combinations were ranked as having equal values (to seven significant figures) of the coefficient of determination, that combination providing the maximum sum of all partial correlation coefficients was chosen. The sets of coefficients were then individually tested to insure that each reproduced its data set to ± 5 percent or better at almost all locations.

Examples of fit fluence plotted together with the data from which they were derived are presented in Figures 7, 8 and 9 for neutron, secondary gamma ray and prompt gamma ray kerma, respectively, from a fission source.

The angular fluence parameterization was retained from ATR 4.

3.3 TRANSPORT PERTURBATION BY AIR MOISTURE VARIATION.

The atmosphere is nominally considered to contain nitrogen, oxygen and argon in descending order of abundance, with the last mentioned being present at levels only a little over a percent of the total mass. The argon is important cause of its large photoelectric cross section which helps make the atmosphere opaque to photons below approximately 30 keV. These three constituents make up the so-called dry atmosphere, which has long been the standard for use in radiation transport calculations. However, the atmosphere also contains moisture in amounts which vary over time, ranging from a few tenths of a percent to as much as one and a half percent by weight. Consequently the atmosphere generally contains up to a few tenths of percent hydrogen atoms by weight or up to more than three percent by number.

As described in section 2.1, ATR5 has been given the capability to accept atmospheric humidity as a meteorological variable. This capability is based on scaling factors which have been incorporated into ATR5. Those scaling factors have been developed from a set of adjoint ANISN, one-dimensional transport calculations, performed to a dry air optical depth of 55 gram per square centimeter, using DLC-31 cross sections (S_{40}, P_3), having moisture contents as follows:

Weight Percent

0.0 (Moisture content default if no moisture specification is input)

0.1

0.2

0.4

0.5645 (ATR5 Uniform Air Data Base)

0.8

1.2

1.6

2.0

The calculations provided tissue kerma as a function of distance from each of 37 neutron and 21 gamma ray source energy groups. These were collapsed into the 18 neutron, 18 gamma ray group source energy structure of ATR5 using the thermonuclear source shape for neutrons and secondary gamma rays and inverse energy for gamma rays, as described in section 3.2. The results for each source energy were fitted as a function of optical depth as ratios of kerma calculated for a particular moisture content and that calculated for the ATR5 data base. As applied in ATR5, the natural logarithm of the moisture content correction factor was expressed as a function of optical depth using the same polynomial form used to fit the uniform air fluence data base. That form is a polynomial series in half integer power steps from a negative three to a positive three. Trials were run to determine the minimum number of coefficients required to fit the ratios to better than five percent accuracy. These determined that four terms (plus a constant) were required to fit the neutron and secondary gamma ray data, while only three terms (plus a constant) were required to fit the gamma ray data. As in the case of the uniform air fluences, while each fit consists of four or five terms they are not necessarily the same four or five terms for each source energy.

Moisture corrections in the form of kerma ratios for various moisture contents are depicted in Figures 10, 11 and 12 for fission neutrons and secondary gamma rays and fusion neutrons, respectively. It should be noted that, as argonne has little effect on the transport of neutrons,

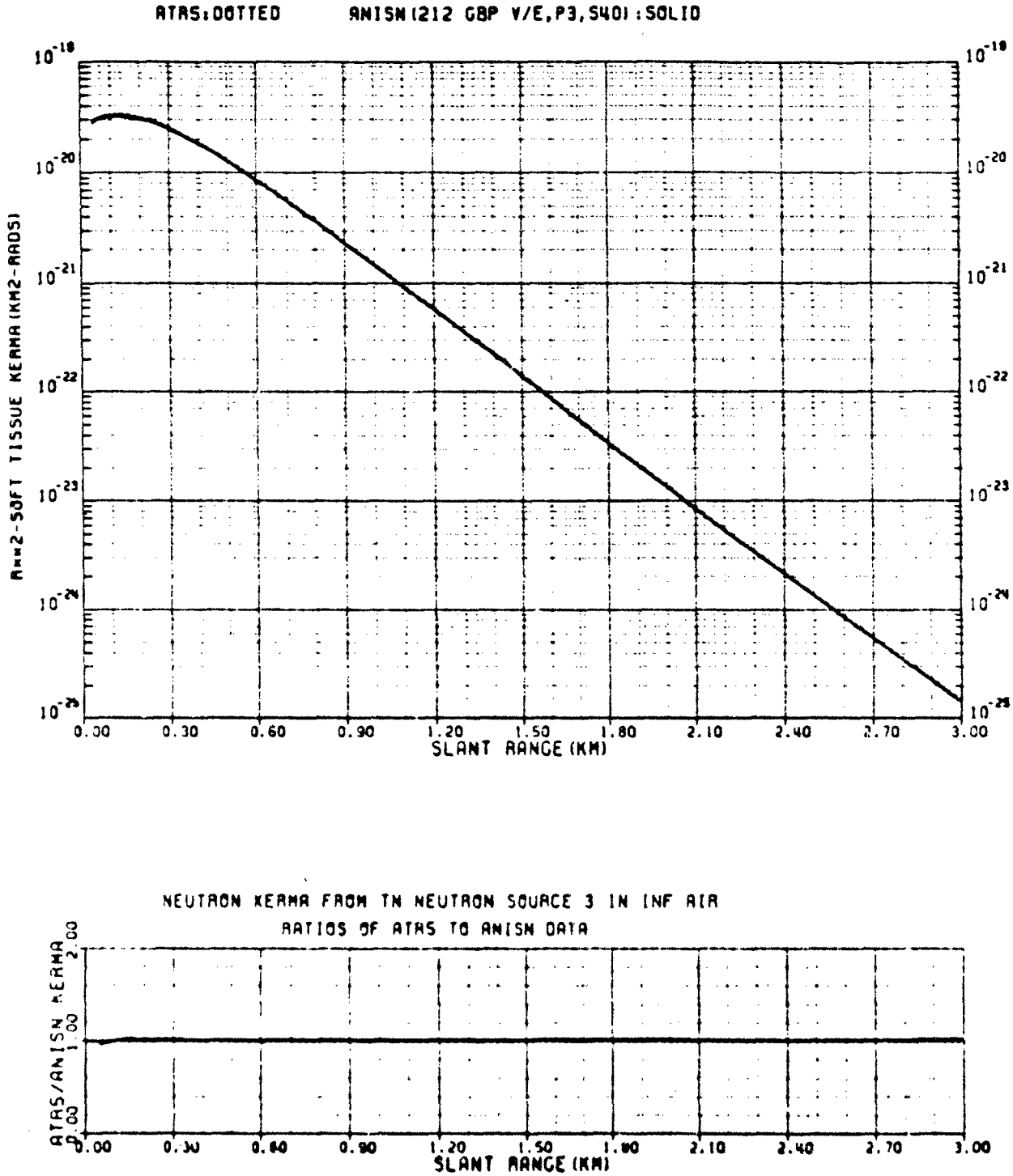

Figure 7. Neutron tissue kerma from a boosted fission source in uniform air, ATR5 and its data base.

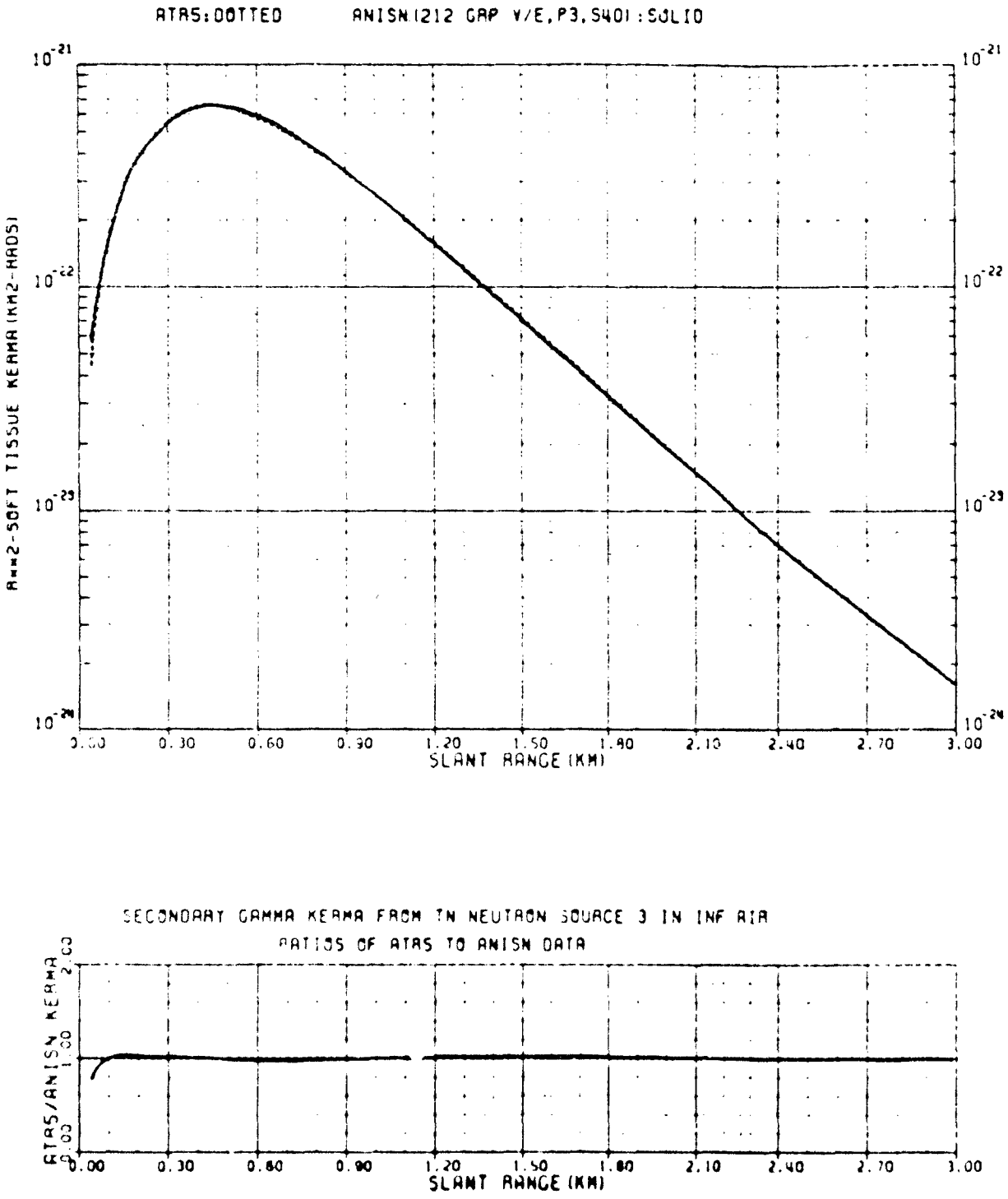

Figure 8. Secondary gamma ray tissue kerma from a boosted fission neutron source in uniform air, ATR5 and its data base.

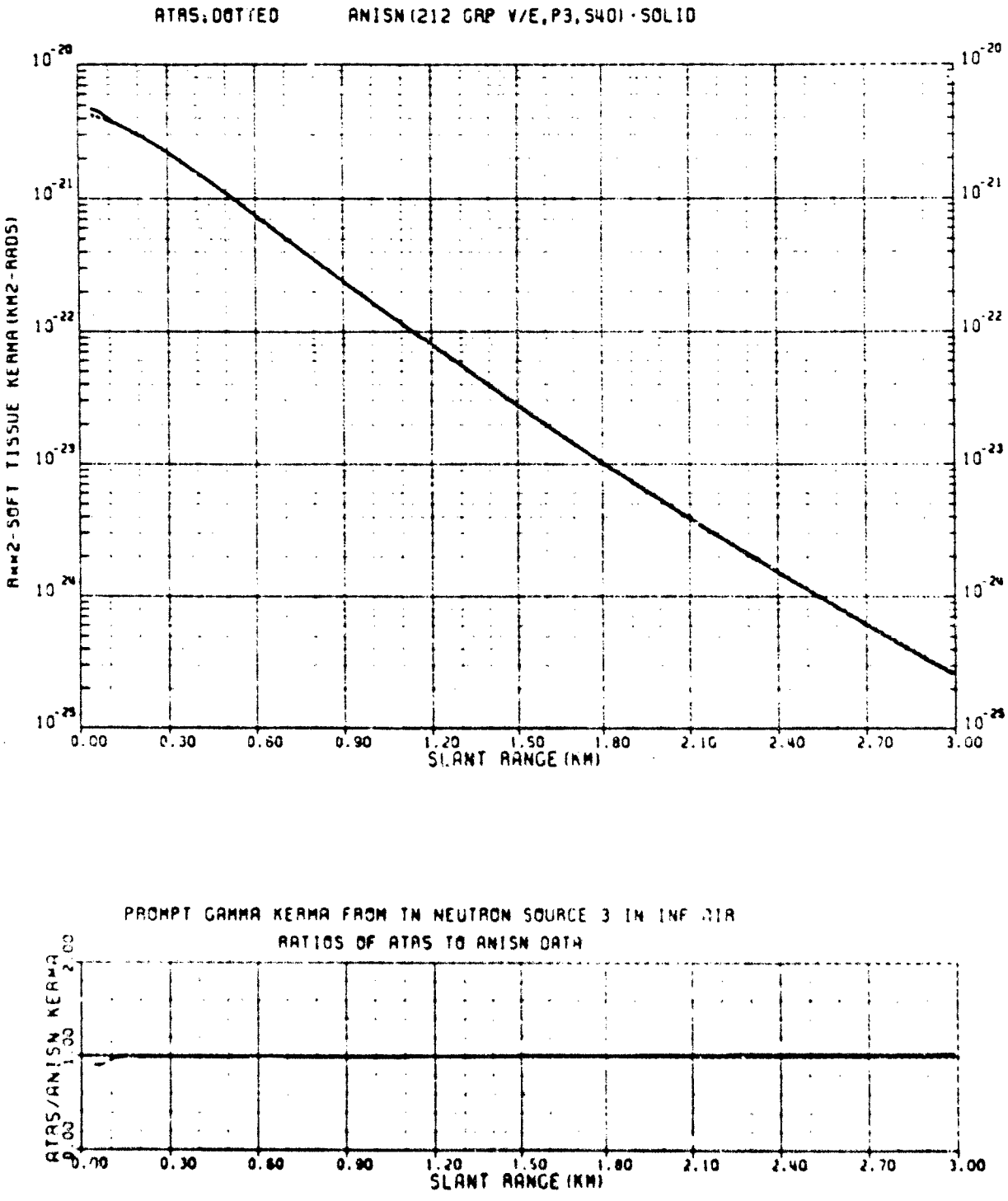

Figure 9. Gamma ray tissue kerma from a boosted fission gamma ray source in uniform air, ATR5 and its data base.

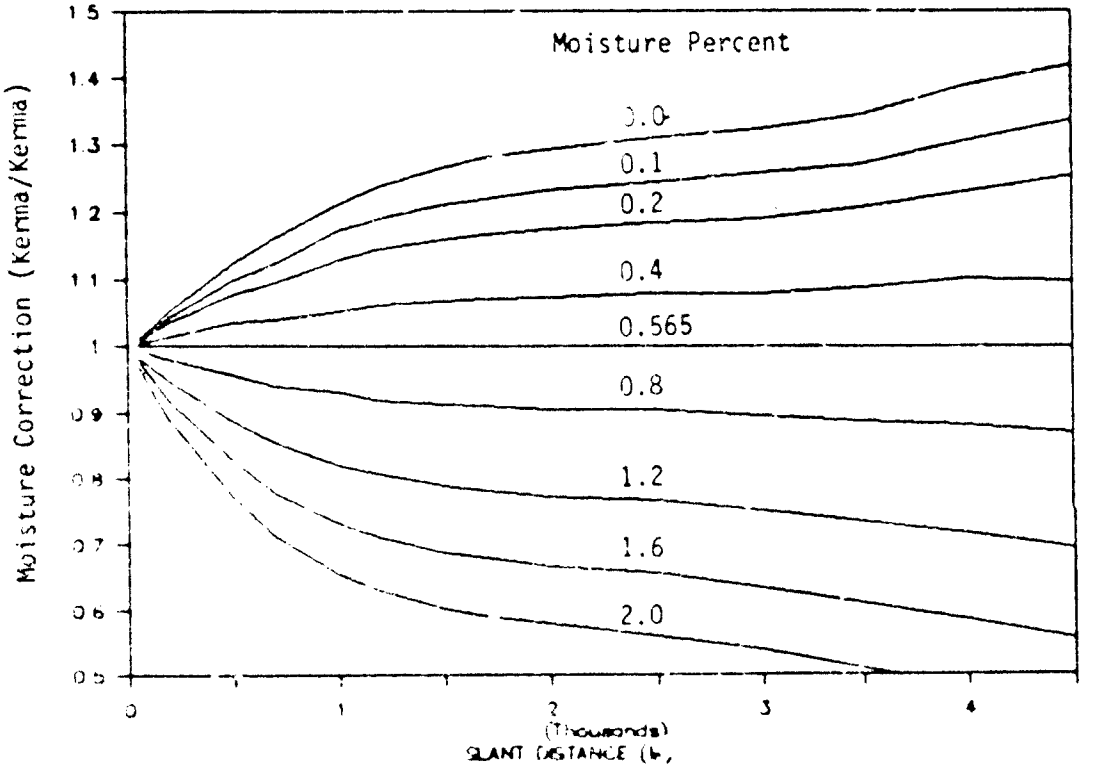

Figure 10. Neutron kerma correction for atmospheric moisture content in uniform air, fission neutron source.

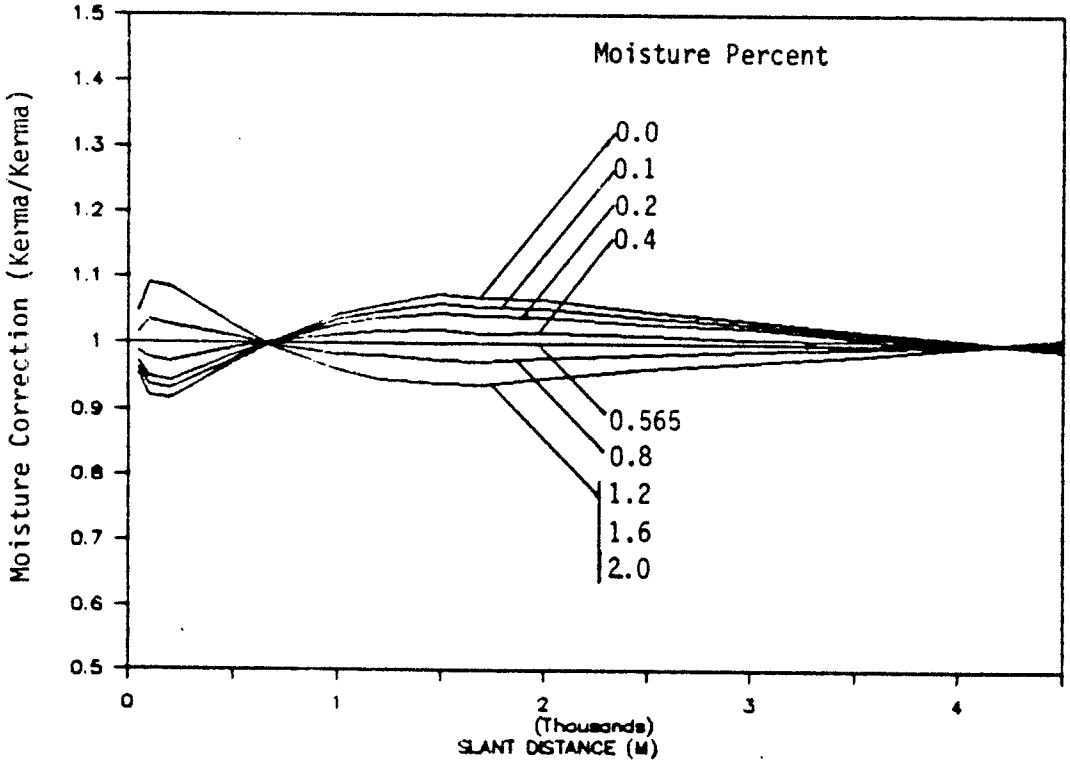

Figure 11. Secondary gamma ray kerma correction for atmospheric moisture content in uniform air, fission neutron source.

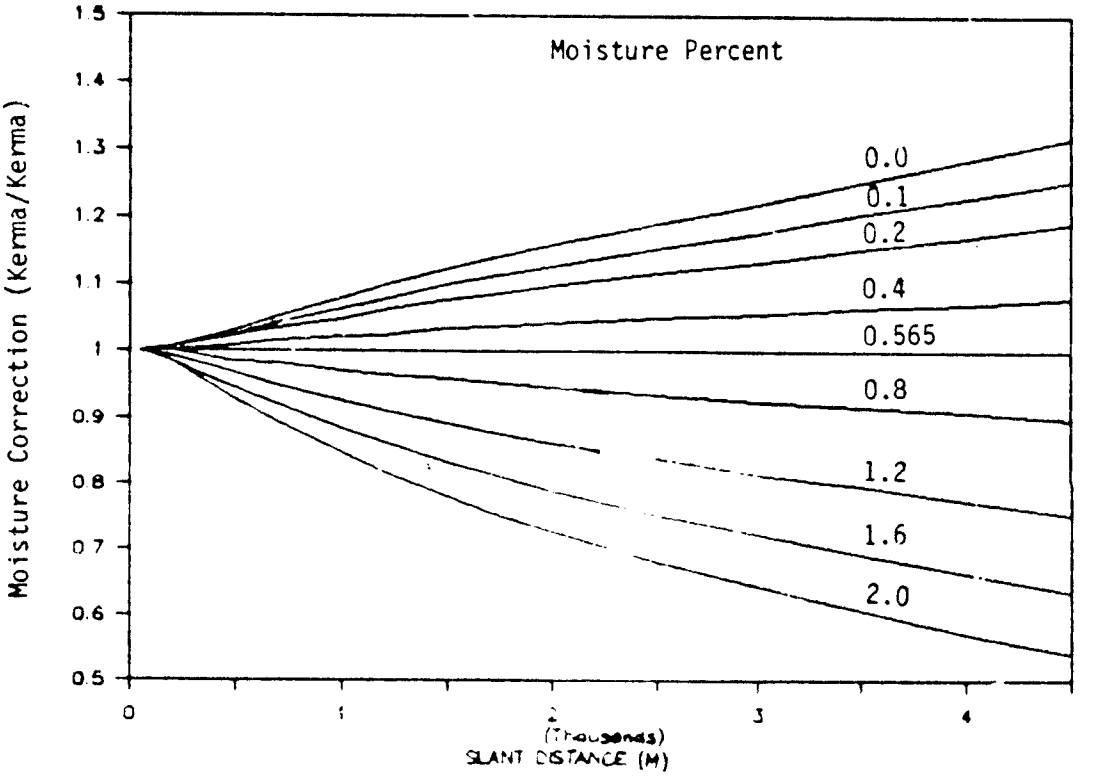

Figure 12. Neutron kerma corrections for atmospheric moisture content in uniform air, fusion (12.2 to 14.9 MeV) source.

moisture has little effect on the transport of source gamma rays. However, moisture has a considerable effect on the transport of neutrons. The nature of this effect is to strip the low energy (less than 1 MeV) neutrons from the transported spectrum. A fission weapon source contains a large number of such neutrons. Hence, its transport is significantly effected initially, much more so than the fusion source. After its initial loss of low energy source neutrons, the transported fission spectrum stabilizes, aided by the oxygen cross section minimum at approximately 2.3 MeV.

The prompt gamma rays and secondary gamma rays from fusion neutrons are essentially unaffected by atmospheric moisture. However, the effect of increasing moisture on secondary gamma rays from a fission neutron source is to decrease the distance from the source at which such gamma rays are produced. This increases the gamma ray kerma at short distances, as shown in Figure 11. At very large distances the effect becomes less important because the source becomes more and more equivalent to a point, regardless of where the gamma rays were produced.

Note that the moisture transport correction used in ATR5 is based on ratios of kerma for each *source* energy and is not detector energy - dependent. Thus, the spectrum is unchanged from that contained in the data base which contains approximately 0.6% moisture by weight. This corresponds to a relative humidity of approximately 50% on a cool day (15°c) and is typical of conditions which are to be found in central Europe in the spring (Ref. 40).

SECTION 4

AIR-GROUND INTERFACE PERTURBATION MODEL

Radiation is scattered and absorbed in the ground to a different extent than in air. Thus, the presence of the air-ground interface causes radiation fluences to be perturbed in energy and angle from those which would otherwise exist at the same distance from the source in uniform air. At the present time, the ATR code does not correct the differential fluence for the presence of the ground. Rather, it corrects the free field tissue kerma, an integral quantity, based on ratios of two-dimensional calculations with and without the ground.

It is important to note that differential fluences produced by ATR for detector locations near the air-ground interface are those for uniform air, adjusted by scalar multipliers, which are functions of source energy, horizontal distance and burst height, in order to obtain the correct free field tissue kerma. Values for all remaining kerma or dose quantities are obtained in ATR by applying the fluence-to-dose conversion factors described previously to the adjusted uniform air fluence.

The first correction factors placed in ATR to account for the presence of the Air-ground interface were based on the French-Mooney first-last collision estimation method (Ref. 24), normalized to the two-dimensional calculations of Straker (Ref. 53), which pertained to a neutron source at a height of 50 feet. The next improvement was based on the extensive two-dimensional calculations of Pace (Ref. 44), which provided data for source heights to 300 meters, although the source data were limited to fission and fusion spectra. The most recent improvement prior to the current effort used the results of adjoint two-dimensional calculations ratioed to one-dimensional results to obtain a full, source energy-dependent array of adjustment factors (Ref. 26). However, these data suffered from the fact that the ground used in the two-dimensional calculations was unrealistically dry, causing the neutron and secondary gamma ray dose immediately above the ground to be unrealistic as well.

The air-over-ground transport corrections developed for use in thecurrent update of ATR are also based on two-dimensional adjoint calculations, performed this time with a credible amount ground moisture, 13% by weight, which is representative of that contained by mid-European and United States soils under moderate weather conditions (Ref. 6). The elemental constituents and density data for the ground and atmosphere used in the calculations are shown in Table 9. The atmosphere has a graded density based on a model of spring conditions in central Europe, as shown in Figure 13.

The calculations were performed using the DOT two-dimensional discrete ordinates transport code (Ref. 25) with a tissue kerma adjoint source, the 37 neutron, 21 gamma ray group DLC-31 cross section set with P_3 legendry scattering in a S_8 quadrature set modified to S_{40} in the polar direction to minimize streaming along discrete quadrature angles (ray effects). Calculations were performed to a usable source height of 1000 meters and a usable horizontal distance of 2000 meters. As an additional precaution against the effects of quadrature streaming, the uniform air calculations used to develop the correction factors were also performed using the DOT code with an identical atmosphere profile mirrored at the location of the air ground interface.

The results of the calculations, as ratios of the air-ground to uniform air kerma for a fission source are shown in Figures 14, 15 and 16 for neutrons, secondary gamma rays and prompt gamma rays, respectively. Equivalent data for fusion (12.2 to 14.9 MeV) neutrons are given for neutron and secondary gamma ray kerma, respectively, in Figures 17 and 18. The data are very well behaved except within a forty-five degree cone below the source. Beyond that inner region it is clear that the relationship between ground-perturbed and uniform air transport is linear with respect to source height and horizontal distance. This fact has been used to extrapolate the results of these calculations to greater distances. Within the forty-five degree cone, the relationship between the uniform air and air-over-ground results is irregular, probably indicating instabilities in the calculation of the latter case. The irregularities do decrease with increasing burst height. Also, they were more pronounced when kerma ratios were taken with respect to ANISN (one-dimensional) rather than DOT (two-dimensional) calculation results.

Table 9. Air and ground elemental constituents (weight %).

Elements	Dry Ground Constituents	Dry Air Constituents Level 1 0-400m	Level 2 400-800m	Level 3 800-1100m
H	0.14			
C	1.43			
N	0.14	75.72	75.72	75.72
O	50.63	24.28	24.28	24.28
Na	0.79			
Mg	1.14			
Al	4.60			
Si	32.14			
K	1.65			
Ca	2.30			
Mn	0.14			
Fe	2.25			
Ti	0.36			
P	0.12			
Density (g/cc)	1.40	1.155-3*	1.116-3	1.074-3
Free Moisture Density (g/cc)	0.21	6.750-6	6.148-6	4.844-6
Total Density (g/cc)	1.61	1.162-3	1.122-3	1.079-3

*Read as $1.155*10^{-3}$.

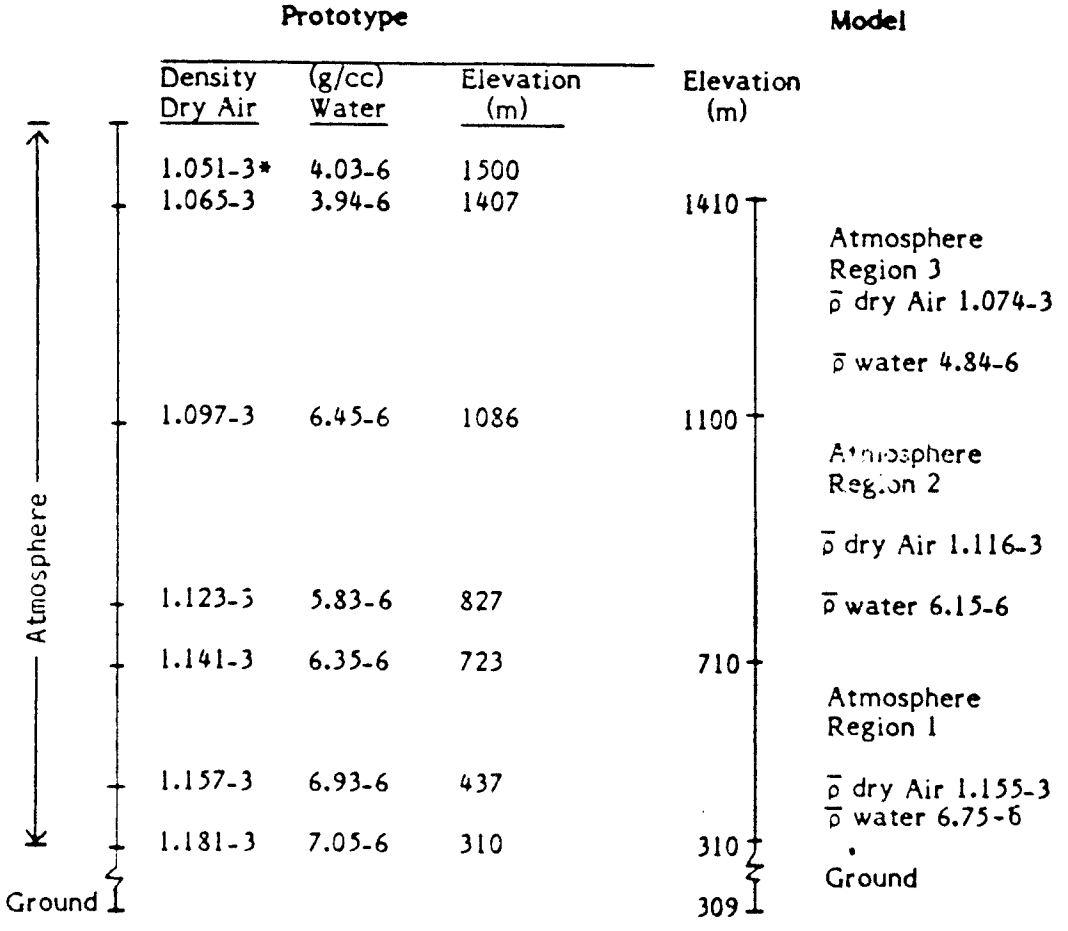

*Read as $1.051 * 10^{-3}$

Figure 13. Atmospheric density and moisture profile.

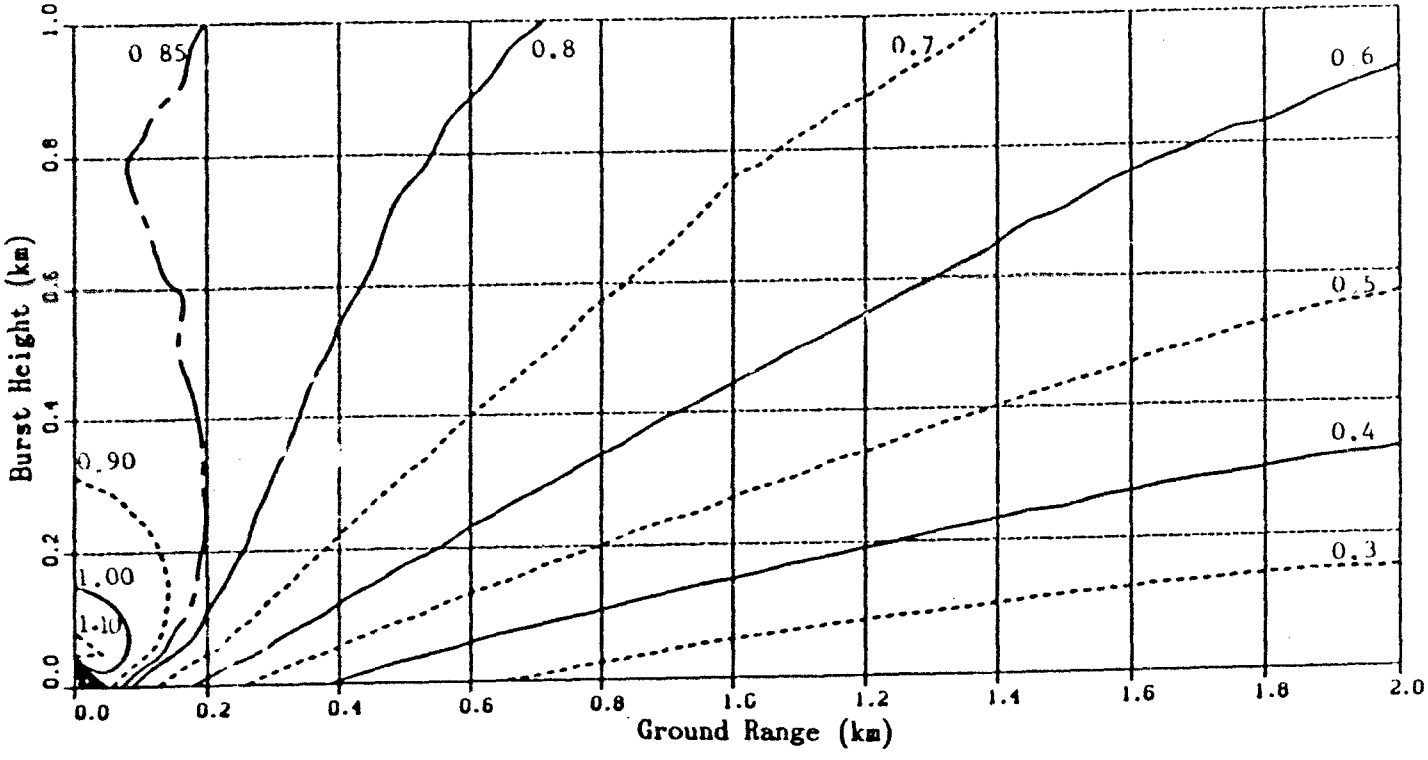

Figure 14. Factors for correcting fission neutron kerma in uniform air for the presence of the air-ground interface, target height one meter.

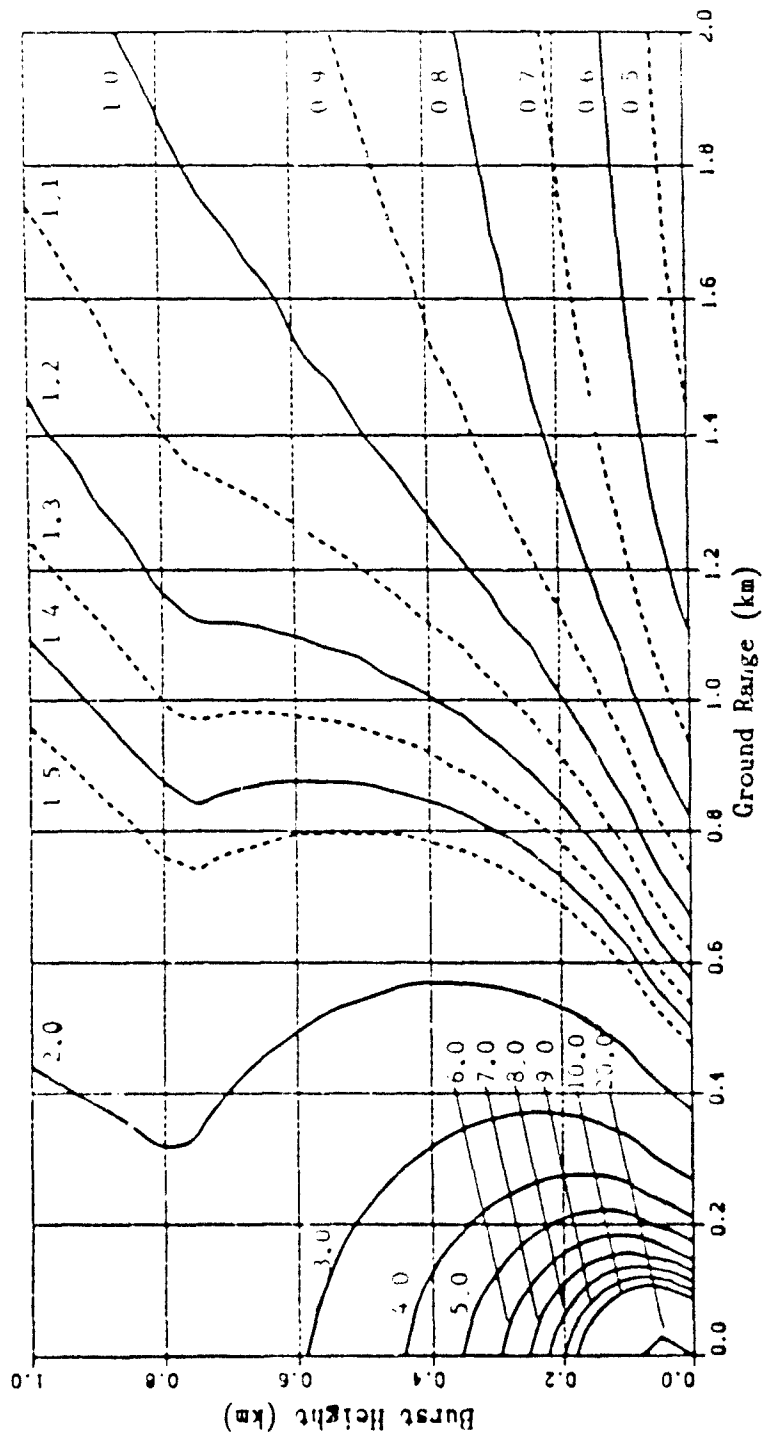

Figure 15. Factors for correcting fission neutron secondary gamma rays kerma in uniform air for the presence of the air-ground interface, target height one meter.

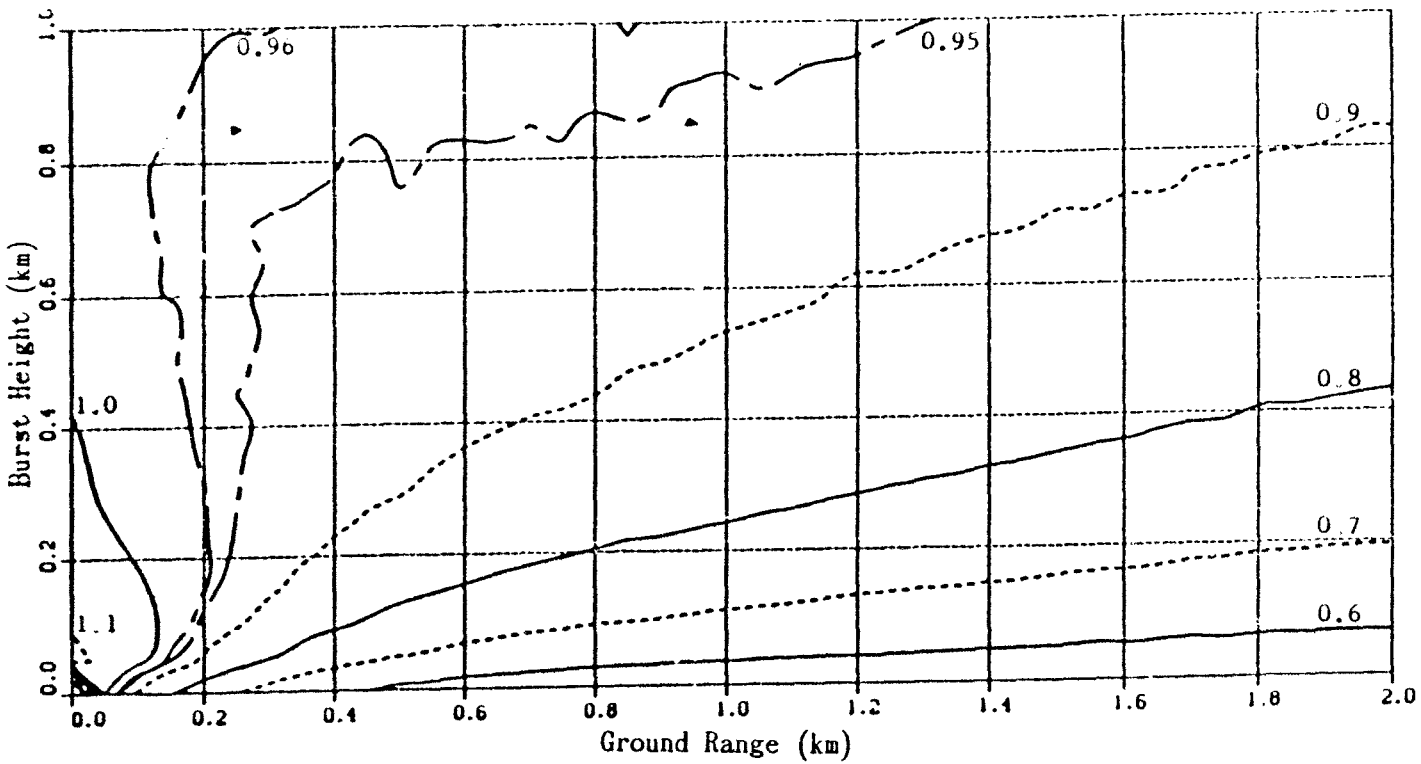

Figure 16. Factors for correcting fission gamma ray kerma in uniform air for the presence of the air-ground interface, target height one meter.

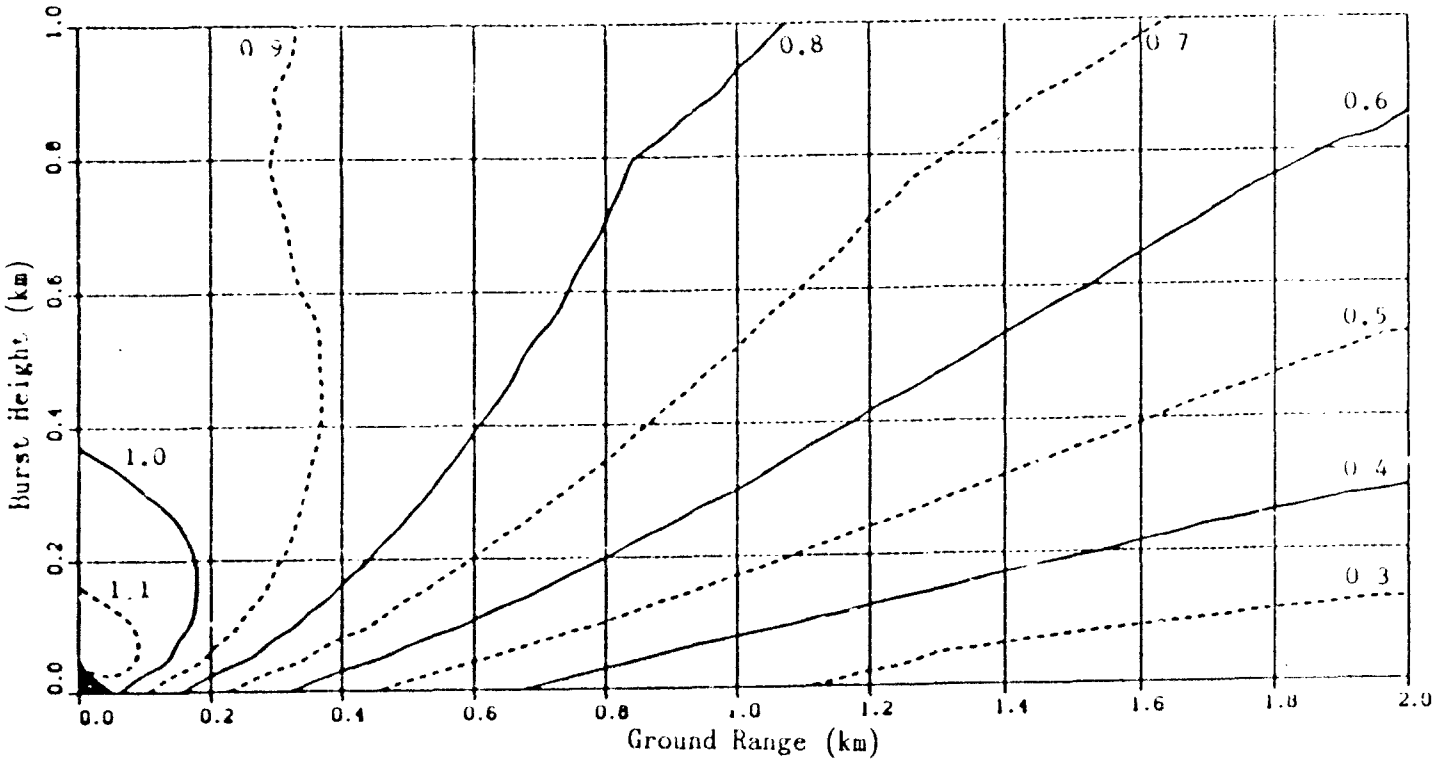

Figure 17. Factors for correcting fusion neutron kerma in uniform air for the presence of the air-ground interface, target height one meter.

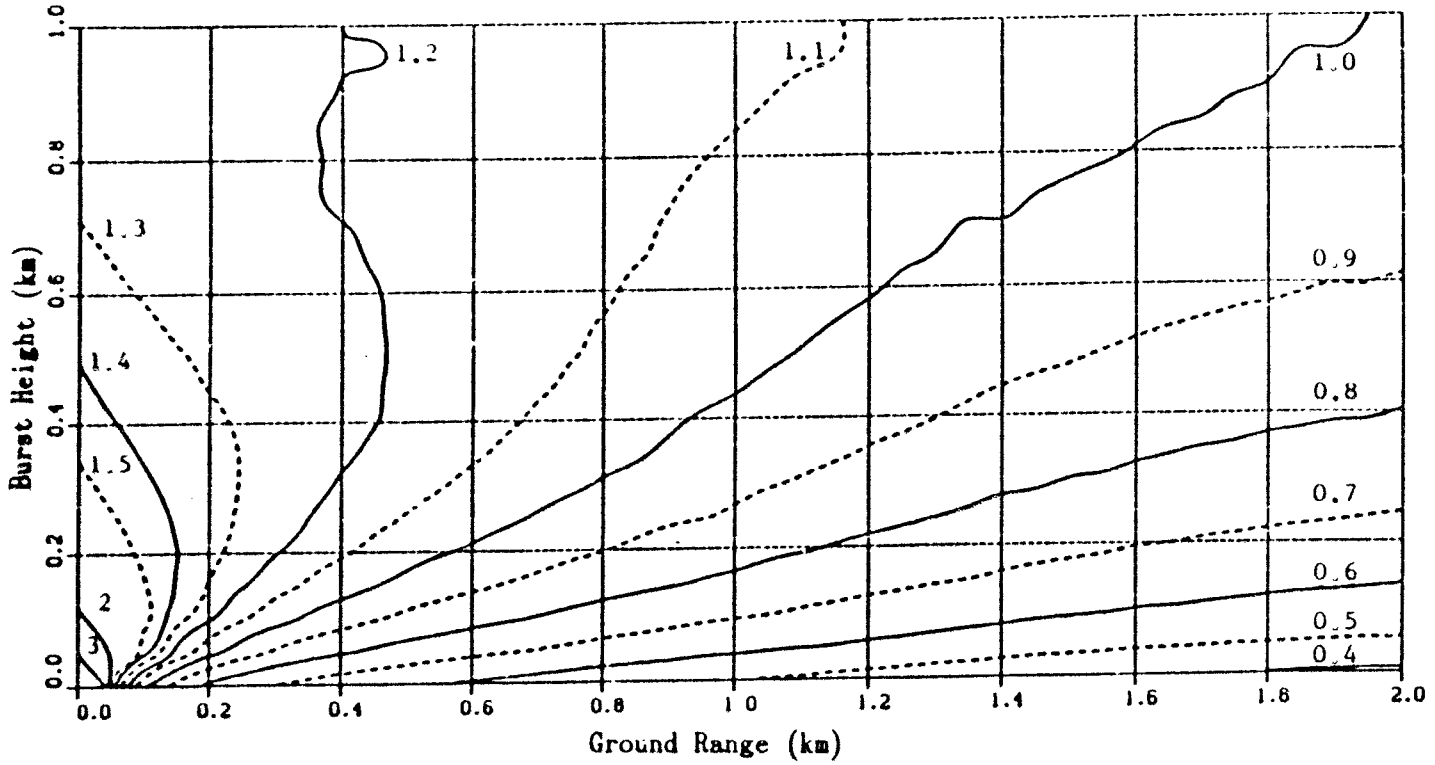

Figure 18. Factors for correcting fusion neutron secondary gamma rays kerma in uniform air for the presence of the air-ground interface, target height one meter.

The ratios of air-over-ground to uniform air tissue kerma were fit with a multi-variable function, including the following terms. Note that all distance quantities (slant range, R, and burst height, H) are expressed as optical depth (mass per unit area).

TRIAL TERMS FOR FITTING AIR-OVER-GROUND CORRECTION FACTORS

R in quarter power steps from 1/4 to 2

H in quarter power steps from 1/4 to 2

(R*H) in half power steps from 1/2 to 2

θ grazing angle, in radians

SIN θ

COS θ

R*SIN θ

R*COS θ

CONSTANT

Trials were run to identify the most important coefficients, fifteen of which were required to reproduce the data everywhere to within five percent or better. Those fifteen terms are as follows:

FINAL TERMS USED TO FIT AIR-OVER-GROUND CORRECTION FACTORS

1. $H^{1/4}$
2. $H^{1/2}$
3. H^{1}
4. H^{2}
5. $R^{1/4}$
6. $R^{1/2}$
7. R^{1}
8. $R^{3/2}$
9. R^{2}
10. θ
11. COS θ
12. SIN θ
13. R*COS θ
14. $(R*H)^{1/2}$
15. CONSTANT

The relative importance of these fifteen terms in fitting the data varies with location. At short distances (less than approximately 300 meters burst height and 500 meters horizontal distance in data base air) the H (burst height) terms dominate the value produced by the function. Beyond those confines the value is dominated by the slant range and grazing angle. At the limits of the data the value is dominated by the grazing angle alone. Thus, the extrapolation of the correction factor beyond the confines of the data base is accomplished on the basis of grazing angle, which is used to determine the applicable correction factor taken from the data base limit.

SECTION 5

DELAYED GAMMA RADIATION

ATR calculates delayed radiation propagation taking into account the time-dependent fission product gamma ray emissions, fireball/weapon debris height and air density surrounding the rising fireball. The fireball rise and air density treatments in ATR5 are based on empirical observations and a one dimensional model, respectively, and are unchanged from those used in ATR4. The balance of the model used in ATR5 differs from that used in ATR4 as follows:

1. The ATR5 source term accounts for differences between spectra and photon emission rates between fissionable isotopes U235, U238 and Pu239, whereas the ATR4 model is applicable to U235 only.

2. The ATR5 delayed gamma ray transport model uses the same data base as that used for the prompt gamma rays, calculating scalar fluence as its primary quantity, whereas ATR4 has a separate photon transport data base consisting of a kerma-optical depth (g/cm^2) relationship.

3. The ATR5 model has been used to calculate dose and dose rate values measured at atmospheric tests and has been empirically adjusted to provide the best agreement with available test data.

Delayed radiation fluences are calculated in ATR5 according to the expression:

$$\phi_j(R) = Y \cdot FFR \cdot \sum_{k=1}^{29} \sum_{l=1}^{18} \phi_{jkl}(r,\rho r,hs) \cdot \int_{\Delta t_k} (dt \sum_{i=1}^{3} (FF_i) \cdot (FFY_i) \cdot S_{il}(t) \qquad (3)$$

where $\phi_j(R)$ is the total gamma ray fluence in energy group j, at a given location R, relative to the burst point.

Y is the total device yield (user input)

FFR is the fraction of the total yield attributable solely to fission (user input)

$\phi_{jkl}(r,\rho r,hs)$ is the gamma ray fluence in energy group j per source photon in source group l, determined according to the parameters r, ρr and hs and the midpoint of time increment k, where r is the source-detector slant distance, ρr is the product of r and the average density (ρ) over its length and hs is the source height above the ground.

(FF_i) is the number of fissions per unit yield of fissile isotope i,

(FFY_i) is the fraction of the fission yield due to isotope i, and

$S_{il}(t)$ is the time-dependent source rate in l energy groups due to isotope i.

Values for quantities Y, FFR and FFY must be input by the user (see section 2). The time increment fluence (ϕ_{jkl}), per source group, is calculated using the same data base as that for prompt gamma radiation transport. The parameters r, ρr, and hs are calculated within ATR5, based on initial conditions of the burst, using models described in the ATR4 Users Guide (DNA 3995F) (Ref. 33). ATR5 integrates the fission product gamma ray dose rate over the period from zero to sixty seconds numerically, using nineteen time steps. The variation of the dose rate with time depends on weapon yield, burst height, target height and distance. Therefore, in order to employ so few time steps the code itself chooses the duration of each step. It does so on the basis of the cumulative uncollided fluence, which it calculates in fifty equal logarithmic time steps from one tenth to sixty seconds, plus points at 0.001 and 0.01 seconds. The code selects the times at which the uncollided fluence is closest to (but larger than) the cumulative value in one-fifteenth increments. The last time step is further divided into five smaller increments, in equal logarithmic intervals, due to the sharp dose rate gradient prevalent at late times.

The number of fissions per kiloton of fission yield (FFi) is stored in the code and need not be entered by the user. The values are:

Isotope	Fissions/kt
U235	1.467E + 23
U238	1.475E + 23
Pu239	1.419E + 23

5.1 FISSION PRODUCT GAMMA RAY SOURCE.

The fission product gamma ray source term $S_{il}(t)$ is a function of isotope (i), energy (l) and time. The most comprehensive measurements of such source spectra have been made by Fisher and Engle (Ref. 22), Dickens, et al. (Ref. 14, 15) and Akiyama and An (Ref. 2). The 1962 measurements included mean times after fast fission as early as 0.35 seconds for U235, U238 and Pu239. Dickens, et.al., measured data as early as approximately two seconds after thermal fission of U235 and Pu239. Akiyama and An measured fast fission - related data for several isotopes but at relatively late times, a few tens of seconds after fission.

The energy emission rates measured by Fisher and Engle are not in agreement with those of the other two groups for times after fission at which no substantial differences should remain between fast and thermal fission. This discrepancy is important because only the Fisher and Engle data provide fission product spectra applicable to all three fissile nuclides at times of greatest interest. Fortunately, the differences between the three sets of data have been reconciled as part of the U.S. - Japan Joint Assessment of Atomic Bomb Radiation Dosimetry in Hiroshima and Nagasaki (Ref. 58). The Fisher and Engle spectral data have been adjusted based on those of Dickens, et al., with a consistent application of that adjustment reproducing the Akiyama and An U238 energy emission rate at 40 seconds. The adjusted spectra, normalized to one gamma ray per fission per second, are given in Tables 10, 11 and 12 for U235, U238 and Pu239, respectively. The development and testing of these source data are described in detail in Appendix E of this report.

In the process of correcting the Fisher and Engle spectra, using the data of Dickens, et al., the energy emission rate was effectively renormalized to that applicable to thermal neutron fission. This problem is alluded to in Appendix E, which describes the correction process and the subsequent testing of the corrected spectra and energy emission rates. Subsequent to the completion of the work described in Appendix E, England and Schenter (Ref. 19) created a data base from a combination of U.S. (ENDF B V and VI) and Japanese (JNDC86) sources, consisting of fission product inventories for each fissile nuclide and the beta and gamma ray energy emission rates for each fission product. These data are available for thermal, fast and 14 MeV neutron fission and reproduce the measurements of Dickens, et al., and Akiyama and An within a few percent. Therefore, the energy emission rates for U235, U238 and Pu239 adopted for use in ATR5 are those taken from England and Schenter for fast fission and fit to the functional form:

$$\text{Energy Emission Rate} = \frac{A}{1+Bt} \quad \text{(MeV per fission per second)} \qquad (4)$$

where t is the time in seconds. The coefficients used in the emission rate model are:

Isotope		Coefficient A	Coefficient B
U235	($0<t<11.42$ sec)	0.606	0.833
	($11.42<t<60$ sec)	4.818	7.234
U238	($0<t<2.19$ sec)	1.191	1.039
	($2.19<t<8.25$ sec)	2.490	2.059
	($8.25<t<15$ sec)	0.878	-1.105
	($15<t<60$ sec)	-0.442	-0.589
Pu239	($0<t<60$ sec)	0.340	0.618

Table 10. Fission product gamma ray source spectra for U235 at mean times after fission of 0.35, 1.5, 4.75, 11.5 and 40 seconds.

Energy Group No.	Upper Energy (MeV)	Gamma rays/MeV-Gamma ray Time (sec): 0.35	1.50	4.75	11.50	40.00
1	0.045[a]	0.000E+00	0.000E+00	0.000E+00	0.000E+00	0.000E+00
2	0.100	0.000E+00	0.000E+00	0.000E+00	0.000E+00	0.000E+00
3	0.150	4.933E-01[b]	3.675E-01	4.307E-01	4.210E-01	3.769E-01
4	0.300	1.038E+00	8.693E-01	9.983E-01	1.010E+00	9.071E-01
5	0.450	6.942E-01	6.720E-01	7.311E-01	7.382E-01	7.324E-01
6	0.700	6.764E-01	7.565E-01	8.226E-01	7.801E-01	6.182E-01
7	1.000	5.391E-01	5.263E-01	4.511E-01	4.589E-01	4.965E-01
8	1.500	3.230E-01	3.388E-01	3.050E-01	3.252E-01	3.648E-01
9	2.000	1.605E-01	1.715E-01	1.728E-01	1.664E-01	1.868E-01
10	2.500	1.066E-01	1.100E-01	1.081E-01	1.065E-01	1.209E-01
11	3.000	6.688E-02	7.002E-02	6.091E-02	6.624E-02	8.265E-02
12	4.000	3.840E-02	4.177E-02	3.993E-02	3.671E-02	3.763E-02
13	5.000	1.396E-02	1.189E-02	1.035E-02	1.091E-02	1.230E-02
14	6.000	2.797E-03	3.618E-03	3.420E-03	3.571E-03	3.628E-03
15	7.000	9.842E-04	8.458E-04	7.598E-04	5.387E-04	4.233E-04
16	8.000	1.399E-04	1.400E-04	1.396E-04	1.399E-04	1.398E-04
17	10.000	0.000E+00	0.000E+00	0.000E+00	0.000E+00	0.000E+00
18	12.000	0.000E+00	0.000E+00	0.000E+00	0.000E+00	0.000E+00

[a]Lower energy bound 0.010 MeV
[b]Read as $4.933*10^{-1}$

Table 11 Fission product gamma ray source spectra for U238 at mean times after fission of 0.35, 1.5, 4.75, 11.5 and 40 seconds.

Energy Group No.	Upper Energy (MeV)	Gamma rays/MeV-Gamma ray Time (sec): 0.35	1.50	4.75	11.50	40.00
1	0.045[a]	0.000E+00	0.000E+00	0.000E+00	0.000E+00	0.000E+00
2	0.100	0.000E+00	0.000E+00	0.000E+00	0.000E+00	0.000E+00
3	0.150	5.568E-01[b]	3.742E-01	5.271E-01	4.505E-01	3.881E-01
4	0.300	1.108E+00	9.559E-01	1.125E+00	1.049E+00	1.009E+00
5	0.450	7.432E-01	7.151E-01	7.608E-01	8.385E-01	7.773E-01
6	0.700	6.223E-01	6.674E-01	7.825E-01	7.532E-01	6.814E-01
7	1.000	4.881E-01	4.934E-01	4.347E-01	4.335E-01	4.891E-01
8	1.500	3.039E-01	3.313E-01	2.826E-01	2.956E-01	3.311E-01
9	2.000	1.564E-01	1.852E-01	1.685E-01	1.663E-01	1.605E-01
10	2.500	1.253E-01	1.151E-01	1.076E-01	1.121E-01	1.211E-01
11	3.000	8.130E-02	8.057E-02	6.249E-02	6.765E-02	8.479E-02
12	4.000	3.971E-02	4.338E-02	4.011E-02	3.923E-02	3.392E-02
13	5.000	1.387E-02	1.180E-02	9.619E-03	1.124E-02	9.236E-03
14	6.000	3.882E-03	3.409E-03	3.587E-03	3.951E-03	3.109E-03
15	7.000	1.409E-03	8.844E-04	7.119E-04	6.154E-04	3.538E-04
16	8.000	1.398E-04	1.399E-04	1.402E-04	1.398E-04	1.403E-04
17	10.000	0.000E+00	0.000E+00	0.000E+00	0.000E+00	0.000E+00
18	12.000	0.000E+00	0.000E+00	0.000E+00	0.000E+00	0.000E+00

[a]Lower energy bound 0.010 MeV
[b]Read as $5.568 \cdot 10^{-1}$

Table 12. Fission product gamma ray source spectra for U239 at mean times after fission of 0.35, 1.5, 4.75, 11.5 and 40 seconds.

Energy Group No.	Upper Energy (MeV)	Gamma rays/MeV-Gamma ray Time (sec): 0.35	1.50	4.75	11.50	40.00
1	0.045[a]	0.000E+00	0.000E+00	0.000E+00	0.000E+00	0.000E+00
2	0.100	0.000E+00	0.000E+00	0.000E+00	0.000E+00	0.000E+00
3	0.150	5.425E-01[b]	3.966E-01	4.769E-01	4.377E-01	3.764E-01
4	0.300	1.094E+00	9.689E-01	1.107E+00	1.145E+00	9.238E-01
5	0.450	7.172E-01	7.560E-01	7.595E-01	8.111E-01	7.964E-01
6	0.700	7.448E-01	8.944E-01	9.002E-01	8.086E-01	6.484E-01
7	1.000	5.210E-01	4.882E-01	4.412E-01	4.426E-01	4.859E-01
8	1.500	2.982E-01	3.194E-01	2.792E-01	2.967E-01	3.430E-01
9	2.000	1.490E-01	1.496E-01	1.698E-01	1.679E-01	1.839E-01
10	2.500	1.014E-01	9.263E-02	9.549E-02	9.966E-02	1.300E-01
11	3.000	7.294E-02	5.696E-02	5.283E-02	5.935E-02	8.725E-02
12	4.000	3.249E-02	3.024E-02	3.116E-02	2.869E-02	3.345E-02
13	5.000	1.250E-02	9.317E-03	6.433E-03	6.850E-03	7.245E-03
14	6.000	2.182E-03	1.805E-03	1.888E-03	1.850E-03	2.019E-03
15	7.000	5.915E-04	5.696E-04	5.417E-04	3.981E-04	3.396E-04
16	8.000	1.398E-04	1.400E-04	1.396E-04	1.397E-04	1.403E-04
17	10.000	0.000E+00	0.000E+00	0.000E+00	0.000E+00	0.000E+00
18	12.000	0.000E+00	0.000E+00	0.000E+00	0.000E+00	0.000E+00

[a]Lower energy bound 0.010 MeV.
[b]Read as $5.425*10^{-1}$

These coefficients reproduce the England and Schenter gamma ray energy emission rate data within two percent or less over the time periods indicated.

The reported emission rate spectra have been assigned to time regimes, the limits of which are the time increment boundaries closest to the mean of the logarithm of adjacent reported times, as follows:

Time (sec)	Time (sec) of Applicable Spectrum
0 - 0.075	0.35
0.75 - 3.25	1.50
3.25 - 7.75	4.75
7.75 - 22.5	11.50
22.5 - 60.0	40.00

5.2 EMPIRICAL CORRECTIONS.

The ATR5 model was used to calculate delayed radiation as measured at several atmospheric weapon tests. These included yields from several kilotons to several megatons and scaled burst heights (HOB(m)/yield to the one-third power) from zero to over one hundred meters. The measurements included time-dependent data from active dosimeters and total dose data from passive dosimeters, such as film badges. The film badge data were used only when the yield was sufficiently large that delayed radiation component was dominant or when the calculated prompt and secondary components were confirmed by time dependent measurements, and could be subtracted from the total to obtain the delayed component.

The calculations and measurements for each shot were compared over all distances and the mean of all comparisons for each shot was compared with those for all the other shots. Upon comparing the calculations and measurements as a function of scaled height of burst, as shown in Figure 19, it was evident that the ATR5 model deviated from the measured data as a strong function of the scaled burst height. Further comparisons against the results of a model which contained the same source and transport components as ATR5 but included a more sophisticated, two-dimensional hydrodynamic model indicated that the primary shortcoming of the ATR5 model lay in its inability to account for the ground-reflected shock wave from the burst. The ground-reflected shock wave fills in the low density region which includes the rising fireball, providing more mass for the fission product gamma rays to penetrate and, consequently, a lower dose rate, as described in Appendix E of this report. This effect is particularly well defined for a burst at 110m scaled height, as shown in Figure 20. The two-dimensional model begins to fill in the line of sight from source to detector at approximately 1 second, similar to the effect shown in the measured data, though the two-dimensional model over-estimates the effect. The data from ATR5, based on a one-dimensional hydrodynamic model, show no such effect and over-predict the dose rate at later times.

Unfortunately, reliable delayed gamma ray dose rate data are not available for scaled burst heights greater than 110.4 meters. However, results of the two-dimensional delayed radiation model combined with detailed calculations of the prompt and secondary radiation components compare well with time-integral measurements of total initial gamma ray dose recorded for bursts having scaled burst height as large as 182.3 meters (Nagasaki) and 235.2 meters (Hiroshima). Thus, the two-dimensional model was used as the standard by which to assess the deviation of the one-dimensional model at scaled burst height greater than 110.4 meters. As can be seen from Figure 19 the one- and two-dimensional models come into agreement at a scaled burst height of 235.2 meters. It is not surprising that this should occur, since at such large heights the reflected shock wave has little or no effect on the rising fireball.

Comparisons of experimental and two-dimensional model dose values with those produced using the one-dimensional model ATR5 were used to produce an empirical correction factor based on scaled burst height. Linear interpolation is used to obtain correction factor values between break point values, as shown below.

Scaled Height of Burst (m)	Correction Factor
0	1.000
17.1	1.000
56.8	0.758
70.1	0.695
110.4	0.560
182.3	0.943
≥235.2	1.000

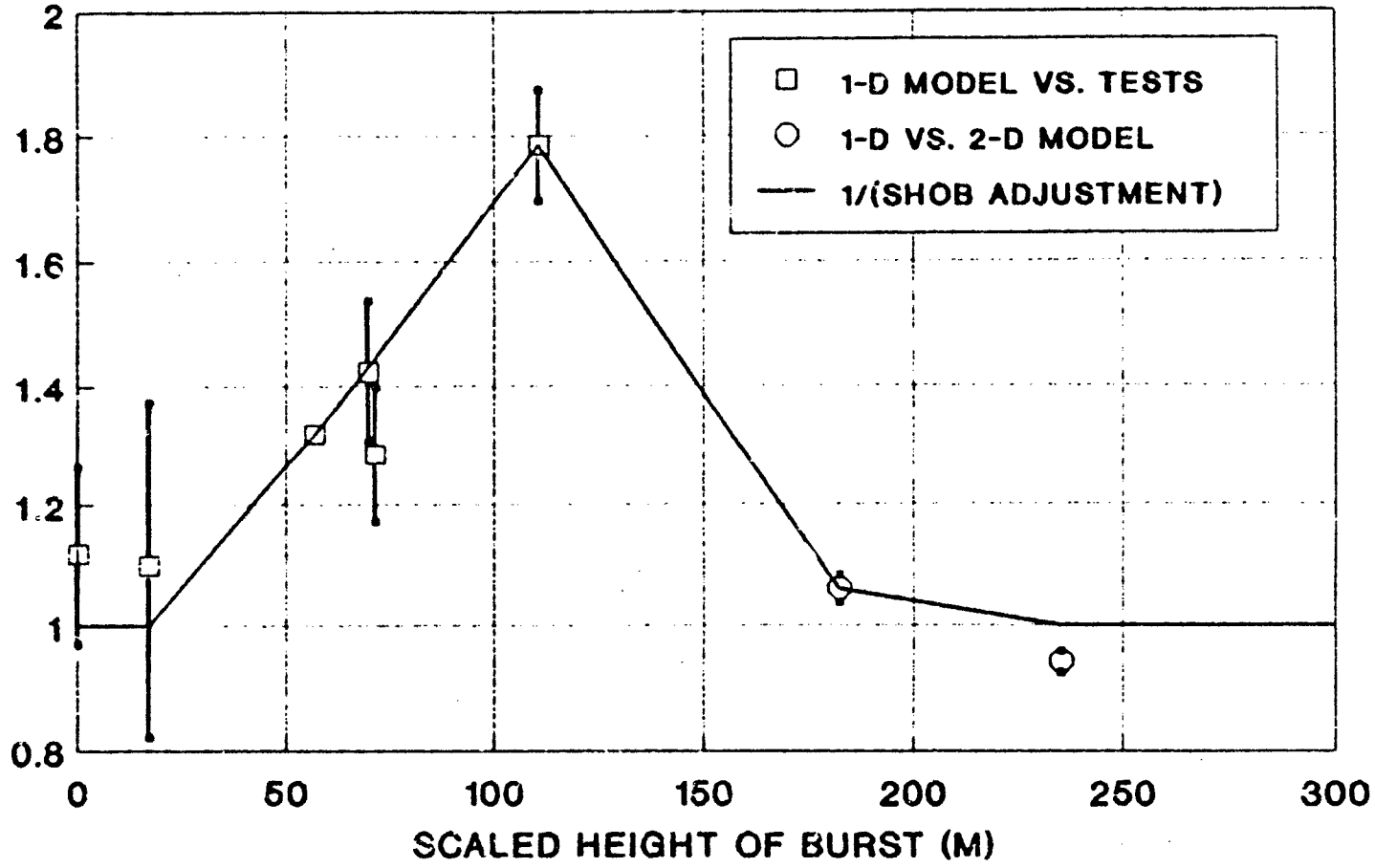

Figure 19. A comparison between time-integral exposure data calculated with a one-demensional model and those measured and calculated using a two-dimentional model, as related to scaled height of burst.

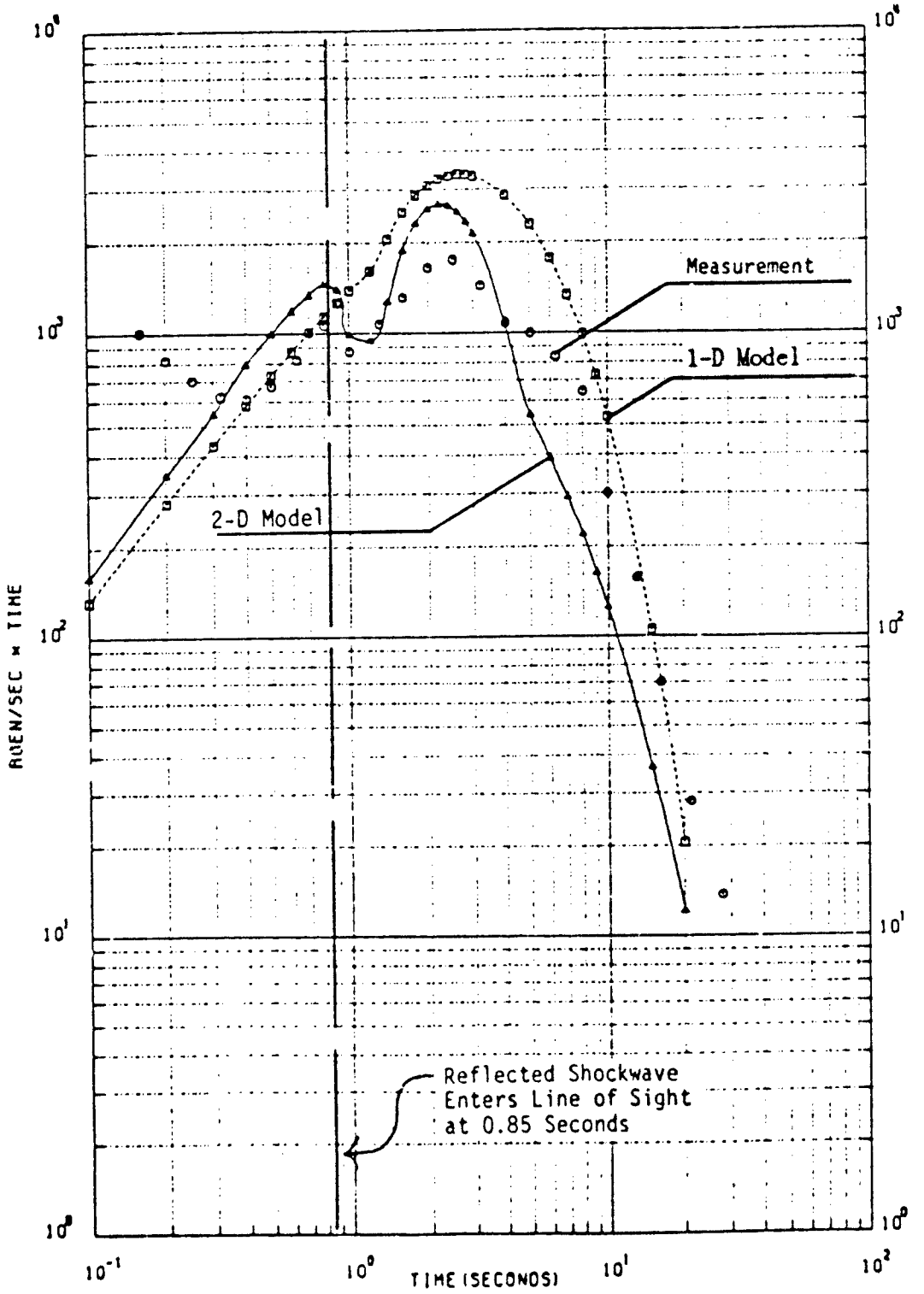

Figure 20. Measured and calculated delayed radiation exposure rates from a 110 m scaled burst height event taken at 914 m horizontal distance.

The correction factors for zero and 17.1 meter scaled burst height were set to unity because the comparisons of ATR5 with available data produced very large uncertainty bands at those burst heights, which included the unity value. Thus, the data did not conclusively indicate that the problem of reflected shock for very low burst heights produced any effect beyond that already accounted for in the model. (For very low burst heights the one-dimensional model includes a provision for increasing the yield for the purpose of calculating the hydrodynamic perturbation of the surrounding air).

Even with the scaled burst height-based empirical correction, problems remain in ATR, probably having to do with other limitations of the hydrodynamic model, such as its inability to describe the movement of the gamma ray source within the fireball or the formation of the torus cloud at late times, as described in Appendix E. These problems are evidenced by range-dependent discrepancies between calculated and measured dose values. These are particularly evident for surface bursts and very low air bursts (SHOB < 50 meters), with the corrected (SHOB effect) model underestimating the measured values by twenty to thirty percent within a few fireball radii and over estimating them by a similar amount at distances of many fireball radii. Unfortunately, there is not a strong enough correlation with fireball radius or any other readily observable parameter to create a scalar correction factor to minimize the error in a systematic and reliable way. It is recommended that future research be directed toward developing a reliable high order model of the phenomena affecting delayed radiation transmission and that such a model be used as the basis for deriving further improvements for ATR, since the available measured data are very limited.

SECTION 6

SAMPLE CALCULATIONS

This section contains samples of calculations which exemplify the new capabilities added to ATR5. The input and output for each calculation are described in detail, particularly as regards ATR5 modifications. Additional explanations of ATR input and output can be obtained from the documentation for ATR4 (DNA 3995F).

6.1 SAMPLE CALCULATION 1, USE OF THE *MET COMMAND.

This calculation illustrates the use of two variations of the *MET command to obtain the same neutron values. In the first entry the *MET command is used to specify the Temperature (20 c), Pressure (1000 mb) and relative humidity (90%). After an *EXC command, which causes the calculation to be executed, the *MET command is re-entered, providing data which supersedes that contained in the previous calculations but leaving all other commands unchanged. The revised *MET entry provides a moist air density (1.179 E-3 g/cc) and a percent moisture by weight (1.3043), which are identical to those obtained using the data from the first *MET entry. The results of the two entries are virtually identical, as should be expected. Note that ATR5 calculates a ground level from the data provided in the *MET command. That ground level will supersede any which is entered by the *GROUND command unless no *MET input is provided.

SAMPLE PROBLEM 1 - INPUT

```
*ATR VERSION 5 - - - SAIC (1   R 1989 REVISION)
*TITLE SAMPLE PROBLEM 1 - AT  ERSION 5
*N-SOURCE(1)
*N-YIELD 10
*N-NORM 2.0E+23
*HS,M,100
*HT,M,*
*MET(1) 20 1000 90
*RH,M, 500(500)2000
*DOSE/N/
*EXC
*MET(3) 1.179E-3 1.3043
*EXC
*STOP
*FIN
```

SAMPLE PROBLEM 1 - OUTPUT

```
ATR PROBLEM NUMBER     1          SAMPLE PROBLEM 1 - ATR VERSION 5

* * * * * * * * * * * * * * * * * * * * * * * * * * * * * * * * * * * * *

NEUTRON  SOURCE     INTERNAL  FISSION
NORMALIZATION=2.000E+23 NEUTRON /KT, YIELD=1.000E+01 KT
 TOTAL OUTPUT=2.000E+24 NEUTRON

                    SOURCE SPECTRUM
 ENERGY(MEV )       N          N/MEV    ENERGY(MEV )       N          N/MEV
1.07E-05-2.90E-05 0.00E+00 0.00E+00 1.83E+00-2.31E+00 2.03E+23 4.24E+23
2.90E-05-1.01E-04 0.00E+00 0.00E+00 2.31E+00-3.01E+00 7.74E+22 1.11E+23
1.01E-04-1.23E-03 0.00E+00 0.00E+00 3.01E+00-4.07E+00 1.10E+23 1.03E+23
1.23E-03-2.19E-02 3.30E+22 1.60E+24 4.07E+00-4.97E+00 2.35E+22 2.62E+22
2.19E-02-1.11E-01 4.12E+23 4.63E+24 4.97E+00-6.38E+00 3.66E+22 2.60E+22
1.11E-01-1.58E-01 3.60E+22 7.66E+23 6.38E+00-8.19E+00 2.55E+22 1.41E+22
1.58E-01-5.50E-01 3.03E+23 7.72E+23 8.19E+00-1.00E+01 1.47E+22 8.11E+21
5.50E-01-1.11E+00 4.32E+23 7.71E+23 1.00E+01-1.22E+01 0.00E+00 0.00E+00
1.11E+00-1.83E+00 2.94E+23 4.08E+23 1.22E+01-1.49E+01 0.00E+00 0.00E+00

* * * * * * * * * * * * * * * * * * * * * * * * * * * * * * * * * * * * *

ATR PROBLEM NUMBER     1          SAMPLE PROBLEM 1 - ATR VERSION 5

* * * * * * * * * * * * * * * * * * * * * * * * * * * * * * * * * * * * *

 GROUND LEVEL        .500KM,  59.819GM/CM**2,  1.641KFT,   .311MILES
 HORIZ. RANGE RH=    .500KM,  57.782GM/CM**2,  1.640KFT,   .311MILES
*SLANT RANGE  RS=    .510KM,  60.096GM/CM**2,  1.672KFT,   .317MILES
 TARGET ALT.  HT=    .001KM,    .117GM/CM**2,   .003KFT,   .001MILES
 SOURCE ALT.  HS=    .100KM,  11.613GM/CM**2,   .328KFT,   .062MILES
*SLANT ANGLE  AN= -11.200DEGREES (COS=  .98096)
        *CALCULATED FROM OTHER COORDINATES

* * * * * * * * * * * * * * * * * * * * * * * * * * * * * * * * * * * * *
```

NEUTRON DOSE VS. HORIZ. RANGE (RADS)

DOSE 1= ANS STANDARD-REM
DOSE 2= SOFT TISSUE
DOSE 3= MID-PHANTOM
DOSE 4= CONCRETE
DOSE 5= AIR
DOSE 6= NON-IONIZING SI.
DOSE 7= IONIZING SILICON
DOSE 8= MID-HEAD
DOSE 9= 1MEV EQ. FLUENCE
DOSE10= USER SUPPLIED

HORIZ. RANGE	DOSE 1	DOSE 2	DOSE 3	DOSE 4	DOSE 5	DOSE 6
5.000E+02 M	4.58E+05	3.44E+04	1.18E+04	3.53E+03	5.41E+03	4.35E+02
1.000E+03 M	7.42E+03	5.61E+02	2.08E+02	5.82E+01	9.83E+01	7.06E+00
1.500E+03 M	2.12E+02	1.65E+01	6.03E+00	1.75E+00	2.91E+00	2.10E-01
2.000E+03 M	9.21E+00	7.34E-01	2.59E-01	7.94E-02	1.27E-01	9.43E-03

DOSE 7	DOSE 8	DOSE 9	DOSE10
4.04E+02	1.59E+04	1.32E+13	0.00E+00
7.05E+00	2.79E+02	2.14E+11	0.00E+00
2.28E-01	8.17E+00	6.34E+09	0.00E+00
1.07E-02	3.55E-01	2.85E+08	0.00E+00

* *

**EXECUTION COMPLETED

6.2 SAMPLE CALCULATION 2, USER-SUPPLIED *FLUXWT.

A gamma-ray source is used to illustrate *FLUXWT input and output in ATR5. The *FLUXWT command allows the user to provide his own fluence-to-dose factors. These are entered after the units are given (up to 16 characters not including the bracketing commas) in energy order low to high. In ATR5, the resulting dose values are printed as part of the *DOSE command in position 8 for gamma rays and position 10 for neutrons.

SAMPLE PROBLEM 2 - INPUT

```
*ATR VERSION 5 - - - SAIC (1 APR 1989 REVISION)

*TITLE SAMPLE PROBLEM 2 - ATR VERSION 5
*G-SOURCE(1)
*G-YIELD 10
*G-NORM 7.5E+22
*GROUND,M,500
*HS,M,50
*HT,M,1
*RH,M, 500(500)2000
*DOSE/G/
*FLUXWT/G/,ROENTGENS,7.185E-11 3.616E-11 5.464E-11 1.079E-10
1.993E-10 3.066E-10 4.433E-10 6.054E-10 7.820E-10 9.069E-10
1.110E-09 1.255E-09 1.487E-09 1.707E-09 1.890E-09 2.192E-09
2.448E-09 2.823E-09
*EXC
*STOP
*FIN
```

SAMPLE PROBLEM 2 - OUTPUT

ATR PROBLEM NUMBER 1 SAMPLE PROBLEM 2 - ATR VERSION 5

* *

GAMMA SOURCE INTERNAL FISSION
NORMALIZATION=7.500E+22 GAMMA /KT, YIELD=1.000E+01 KT
TOTAL OUTPUT=7.500E+23 GAMMA

SOURCE SPECTRUM

ENERGY(MEV)	G	G/MEV	ENERGY(MEV)	G	G/MEV
1.00E-02-4.50E-02	2.44E+22	6.98E+23	2.00E+00-2.50E+00	2.81E+22	5.61E+22
4.50E-02-1.00E-01	1.23E+22	2.24E+23	2.50E+00-3.00E+00	1.67E+22	3.34E+22
1.00E-01-1.50E-01	3.66E+22	7.32E+23	3.00E+00-4.00E+00	1.58E+22	1.58E+22
1.50E-01-3.00E-01	7.74E+22	5.16E+23	4.00E+00-5.00E+00	5.59E+21	5.59E+21
3.00E-01-4.50E-01	1.02E+23	6.79E+23	5.00E+00-6.00E+00	1.99E+21	1.99E+21
4.50E-01-7.00E-01	1.52E+23	6.08E+23	6.00E+00-7.00E+00	6.94E+20	6.94E+20
7.00E-01-1.00E+00	1.22E+23	4.08E+23	7.00E+00-8.00E+00	2.83E+20	2.83E+20
1.00E+00-1.50E+00	1.06E+23	2.11E+23	8.00E+00-1.00E+01	1.18E+20	5.90E+19
1.50E+00-2.00E+00	4.82E+22	9.64E+22	1.00E+01-1.20E+01	0.00E+00	0.00E+00

* *

ATR PROBLEM NUMBER 1 SAMPLE PROBLEM 2 - ATR VERSION 5

* *

GROUND LEVEL	.500KM,	59.787GM/CM**2,	1.640KFT,	.311MILES
HORIZ. RANGE RH=	.500KM,	58.065GM/CM**2,	1.640KFT,	.311MILES
*SLANT RANGE RS=	.502KM,	58.482GM/CM**2,	1.648KFT,	.312MILES
TARGET ALT. HT=	.001KM,	.117GM/CM**2,	.003KFT,	.001MILES
SOURCE ALT. HS=	.050KM,	5.821GM/CM**2,	.164KFT,	.031MILES

*SLANT ANGLE AN= -5.597DEGREES (COS= .99523)
*CALCULATED FROM OTHER COORDINATES

* *

GAMMA DOSE VS. HORIZ. RANGE (RADS)

DOSE 1= ANS STANDARD-REM
DOSE 2= SOFT TISSUE
DOSE 3= MID-PHANTOM
DOSE 4= CONCRETE
DOSE 5= AIR
DOSE 6= IONIZING SILICON
DOSE 7= MID-HEAD
DOSE 8= USER SUPPLIED

HORIZ. RANGE	DOSE 1	DOSE 2	DOSE 3	DOSE 4	DOSE 5	DOSE 6	DOSE 7	DOSE 8
5.000E+02 M	1.72E+03	1.30E+03	7.95E+02	1.71E+03	1.18E+03	1.83E+03	9.25E+02	1.36E+03
1.000E+03 M	4.55E+01	3.64E+01	2.32E+01	4.34E+01	3.31E+01	4.57E+01	2.64E+01	3.80E+01
1.500E+03 M	2.90E+00	2.41E+00	1.57E+00	2.69E+00	2.18E+00	2.81E+00	1.77E+00	2.51E+00
2.000E+03 M	2.83E-01	2.40E-01	1.59E-01	2.61E-01	2.18E-01	2.71E-01	1.78E-01	2.50E-01

* *

**EXECUTION COMPLETED

6.3 SAMPLE CALCULATION 3, USE OF THE *FP COMMANDS.

ATR5 allows the user to specify the fractions of fission yield due to the three primary fissile materials U-235, U-238 and Pu-239. These fractions are input via the *FP-I command and are used only in the calculation of the fission product (delayed) component. Failure to provide a *FP-I command when calculating delayed radiation results in U-235 fission by default. In the case of the sample problem, a hypothetical weapon having a total yield of 100 kt, of which 95% is due to fission, is specified using the *FP-Y and *FP-F commands, respectively. The *FP-I command stipulates that 95% of the yield is due to U-235, 5% is due to U-238 and no yield is derived from Pu-239.

SAMPLE PROBLEM 3 - INPUT

```
*ATR VERSION 5 - - - SAIC (1 APR 1989 REVISION)

*TITLE SAMPLE PROBLEM 3 - ATR VERSION 5
*FP-Y 100
*FP-F 0.95
*FP-I 0.95 0.05 0.0
*HS,M,250
*HT,M,1
*GROUND,M,500
*RH,M,500
*RH,M, 1000(500)2500
*DOSE,FP/
*EXC
*STOP
*FIN
```

SAMPLE PROBLEM 3 - OUTPUT

```
ATR PROBLEM NUMBER     1          SAMPLE PROBLEM 3 - ATR VERSION 5

* * * * * * * * * * * * * * * * * * * * * * * * * * * * * * * * * * * *

FISSION PRODUCT YIELD=1.00E+02KT,  FISSION FRACTION= 9.50E-01

* * * * * * * * * * * * * * * * * * * * * * * * * * * * * * * * * * * *

ATR PROBLEM NUMBER     1          SAMPLE PROBLEM 3 - ATR VERSION 5

* * * * * * * * * * * * * * * * * * * * * * * * * * * * * * * * * * * *
 GROUND LEVEL       .500KM,  59.787GM/CM**2,  1.640KFT,   .311MILES
 HORIZ. RANGE RH=  1.000KM, 113.897GM/CM**2,  3.281KFT,   .621MILES
*SLANT RANGE  RS=  1.031KM, 118.805GM/CM**2,  3.381KFT,   .640MILES
 TARGET ALT.  HT=   .001KM,    .117GM/CM**2,   .003KFT,   .001MILES
 SOURCE ALT.  HS=   .250KM,  28.823GM/CM**2,   .820KFT,   .155MILES
*SLANT ANGLE  AN= -13.982DEGREES (COS=  .97037)
        *CALCULATED FROM OTHER COORDINATES

* * * * * * * * * * * * * * * * * * * * * * * * * * * * * * * * * * * *

   FISSION PRODUCT DOSE  VS.  HORIZ. RANGE     (RADS        )
                  DOSE 1=  ANS STANDARD-REM
                  DOSE 2=  SOFT TISSUE
                  DOSE 3=  MID-PHANTOM
                  DOSE 4=  CONCRETE
                  DOSE 5=  AIR
                  DOSE 6=  IONIZING SILICON
                  DOSE 7=  MID-HEAD
                  DOSE 8=  USER SUPPLIED
```

HORIZ. RANGE		DOSE 1	DOSE 2	DOSE 3	DOSE 4	DOSE 5	DOSE 6
1.000E+03 M	*	1.04E+04	7.99E+03	4.95E+03	1.03E+04	7.27E+03	1.09E+04
1.500E+03 M		8.92E+02	7.12E+02	4.52E+02	8.52E+02	6.46E+02	8.96E+02
2.000E+03 M		9.15E+01	7.54E+01	4.88E+01	8.51E+01	6.83E+01	8.88E+01
2.500E+03 M		1.11E+01	9.31E+00	6.12E+00	1.02E+01	8.43E+00	1.06E+01

DOSE 7	DOSE 8
5.72E+03	0.00E+00
5.15E+02	0.00E+00
5.51E+01	0.00E+00
6.85E+00	0.00E+00

* *

**EXECUTION COMPLETED

6.4 SAMPLE CALCULATION 4, CALCULATING TOTAL DOSE (*DOSE/T/).

ATR5 has completely integrated the fission product (delayed) radiation module into the code for the purpose of calculating dose, as specified using the *DOSE command. The commands:

*DOSE/N/

*DCSE/G/

*DOSE/NG/

*DOSE/FP/

provide only the values computed for each component, respectively. The command *DOSE/GG/ provides the total gamma-ray dose for all sources specified including fission production radiation, regardless of whether the individual dose components are requested. The *DOSE/GG/ command should not be used when only on source of gamma rays (including neutrons) is stipulated. Likewise, the *DOSE/T/ command provides a total of all components resulting from the sources stipulated, including fission product radiation, regardless of whether the dose components are requested individually.

SAMPLE PROBLEM 4 - INPUT

```
*ATR VERSION 5 - - - SAIC (1 APR 1989 REVISION)


*TITLE SAMPLE PROBLEM 4 - ATR VERSION 5
*N-SOURCE(2)
*N-YIELD 200
*N-NORM 2.0E+23
*G-SOURCE(1)
*G-YIELD 200
*G-NORM 7.5E+22
*FP-Y 200
*FP-F 0.9
*FP-I 0.0 0.2 0.8
*GROUND,M,500
*HS,M,300
*HT,M,1
*RH,M, 1500(500)3000
*DOSE/N/
*DOSE/G/
*DOSE/NG/
*DOSE/FP/
*DOSE/GG/
*DOSE/T/
*EXC
*STOP
*FIN
```

SAMPLE PROBLEM 4 - OUTPUT

ATR PROBLEM NUMBER 1 SAMPLE PROBLEM 4 - ATR VERSION 5

* *

NEUTRON SOURCE INTERNAL THERMONUCLEAR
NORMALIZATION=2.000E+23 NEUTRON /KT, YIELD=2.000E+02 KT
TOTAL OUTPUT=4.000E+25 NEUTRON

SOURCE SPECTRUM

ENERGY(MEV)	N	N/MEV	ENERGY(MEV)	N	N/MEV
1.07E-05-2.90E-05	0.00E+00	0.00E+00	1.83E+00-2.31E+00	1.04E+24	2.16E+24
2.90E-05-1.01E-04	8.00E+22	1.11E+27	2.31E+00-3.01E+00	1.04E+24	1.49E+24
1.01E-04-1.23E-03	2.29E+24	2.03E+27	3.01E+00-4.07E+00	1.04E+24	9.81E+23
1.23E-03-2.19E-02	1.38E+25	6.66E+26	4.07E+00-4.97E+00	6.80E+23	7.56E+23
2.19E-02-1.11E-01	4.39E+24	4.92E+25	4.97E+00-6.38E+00	7.20E+23	5.11E+23
1.11E-01-1.58E-01	4.57E+23	9.72E+24	6.38E+00-8.19E+00	5.88E+23	3.25E+23
1.58E-01-5.50E-01	3.62E+24	9.24E+24	8.19E+00-1.00E+01	5.64E+23	3.12E+23
5.50E-01-1.11E+00	3.40E+24	6.07E+24	1.00E+01-1.22E+01	1.02E+24	4.65E+23
1.11E+00-1.83E+00	2.48E+24	3.44E+24	1.22E+01-1.49E+01	2.82E+24	1.05E+24

```
* * * * * * * * * * * * * * * * * * * * * * * * * * * * * * * * * * * * *

ATR PROBLEM NUMBER     1          SAMPLE PROBLEM 4 - ATR VERSION 5

* * * * * * * * * * * * * * * * * * * * * * * * * * * * * * * * * * * * *

GAMMA    SOURCE     INTERNAL  FISSION
NORMALIZATION=7.500E+22 GAMMA   /KT, YIELD=2.000E+02 KT
 TOTAL OUTPUT=1.500E+25 GAMMA

                    SOURCE SPECTRUM
 ENERGY(MEV )       G          G/MEV    ENERGY(MEV )       G          G/MEV
1.00E-02-4.50E-02 4.89E+23 1.40E+25 2.00E+00-2.50E+00 5.61E+23 1.12E+24
4.50E-02-1.00E-01 2.47E+23 4.48E+24 2.50E+00-3.00E+00 3.34E+23 6.68E+23
1.00E-01-1.50E-01 7.32E+23 1.46E+25 3.00E+00-4.00E+00 3.16E+23 3.16E+23
1.50E-01-3.00E-01 1.55E+24 1.03E+25 4.00E+00-5.00E+00 1.12E+23 1.12E+23
3.00E-01-4.50E-01 2.04E+24 1.36E+25 5.00E+00-6.00E+00 3.97E+22 3.97E+22
4.50E-01-7.00E-01 3.04E+24 1.22E+25 6.00E+00-7.00E+00 1.39E+22 1.39E+22
7.00E-01-1.00E+00 2.45E+24 8.17E+24 7.00E+00-8.00E+00 5.66E+21 5.66E+21
1.00E+00-1.50E+00 2.11E+24 4.22E+24 8.00E+00-1.00E+01 2.36E+21 1.18E+21
1.50E+00-2.00E+00 9.64E+23 1.93E+24 1.00E+01-1.20E+01 0.00E+00 0.00E+00

* * * * * * * * * * * * * * * * * * * * * * * * * * * * * * * * * * * * *

ATR PROBLEM NUMBER     1          SAMPLE PROBLEM 4 - ATR VERSION 5

* * * * * * * * * * * * * * * * * * * * * * * * * * * * * * * * * * * * *

 FISSION PRODUCT YIELD=2.00E+02KT,  FISSION FRACTION= 9.00E-01
```

```
* * * * * * * * * * * * * * * * * * * * * * * * * * * * * * * * * * * * * * *

ATR PROBLEM NUMBER     1          SAMPLE PROBLEM 4 - ATR VERSION 5

* * * * * * * * * * * * * * * * * * * * * * * * * * * * * * * * * * * * * * *

 GROUND LEVEL       .500KM,  59.787GM/CM**2,  1.640KFT,   .311MILES
 HORIZ. RANGE RH=  1.500KM, 170.018GM/CM**2,  4.921KFT,   .932MILES
*SLANT RANGE  RS=  1.530KM, 175.904GM/CM**2,  5.018KFT,   .950MILES
 TARGET ALT.  HT=   .001KM,    .117GM/CM**2,   .003KFT,   .001MILES
 SOURCE ALT.  HS=   .300KM,  34.504GM/CM**2,   .984KFT,   .186MILES
*SLANT ANGLE  AN= -11.273DEGREES (COS=  .98071)
        *CALCULATED FROM OTHER COORDINATES

* * * * * * * * * * * * * * * * * * * * * * * * * * * * * * * * * * * * * * *

   NEUTRON          DOSE  VS.  HORIZ. RANGE     (RADS        )
                    DOSE 1=  ANS STANDARD-REM
                    DOSE 2=  SOFT TISSUE
                    DOSE 3=  MID-PHANTOM
                    DOSE 4=  CONCRETE
                    DOSE 5=  AIR
                    DOSE 6=  NON-IONIZING SI.
                    DOSE 7=  IONIZING SILICON
                    DOSE 8=  MID-HEAD
                    DOSE 9=  1MEV EQ. FLUENCE
                    DOSE10=  USER SUPPLIED

HORIZ. RANGE      DOSE 1   DOSE 2   DOSE 3   DOSE 4   DOSE 5   DOSE 6
 1.500E+03 M    1.82E+04 1.52E+03 5.50E+02 1.84E+02 2.65E+02 1.96E+01
 2.000E+03 M    1.18E+03 9.89E+01 3.50E+01 1.17E+01 1.70E+01 1.28E+00
 2.500E+03 M    8.76E+01 7.34E+00 2.56E+00 8.58E-01 1.25E+00 9.51E-02
 3.000E+03 M    6.93E+00 5.80E-01 2.01E-01 6.70E-02 9.88E-02 7.53E-03
```

DOSE 7	DOSE 8	DOSE 9	DOSE10
3.70E+01	7.55E+02	5.92E+11	0.00E+00
2.22E+00	4.83E+01	3.86E+10	0.00E+00
1.53E-01	3.55E+00	2.88E+09	0.00E+00
1.13E-02	2.79E-01	2.28E+08	0.00E+00

* *

GAMMA DOSE VS. HORIZ. RANGE (RADS)

DOSE 1= ANS STANDARD-REM
DOSE 2= SOFT TISSUE
DOSE 3= MID-PHANTOM
DOSE 4= CONCRETE
DOSE 5= AIR
DOSE 6= IONIZING SILICON
DOSE 7= MID-HEAD
DOSE 8= USER SUPPLIED

HORIZ. RANGE	DOSE 1	DOSE 2	DOSE 3	DOSE 4	DOSE 5	DOSE 6
1.500E+03 M	7.05E+01	5.84E+01	3.80E+01	6.56E+01	5.29E+01	6.84E+01
2.000E+03 M	7.21E+00	6.11E+00	4.04E+00	6.65E+00	5.53E+00	6.91E+00
2.500E+03 M	9.42E-01	8.08E-01	5.41E-01	8.66E-01	7.31E-01	8.98E-01
3.000E+03 M	1.42E-01	1.23E-01	8.32E-02	1.31E-01	1.11E-01	1.36E-01

DOSE 7	DOSE 8
4.29E+01	0.00E+00
4.52E+00	0.00E+00
6.01E-01	0.00E+00
9.21E-02	0.00E+00

* *

NEUTRON GAMMA DOSE VS. HORIZ. RANGE (RADS)

DOSE 1= ANS STANDARD-REM
DOSE 2= SOFT TISSUE
DOSE 3= MID-PHANTOM
DOSE 4= CONCRETE
DOSE 5= AIR
DOSE 6= IONIZING SILICON
DOSE 7= MID-HEAD
DOSE 8= USER SUPPLIED

HORIZ. RANGE	DOSE 1	DOSE 2	DOSE 3	DOSE 4	DOSE 5	DOSE 6	DOSE 7	DOSE 8
1.500E+03 M	1.42E+03	1.26E+03	8.72E+02	1.32E+03	1.14E+03	1.38E+03	9.67E+02	0.00E+00
2.000E+03 M	2.01E+02	1.78E+02	1.24E+02	1.86E+02	1.61E+02	1.94E+02	1.37E+02	0.00E+00
2.500E+03 M	3.35E+01	2.99E+01	2.07E+01	3.11E+01	2.70E+01	3.24E+01	2.29E+01	0.00E+00
3.000E+03 M	6.24E+00	5.58E+00	3.89E+00	5.81E+00	5.04E+00	6.05E+00	4.27E+00	0.00E+00

* *

COUPLED GAMMA DOSE VS. HORIZ. RANGE (RADS)

DOSE 1= ANS STANDARD-REM
DOSE 2= SOFT TISSUE
DOSE 3= MID-PHANTOM
DOSE 4= CONCRETE
DOSE 5= AIR
DOSE 6= IONIZING SILICON
DOSE 7= MID-HEAD
DOSE 8= USER SUPPLIED

HORIZ. RANGE	DOSE 1	DOSE 2	DOSE 3	DOSE 4	DOSE 5	DOSE 6
1.500E+03 M	3.55E+03	2.93E+03	1.92E+03	3.38E+03	2.66E+03	3.55E+03
2.000E+03 M	4.20E+02	3.57E+02	2.38E+02	3.92E+02	3.23E+02	4.09E+02
2.500E+03 M	5.99E+01	5.18E+01	3.51E+01	5.55E+01	4.69E+01	5.78E+01
3.000E+03 M	9.83E+00	8.60E+00	5.88E+00	9.10E+00	7.78E+00	9.47E+00

DOSE 7	DOSE 8
2.17E+03	0.00E+00
2.66E+02	0.00E+00
3.90E+01	0.00E+00
6.50E+00	0.00E+00

* *

TOTAL DOSE VS. HORIZ. RANGE (RADS)

DOSE 1= ANS STANDARD-REM
DOSE 2= SOFT TISSUE
DOSE 3= MID-PHANTOM
DOSE 4= CONCRETE
DOSE 5= AIR
DOSE 6= IONIZING SILICON
DOSE 7= MID-HEAD
DOSE 8= USER SUPPLIED

HORIZ. RANGE	DOSE 1	DOSE 2	DOSE 3	DOSE 4	DOSE 5	DOSE 6	DOSE 7	DOSE 8
1.500E+03 M	2.18E+04	4.45E+03	2.47E+03	3.56E+03	2.92E+03	3.59E+03	2.92E+03	0.00E+00
2.000E+03 M	1.60E+03	4.55E+02	2.73E+02	4.03E+02	3.40E+02	4.11E+02	3.14E+02	0.00E+00
2.500E+03 M	1.48E+02	5.92E+01	3.76E+01	5.64E+01	4.81E+01	5.79E+01	4.25E+01	0.00E+00
3.000E+03 M	1.68E+01	9.18E+00	6.08E+00	9.17E+00	7.88E+00	9.48E+00	6.78E+00	0.00E+00

* *

FISSION PRODUCT DOSE VS. HORIZ. RANGE (RADS)

DOSE 1= ANS STANDARD-REM
DOSE 2= SOFT TISSUE
DOSE 3= MID-PHANTOM
DOSE 4= CONCRETE
DOSE 5= AIR
DOSE 6= IONIZING SILICON
DOSE 7= MID-HEAD
DOSE 8= USER SUPPLIED

HORIZ. RANGE	DOSE 1	DOSE 2	DOSE 3	DOSE 4	DOSE 5	DOSE 6
1.500E+03 M	2.05E+03	1.61E+03	1.01E+03	1.99E+03	1.46E+03	2.11E+03
2.000E+03 M	2.12E+02	1.72E+02	1.10E+02	1.98E+02	1.5[illegible]E+02	2.08E+02
2.500E+03 M	2.55E+01	2.12E+01	1.38E+01	2.35E+01	1.92E+01	2.45E+01
3.000E+03 M	3.44E+00	2.90E+00	1.91E+00	3.16E+00	2.63E+00	3.28E+00

DOSE 7	DOSE 8
1.16E+03	0.00E+00
1.25E+02	0.00E+00
1.55E+01	0.00E+00
2.14E+00	0.00E+00

* *

**EXECUTION COMPLETED

SECTION 7

REFERENCES

1. M.A. Abdou, et al., "MACK: A Computer Program to Calculate Neutron Energy Release Parameters (Fluence-to-KERMA Factors) and Multigroup Neutron Reaction Cross Sections from Nuclear Data in ENDF Format," Oak Ridge National Laboratory, Oak Ridge, TN, ORNL TM-3994 (July 1973).

2. M. Akiyama and S. An, "Measurements of Fission-Product Decay for Fast Reactors", In Nuclear Data for Science and Technology, K.H. Brockhoff, Ed., pp.237-43, Proceedings of an International Conference held Antwerp, Belgium, September 6-10, 1982 (1982).

3. American National Standard Neutron and Gamma-Ray Flux-to-Dose-Rate Factors, ANSI/ANS-6.1.1-1977 (N666), American Nuclear Society, LaGrange Park, Illinois (1977).

4. D.E. Bartine, et al., "Production and Testing of the DNA Few-Group Coupled Neutron-Gamma Cross-Section Library," Oak Ridge, TN: Oak National Laboratory, report ORNL/TM-4840 (1977).

5. J.E. Campbell and H.S. Sandmeier, "Radiation Transport in Air-Over-Ground and Air-Over-Seawater for Application to Low-Altitude, Low-Yield Tactical Nuclear Detonations," NWEF 1102 (April 1973).

6. U.S. Army Engineering Intelligence Note 32, "Chemical Composition and Neutron-Induced Radioactivity Potential of Selected Rocks and Limestone," (June 1959).

7. M. Cristy, "Mathematical Phantoms Representing Children of Various ages for use in Estimates of Internal Dose", Oak Ridge National Laboratory Oak Ridge, TN, ORNL-TM-367 (1980).

8. M. Cristy and K.F. Eckerman, "Specific Absorbed Fractions of Energy Various Ages from Internal Photon Sources, I-Methods," Vol. 1, Oak Ridge National Laboratory, Oak Ridge, TN, ORNL-TM-8381 '1983).

9. D. Dean, McDonnell-Douglas Corporation, Private Communication (1982).

10. Defense Atomic Support Agency, "Improved Models for Predicting Weapon Initial Radiation Environments," Unpublished.

11. Defense Atomic Support Agency, "Initial-Gamma Radiation Intensity and Neutron-Induced Gamma Radiation of NTS Soil," Unpublished.

12. Defense Nuclear Agency, "Photographic Atlas of Event Climax", Unpublished.

13. Defense Nuclear Agency Working Cross Section Library, Oak Ridge, TN, Oak Ridge National Laboratory, ORNL-RSIC-34, (June 1975).

14. J.K. Dickens, et. al., "Fission-Product Energy Release for Times Following Thermal-Neutron Fission of ^{235}U between 2 and 14000 Seconds," Nucl. Sci. Eng. 74:106-129 (1980).

15. J.K. Dickens, et. al., "Product Energy Release for Times following Thermal-Neutron Fission of ^{239}Pu and ^{241}Pu Between 2 and 14000 Seconds, Nucl. Sci. Eng. 78:126-146 (1981).

16. M. Ehrlich, "Energy Dependence of Instrument Sensitivity," presented at the Workshop of Radiation Survey Instruments and Calibration, National Bureau of Standards (July 1984).

17. C.M. Eisenhauer and G.L. Simmons, "Point Isotropic Gamma-Ray Buildup Factors in Concrete," Nucl. Sci. Eng., Vol. 56, pp. 263-270, (1975).

18. T. England, Los Alamos National Laboratory, Private Communication (1985).

19. T.R. England and R.E. Schenter, "The ANS Standard Curves of 1979 and Other Standards in the Light of New Experimental Information", LA-UR-2957, Los Alamos National Laboratory, Presented at the Specialists Meeting on Data for Decay Heat Predictions, Studsvik, Sweden, 7-10, 1987.

20. W.W. Jr. Engle, "A Users Manual for ANiSN-A One-Dimensional Discrete Ordinates Transport Code With Anisotropic Scattering," Oak Ridge Gaseous Diffusion plant, report K-1693 (1967).

21. P.C. Fisher and L.B. Engle, "Energy and Time Dependence of Delayed Gammas from Fission," Los Alamos Scientific Laboratory, LAMS-2642 (1962)

22. P.C. Fisher and L.B. Engle, "Delayed Gamma for Fast-Neutron Fission of ^{232}Th, ^{233}U, ^{235}U, ^{238}U, and ^{239}Pu," Phys. Rev. 134(4B):796-816 (1964).

23. R.G. Fleagle and J.A. Businger, An Introduction to Atmospheric Physics Academic Press, New York (1963).

24. R.L. French, "A First-Last Collision Model of the Air/Ground Interface Effects on Fast-Neutron Distributions," Nucl. Sci. Eng. 19, 151 (1964).

25. M.L. Gritzner, "A User's Manual for the Two-Dimensional Discrete Ordinate Code DOTSAI," SAI-75-747-HV, SAI (1973).

26. M.L. Gritzner, et al., "Radiation Environments from Tactical Nuclear Weapons," DNA 4267F (July 1976).

27. F.F. Haywood and J.A. Auxier, "Technical Concept-Operation HENRE CEX-65.02, U.S. Atomic Energy Commission (1965).

28. F.F. Haywood, J.A. Auxier and E.T. Loy, "An Experimental Investigation of the Spatial Distribution of Dose in an Air-Over-Ground Geometry CEX-62.14, U.S. Atomic Energy Commission" (October 1964).

29. S.L. Hess, Introduction to Theoretical Meteorology, Holt, Rinehart and Wiston, New York (1959).

30. J.H. Hubbell, "Photon Mass Attenuation and Mass Energy-Absorption Coefficients for H, C, N, O, Ar, and Seven Mixtures from 0.1 keV to 20 MeV," Radiat. Res., Vol. 70, pp. 58-81 (1977).

31. J.H. Hubbell, "Photon Mass Attenuation and Energy-Absorption Coefficients from 1 keV to 20 MeV," Int. J. Appl. Radiat. Isot., 33, pp. 1269-1290 (1982).

32. Illinois Institute of Technology Research Institute, "Study of Initial Gamma Dose and Dose Rate Measurements," Unpublished.

33. L. Huszar, et. al., "Version 4 of ATR (Air Transport of Radiation"), Defense Nuclear Agency, DNA 3995F (January 1976).

34. L. Huszar, et al., "Energy Dependent Air/Ground Correction Factors for the ATR (Air Transport of Radiation) Code," BRL Contract Report 345 (August 1977).

35. G.D. Kerr, "Photon and Neutron Fluence-to-Kerma Conversion Factors ICRP-1975 Reference Man Using Improved Elemental Compositions for Bone and Marrow of the Skeleton," Oak Ridge, TN: Oak Ridge Laboratory, ORNL/TM-8318 (November 1982).

36. Los Alamos Scientific Laboratory, "Gamma Ray Exposure as a Function Distance," Unpublished.

37. Los Alamos Scientific Laboratory, "Gamma Ray Exposure as a Function Distance, Operation Ranger," Unpublished

38. F.C. Maineschein, et. al., "Camma Rays Associated with Fission," from United Nations Peaceful Uses of Atomic Energy, Proceedings of the Second International Conference, Geneva Vol. 15 (September 1958).

39. F.C. Maineschein, "Prompt-Fission Gamma Rays," from Engineering Compendium on Radiation Shielding: Vol. 1, Sheilding Fundamentals and Methods, R.G. Jaeger ed., IAEA, Spring-Verlag, New York (1968).

40. B. Miers, Atmospheric Sciences Laboratory, White Sands Missile Range Private Communication (12 April 1983).

41. L.G. Mooney, "Utilization Instructions for FPR, A Code for Computing Fission Product Gamma Dose and Dose Rates," RRA-N7236 (October 1972).

42. F.R. Mynatt, et al., "Calculations of the Penetration of Nuclear Weapons Radiation into a Missile Silo," ORNL-TM-4021 (1973).

43. C.E. Needham and L.A. Wittwer, "Low Altitude Multiple Burst (LAMB) (Models," Air Force Weapons Laboratory, report AFW-DYS-TN-75-2, Albuquerque, NM (1975).

44. J.V. Pace, III, et al., "Neutron and Secondary-Gamma-Ray Transport Calculations for 14 MeV and Fission Neutron Sources in Air-Over-Ground and Air-Over-Seawater Geometries," ORNL-TM-4841 (August 1975).

45. V.C. Rogers, et al., "Silicon Ionization and Displacement KERMA for Neutrons from Thermal to 20 MeV," IEEE Trans. Nucl. Sci., Vol. No. 6, pp. 2326-2329 (December 1975).

46. V.C. Rogers, et al., "ERRATUM Silicon Ionization and Displacement KERMA for Neutrons from Thermal to 20 MeV," IEEE Trans. Nucl. Sci. Vol. NS-23, No. 1., pp. 875-876 (February 1976).

47. W.A. Rhoades, "Development of a Code System for Determining Radiation Protection of Armored Vehicles (the VCS Code)," Oak Ridge National Laboratory, Oak Ridge, TN, ORNL-TM-4664 (1974).

48. R.W. Roussin, et. al., "Vitamin-C: The CTR Processed Multigroup Cross-Section Library for Neutronics Studies," Oak Ridge National Laboratory, Oak Ridge, TN, ORNL/RSIC-37 (July 1980).

49. W.H. Scott, "Recommendations for Si Dose and 1 MeV Equivalent Response for Neutrons," unpublisned paper, Science Applications Inc., La Jolla, California (February 1982).

50. R.H. Simpson, "On the Computation of Equivalent Potential Temperature, Monthly Weather Review - Vol. 106, pp 124-130 (January 1978).

51. J.A. Stoddard, et. al., "The Vehicle Code System with In-Group Energy Bias and Gifts Geometry," Defense Nuclear Agency, DNA-TR-87-23 (January 16, 1987).

52. E. Storm, Memo to John Malik, Subject: Gamma vs. Distance LA Film Badge Correction Factors for the 1951-55 Nevada Tests, Los Alamos National Laboratory (October 1981).

53. E.A. Straker, "Time-Dependent Neutron and Secondary Gamma Ray Transport in Air-Over-Ground Geometry," ORNL 4289, (September 1968).

54. E.A. Straker, "Investigation of the Adequacy of Nitrogen Cross Section Sets: Comparison of Neutron and Secondary Gamma-Ray Transport Calculations with Integral Experiments," ORNL-TM-3768 (August 1972).

55. E.A. Straker, et al., "IDEA - An Integrated Dose Environment Analysis Code for Nuclear Weapons Effects," DNA 3763F (May 1976).

56. E.A. Straker and M. Gritzner, "Neutron and Secondary Gamma Ray Transport in Infinite Homogeneous Air," ORNL 4464, (December 1969).

57. E.A. Straker, et al., "The MORSE Code with Combinatorial Geometry," Defense Nuclear Agency, DNA 2860T (1972).

58. US-Japan Joint Reassessment of Atomic Bomb Radiation Dosimetry in Hiroshima and Nagasaki-Volumn 1, The Radiation Effects Research Foundation, Hiroshima, Japan, W.C. Roesch, Ed. (1987).

59. V.V. Verbinski, N.A. Lurie and V.C. Rogers, "Threshold-Foil Measurements of Reactor Neutron Spectra for Radiation Damage Applications," Nucl. Sci. Eng., Vol. 65, pp. 316-330 (1978).

60. C.R. Weisbin, et. al., "Vitamin-E: An ENDF/B-V Multigroup Cross-Section Library for LMFBR Core and Shield, LWR Shield, Dosimetry, and Fusion Blanket Technology," Oak Ridge, TN: Oak Ridge National Laboratory, report ORNL-5505 (1979)

61. P.G. Young and D.G. Foster, Jr., "An Evaluation of the Neutron and Photon-Production Cross Sections for Nitrogen," LA-4725, Los Alamos Scientific Laboratory (1972).

62. P.G. Young and D.G. Foster, Jr., "An Evaluation of the Neutron and Photon-Production Cross Sections for Oxygen," LA-4780, Los Alamos Scientific Laboratory (1972).

APPENDIX A

HISTORY OF ATR

Considerable effort was devoted to the understanding of weapons radiation transport in the atmosphere, especially near the air-ground interface, in the decade of the 60's. This effort was a combination of experimental and analytical studies, a large portion of which were supported by DNA (then DASA). All the experimental work was performed at the Nevada Test Site and included the two tower experiments, BREN (Ref. 28) and HENRE (Ref. 27), the former using a bare fast reactor source and the latter using an accelerator-driven 14 MeV neutron source. There was also interest in trying to predict analytically the radiation dose and fluence levels measured in the NTS atmospheric shots of the 50's.

The DNA-sponsored efforts culminated in publications by Straker (Refs. 53 and 56) and by L.G. Mooney and R.L. French (Ref. 10). The Mooney and French work was the most comprehensive ever attempted to completely describe the initial radiation intensity from actual tests, selected from Teapot, Plumbbob and later series. It used the Straker air-over-ground data, adjusted for height-of-burst using the method of French (Ref. 24), and incorporated a method for estimating the contribution of debris radiation to the total. Mooney and French developed their debris radiation predictive model based on the work of Loewe (Ref. 32).

The work of Mooney and French showed quite encouraging agreement with test shot data. Unfortunately, no attempt was made to incorporate their methods into a general tool for initial weapon radiation transport prediction. However, a proposal to do exactly that was submitted to DNA (DASA (RARP)) by Science Applications, Inc. in 1970. Oddly, this proposal did not arise from review of the RRA work, but from needs perceived by Dr. James Lonergan of SAIC, pertaining to in-flight radiation vulnerability analysis of strategic missiles. Dr. Lonergan's concept was to couple the energy and angle-dependent response calculated in the adjoint mode for important internal missile components with the results of uniform air transport calculations of the type published by Straker. To do this efficiently, it was necessary that the air transport data be placed in a format suitable for easy retrieval by computer. SAIC, under the resulting contract and follow-ons and under an additional study funded by Ballistic Research Laboratories (BRL), produced five successive versions of that prediction tool, which was given the name Air Transport of Radiation (ATR). The documentation for these versions of ATR are listed in Table 13.

The code released as Version 1 was an interim version and included only the neutron and secondary gamma-ray portion of the data base. Version 2 was actually the first complete version of ATR as originally proposed. It had functional fits of the Straker energy and angular-differential uniform air neutron and secondary gamma-ray transport data and an additional data base for gamma ray and x-ray transport, generated in a like format to the Straker data. It also incorporated an air-over-ground transport correction approach for integral dose based on the French method and normalized to the Straker air-over-ground calculated data. There were no plans at the time to incorporate a debris radiation model in the code. The reason for this is that radiation transport research of the early 70's was preoccupied with strategic applications, particularly the penetration of missile silos. Works such as that by Mynatt, et al. (Ref. 42), indicated that the most important components of initial weapons radiation for this application were the neutrons, which produced gamma rays in the silo cover, and the high-energy secondary gamma radiation, particularly that produced above the silo. The moderately energetic (~1.0 MeV) debris radiation is much less penetrating through such facilities, particularly if incident at an oblique angle.

In 1972, new neutron cross section evaluations for nitrogen and oxygen, sponsored by DNA (RARP), were published by Young and Foster of LASL (Refs. 61 and 62). These cross sections predicted half of the secondary gamma radiation from 14 MeV neutrons in nitrogen called for by the earlier Straker set. The reason given was that the earlier set had underestimated the competition from charged particle emission at high neutron energies. At the same time, the Young-Foster data also predicted higher transmitted dose of high energy neutrons and greater secondary gamma-ray production by low energy neutrons that did the Straker set. The appearance of the new cross sections caused consider-

Table 13. ATR documentation summary.

REPORT	CONTENT
SAI-71-565-LJ November 1971	Paper given at RSIC Workshop on Radiation Transport in Air. Describes logic of code and some data base development.
DNA2803I May 1972	First report describing basic concepts of ATR and the first distributed version of the code; describes neutron and secondary gamma-ray data base generation. Includes air/ground and exponential air correction factors.
DNA3144A April 1973	Users manual for ATR-2 version of the code; does not describe data base generation.
DNA3279T August 1974	Describes data base generation for photons (prompt gamma rays and x-rays) and the prompt gamma-ray air/ground correction factors.
DNA3362Z August 1974	Summary of the capabilities of the ATR code with updates to ATR-2.
DNA3813F July 1975	Describes ATR-3 including new data base using DNA cross section library, new air/ground correction factors, low energy x-rays, and new REGROUP routine.
DNA4061 January 1976	Describes TDATR, the time-dependent prompt photon and secondary gamma-ray version of ATR.
DNA3395F January 1976	Describes fission product model and summarizes total capability of the ATR-4 code.
BRL CR 343 August 1977	Describes ATR-4.1 with energy-dependent air/ground correction factors. Work supported by BRL.

able argument. It was found that they predicted the results measured in laboratory experiments but did not predict the results of the HENRE experiment. The opposite was found to be true of the Straker set (Ref. 54).

Accepting the laboratory experiments as the more reliable comparison, DNA and the Cross Section Evaluation Working Group (CSEWG) accepted the Young-Foster data to supplant that of Straker in the Evaluated Nuclear Data File (ENDF) library. Subsequently, it was decided by DNA to sponsor an update of ATR to include air transport data generated using the Young-Foster cross sections. SAIC produced the homogeneous air transport results in a format identical to the original Straker calculations and Oak Ridge National Laboratory produced a set of source altitude-dependent integral dose calculations (Ref. 44), all under DNA sponsorship. SAIC then incorporated these data into ATR, applying the air-over-ground correction factors for 14 MeV neutron-produced integral dose to all neutron source energies above 5 MeV and those for the fission weapon source to all neutron source energies below 5 MeV. Improvements were also made in the x-ray transport at the time. The results were published as Version 3 of ATR.

During the period in which Version 3 of ATR was being produced, a new interest in debris radiation developed. The driving force behind this interest was the possibility that low altitude ABM missiles might have to fly through the debris cloud of another such missile. Both Radiation Research Associates (RRA) and SAIC were sponsored by DNA to study the debris radiation problem. The SAIC product was the Integral Dose Environment Analysis (IDEA) Code (Ref. 55), which used the ATR3 data base and "ρr" scaling to estimate the transport of radiation from all weapon source components through a perturbed atmosphere. The time dependent hydrodynamic behavior of the atmosphere surrounding a burst was described using a complex model (LAMB) (Ref. 43) produced by the Air Force Weapons Laboratory. Near the end of ATR 3 development, it was decided to incorporate a debris radiation model on ATR. However, it was found that the hydrodynamic and cloud rise model used in IDEA was too long running and complex to use as it stood. Therefore, it was decided to use the simpler models developed by RRA (Ref. 41). These were essentially the same models used to compute debris radiation dose in the RRA report on weapon tests referred to previously. Air-over-ground correction factors for the debris radiation dose were based on the French "First-Last Collision Method," as were those for prompt gamma rays. This was known not to be very satisfactory for gamma ray applications, however, no suitable body of data similar to the Pace calculations existed for gamma-ray transport in an air-over-ground configuration. The resulting code became Version 4 of ATR, the first version of the code capable of calculating all of the most important initial radiation components. The capabilities of ATR4 are summarized in Figure 21.

Version 4 of ATR, released in January of 1976 was, in fact, the conceptual embodiment of all aspects of the RRA study of test shot dose distribution analysis published almost exactly 6 years earlier. Some nuclear data changes had occurred in the interim, but that original concept of estimating the radiation dose distribution resulting from any device, based on a single comprehensive set of pre-calculated data came to fruition in ATR4.

In April of 1973, a report containing a large compilation of air-over-ground transport calculations was published by the Naval Weapons Evaluation Facility (Ref. 5). It was thought at the time that those results might be used to produce the air-over-ground correction factors for use in ATR3 as then contemplated. However, upon review by DNA and SAIC, it was found that the NWEF data contained many errors and inconsistencies which made it unsuitable for such use. Among these were the use of Pre-Young-Foster cross sections, insufficient problem dimensions and oscillations in the fine-mesh dose distribution data. The results of this review were forwarded to NWEF. In spite of this, a group at Los Alamos Scientific Laboratory (LASL), including T.W. Dowler and H.A. Sandmeier, used the NWEF data base to calculate dose distributions from actual tactical nuclear devices. The resulting report was reviewed by DNA, which determined that it was necessary to rebut its findings. At first, it was thought that ATR3, then in preparation might be used for this purpose. However, it was finally decided by DNA that such a rebuttal must be done on the basis of state-of-the-art transport technology in order to have the greatest effect. Therefore, E.A. Straker, by then at SAIC, was sponsored to perform a complete set of two-dimensional neutron, secondary gamma-ray prompt gamma- ray and debris gamma-ray calculations applicable to tactical device detonations. It was further decided that, since the number of response functions of interest was lim-

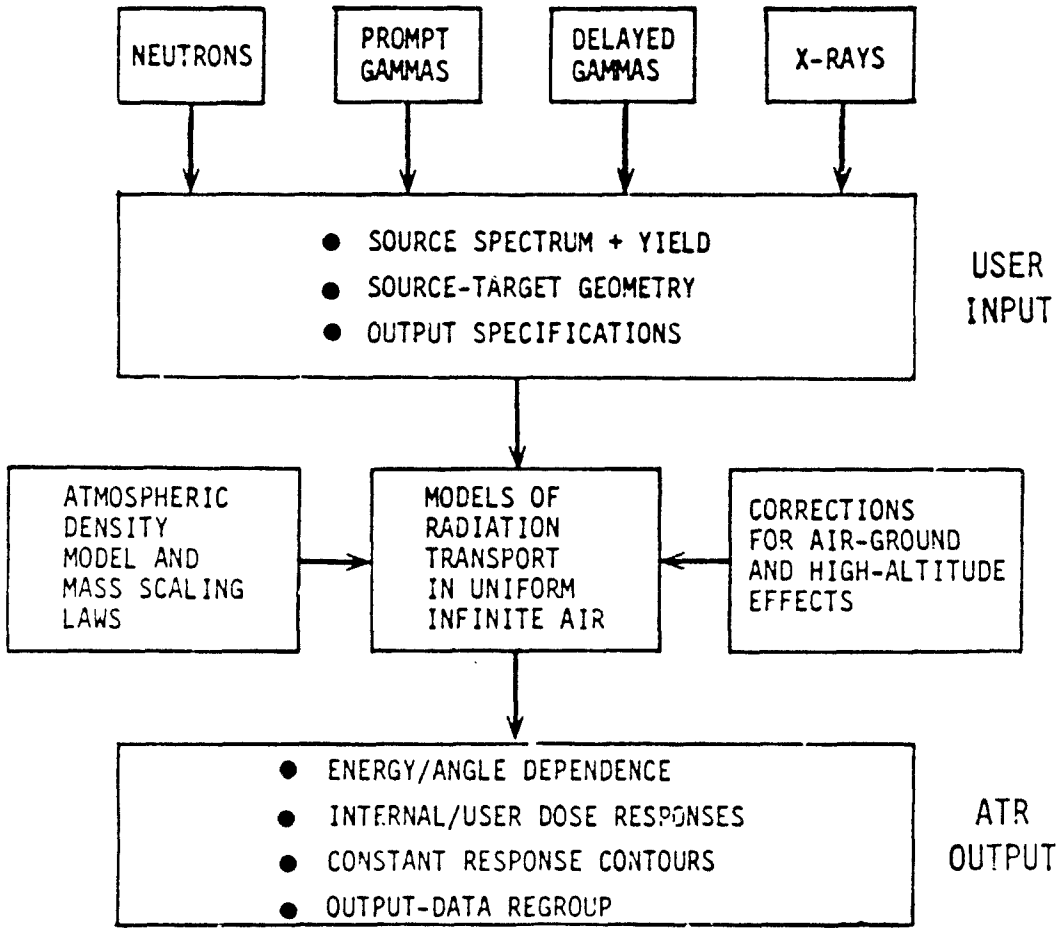

Figure 21. ATR model.

ited, whereas the number of sources was potentially limitless, the problems would be run in the adjoint mode. This would provide integrated dose data at any range of interest for an arbitrary isotropic source at any altitude. As part of this effort, it was decided to investigate the effect of soil composition, particularly moisture content, on radiation transport. A one-dimensional analysis of this effect was performed, revealing that such a dependence did exist. Therefore, pains were taken to perform the 2-D calculation using an area-weighted central German soil.

The results of the DNA-sponsored tactical nuclear weapon radiation environment study (Ref. 26) were published in 1976. Shortly thereafter it was proposed by SAIC to DNA that the full source-energy-dependent air-over-ground correction factors for all radiation types available from the new calculations be incorporated in ATR. The proposal was not accepted by DNA. However, Ballistic Research Laboratories (BRL) did offer to sponsor the project. The result of this was ATR4.1 (Ref. 34), which differs from ATR4 as described in Table 14.

Table 14. Comparison of transport data bases used for air-over-ground correction factors in ATR4 and ATR4.1.

	ATR4	ATR4.1
Description	DOT calculations by Pace, ORNL	TWEEDEE data base from Adjoint DOT calculations by Gritzner, Straker
Source Energy Dependence	Two sources o 14 MeV o Degraded fission	23 neutron source energy bands from 15 MeV to thermal. 19 photon source energy bands from 10 MeV to 0.01 MeV
HOB	Three source heights	Continuous from 0 to 1000 m
Radiation Components	Tissue dose for neutrons and secondary gammas	Tissue dose for neutrons, secondary gammas, and prompt gammas
Energy and Angular Dependent Effects at Detector	No	No
Soil	NTS	Dry (no free water) area weighted West German
Target Altitude	Continuous from 0 to 1000 m	1 m
Ground Range	∿1.3 km	∿1.3 km

APPENDIX B

EQUATIONS TO CALCULATE METEOROLOGICAL VARIABLES PRESENT IN A MOIST ATMOSPHERE

The following paragraphs briefly describe a procedure to compute the more important meteorological variables present in a moist atmosphere. Equations and constants used in this procedure for calculating these variables were obtained from References 29, 23 and 50.

Equations Used

(1) Latent Heats (L)

(a) Vaporization ($T \geq -20\ ^{\circ}C$) = 597.2 - .543t $^{\circ}C$ (cal/g) (5)

(b) Sublimation ($T < -20\ ^{\circ}C$) = 677.0 - .0356t $^{\circ}C$ (cal/g) (6)

(2) Dew Point Temperature (T_d) / Frost Point Temperature (T_F) for $T < -20\ ^{\circ}C$

$$T_F = C_1 / \{C_2 - 1n\ [(RH/100) \times \exp\ (C_2 - C_1/T)]\}\ (K) \quad (7)$$

where: $C_1 = L / R_v$ (8)

$$C_2 = L / 273.155 \times R_v \quad (9)$$

and R_v is the gas constant for water vapor = 0.11025 cal/g K.

(3) Relative Humidity (RH%)

$$RH = \exp\ [C_1 \times (1/T - 1/T_d)] \times 100\ T,\ T_d \text{ in K } (\%) \quad (10)$$

(4) Saturation Vapor Pressure (e_s)

$$e_s = 6.11 \times \exp\ (C_2 - C_1/T)\ (mb) \quad (11)$$

(5) Saturation Mixing Ratio (W_s)

$$W_s = \epsilon \times e_s / (P - e_s)\ (ppm) \text{ multiply by } 10^3 \text{ to get g/kg.} \quad (12)$$

where: P is pressure (mb)

and $\epsilon = (M_v / M_d) = (18.016\ g/mole / 28.966\ g/mole) = .622$ (13)

(6) Mixing Ratio (w)

$$w = RH \times W_s / 100\ (ppm) \quad (14)$$

also $w = \rho_v / \rho_d$ (15)

where ρ_v = density of water vapor present

ρ_d = density of dry air containing the vapor

(7) Vapor Pressure (e)

$$e = w \times P / (\epsilon + w)\ (mb) \quad (16)$$

(8) Virtual Temperature (T^*)

$$T^* = T \times [(1 + w/\epsilon) / (1 + w)]\ (K) \quad (17)$$

(9) Density of Moist Air (ρ_m)

$$\rho_m = P / (R_d \times T^*) = 3.4838 \times 10^{-4} (P / T^*) \ (g/cm^3) \quad (18)$$

where R_d is the gas constant for dry air = .06857 cal/gm

(10) Density of Dry Air (ρ_d)

$$\rho_d = \rho_m / (1 + w) \ (g/cm^3) \quad (19)$$

(11) Absolute Humidity $\rho_v = \rho_m - \rho_d$ (g cm^{-3}) (20)

(12) Specific Humidity (q)

$q = \rho_v / \rho_m$ from (6) we see that $q : w$ (21)

(13) Potential Temperature (Θ)

$$\Theta = T \times (1000 / (P - e)^{K_d} \ (K) \quad (22)$$

where: T is in K

and $K_d = R_d / C_p$ (23)

and C_p = specific heat capacity at constant pressure = 2.4 cal/g K.

(14) Equivalent Potential Temperature (Θe)

$$\Theta_e = \Theta \times \exp [L \times W_s / C_p \times T] \ (K) \quad (24)$$

where t is in K.

APPENDIX C

GENERATION AND TESTING OF ATR5 RESPONSE FUNCTIONS

NEUTRON RESPONSE FUNCTIONS.

Neutron response functions span the energy range from 1.00×10^{-11} MeV to 14.9 MeV using 22 energy groups. Energy-specific KERMA values were collapsed into this 22 group format using a fluence spectrum that consisted of a 300 K Maxwell-Boltzman distribution for neutron energies below 5 KT (0.129 eV) and a 1/E distribution for neutron energies above 5 KT. This fluence spectrum is representative of the spectrum that exists at distances of 500 m to 5000 m in air from a typical fission source.

The ANS Standard response function is based on the neutron flux-to-dose rate factors published by the American Nuclear Society (Ref. 3).

The Soft Tissue response function is based on Kerr's model (Ref. 35).

The Mid-Phantom and Mid-Head response functions are based on the work described in Appendix D.

The Concrete response function is for the concrete composition given in Table 15. The elemental KERMA factors were generated from the DNA Working Cross Section Library (Ref. 13) using the MACK code (Ref. 1).

Table 15. Composition of concrete*.

Element	Weight Fraction
Hydrogen	0.0056
Oxygen	0.4983
Sodium	0.0171
Magnesium	0.0024
Aluminum	0.0456
Silicon	0.3158
Sulfur	0.0012
Potassium	0.0192
Calcium	0.0826
Iron	0.0122
Total	1.0000

* This concrete is termed White-Grodstein "typical" composition in Reference 31 and "NBS" concrete in Reference 50. It has a density of 2.35 g/cm3

The Dry Air response function is for the air composition given in Table 16. The elemental KERMA factors were generated from the DNA Working Cross Section Library using the MACK code.

The Non-Ionizing Silicon and Ionizing Silicon response functions are based on the work reported by Rogers et al. (Refs. 45 and 46) and their tabulated results (Ref. 59). The 1 MeV Equivalent Fluence response function is based on the recommendations of Scott (Ref. 49).

GAMMA RAY RESPONSE FUNCTIONS.

Gamma ray response functions span the energy range from 0.01 MeV to 12.0 MeV using 18 energy groups. Energy-specific KERMA values were collapsed into this 18 group format using a fluence spectrum that consisted of an E^3 distribution for photon energies below 0.045 MeV and a 1/E distribution for photon energies above 0.045 MeV. This fluence spectrum is representative of the spectrum that exists at distances of 500 m to 5000 m in air from a prompt gamma fission source.

The ANS Standard response function is based on the gamma-ray flux-to-dose-rate factors published by the American Nuclear Society (Ref. 3).

The Soft Tissue response function is based on Kerr's model (Ref. 35).

The Mid-Phantom and Mid-Head response functions are based on the work described in Appendix C.

The Concrete response function is based on Hubbell's work (Ref. 31). The concrete composition is given in Table 15.

The Dry Air response function is based on Hubbell's work (Ref. 31). The air composition is given in Table 16.

The Ionizing Silicon response function is based on Hubbell's work (Ref. 31).

COMPARISON OF OLD AND NEW RESPONSE FUNCTIONS.

Table 17 provides representative neutron and gamma-ray fluences for this comparison of response functions. The neutron fluence is for a distance of 1000 m from a 1 KT fission/fusion (0.5/0.5) neutron source; the fluence was calculated using ATR4 with subsequent regrouping to the ATR5 neutron energy group format. The gamma-ray fluence is for a distance of 1000 m from

Table 16. Composition of dry air*.

Element	Weight Fraction For Gamma KERMA	For Neutron KERMA
Oxygen	0.232	0.245
Nitrogen	0.755	0.755
Argon	0.013	0.000
Total	1.000	1.000

* The dry air composition used for gamma ray KERMA is that used by Hubbell in Reference 31 as reported in Reference 10. Since elemental neutron KERMA factors are not available for Argon, for the neutron KERMA of dry air the Argon fraction was assigned to Oxygen.

Table 17. Representative neutron and gamma-ray fluences used to illustrate difference in kerma factors between ATR4 and ATR5*.

	Neutron Fluence		Gamma-Ray Fluence	
Group No.	ATR4 Group	ATR5 Group	ATR4 Group	ATR5 Group
1	2.94E-13	2.94E-13	1.54E-14	1.29E-14
2	3.25E-13	3.25E-13	6.16E-14	6.78E-14
3	3.89E-13	3.89E-13	4.15E-14	2.82E-14
4	5.43E-13	5.43E-13	1.89E-14	3.21E-14
5	4.58E-13	4.58E-13	9.49E-15	1.30E-14
6	5.88E-13	5.88E-13	1.18E-14	1.25E-14
7	8.55E-13	1.13E-12	7.24E-15	7.98E-15
8	9.04E-13	1.12E-12	4.94E-15	8.70E-15
9	2.26E-12	1.78E-12	3.08E-15	6.29E-15
10	1.38E-12	1.60E-13	4.78E-15	5.01E-15
11	7.39E-13	1.22E-12	4.13E-15	4.21E-15
12	3.65E-13	7.39E-13	5.01E-15	6.64E-15
13	1.79E-13	3.65E-13	4.21E-15	5.14E-15
14	3.74E-14	1.65E-13	6.64E-15	4.20E-15
15	1.09E-13	1.60E-13	5.14E-15	3.42E-15
16	1.04E-13	1.04E-13	6.08E-15	1.46E-15
17	9.83E-14	9.83E-14	3.01E-15	7.39E-16
18	1.09E-13	1.10E-13	7.39E-16	0.00E-00
19	7.24E-14	7.13E-14		
20	4.31E-14	4.31E-14		
21	4.79E-14	4.79E-14		
22	1.21E-13	1.16E-13		

* The neutron fluence was calculated using ATR4, and then regrouped into ATR5 format. The gamma ray fluence was calculated using ATR5, and then regrouped into ATR4 format.

ε 1 kT prompt gamma fission source; this fluence was calculated using ATR5 with subsequent regrouping to the ATR4 gamma ray energy group format.

Table 18 shows the responses calculated using the fluences from Table 17 and the old (ATR4) and the new (ATR5) response functions.

Table 19 shows the change in calculated responses for comparable response functions.

Table 18. Neutron and gamma-ray kerma and dose values calculated from ATR4 and ATR5 with identical fluence values*.

Neutron Responses

ATR4		ATR5	
Henderson Tissue	= 8.28E-21		
Snyder-Neufeld	= 1.51E-20		
Tissue	= 9.14E-21	Soft Tissue	= 9.32E-21
Mid-Phantom	= 3.65E-21	Mid-Phantom	= 3.33E-21
Concrete	= 1.22E-21	Concrete	= 1.24E-21
Air	= 1.64E-21	Air	= 1.58E-21
Non-Ionizing Silicon	= 1.13E-22	Non-Ionizing Silicon	= 1.18E-22
Ionizing Silicon	= 3.00E-22	Ionizing Silicon	= 3.10E-22
		ANS Standard	= 1.09E-19
		Mid-Head	= 4.52E-21
		1 MeV Equil. Flu.	= 3.56E-12

Gamma Ray Responses

ATR4		ATR5	
Henderson Tissue	= 7.18E-23		
Concrete	= 8.30E-23	Concrete	= 7.53E-23
Air	= 6.85E-23	Air	= 6.30E-23
Silicon	= 7.93E-23	Ionizing Silicon	= 7.84E-23
		ANS Standard	= 8.10E-23
		Soft Tissue	= 6.96E-23
		Mid-Phantom	= 4.69E-23
		Mid-head	= 5.22E-23

* Since the ATR4 and ATR5 fluences are based on one fluence regrouped into the other energy group format, the fluences are essentially equivalent. Accordingly, this table shows the effect of changing the response function.

Table 19. Changes in selected kerma and dose values due to fluence-to-kerma or -dose factor changes*.

	Percent Change	
Response	Neutron	Gamma Ray
Tissue	+2%	NA
Mid-Phantom	-9%	NA
Concrete	+2%	-9%
Air	-4%	-8%
Non-Ionizing Silicon	+4%	NA
Ionizing Silicon	+3%	-1%

---

* ("ATR5" - "ATR4") / "ATR4".

So, for example, if ATR4 and ATR5 were used to calculate Concrete kerma, at a range of 1000 m from a 1 kT prompt gamma source, the ATR5 kerma would be 9% less than the ATR4 kerma, assuming the transported fluences were the same.

APPENDIX D

KERMA IN AN ANTHROPOMORPHIC PHANTOM

This Appendix describes the procedure used to calculate neutron and gamma-ray Mid-Phantom and Mid-Head energy-angle differential response functions. This task was performed under a DNA sponsored effort, Contract No. DNA001-83-C-0252.

The transport of externally incident fluence to points at the mid-head and mid-thorax of an anthropomorphic phantom has been assessed using the VCS code system (Ref. 47) which incorporates the MORSE Monte Carlo transport code (Ref. 57). The MORSE code performs transport calculations in three dimensions.

Computations were performed using a three-dimensional adult male anthropomorphic phantom developed by Cristy, (Ref. 7) having a total mass of approximately 74 Kg. This phantom and its internal lung and skeletal detail are depicted in Figure 22. Specifications of elemental constituents, as recently published by Kerr, (Ref. 35) are provided in Table 20 along with revised density values (Ref. 8).

Transport computations have been performed using the DNA Few Group Cross Section Library (DLC-31) with P_3 Legendre expansion. Calculations have been performed in the adjoint mode. In this mode the physics of the radiation transport are reversed by inverting the energy dependent quantities and reflecting the angular variables through the origin. This causes neutrons and gamma rays in the computation to gain energy in scattering and causes gamma rays to "produce" neutrons.

The adjoint approach is employed by starting a particle at a detector point and following it until it leaks from the system along a direction Ω' and at a leakage surface defined by its normal vector n. The correlated descriptions of the starting and leaking particles are saved.

The system leakage fluence $(n \cdot \Omega')\phi^*(E', \Omega')$ may be viewed as having the qualities of detector weighted by the transport through the intervening media. It may be convoluted with any fluence $\phi(E', \Omega')$ defined as incident on the system from which the leakage is scored to obtain the detector response for that particular incident fluence, as in the expression:

$$\text{Total Kerma} = \int \int d\Omega' dE' \phi(E', \Omega')(n \cdot \Omega')\phi^*(E', \Omega') \; \Omega' \; E' \qquad (25)$$

at some range r from the radiation source. This process is shown schematically in Figure 23.

To obtain an energy differential response function, the angular integration is carried out in advance, yielding the energy dependent (isotropic) transport-weighted Kerma factors, $\phi^*(E)$.

Computations of transport in the anthropomorphic phantom have been performed for two detector locations. The first location is mid-head, which is specified to be the geometric center of the ellipsoid head of the phantom. The second location is mid-thorax, which is specified to be at the geometric center of the elliptical torso cross section, midway between the top of the pelvis and the top of the torso. Starting histories were sampled uniformly from 58 (37 neutron, 21 gamma-ray) energy groups. A total of 60,000 starting histories were used for the mid-head location, while a total of 45,300 were used for the mid-thorax location. Due to splittings of histories in the Monte Carlo process, approximately twice the number of starting histories were actually tallied as having leaked from the system, a few more for the mid-thorax location, a few less for the mid-head location. The results of these calculations may be considered to be highly reliable, statistically, in terms of total Kerma transmission.

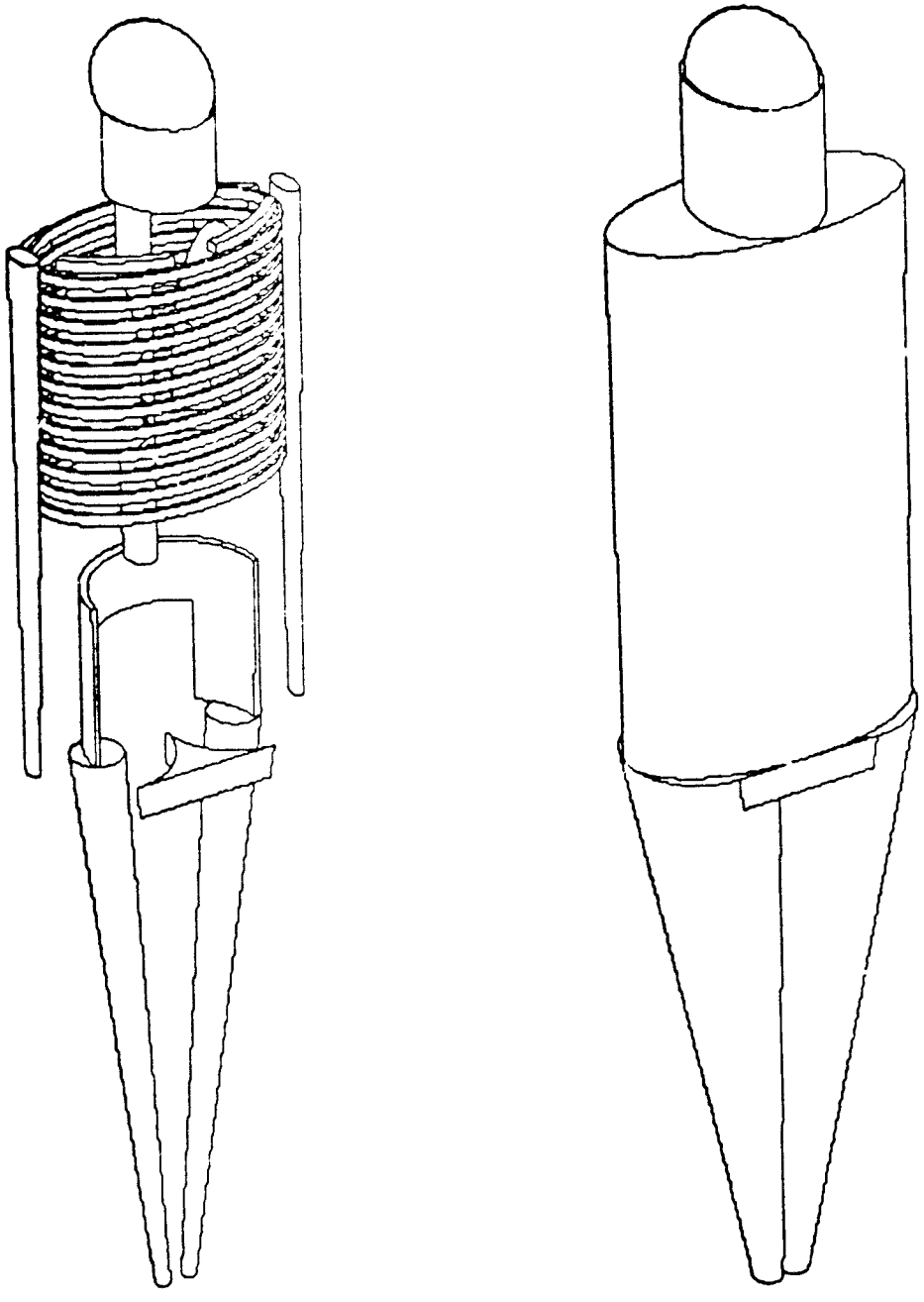

Figure 22. Adult male reference man.

Table 20. Elemental composition for various components of reference man.

Element	Percent by Weight		
	Lung	Skeleton	Soft Tissue
H	10.21	7.28	10.51
C	10.24	24.64	22.63
N	2.91	3.06	2.34
O	75.63	46.88	63.69
Na	0.19	0.32	0.011
Mg	0.007	0.11	0.013
P	0.080	5.03	0.13
S	0.23	0.31	0.20
Cl	0.27	0.14	0.14
K	0.20	0.15	0.20
Ca	0.009	12.07	0.024
Fe	0.037	0.008	0.006
Density (g/cm^3)	0.296	1.40	1.04

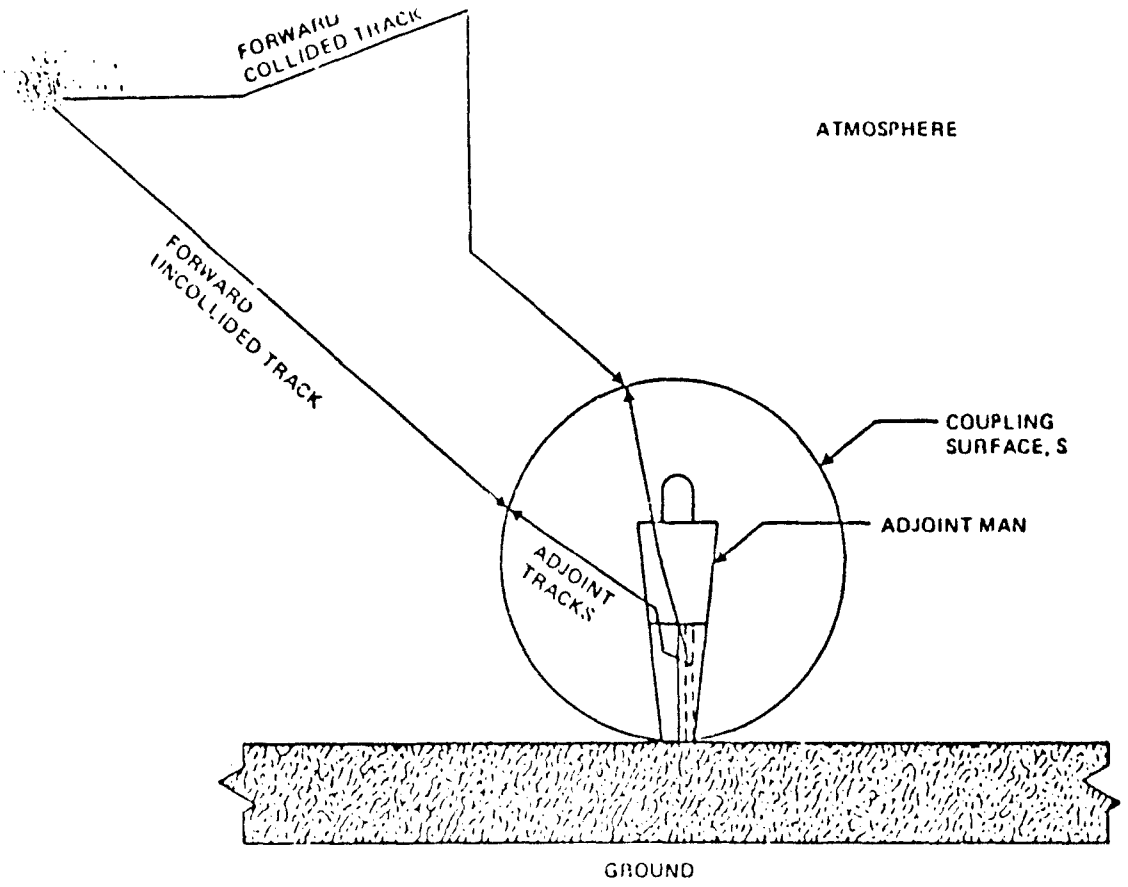

Figure 23. Illustration of forward-adjoint coupling.

APPENDIX E

DELAYED GAMMA RADIATION TRANSPORT METHODOLOGY DEVELOPMENT

INTRODUCTION.

The improvement of the ATR delayed radiation model has been based on the study of empirical data from the atmospheric tests conducted in Nevada and Pacific test sites and the study of alternative models. This Appendix describes the development and study of an alternative model to that contained in ATR. Study of this alternative model yielded significant insights into possible shortcomings of the ATR model, particularly the hydrodynamic model. Unfortunately, the alternative hydrodynamic model was too complex for direct inclusion in ATR. However, it did provide additional data from which to develop the scaled height-of-burst correction factor described in the body of this report. In addition, it provided the fission product radiation source terms incorporated in ATR5.

Delayed gamma radiation is that component of initial nuclear weapon radiation (radiation emitted within the first 60 seconds following initiation) emitted by products of fission and neutron activation which are parts of the debris of the nuclear explosion. These debris initially reside within the fireball, a luminous sphere of hot gases generated by the interaction with the air of x-rays radiated from the hot debris within a millionth of a second after initiation.

The fireball also defines the edge of a region of very low density air, a density well, created by the expansion of the very hot gases within. The high pressure region created at the edge of that density well forms a shock wave which breaks away from the fireball and travels outward, superimposed on the ambient air. The net effect of these perturbations is to decrease the amount of air on a line from source to target, thereby enhancing the transmission of delayed radiation over that which would occur in unperturbed air. This effect is often referred to as hydrodynamic enhancement.

The density well is buoyant and begins to rise within a fraction of a second of its creation. Its momentum is augmented by the returning shock wave, now reflected off the ground. The rise of the fireball, which includes the radiation source, causes the distance between source and target to increase, thereby causing the radiation transmission to decrease once the expansion of the fireball has slowed or stopped.

As the fireball rises the outer surface cools and is subject to drag forces from the surrounding atmosphere. That causes the spherical fireball to become a toroid-shaped cloud of condensed gases, containing the weapon debris.

Throughout this process the weapon debris, including the fission products, are in motion relative to the fireball. First, the debris are propelled toward the top of the fireball with an initial impulse provided by the reflected shock. Eventually the debris pierce the top of the rising fireball and flow down the side, with most becoming incorporated in the torus itself or in the cloud skirt below the torus. Those effects become less pronounced as the scaled burst height increases, where the scale burst height is defined to be the burst height divided by yield to the one third power ($HOB/y^{1/3}$).

This complex system, consisting of a radioactive, hence time-varying, source of gamma rays and similarly time-varying geometry, in which the amount of air between source and target is changing, even as the source rises from its original location, must be modeled in some detail in order to properly describe the intensity of the delayed radiation component. The motivation for doing so is that delayed gamma radiation comprises the majority of the gamma ray field strength from large yield weapons.

Three technical areas must be addressed in the modeling process. These are:

Fission Product Gamma Ray Source

Gamma Ray Transport

Nuclear Weapon Hydrodynamics

Data required for modeling the processes of interest in these areas have been acquired through laboratory and field measurements. However, these data are by no means complete. Here follows a discussion of such modeling.

FISSION PRODUCT GAMMA RAY SOURCE.

Measurements of gamma and beta radiation source rates as functions of time after fission have been made in the laboratory. Maienschein, et al., (Refs. 38 and 39), reported measurements made in the late 1950's and early 1960's at Oak Ridge National Laboratory in terms of spectra, total number and total energy emission rates. In the early 1960's, Fisher and Engle (Refs. 21 and 22), of Los Alamos National Laboratory performed similar experiments using a fast reactor source, which allowed them to obtain results at very early times (.35 sec). They also performed such measurements for several fissionable materials including U-235, Pu-239 and U-238.

Dickens et al., (Ref. 14 and 15), have published results of recent measurements made ORNL, including those of spectra, again using thermal neutron fission. Also, Japanese scientists Akiyama and An (Ref. 2) have published results of their measurements using a fast reactor source. The Japanese data are in terms of total energy rate only, and are limited to times of twenty seconds or greater.

Results of several measurements in terms of energy emission rates at forty seconds, the earliest time common to all the available measurements, are provided in Table 21. There is a limit to what can be construed from these data because of disparities in the uncertainties quoted by the individual measurers. The Maienschein et al., data are assigned a standard deviation of approximately twenty-five percent, those of Fisher and Engle twelve percent (U-235 and U-238) and twenty one percent (Pu-239) and those of Dickens et al., and Akiyama and An less than five percent. Nevertheless, the data having the lowest uncertainties are consistent with each other and are not inconsistent with the value provided by Maienschein et al., whereas the data of Fisher stand apart from the high precision data. Unfortunately, the latter provide the only available spectral data for very early times and for U-238 fission. Therefore, it is desirable to reconcile them to those of the other measurers. To accomplish this, the spectra of Dickens, et al., and of Fisher and Engle are compared for U-235 and Pu-239, common to both experiments (Table 22, columns three and four). It is found that the two sets of spectra differ from each other by the same energy-dependent ratio (last column) after removal of a constant correction term in the Fisher and Engle Pu-239 measurement (.85, column 5). That correction is consistent with the Fisher and Engle disclaimer concerning their estimation of the number of fissions in the Pu sample. The energy dependent relationship found to exist between the Dickens, et al., and the Fisher and Engle U-235 and Pu-239 may also be applied to the latter's U-238 measurements. The result, in terms of total gamma ray energy emission rate agrees within a few percent with the value reported by Akiyama and An at 40 seconds post-irradiation time. Therefore, it is concluded that a systematic error must be present in the Fisher and Engle data but that it can be removed through the use of the Dickens, et al - related, energy-dependent corrections. The resulting source rate models for three representative energy groups along with supporting experimental data are shown as functions of time in Figures 24, 25 and 26. Figure 26 also indicates some additional empirical corrections represented by the dotted lines made to the Fisher and Engle data to make their temporal behavior self-consistent and also more consistent with those of Dickens et al. The resulting source rate models are not only consistent with recent experiments but are also inclusive of early times and data for U-238. Source rate spectra for five times, .35 through 40 seconds, are given for U-235, U-238 and Pu-239 in Tables 23, 24 and 25, respectively. Source rates for times other than those shown are obtained by 1n-1n interpolation. For times earlier than .35 seconds the source rate is obtained by 1n-1n extrapolation, based on the earliest two times, .35 and 1.5 The contribution from sources beyond 30 seconds is negligible Therefore, no extrapolation to times greater than 40 seconds is performed.

An addition complication has not been taken into account in the delayed gamma radiation source model. Calculations using nuclide-specific gamma emission rates (Ref. 18) indicate that fast fission produces more gamma ray energy at early times than does thermal fission (Table 26). This is supported to some extent by a comparison of the new American (thermal fission) and Japanese (fast fission) data in Table 21. Having in effect normalized Fisher and Engle's results to those of Dickens, et al., the former are now consistent with those for thermal rather than fast fission.

Table 21. Fission product gamma ray source energy emission rate (0.1 to 5 MeV) at 40 sec after fission.

Experimentor \ Nuclide	MeV/fis-sec U-235	U-238	Pu-239
Maienschein, et al.	0.0193*	-	-
Fisher and Engle	0.0216	0.0275	0.0194
Dickens, et al.	0.0166	-	0.0130
Akiyama and An	0.0171	0.0205	0.0131

*Energy contribution $0.1 < E < 0.28$ estimated by extrapolation.

Table 22. Mean values of Dickens to Fisher and Engle source ratios by energy group for U-235 and Pu-239.

Group No.	Upper Energy (MeV)	$S_D/S_{F\&E}$ U-235	$S_D/S_{F\&E}$ PU-239	R_{239}/R_{235}[a]	$S_D/S_{F\&E}$ Pu-239 Adjusted	$S_D/S_{F\&E}$ Mean
1	6.419	.394(.179)[b]	.360(.161)	.914	.424	.409(.170)
2	5.636	.820(.096)	.654(.217)	.798	.769	.795(.164)
3	4.918	.627(.416)	.630(.103)	1.005	.741	.684(.281)
4	4.257	.866(.095)	.734(.059)	.848	.864	.865(.079)
5	3.655	.958(.048)	.817(.044)	.853	.961	.960(.046)
6	3.110	.852(.076)	.730(.031)	.857	.859	.856(.058)
7	2.620	.904(.046)	.779(.025)	.862	.916	.910(.037)
8	2.189	.869(.028)	.738(.026)	.849	.868	.869(.027)
9	1.808	.779(.034)	.674(.045)	.865	.793	.786(.040)
10	1.478	.787(.049)	.688(.033)	.874	.809	.798(.042)
11	1.195	.722(.044)	.615(.035)	.852	.724	.723(.040)
12	.954	.751(.035)	.620(.012)	.826	.729	.740(.026)
13	.749	.674(.100)	.515(.084)	.764	.606	.640(.093)
14	.575	.671(.086)	.569(.082)	.848	.669	.670(.084)
15	.428	.577(.106)	.495(.104)	.858	.582	.580(.105)
16	.309	.484(.038)	.448(.094)	.926	.527	.506(.074)
17	.213	.394(.077)	.345(.160)	.876	.406	.400(.127)
	.137		mean[c]	.854(0.040)		

[a] Ratio of the Pu-239 source ratio to that of U-235.

[b] read as mean and (fractional standard deviation of the sample = σ_{n-1} /mean).

[c] mean of group values E < 4.257 MeV.

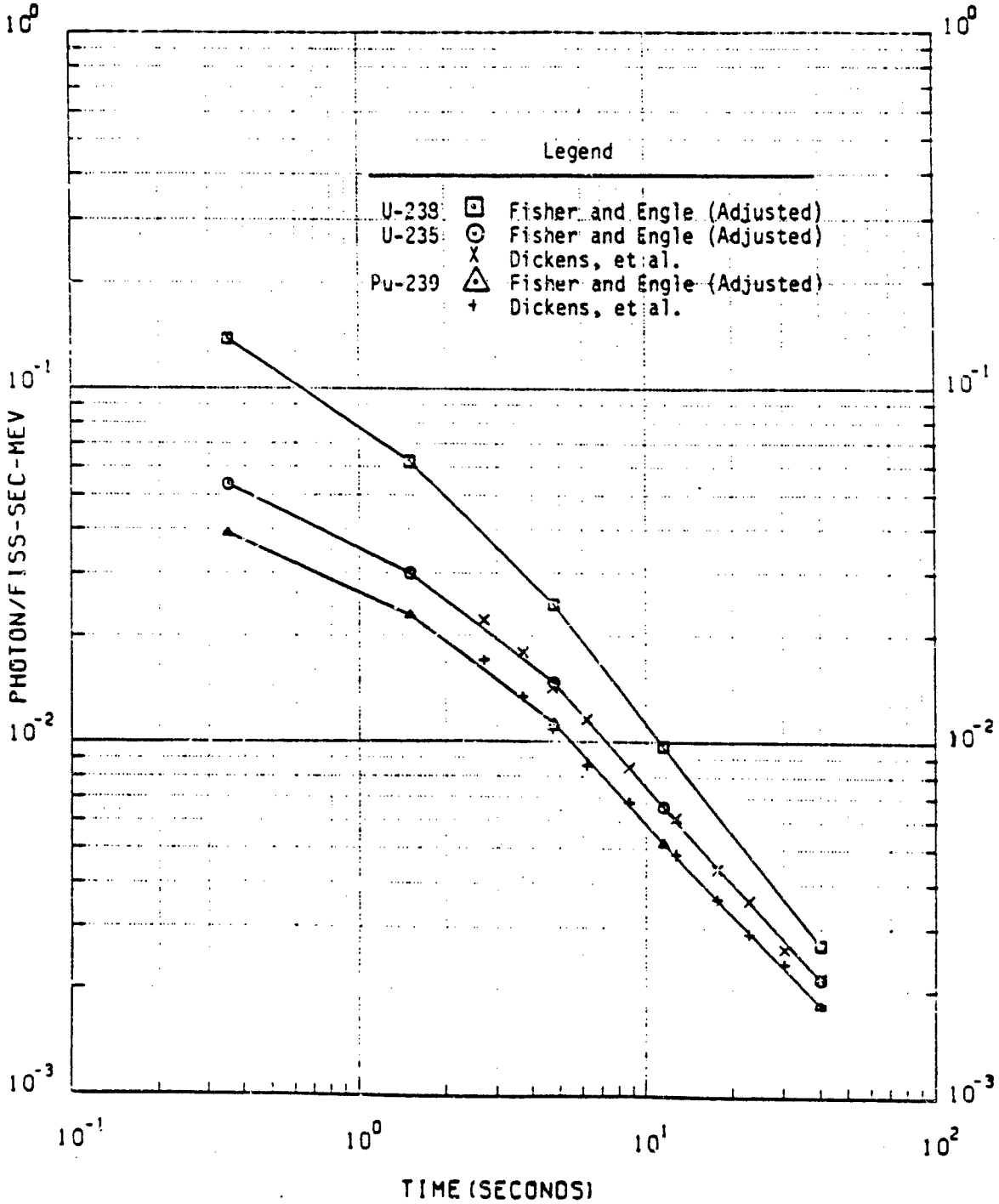

Figure 24. Fission product photon emission rates vs time, 1.81 < E ≤ 2.19 MeV, for U-235, U-239 and Pu-239.

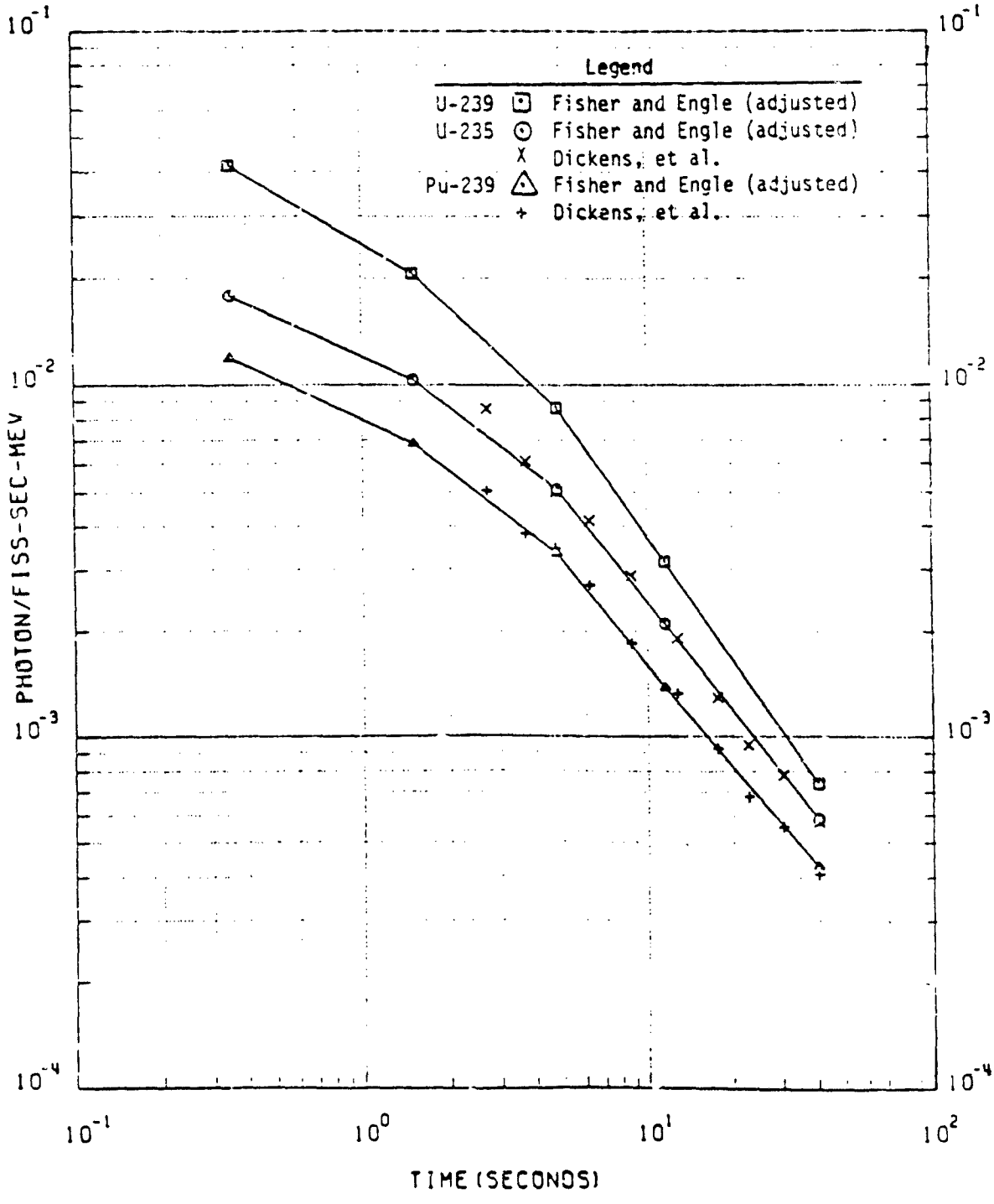

Figure 25. Fission product photon emission rates vs time, 3.11 < E ≤ 3.68 MeV, for U-235, U-239 and Pu-239.

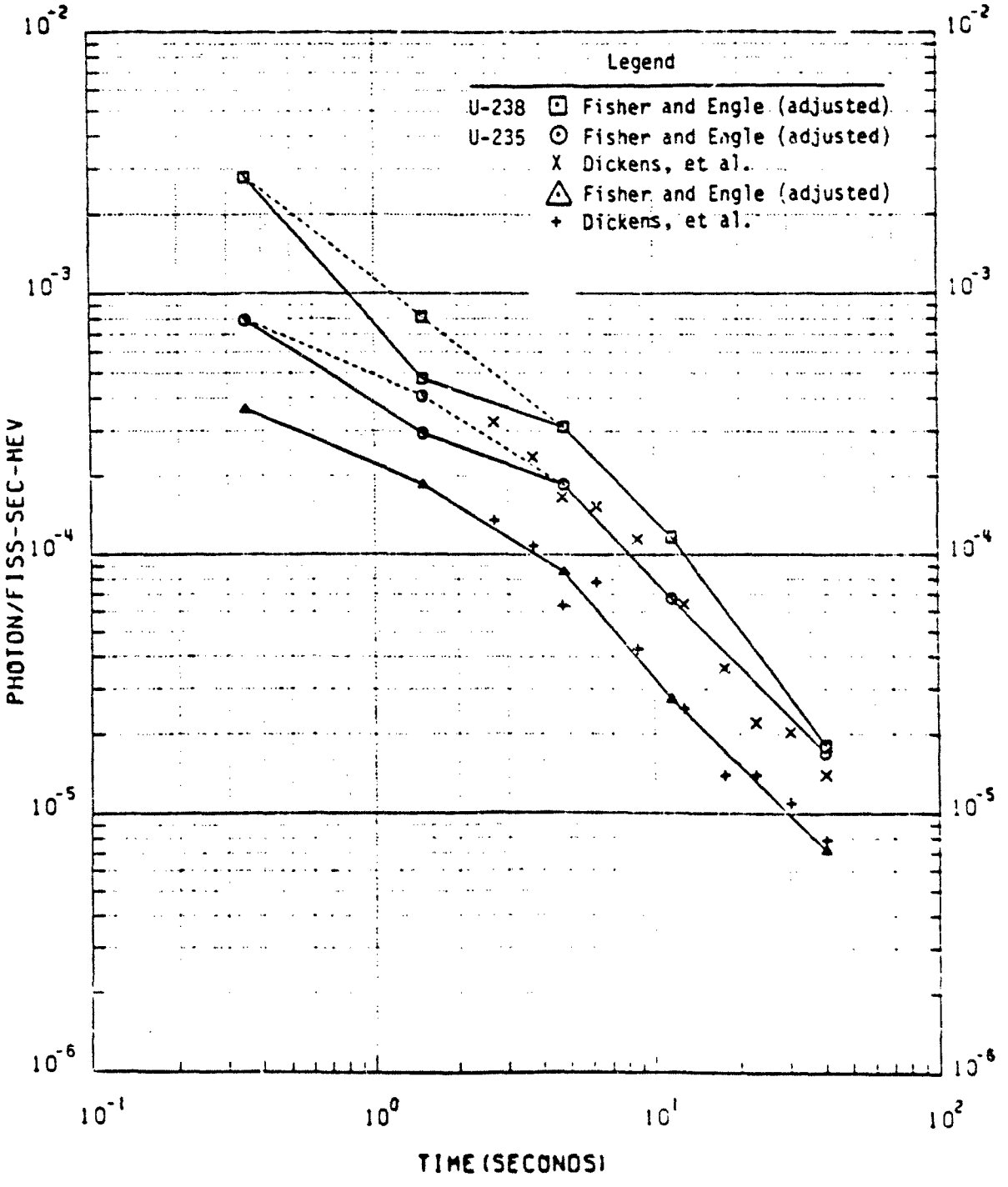

Figure 28. Fission product photon emission rates vs time, 5.64 < E ≤ 6.42 MeV, for U-235, U-239 and Pu-239.

Table 23. Fission product gamma ray source rate spectra for U-235 at mean times after fission of 0.35, 1.5, 4.75, 11.5 and 40 seconds.

Group No.	Upper Energy (MeV)	Gamma Rays/Fission-second-MeV				
		0.35	1.5	4.75	11.5	40.
1	14.0	0.0	0.0	0.0	0.0	0.0
2	10.0	0.0	0.0	0.0	0.0	0.0
3	8.0	5.50-5*	2.98-5	1.51-5	7.01-6	2.08-6
4	7.0	3.87-4	1.80-4	8.22-5	2.70-5	6.30-6
5	6.0	1.10-3	7.70-4	3.70-4	1.79-4	5.40-5
6	5.0	5.49-3	2.53-3	1.12-3	5.47-4	1.83-4
7	4.0	1.51-2	8.89-3	4.32-3	1.84-3	5.60-4
8	3.0	2.63-2	1.49-2	6.59-3	3.32-3	1.23-3
9	2.5	4.19-2	2.34-2	1.17-2	5.34-3	1.80-3
10	2.0	6.31-2	3.65-2	1.87-2	8.34-3	2.78-3
11	1.5	1.27-1	7.21-2	3.30-2	1.63-2	5.43-3
12	1.0	2.12-1	1.12-1	4.88-2	2.30-2	7.39-3
13	.70	2.66-1	1.61-1	8.90-2	3.91-2	9.20-3
14	.45	2.73-1	1.43-1	7.91-2	3.70-2	1.09-2
15	.30	4.08-1	1.85-1	1.08-1	5.06-2	1.35-2
16	.15	1.94-1	7.82-2	4.66-2	2.11-2	5.61-3
17	.10	0.0	0.0	0.0	0.0	0.0
18	.07	0.0	0.0	0.0	0.0	0.0
19	.045	0.0	0.0	0.0	0.0	0.0
20	.030	0.0	0.0	0.0	0.0	0.0
21	.020	0.0	0.0	0.0	0.0	0.0
	.010					

*read as $5.5*10^{-5}$.

Table 24. Fission product gamma ray source rate spectra for U-238 at mean times after fission of 0.35, 1.5, 4.75, 11.5 and 40 seconds.

Group No.	Upper Energy (MeV)	Gamma Rays/Fission-second-MeV				
		0.35	1.5	4.75	11.5	40.
1	14.0	0.0	0.0	0.0	0.0	0.0
2	10.0	0.0	0.0	0.0	0.0	0.0
3	8.0	1.26-4*	5.87-5	2.58-5	9.84-6	2.78-6
4	7.0	1.27-3	3.71-4	1.31-4	4.33-5	7.01-6
5	6.0	3.50-3	1.43-3	6.60-4	2.78-4	6.16-5
6	5.0	1.25-2	4.95-3	1.77-3	7.91-4	1.83-4
7	4.0	3.58-2	1.82-2	7.38-3	2.76-3	6.72-4
8	3.0	7.33-2	3.38-2	1.15-2	4.76-3	1.68-3
9	2.5	1.13-1	4.83-2	1.98-2	7.89-3	2.40-3
10	2.0	1.41-1	7.77-2	3.10-2	1.17-2	3.18-3
11	1.5	2.74-1	1.39-1	5.20-2	2.08-2	6.56-3
12	1.0	4.40-1	2.07-1	8.00-2	3.05-2	9.69-3
13	.70	5.61-1	2.80-1	1.44-1	5.30-2	1.35-2
14	.45	6.70-1	3.00-1	1.40-1	5.90-2	1.54-2
15	.30	9.99-1	4.01-1	2.07-1	7.38-2	2.00-2
16	.15	5.02-1	1.57-1	9.70-2	3.17-2	7.69-3
17	.10	0.0	0.0	0.0	0.0	0.0
18	.070	0.0	0.0	0.0	0.0	0.0
19	.045	0.0	0.0	0.0	0.0	0.0
20	.030	0.0	0.0	0.0	0.0	0.0
21	.020	0.0	0.0	0.0	0.0	0.0
	.010					

*read as $1.26*10^{-4}$.

Table 25. Fission product gamma ray source rate spectra for Pu-239 at mean times after fission of 0.35, 1.5, 4.75, 11.5 and 40 seconds.

Group No.	Upper Energy (MeV)	Gamma Rays/Fission-second-MeV				
		0.35	1.5	4.75	11.5	40.
1	14.0	0.0	0.0	0.0	0.0	0.0
2	10.0	0.0	0.0	0.0	0.0	0.0
3	8.0	4.56-5*	2.63-5	1.25-5	5.65-6	1.64-6
4	7.0	1.93-4	1.07-4	4.85-5	1.61-5	3.97-6
5	6.0	7.12-4	3.39-4	1.69-4	7.48-5	2.36-5
6	5.0	4.08-3	1.75-3	5.76-4	2.77-4	8.47-5
7	4.0	1.06-2	5.68-3	2.79-3	1.16-3	3.91-4
8	3.0	2.38-2	1.07-2	4.73-3	2.40-3	1.02-3
9	2.5	3.31-2	1.74-2	8.55-3	4.03-3	1.52-3
10	2.0	4.86-2	2.81-2	1.52-2	6.79-3	2.15-3
11	1.5	9.73-2	6.00-2	2.50-2	1.20-2	4.01-3
12	1.0	1.70-1	9.17-2	3.95-2	1.79-2	5.68-3
13	.70	2.43-1	1.68-1	8.06-2	3.27-2	7.58-3
14	.45	2.34-1	1.42-1	6.80-2	3.28-2	9.31-3
15	.30	3.57-1	1.82-1	9.91-2	4.63-2	1.08-2
16	.15	1.77-1	7.45-2	4.27-2	1.77-2	4.40-3
17	.10	0.0	0.0	0.0	0.0	0.0
18	.070	0.0	0.0	0.0	0.0	0.0
19	.045	0.0	0.0	0.0	0.0	0.0
20	.030	0.0	0.0	0.0	0.0	0.0
21	.020	0.0	0.0	0.0	0.0	0.0
	.010					

*read as $4.56*10^{-5}$.

Table 26. Fast/thermal fission product gamma ray energy emission ratios.

Calculated Using ENDF/B-V

Time (sec)	Nuclide U235	Pu239
0.1	1.049	1.072
1.0	1.062	1.062
5.0	1.025	1.037
10.0	1.004	1.029
20.0	0.993	1.020

Calculated by England and Schenter

0.1	1.038	0.945
1.0	1.067	0.986
5.0	1.052	1.002
10.0	1.032	0.997
20.0	1.020	1.002
50.0	1.018	1.019

No action was taken to correct the source for the fast-thermal fission effect at the time the corrections were made to the Fisher and Engle source data. This was due to questions regarding the accuracy of calculations using individual nuclide data. Those questions were apparently well founded, at least for Pu239, based on the more recent analysis of England and Schenter (Ref. 19), data from which also appear in Table 26. The ATR5 delayed gamma ray energy emission source rates are taken from England and Schenter data applicable to fast neutron fission.

GAMMA RAY TRANSPORT.

The capability of current codes and cross sections to model gamma ray transport in uniform air was tested using BREN Co-60 source-measurement data (Ref. 28) as shown in Figure 27. Those calculations were performed for a source 343m above ground using the two-dimensional discrete ordinate code DOT (Ref. 25) with the 36 energy group Vitamin C cross section set (Ref. 48). Ideally, it would be desirable to use the DOT code to calculate the delayed radiation transport. However, because the debris/fireball/ ground geometry is dynamic, it would require thirty or more separate calculations to adequately represent the propagation of delayed radiation from any given weapon burst. Therefore, an alternative method has been found which provides a more practical approach to the problem. According to this approach the gamma ray transport is modeled in a one-dimensional system of uniform air. The amount of air along a line from the debris (the gamma ray source) to the target at a specific time is determined using a hydrodynamic model, which will be discussed later in this section. The energy and angle-differential fluence rate at the target is determined for the time-specific source rate spectrum transported through an identical thickness of air, using the uniform air transport data base. This uniform-for-perturbed air substitution is a good approximation for gamma rays, the transport of which is dominated by absorption and forward scattering.

An early version of the one-dimensional uniform air data base was taken from the Air Transport of Radiation (ATR) code (Ref. 33). These data were shown to be in error when compared with those generated using the more recent Vitamin C cross sections as shown in Figure 2i . The current data base has been developed using the latest cross section set, Vitamin E (Ref. 60), the results from which agree well with those calculated using Vitamin C, as shown in Figure 28.

A single one-dimensional, uniform air gamma ray transport data base has been developed to serve prompt and delayed applications. Calculations of gamma ray energy and angle-differential fluence as a function of distance through 550 grams/cm^2 or approximately 5000 meters have been performed for sources in each of the 38 Vitamin E energy groups, as shown in Table 27. The calculations were performed using a S_{40} quadrature and a P_3 Legendre scattering representation. The results of the calculations have been collapsed into the 18 gamma ray energy group, structure common to ATR5. That structure is also shown in Table 27. The collapsing procedure has been performed using a gamma ray source spectrum inversely proportions to energy. The effect of the ground on gamma ray transport is accounted for using the correction factor approach described in the body of this report.

NUCLEAR WEAPON HYDRODYNAMICS.

A schematic representation of nuclear weapon hydrodynamics, exclusive of fireball rise, is given in Figure 29. In an air-ground environment the initial air shock wave created by the rapid expansion of hot gasses around the weapon reflects off the ground and rises after the initial wave, forming the Mach stem, in which the initial and reflected shock unite.

Observations of field tests and small scale high explosive experiments have been used to develop large empirical and semi-empirical models of weapon hydrodynamics. These are embodied in computer codes which are by and large too cumbersome for use in conjunction with transport data for delayed gamma ray modeling. However, small codes which scale data generated by more complex codes have been developed. STLAMB (Ref 9) a more recent variant of the Low Altitude Multi Burst (LAMB) code developed by Needham and Wittwer (Ref. 43) is one of these. This code interpolates between and extrapolates from hydrodynamic data obtained from model calculations for one kiloton and one megaton yields in uniform air. It accounts for the presence of the ground and, hence, the reflected shock by means of an image burst below the ground plane. STLAMB is used as the hydrodynamic model in the delayed gamma radiation system used to calculate survivor air density profiles as a function of time and computes the amount of air between source and detector. It also calculates cloud rise.

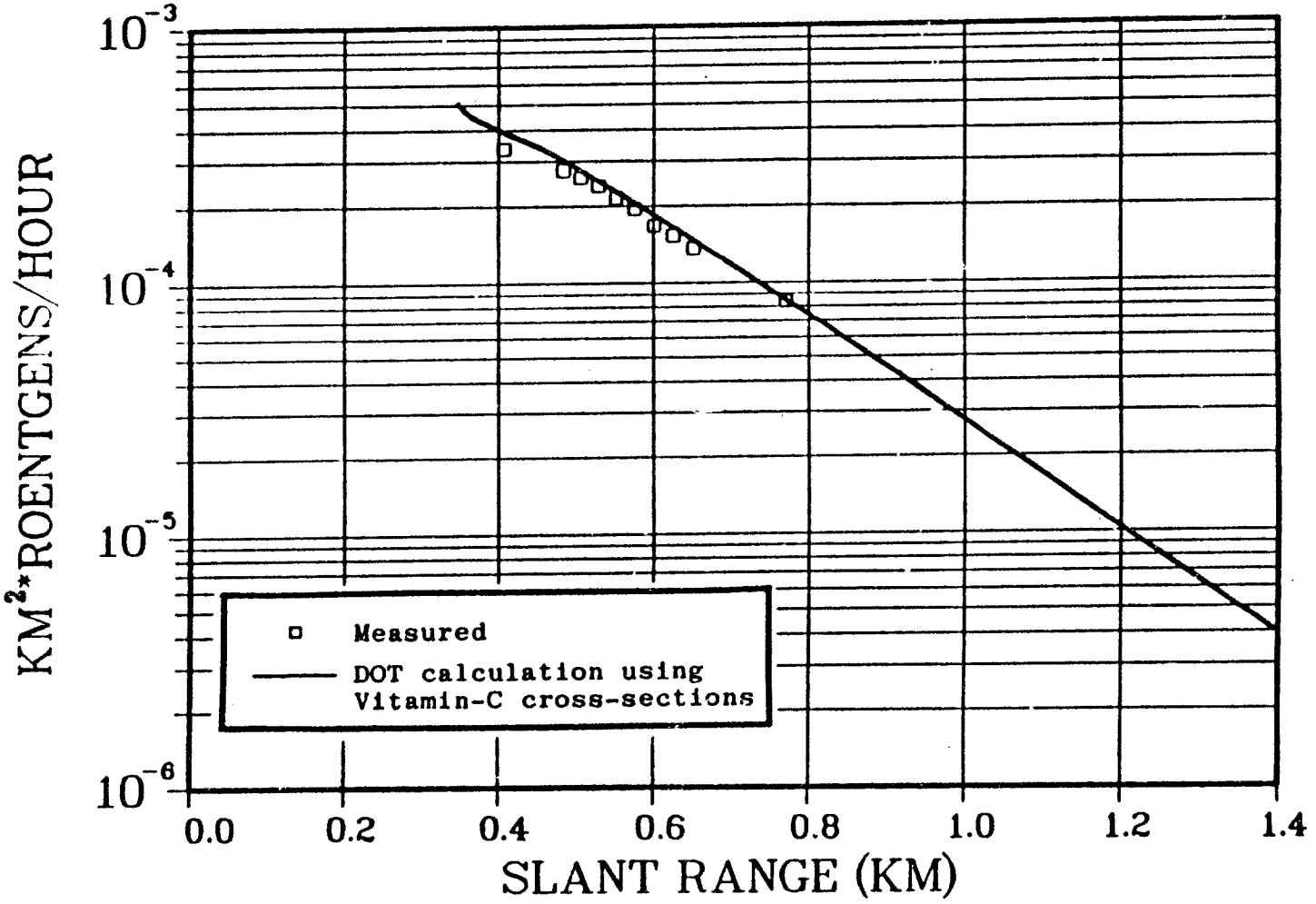

Figure 27. Bren Co-60 dose at 1 m detector height.

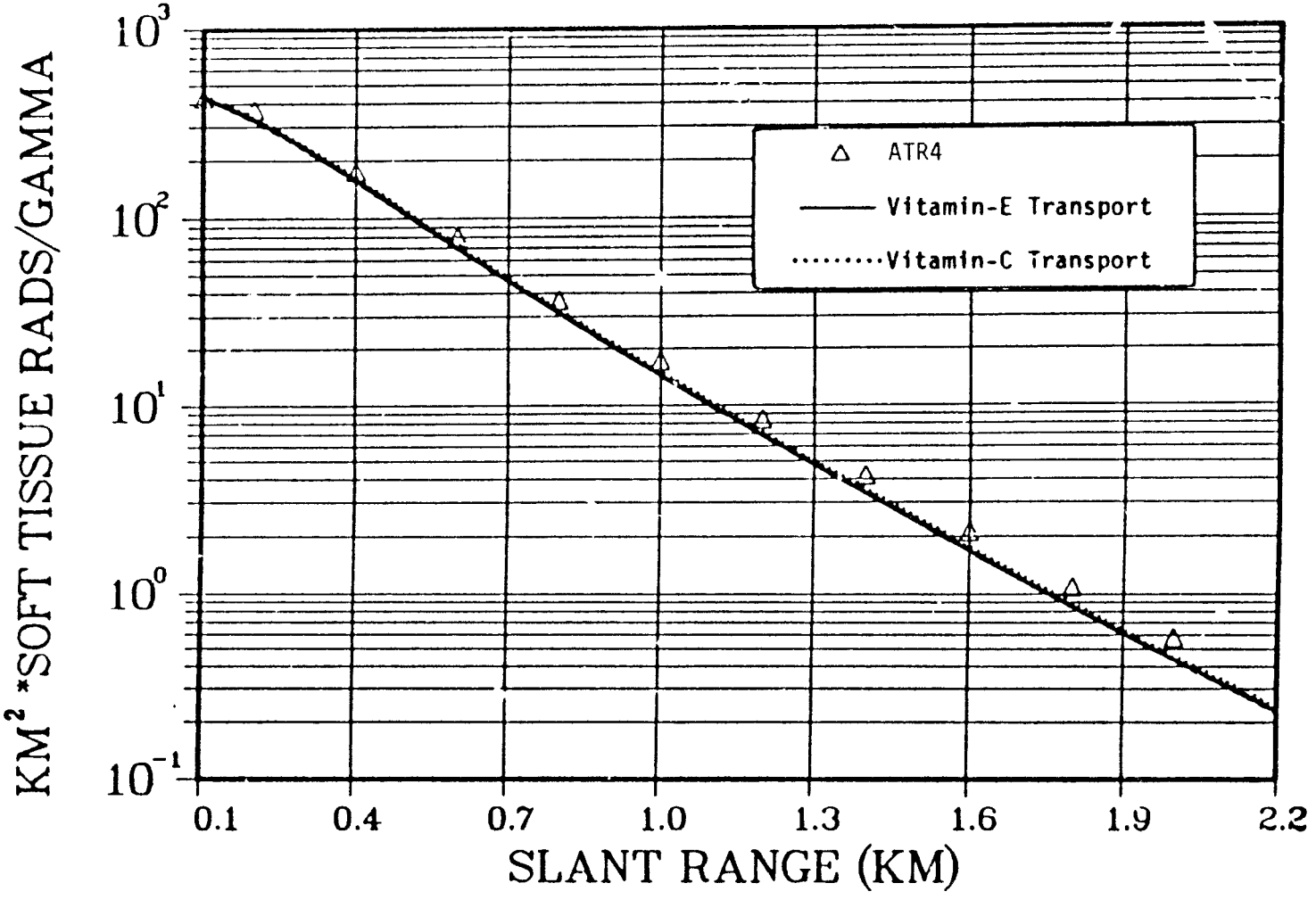

Figure 28. Uniform air tissue kerma from a Fisher and Engle U-235 gamma ray source at one second.

Table 27. Vitamin E and ATR5 gamma ray cross section library energy group structures.

	Upper Energy (MeV)	Vitamin E Group No.	ATR5 Group No.
	2.00+1*	1	
	1.40+1	2	
	1.20+1	3	18**
	1.00+1	4	17
	8.00+0	5	16
	7.50+0	6	
	7.00+0	7	15
	6.50+0	8	
	6.00+0	9	14
	5.50+0	10	
	5.00+0	11	13
	4.50+0	12	
	4.00+0	13	12
	3.50+0	14	
	3.00+0	15	11
	2.50+0	16	10
	2.00+0	17	9
	1.66+0	18	
	1.50+0	19	8
	1.33+0	20	
	1.00+0	21	7
	8.00-1	22	
	7.00-1	23	6
	6.00-1	24	
	5.12-1	25	
	5.10-1	26	
	4.50-1	27	5
	4.00-1	28	
	3.00-1	29	4
	2.00-1	30	
	1.50-1	31	3
	1.00-1	32	2
	7.50-2	33	
	7.00-2	34	
	6.00-2	35	
	4.50-2	36	1
	3.00-2	37	
	2.00-2	38	
Lower Bound	1.00-2	28	

*Read as $2.0*10^{1}$.

**ATR energies are numbered from low to high energy.

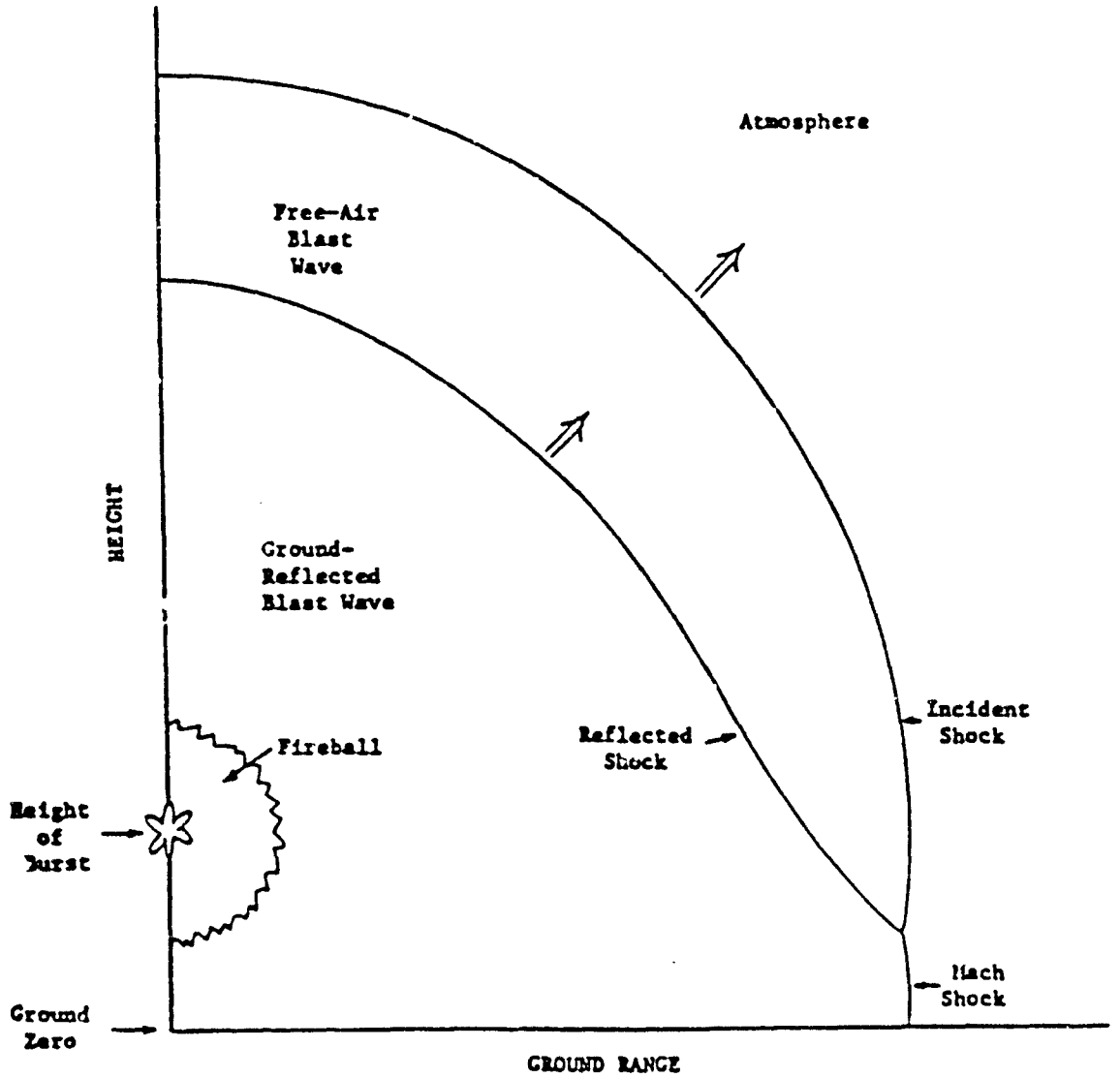

Figure 29. Principal physical features of a nuclear blast wave reflected from a plane ground surface.

Figures 30 through 36 show the development of the system of hydrodynamically perturbed air surrounding a burst at 110 meters scaled height of burst (Burst height + yield $^{1/3}$) as modeled using STLAMB. Time-dependent gamma ray KERMA measurements were made on an equivalent test (Ref. 11), which can be used to help validate the delayed gamma ray model. The development of the weapon hydrodynamic process includes a spherical density well which is later perturbed by the reflected shock front. By 1 second the reflected shock is shown to be passing through the approximate center of the original fireball region. Thereafter, the shock moves rapidly above the now rising fireball, which eventually forms a toroid shaped system and moves well above its starting point.

Figures 37 through 44 show a similar progression for a burst at 73 meters scaled height of burst, also a subject of gamma ray KERMA rate measurements, along with that of a very similar shot (71 meters SHOB). In this case the reflected shock is moving back through the fireball less than a tenth of a second after its initiation. By a second it has passed entirely through the fireball. It is shown to proceed to form a torus similar to that of 110m SHOB shot.

These depictions of density profiles have been created with data from STLAMB and, thus, are the basis for determining the thickness and length of the transport path from source to detector. STLAMB also computes the altitude of the highest temperature in the system, which may be associated with the debris. However, the debris is probably distributed over a larger volume within the fireball. In fact, observations of field tests suggest that the debris actually flows within the fireball, at to the top, later down the sides and, finally, into the torus and skirt. Unfortunately, there are not sufficient data to construct a model of this cloud geometry-debris location system on the basis of actual observations. Thus, the present delayed radiation model has been developed under the assumption that the debris resides at the altitude of the hot spot but at a point on the centerline of the system rather than distributed as a sphere or torus. This assumption has been made to simplify the calculation process and to keep the running time of the computer model at a reasonable level. However, the effect of moving the source to other locations has been examined. Calculations have been made for debris locations on the centerline but *high*, 0.8 of the fireball radius above the fireball center and *low*, 0.8 of the fireball radius below the fireball center. Calculations using these alternative, though not necessarily realistic, debris location have been made for comparison with experimental measurements and to determine the sensitivity of delayed gamma ray fields to such perturbations.

Calculations of time-varying exposure rates (roentgen per second) as measured by shielded ionization chambers (Conrad devices) have been performed using the revised Fisher and Engle source values, transport methods as previously described and STLAMB hydrodynamic modeling. The ionization chambers were located near the center of 25 inch lengths of steel pipe oriented vertically above the ground. The outside diameter of the pipe was 5.5 inches and the sides were 3/16 inch thick. Monte Carlo calculations were performed using the pipe-ground geometry system to obtain the adjoint leakage from the detector, which could be convoluted with the free field fluence to obtain the exposure as measured by the ionization chambers. The energy dependent response of the ionization chamber was taken to be that described by Ehrlich (Ref. 16) and depicted along with those for other detector types, relative to fluence-to-roentgen conversion, in Figure 45. The preferential shielding of low energy photons, along with the rapid drop of detector response at low photon energies, tends to remove the excess low energy fluence component present in the free field as described previously. Results have been obtained for the source located at the hot spot altitude and for the two variants described previously.

Figures 46 through 52 present exposure rate measurement and calculation results for the 110m SHOB shot for horizontal distances from 457 to 3261 km. Figures 53 through 58 present results for the 73m SHOB shot for horizontal distances from 457 to 2780 m. Results are presented in terms of exposure rate x time. This is done to reduce the range of numerical values for plotting. Data corresponding to the *nominal* or hot spot location is depicted using a *heavy solid line*. That corresponding to the *low* source location is depicted using the *dotted line*, that for the *high* using the *dashed line*. The *light solid line* depicts a case in which the effect of the ground reflection of the shock is removed, which is the equivalent of the model used in ATR and which will be discussed later.

(SOLID POINT IS DEBRIS SOURCE LOCATION)

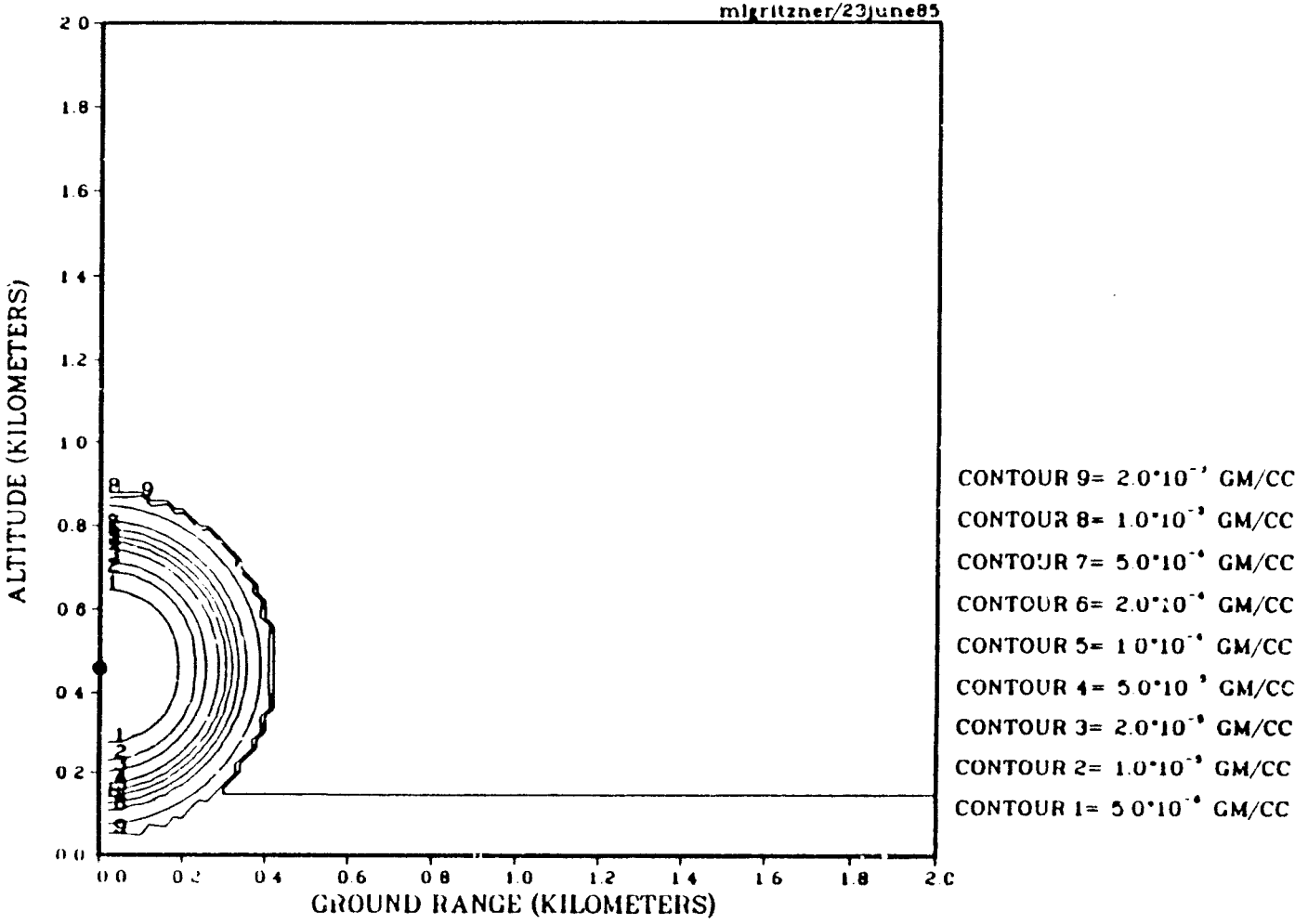

Figure 30. Air density iso-contours, 110m SHOB at 0.221 seconds.

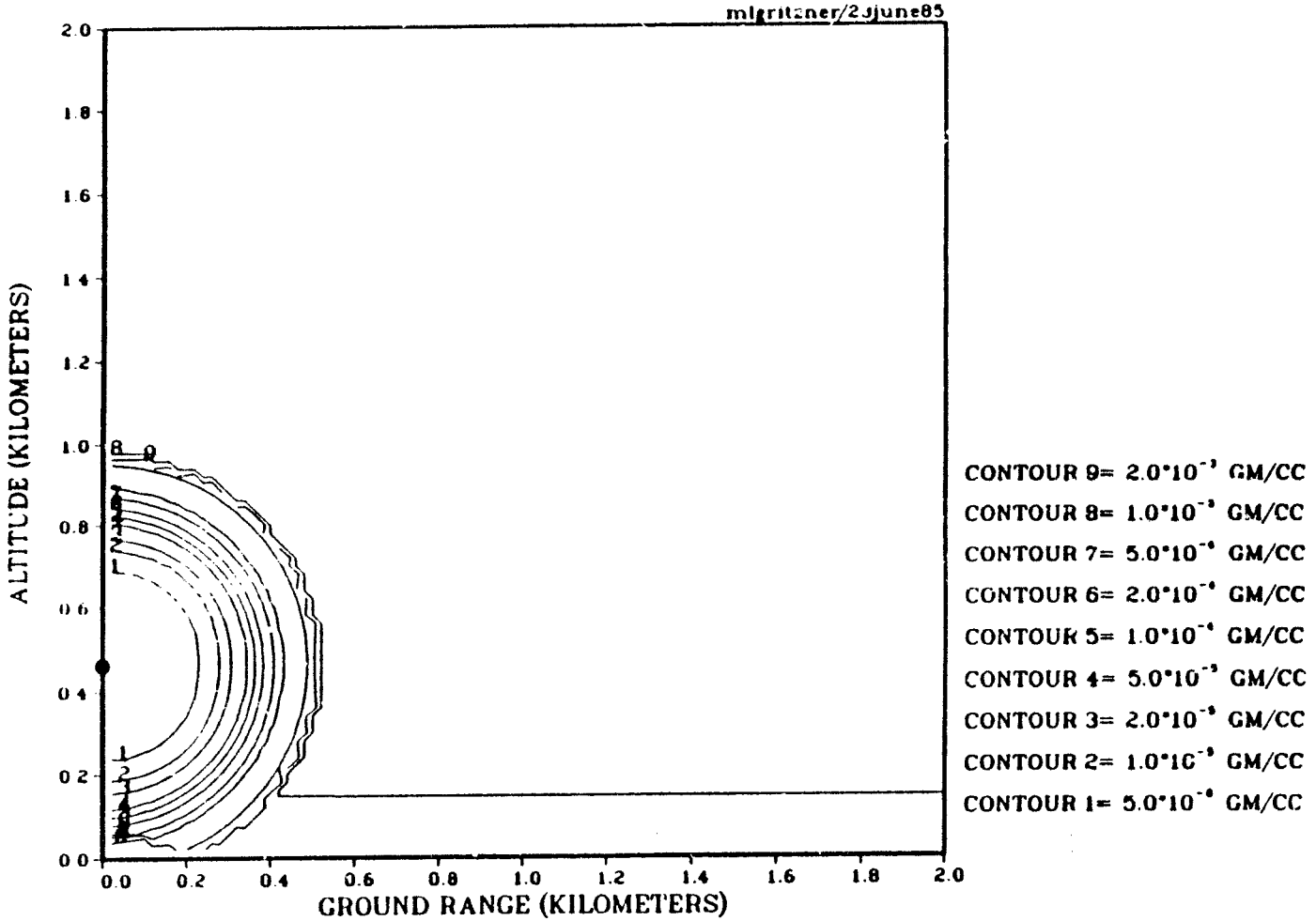

Figure 31. Air density iso-contours, 110m SHOB at 0.354 seconds.

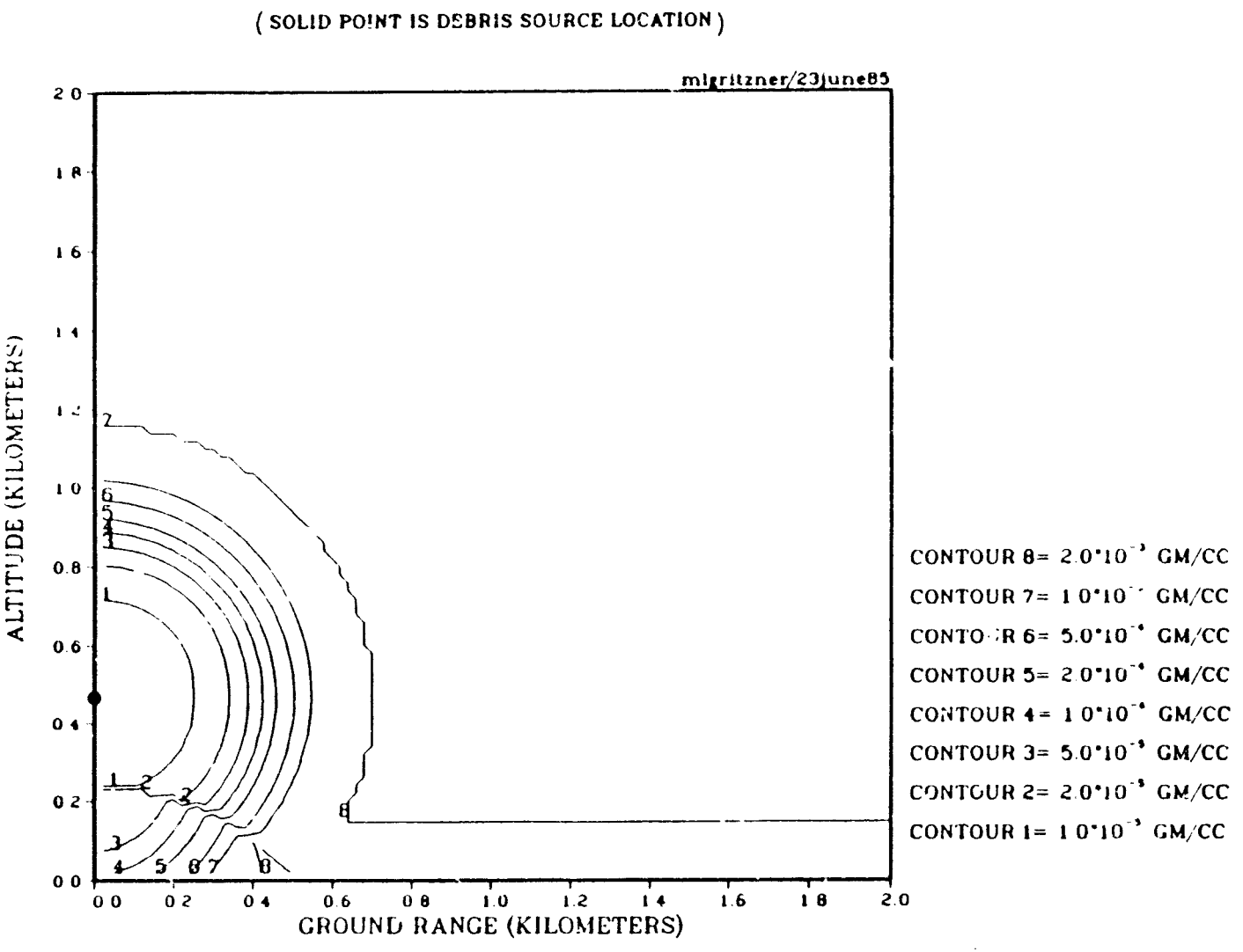

Figure 32. Air density iso-contours, 110m SHOB at 0.662 seconds.

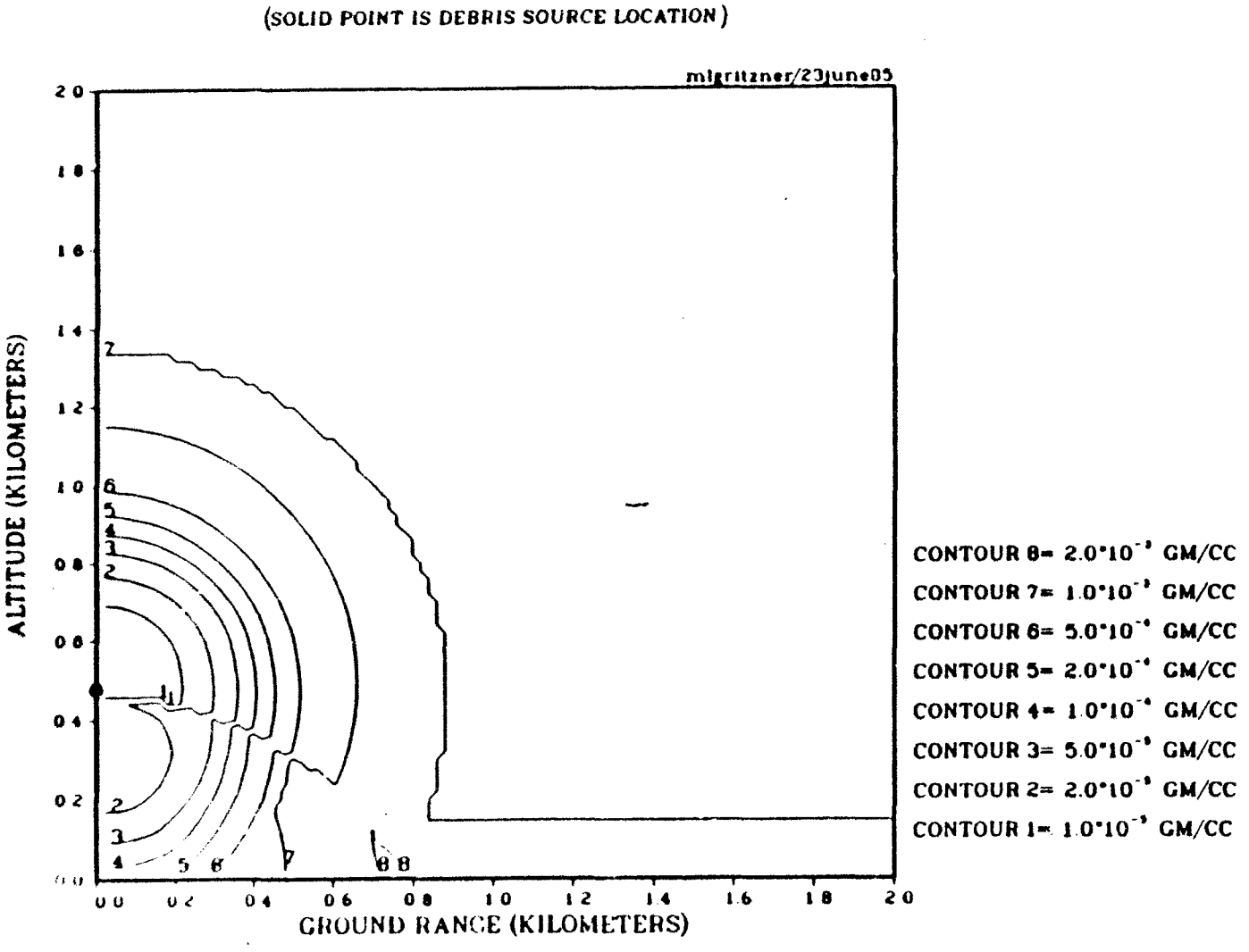

Figure 33. Air density iso-contours, 110m SHOB at 1.034 seconds.

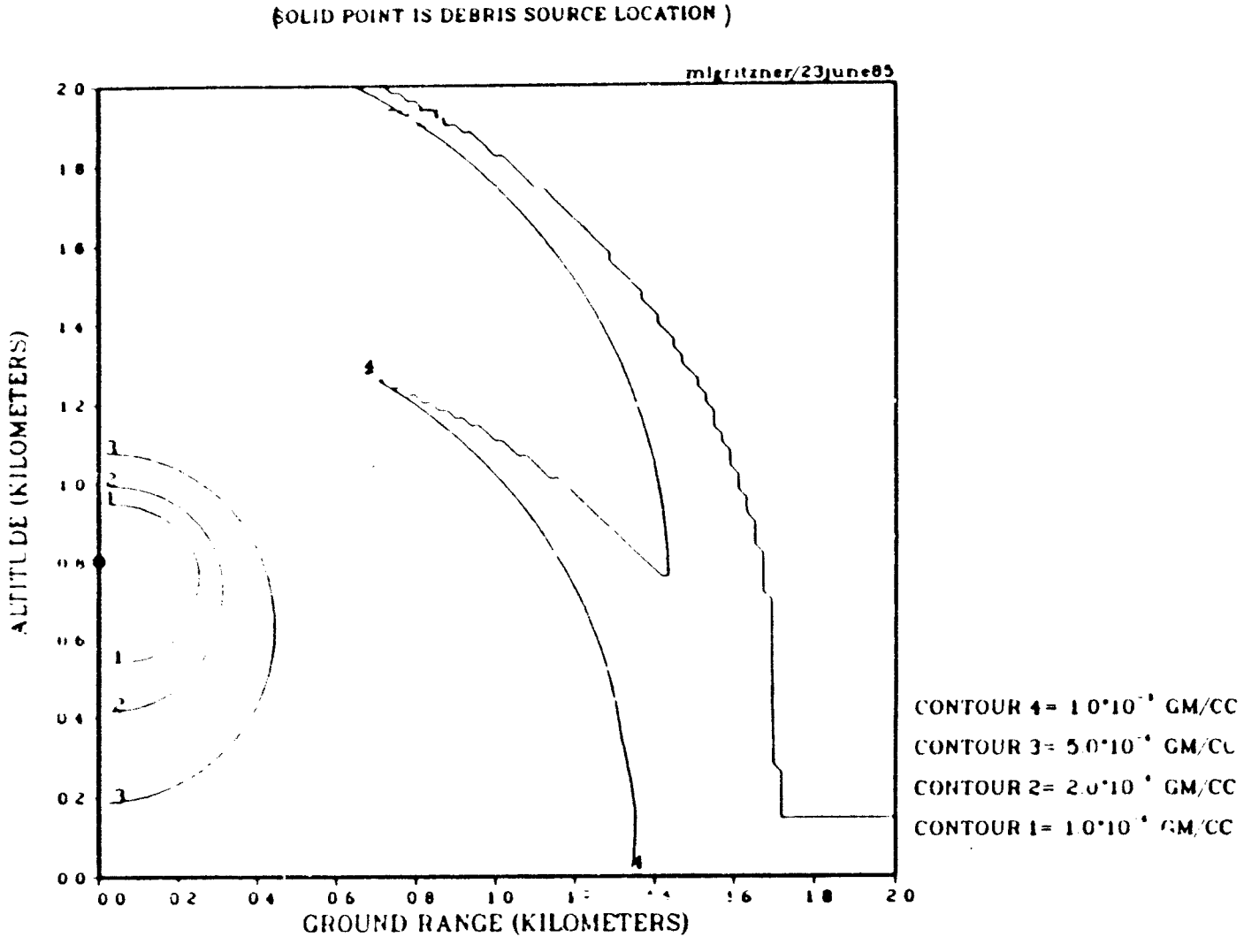

Figure 34. Air density iso-contours, 110m SHOB at 3.067 seconds.

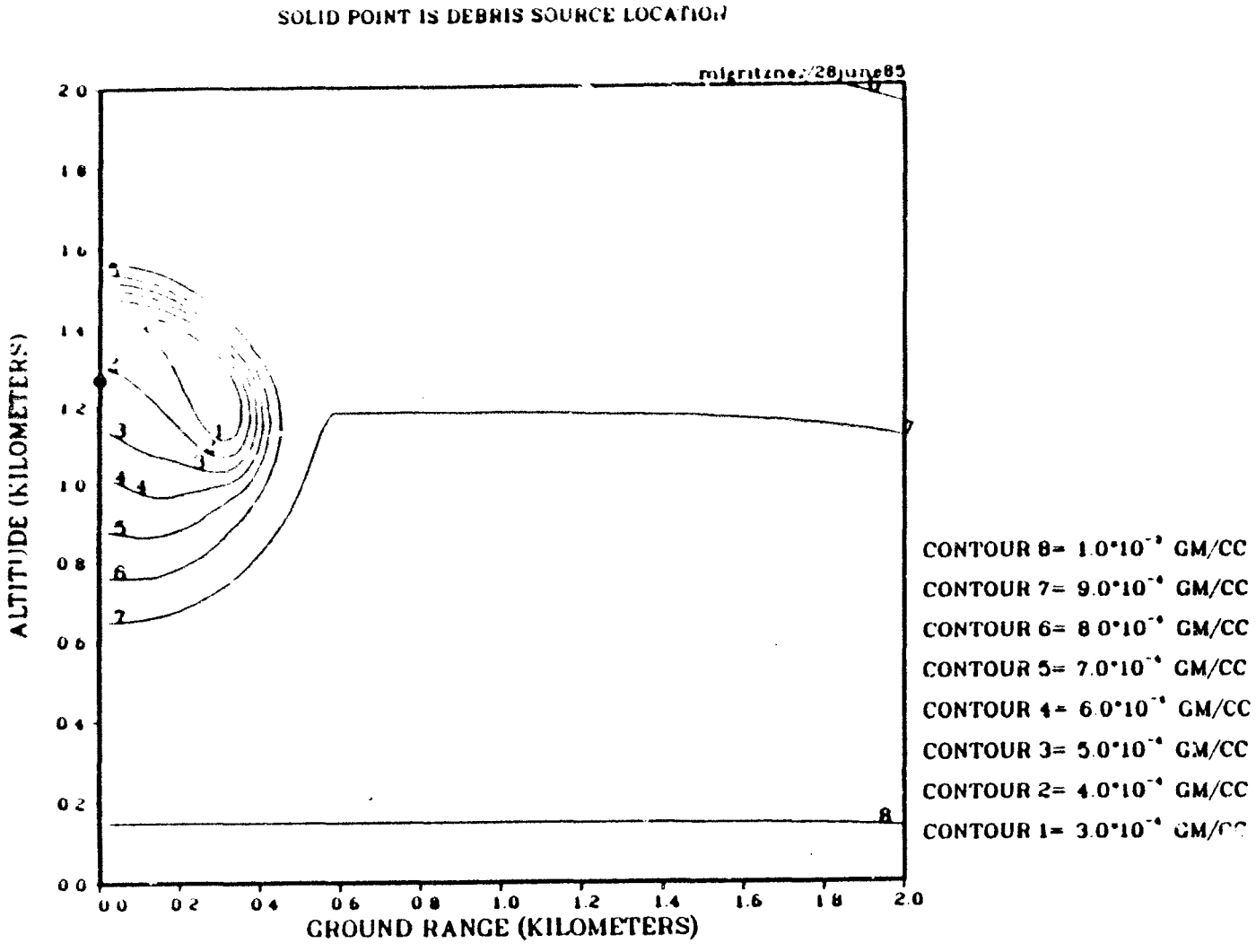

Figure 35. Air density iso-contours, 110m SHOB at 9.725 seconds.

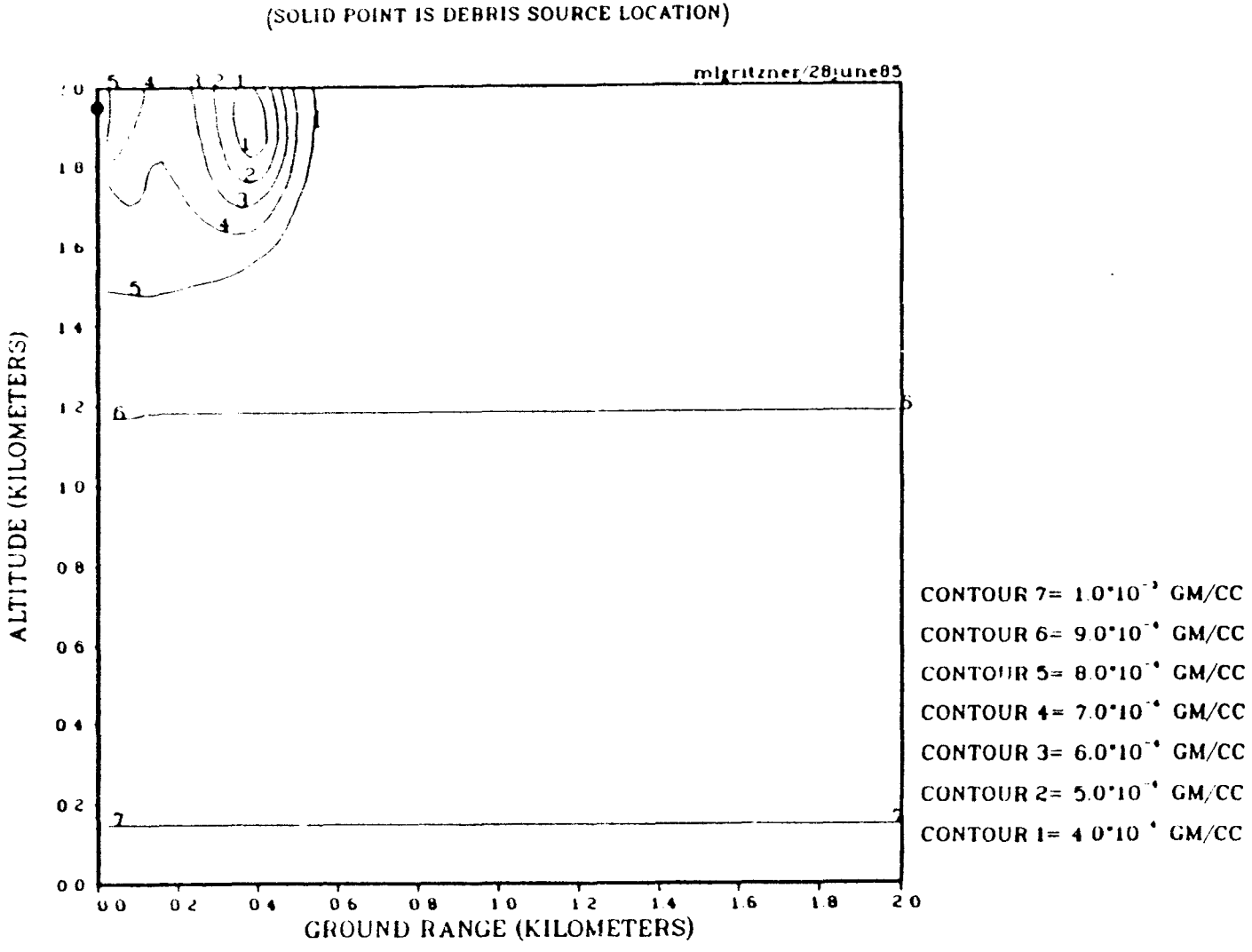

Figure 38. Air density iso-contours, 110m SHOB at 20.004 seconds.

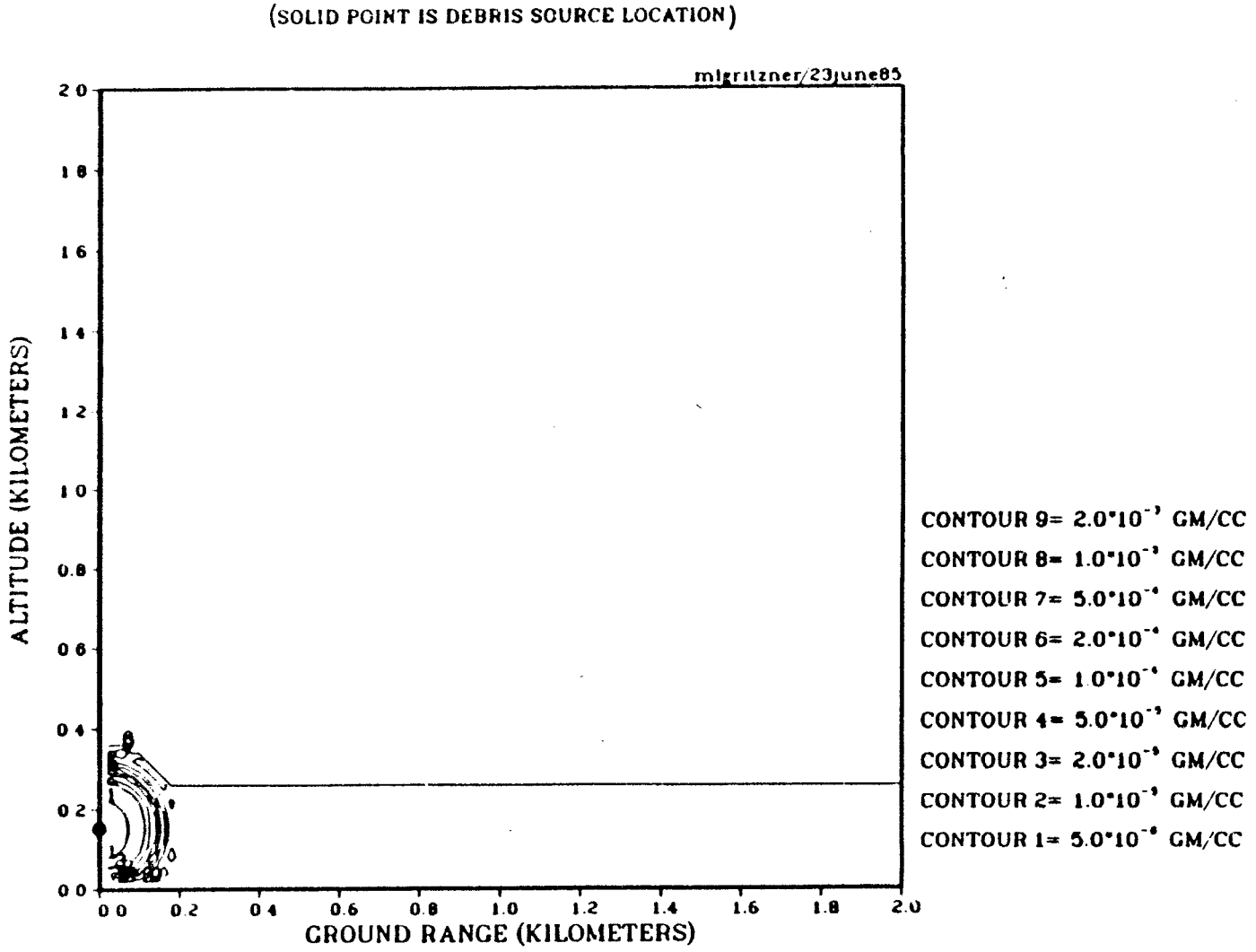

Figure 37. Air density iso-contours, 73m SHOB at 0.100 seconds.

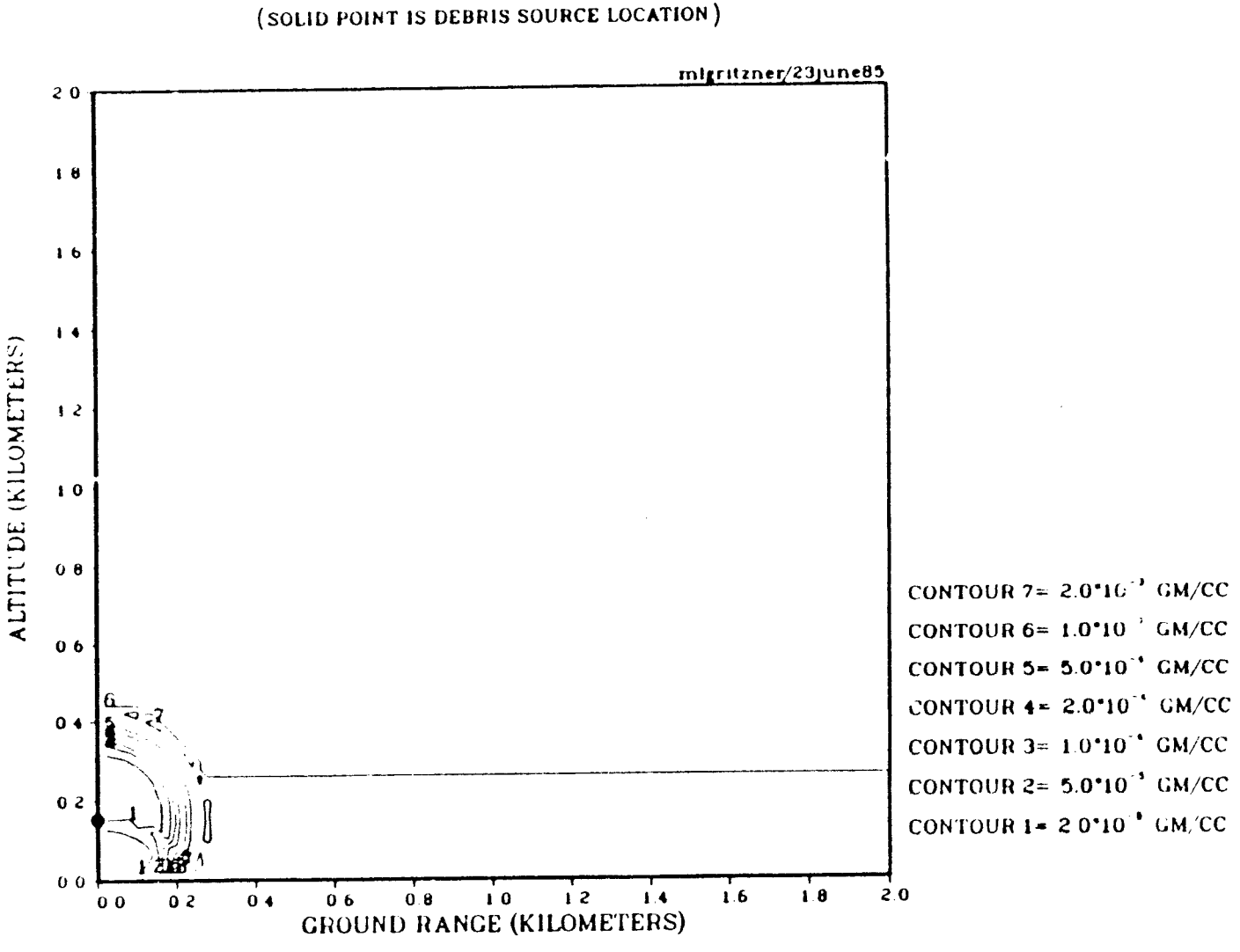

Figure 38. Air density iso-contours, 73m SHOB at 0.221 seconds.

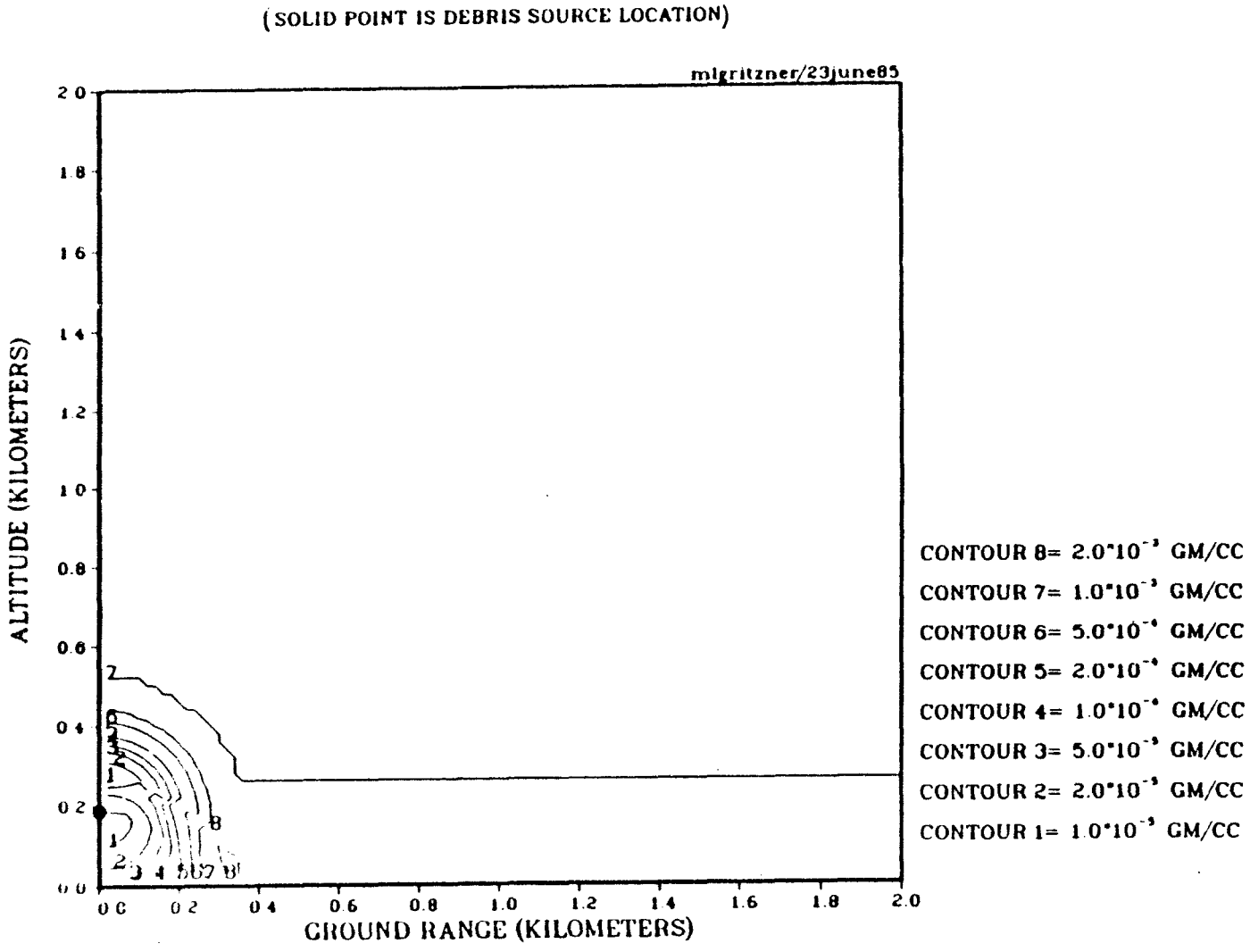

Figure 39. Air density iso-contours, 73m SHOB at 0.354 seconds.

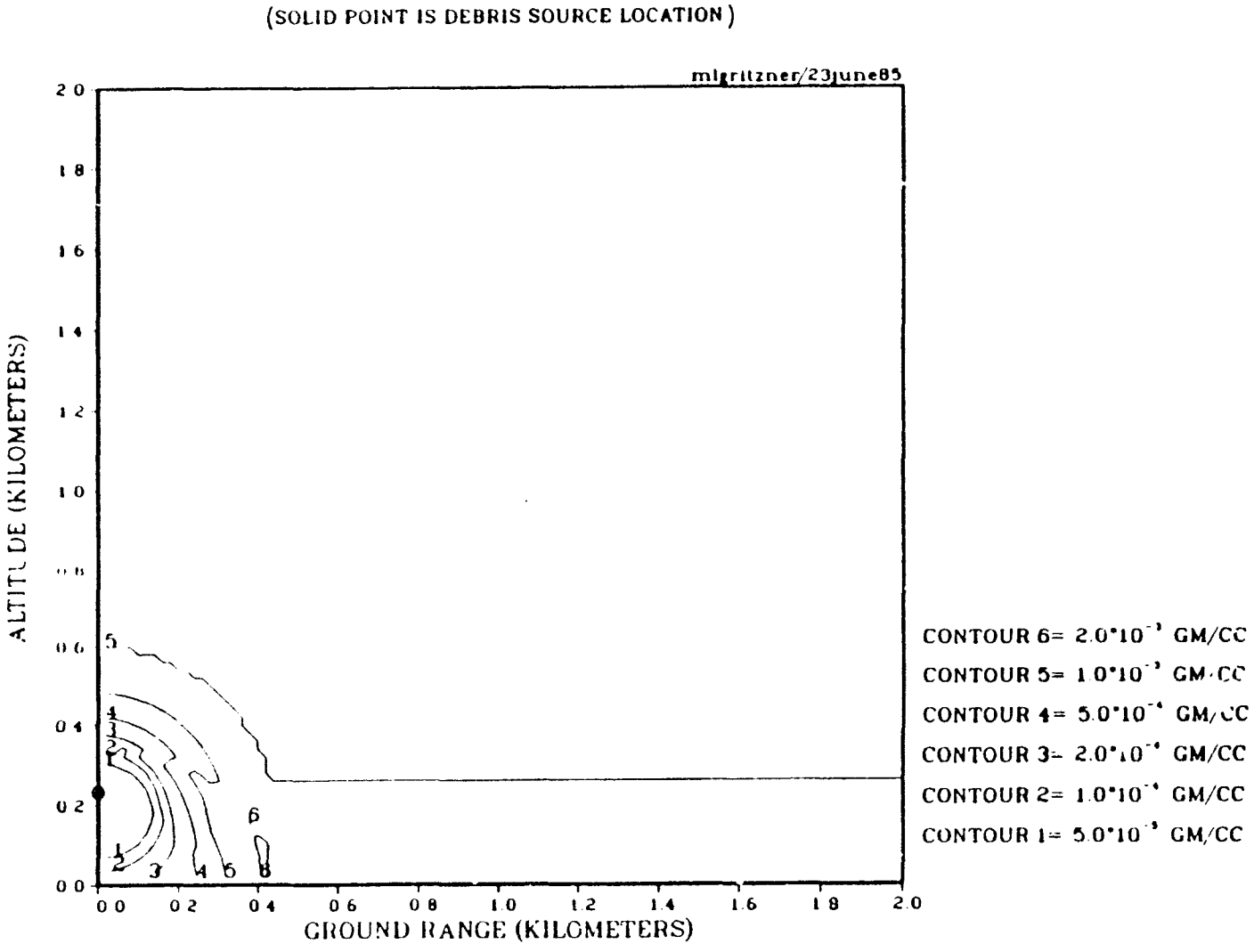

Figure 40. Air density iso-contours, 73m SHOB at 0.501 seconds.

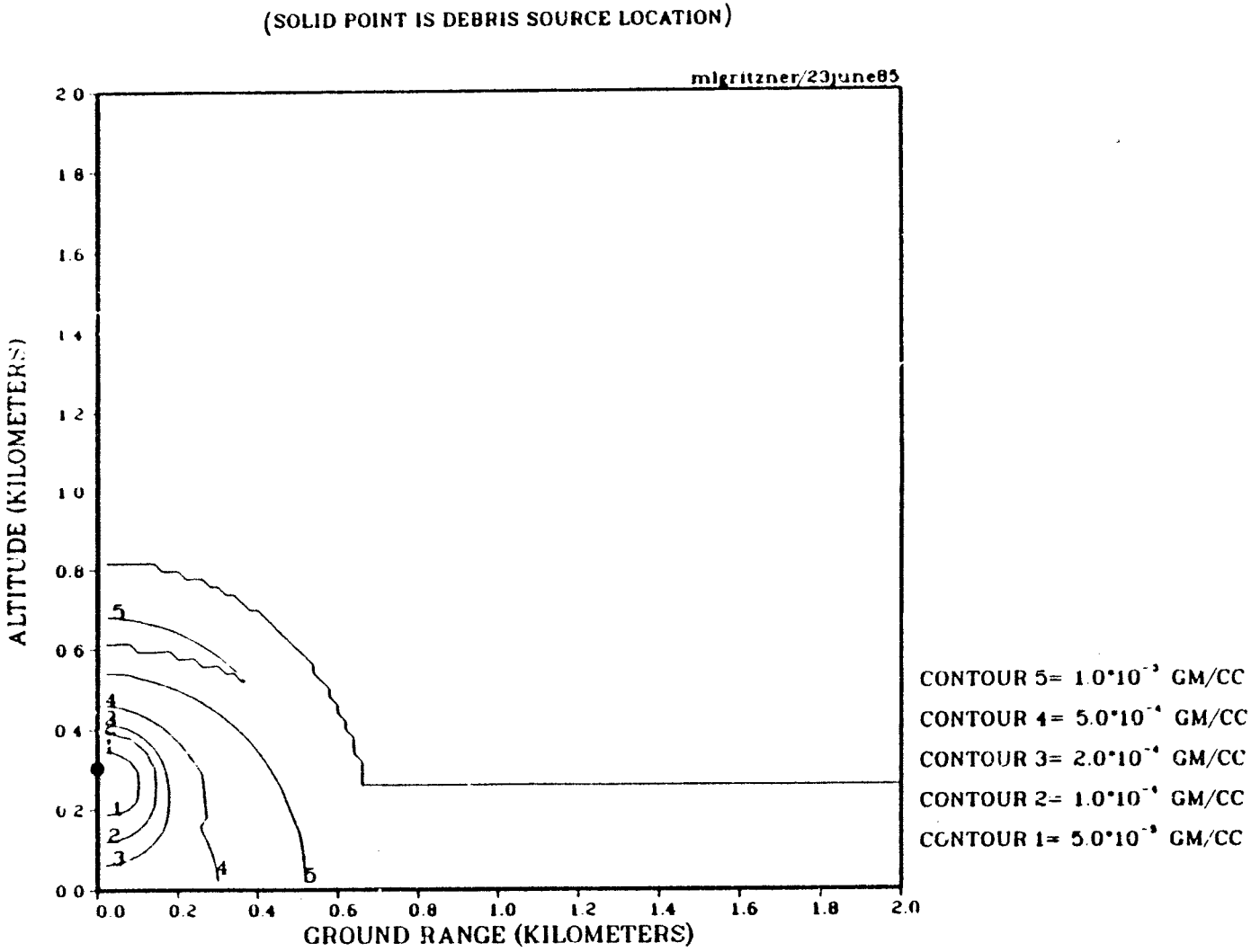

Figure 41. Air density iso-contours, 73m SHOB at 1.034 seconds.

(SOLID POINT IS DEBRIS SOURCE LOCATION)

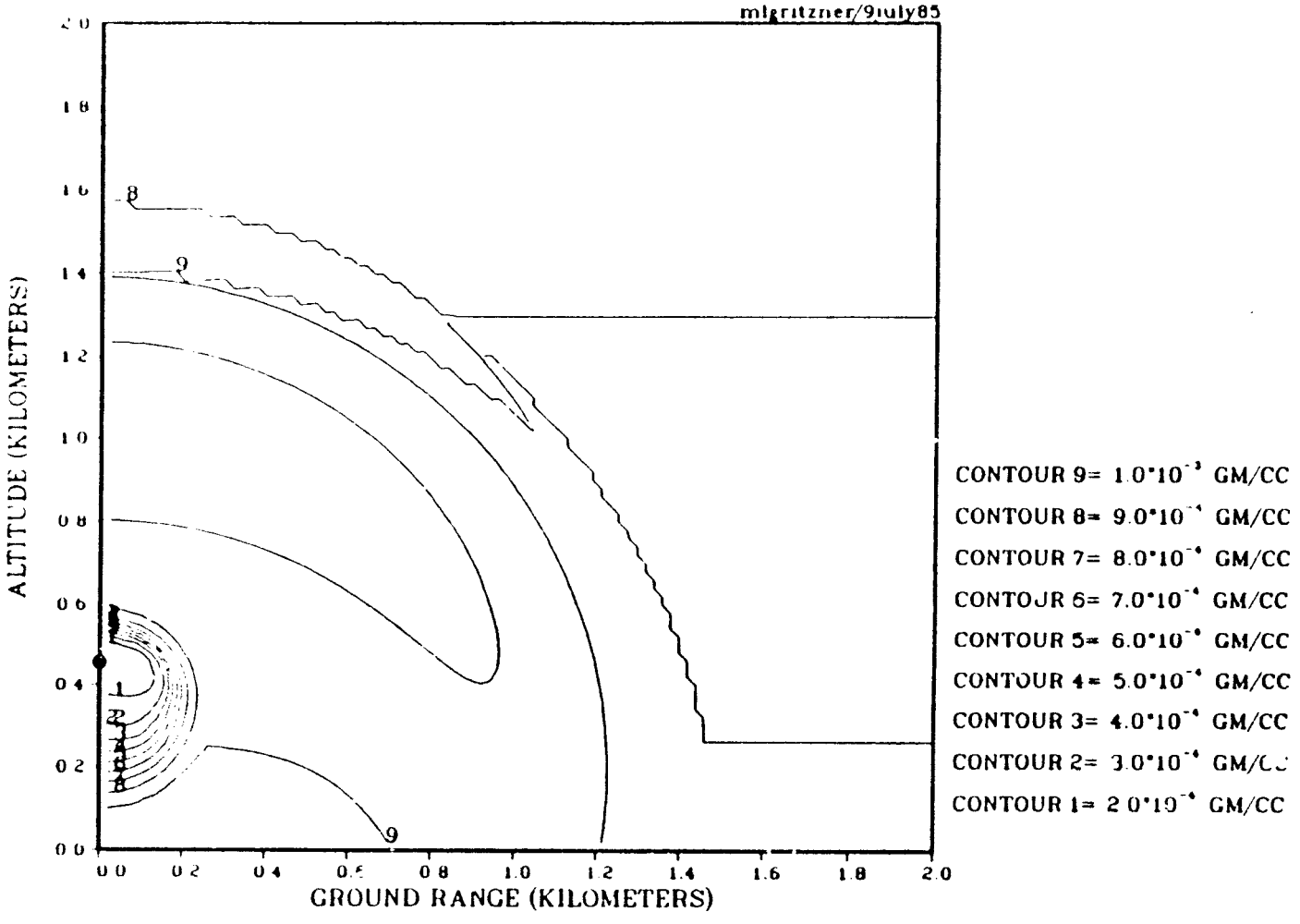

Figure 42. Air density iso-contours, 73m SHOB at 3.067 seconds.

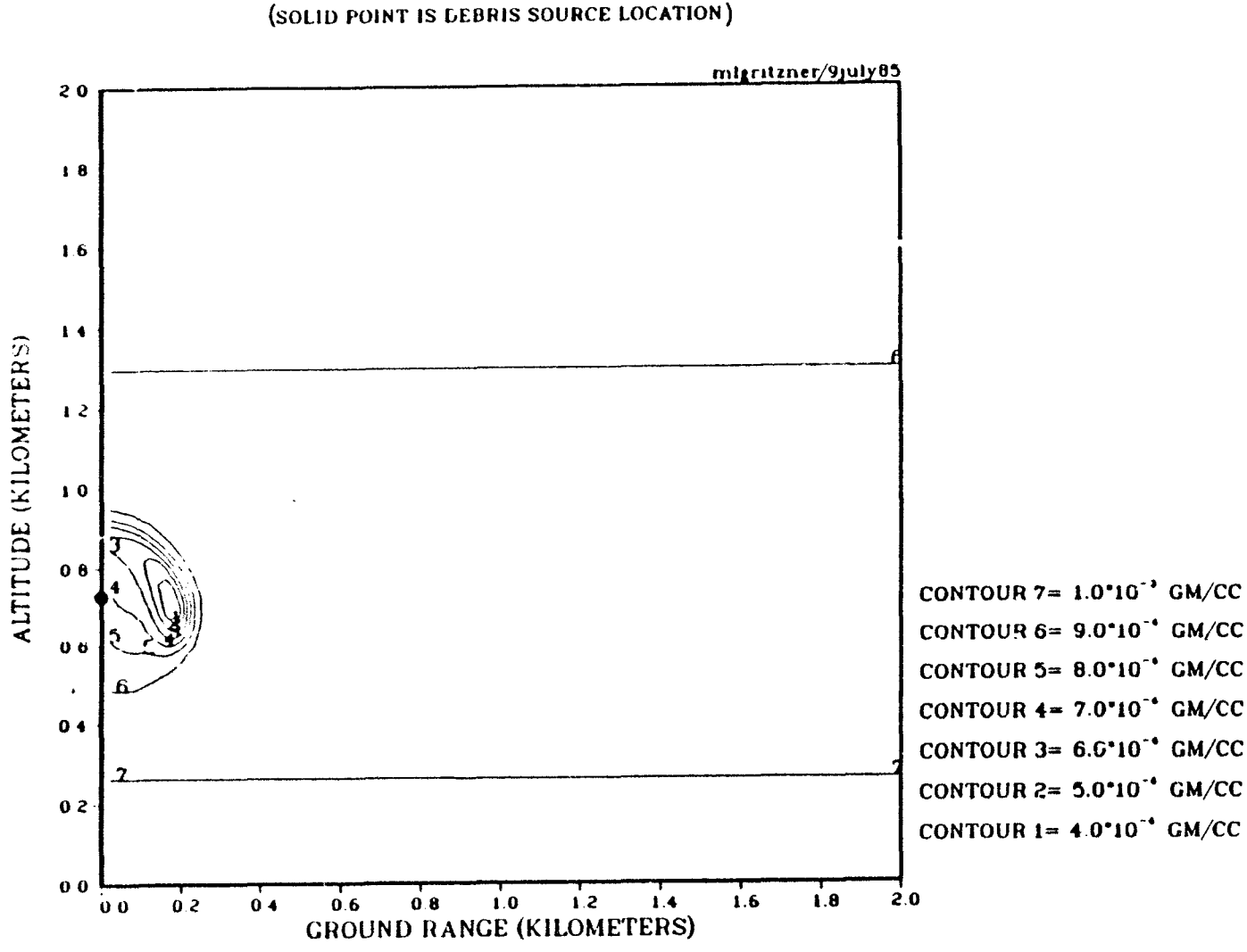

Figure 43. Air density iso-contours, 73m SHOB at 9.725 seconds.

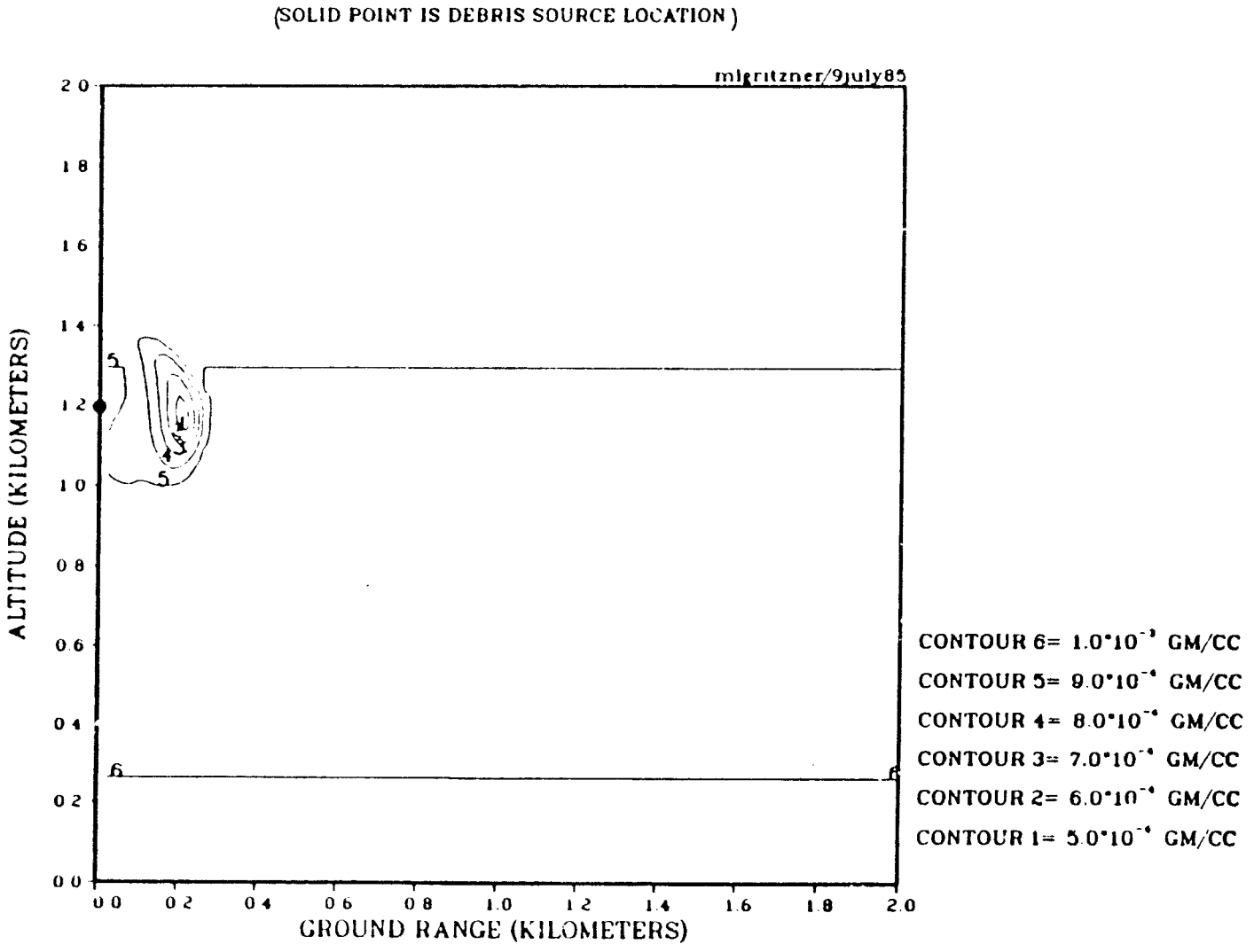

Figure 44. Air density iso-contours, 73m SHOB at 20.004 seconds.

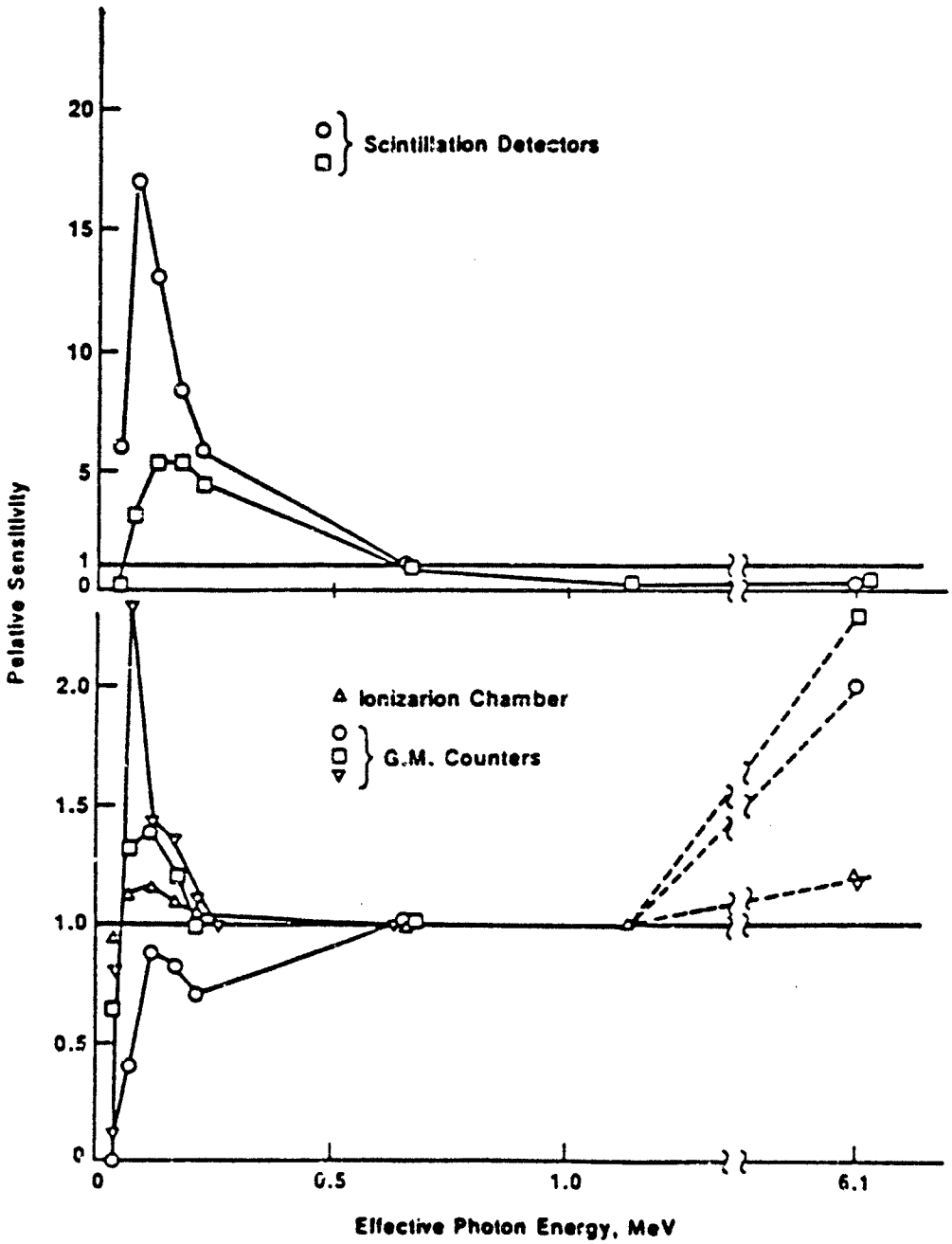

Figure 45. Highlights of energy dependence of instrument sensitivity.

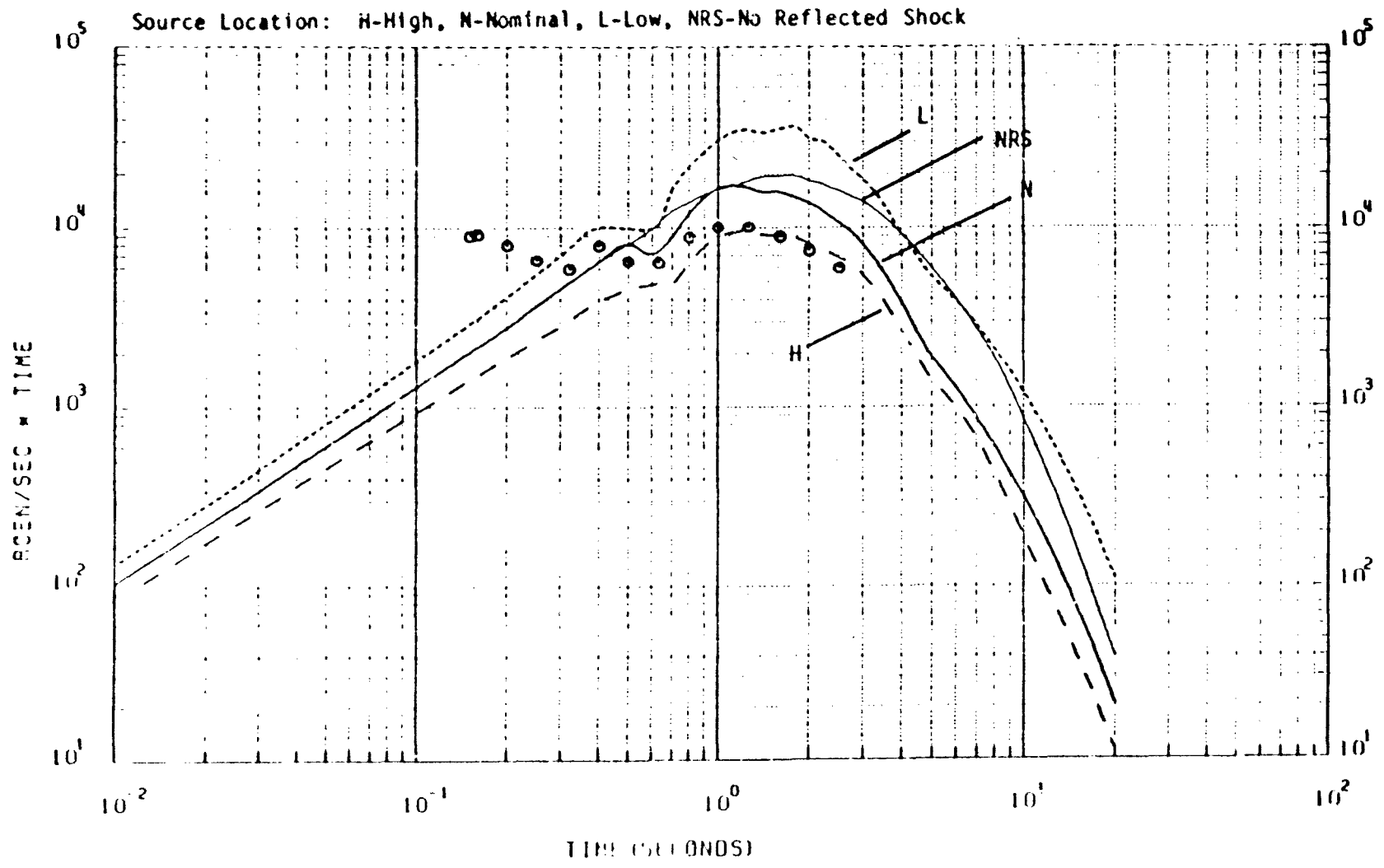

Figure 46. Measured and calculated exposure rates at 457 m, 110m SHOB.

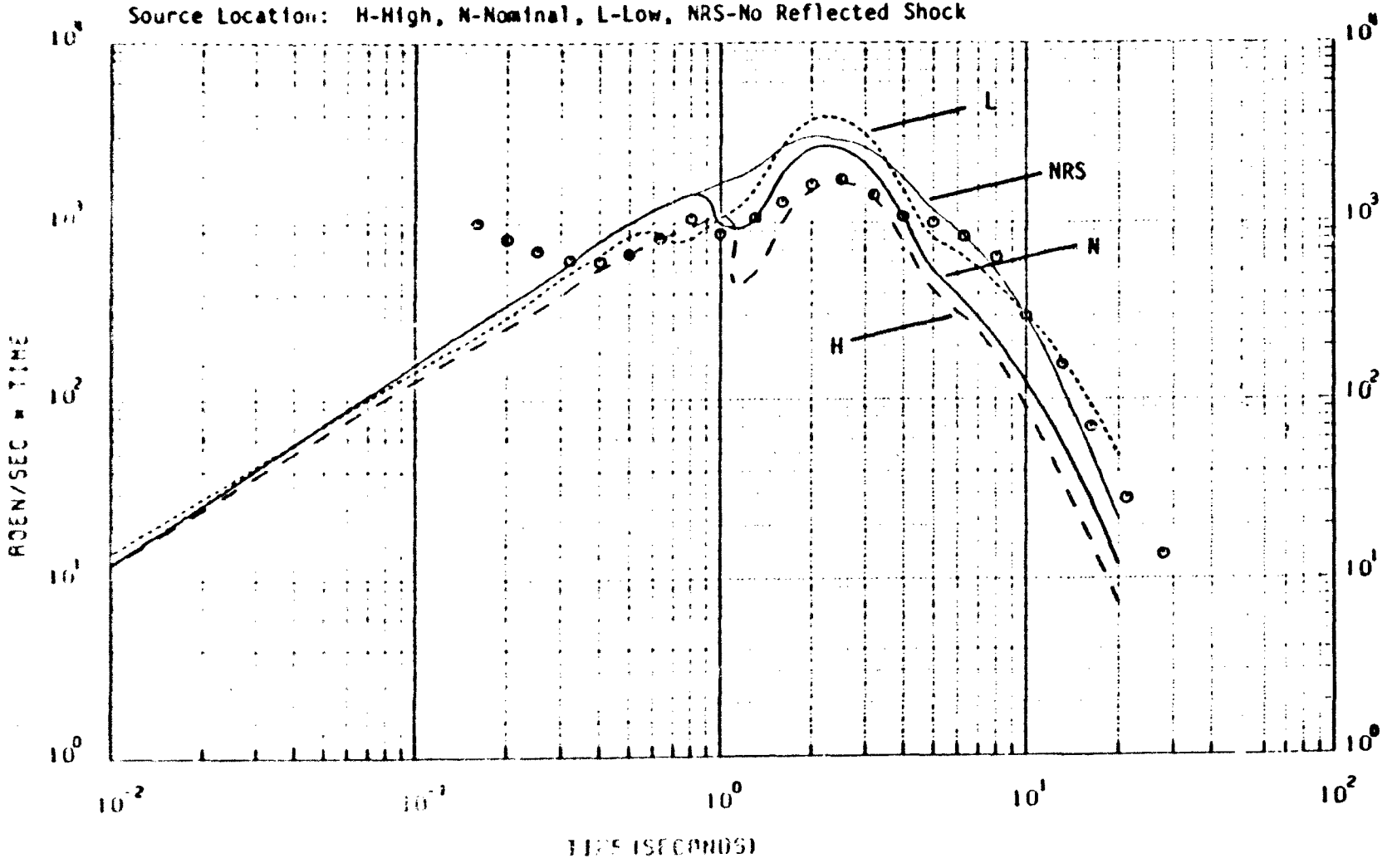

Figure 47. Measured and calculated exposure rates at 914 m, 110m SHOB.

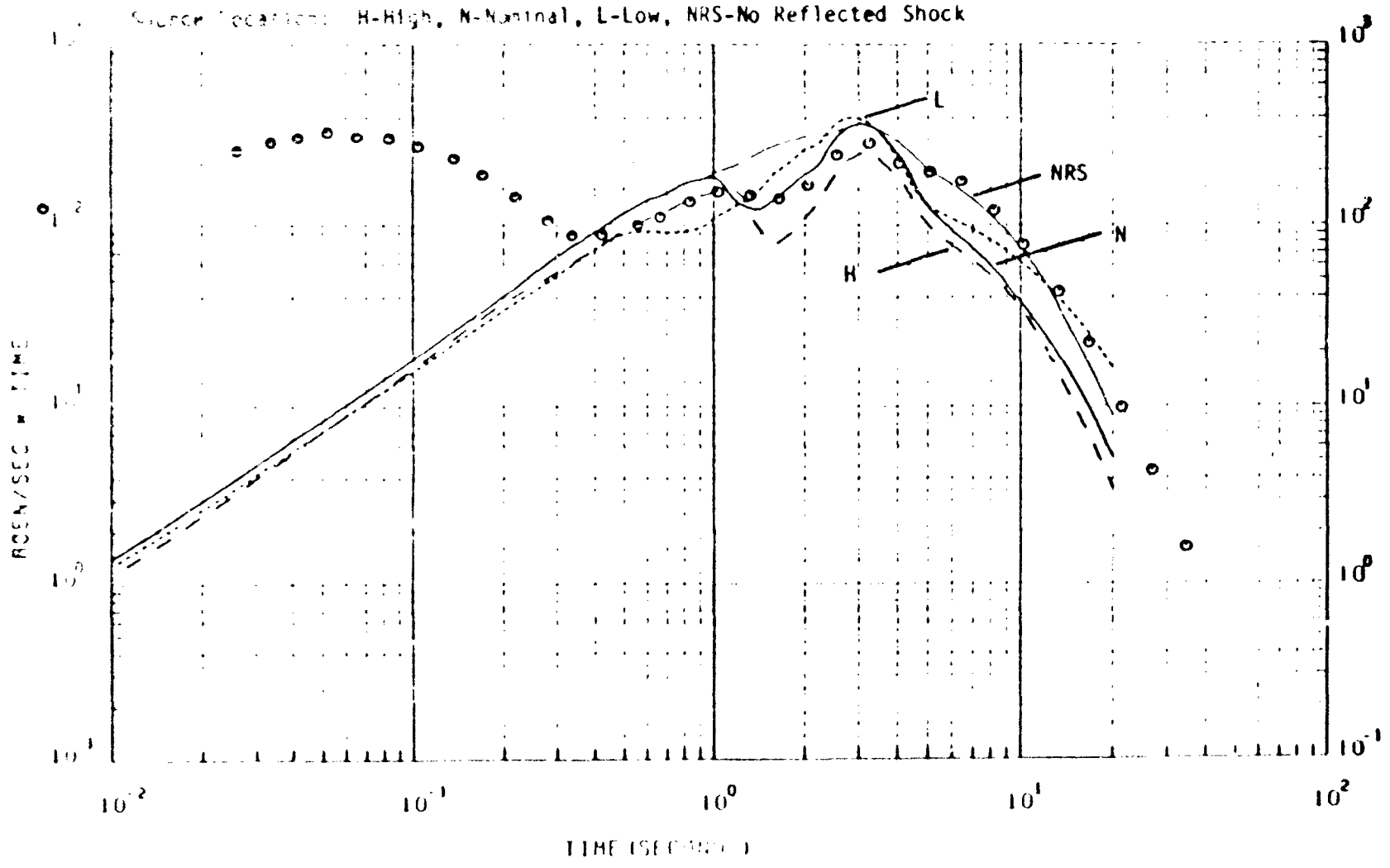

Figure 48. Measured and calculated exposure rates at 1371 m, 110m SHOB.

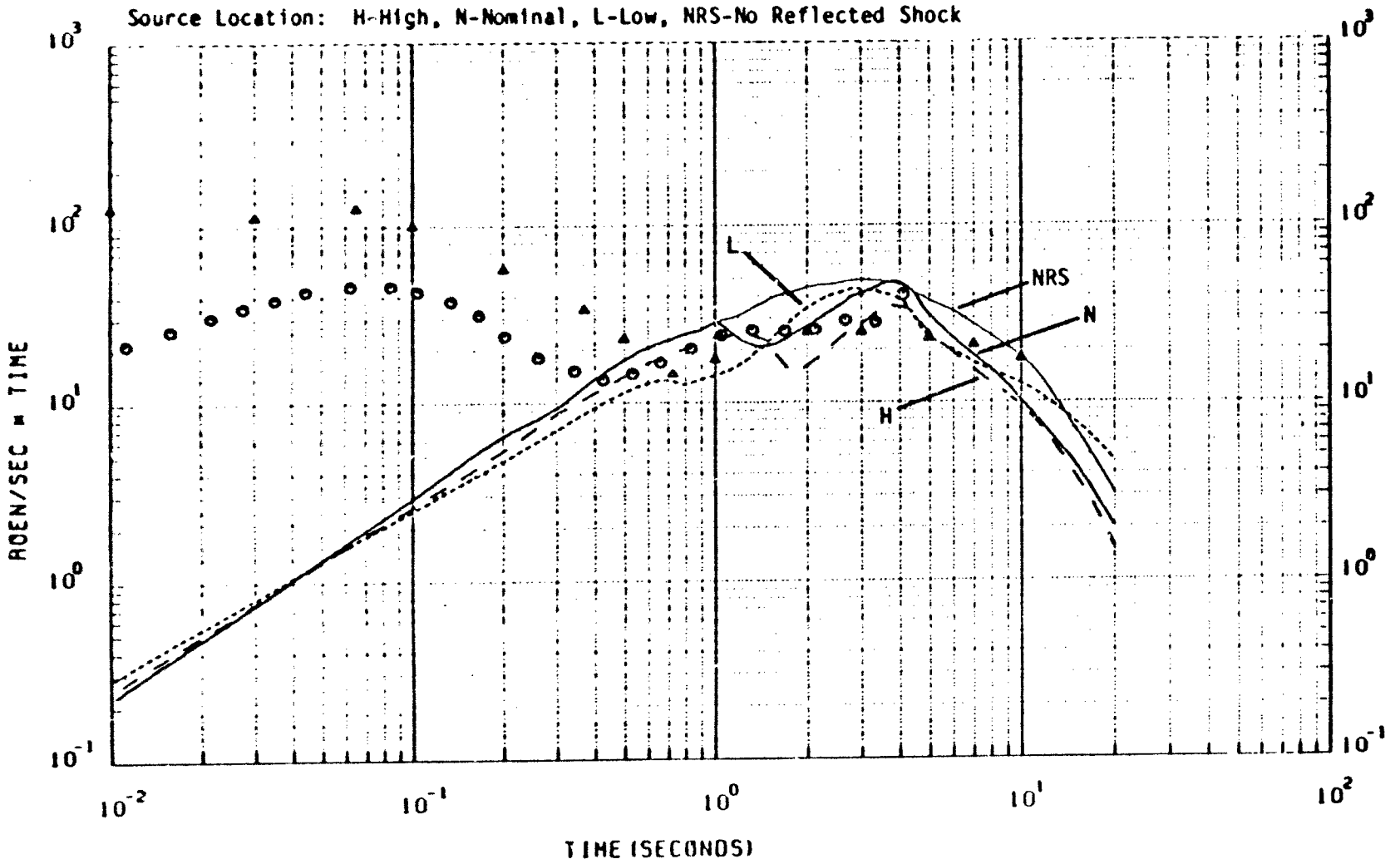

Figure 49. Measured and calculated exposure rates at 1828 m, 110m SHOB.

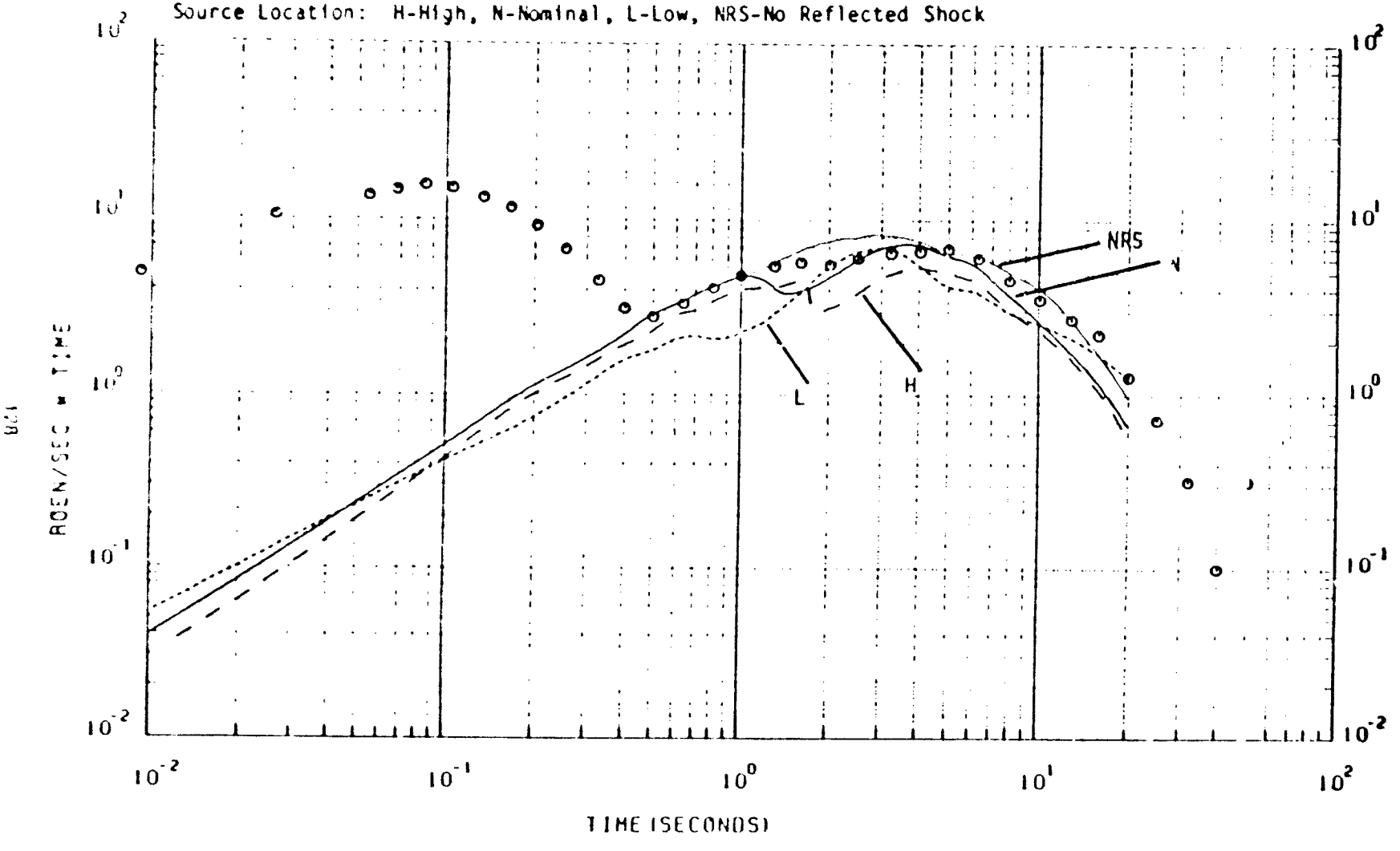

Figure 50. Measured and calculated exposure rates at 2286 m, 110m SHOB.

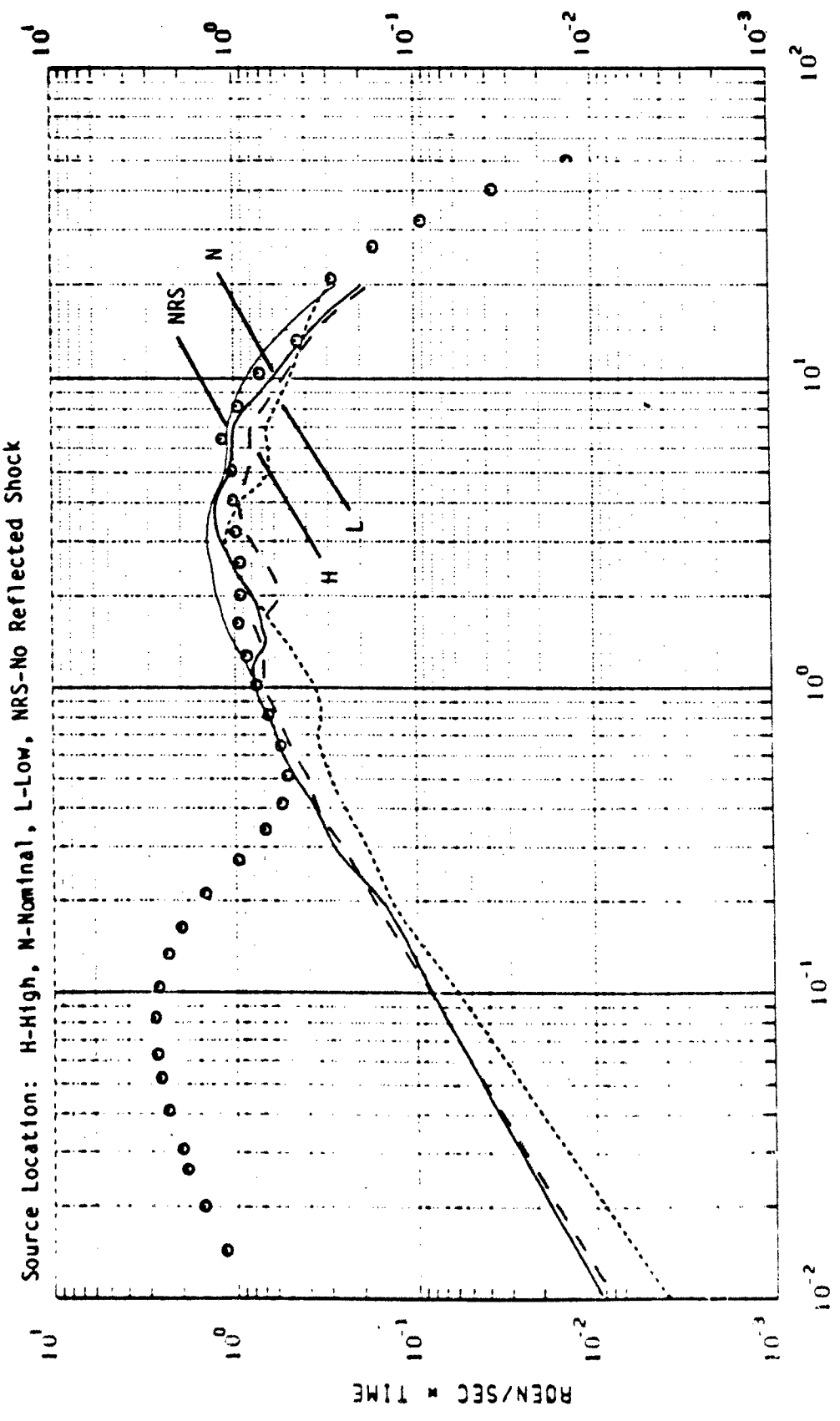

Figure 51. Measured and calculated exposure rates at 2279 m, 110m SHOB.

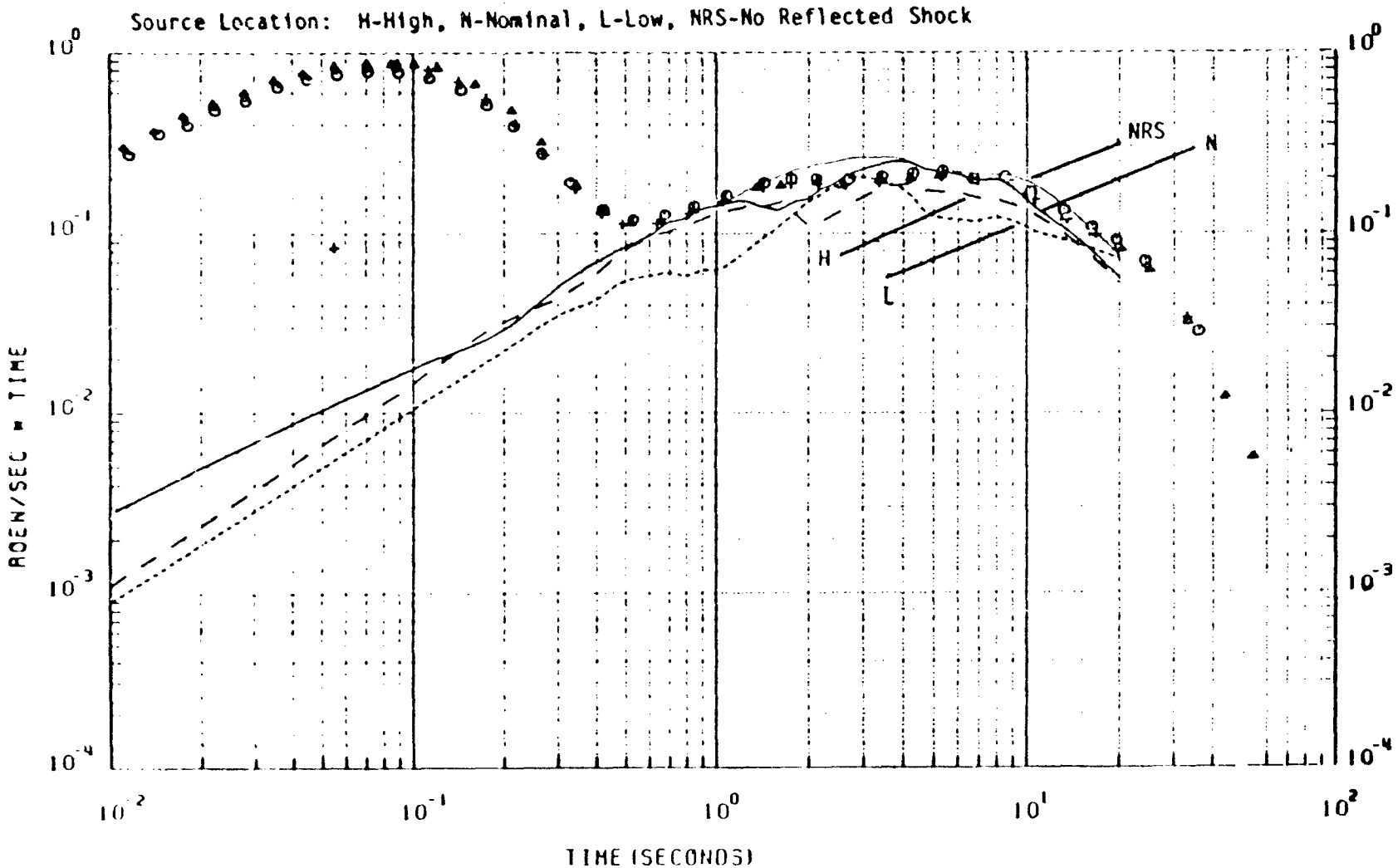

Figure 52. Measured and calculated exposure rates at 3261 m, 110m SHOB.

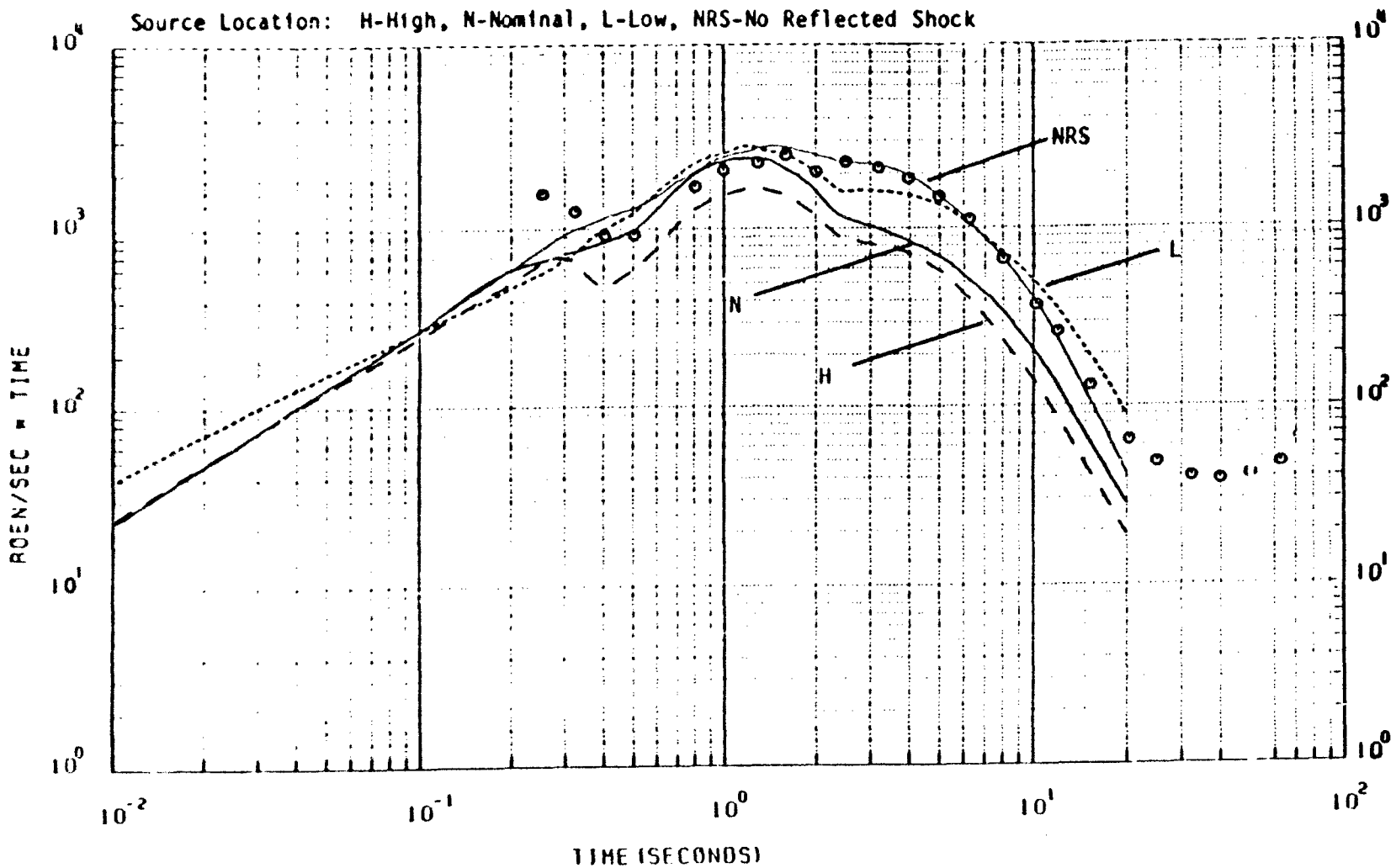

Figure 53. Measured and calculated exposure rates at 457 m, 73m SHOB.

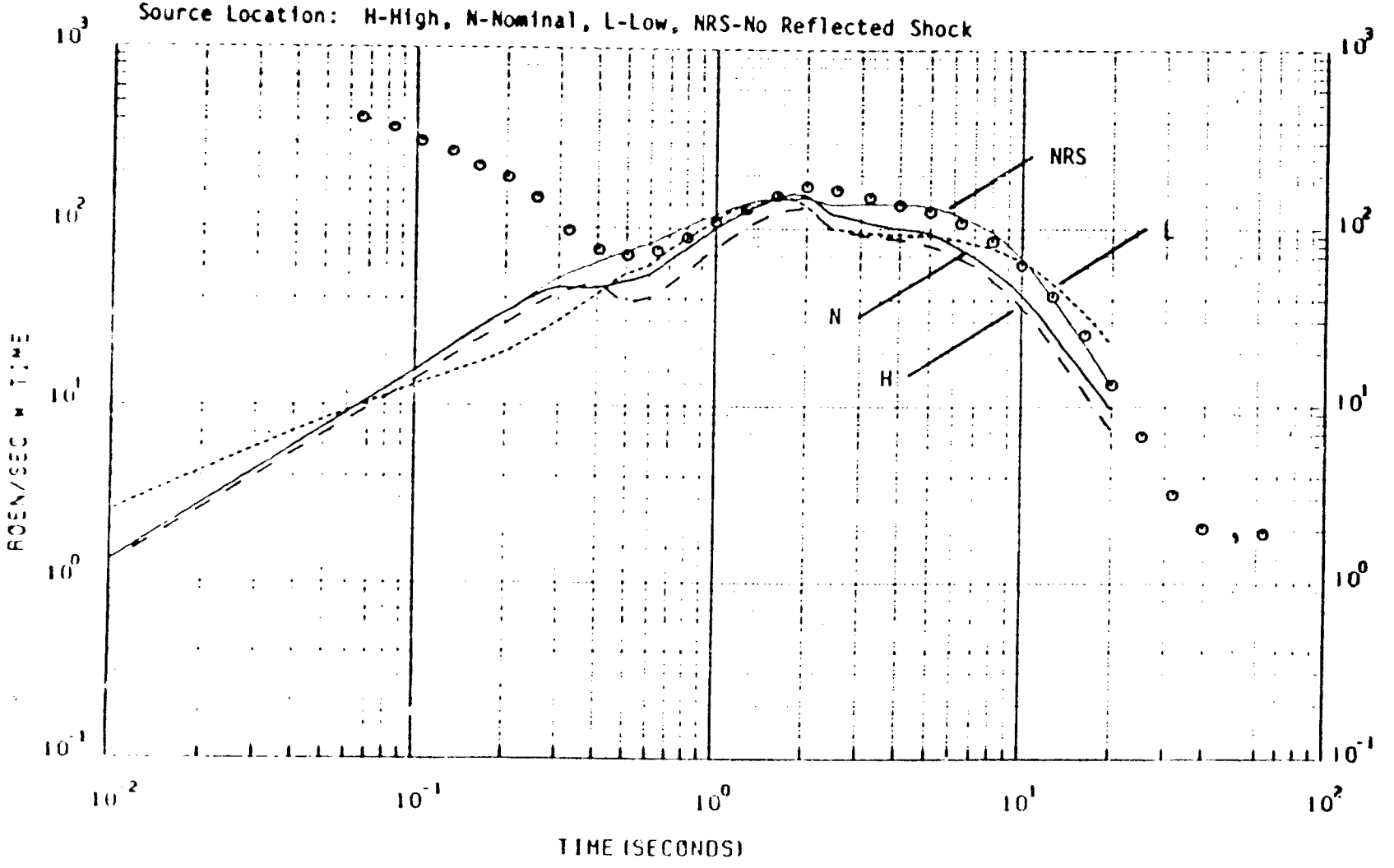

Figure 54. Measured and calculated exposure rates at 914 m, 73m SHOB.

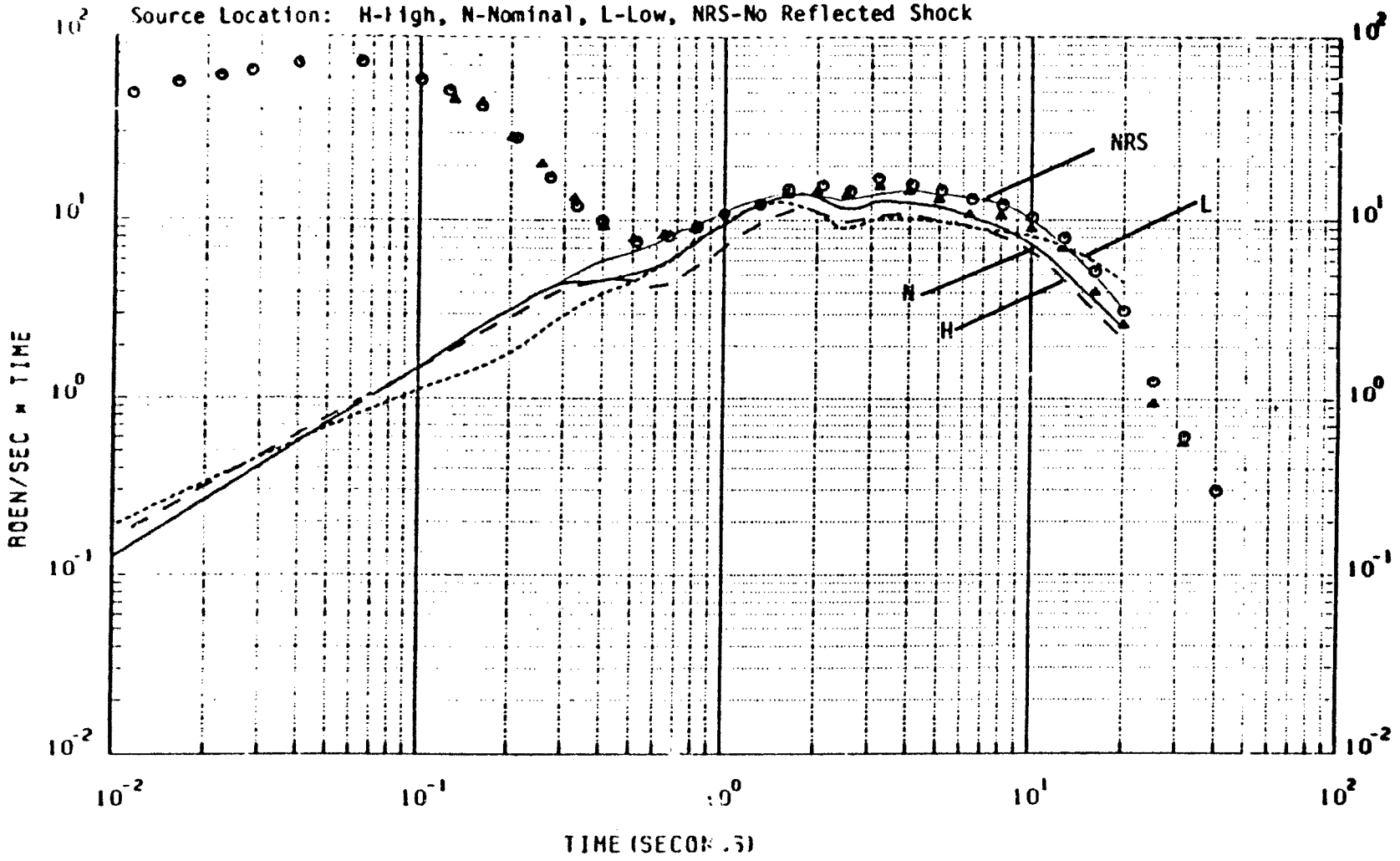

Figure 55. Measured and calculated exposure rates at 1372 m, 73m SHOB.

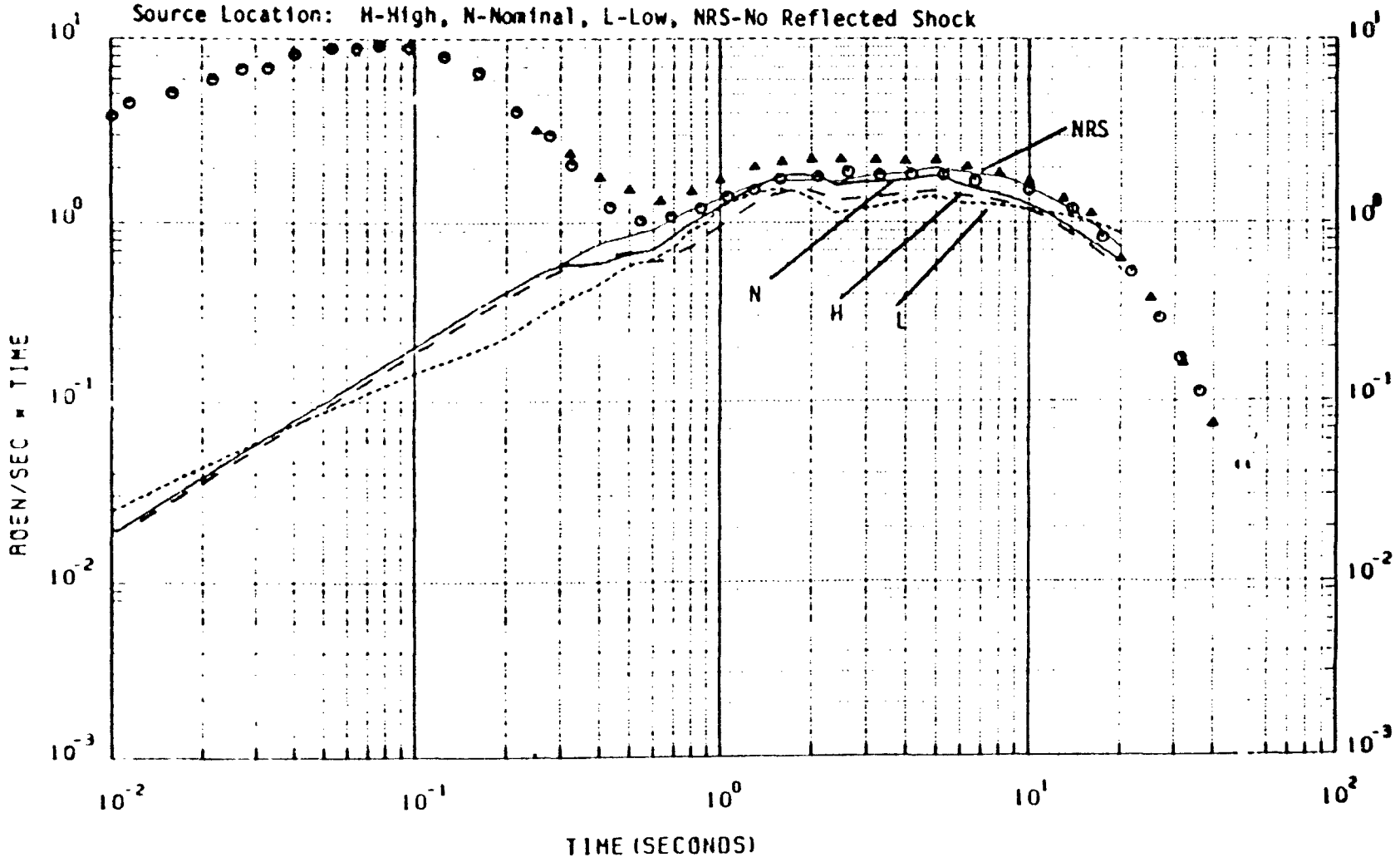

Figure 56. Measured and calculated exposure rates at 1829 m, 73m SHOB.

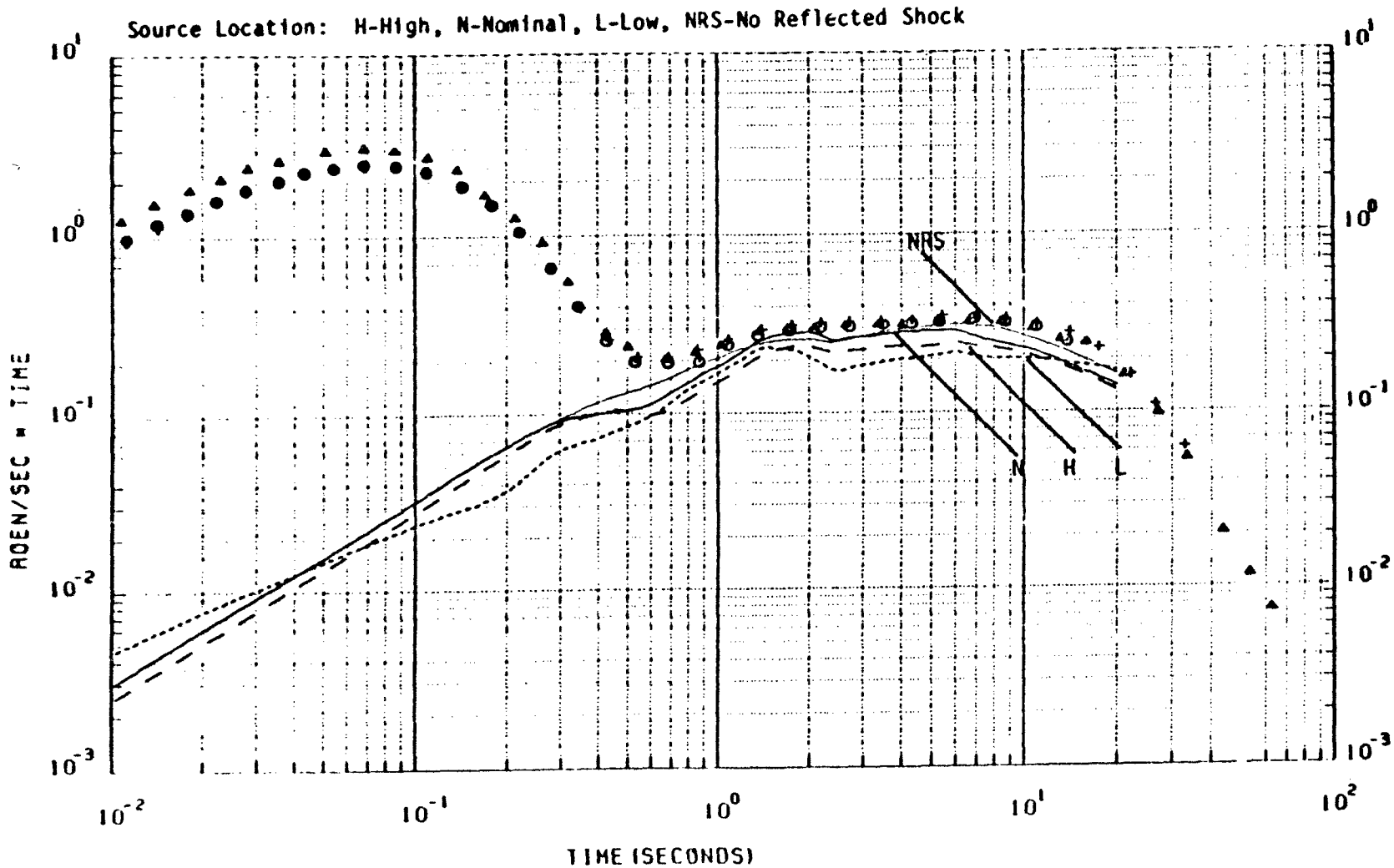

Figure 57. Measured and calculated exposure rates at 2286 m, 73m SHOB.

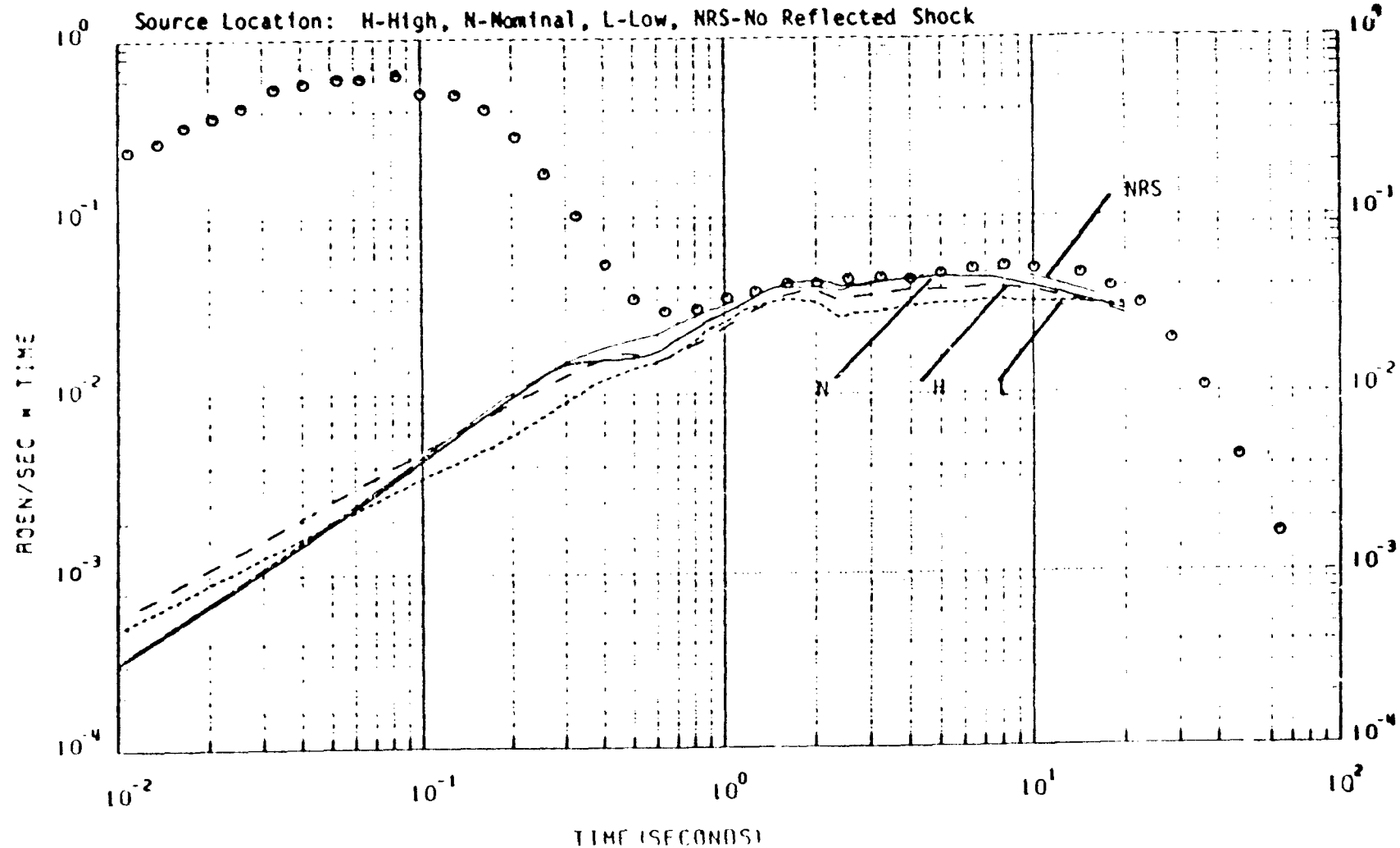

Figure 58. Measured and calculated exposure rates at 2780 m, 73m SHOB.

The calculations follow the general shape of the measured data for times beyond a few tenths of a second. At earlier times gamma rays from air and ground capture of prompt neutrons dominate the exposure rate. Those are not part of the delayed radiation model. At times between a few tenths of a second and a few seconds the calculations display the effect of the reflected shock wave passing through the fireball. The measurements made on the 110m SHOB shot also show this, while the effect is hidden by the dominant secondary gamma rays for the other shot. Beyond a few seconds the calculations are lower than the measurements, quite a bit lower in the case of the 110m SHOB shot.

Before examining the potential effects of source movement within the fireball system and other factors which may effect the calculation-measurement comparison it is useful to examine the calculated and measured exposure rate data in time intervals which allow identification of data trends in time and space. The exposure values calculated in four intervals using the nominal (hot spot) source locations are presented as ratios to the equivalent measured values in Table 28. There are several types of errors to look for from the evidence of these ratios. A source magnitude error should cause a uniform discrepancy at all ranges, as should an error in calculating the size of the density well. An error in fireball rise should cause a discrepancy which is range-dependent, as should an error in specifying the source location relative to the fireball.

During the earliest period the calculation-measurement ratios for the 110m SHOB shot exhibit a range dependence. Either a faster fireball rise or a rise of the debris within the fireball would reduce the discrepancy. However, photographic evidence (Ref.12) indicates that for a similar shot, Upshot-Knothole CLIMAX, the debris remain in the fireball center through approximately one second. This leaves the fireball rise rate as suspect, particularly for large yields, a suspicion which is supported by the same photographic evidence. During the period from one to three seconds the calculation-measurement ratios for Shot the 110m SHOB shot still exhibit a discrepancy at close range through to a lesser extent than during the prior period. The higher fireball caused by an increased rise rate during the period to one second would probably account for most of the discrepancy. In addition photographic evidence suggests that the source is rising relative to the center of the fireball.

In the case of the 73m and 71m SHOB shots the calculation-measurement ratios during the first two periods show good agreement in the first two periods, the mean ratio for the first period being 1.02 ± .12 and that for the second being .88 ± .10, where the means are based on the ratios for both shots and the uncertainty is the standard error of the distribution.

During the periods beyond three seconds the calculation-measurement ratios for all three exhibit systematic variations with distance, being low close in and high far out. According to the Figures 46 through 58 those discrepancies could be eliminated removing the provision for ground-shock reflection from the model. The results of such a modification are depicted as a light solid line in the figures. However, the early time structure observed in the measurements is no longer observed in the calculations after eliminating the reflected shock. Also, the resulting fireball rise rate is unrealistically slow, as compared to test shot photographs. However, this contributes to the improved ability of the unreflected model to calculate dose rates at late times. The hydrodynamic model used in ATR is essentially equivalent to the non-reflected shock variant of the LAMB model described above. Like that model, ATR over-predicts the dose rate in the important period over the first few seconds after the reflected shock wave has passed through the fireball. However, unlike the LAMB model the ATR cloud rise model is independent of the shock propagation process, being based on atmospheric test observations.

The comparison between (STLAMB) calculated and measured exposures in the three to twenty second time periods can be improved by lowering the source relative to the fireball center. Photographic evidence suggeststhat such as phenomenon does occur after the debris rises to the top of the fireball, which takes place at approximately three seconds. Table 29 provides an estimate of the effect of lowering the source (but not the fireball). Those data are based on those presented in Figures 46 through 58. As shown in the Table, H stands for high source, N for nominal and L for low. Intermediate locations are given as NG and NL and are simple averages, representing a midpoint between the two cases for which calculations have been performed. Note that raising the source for Shot Hood between one and three seconds reduces but does not eliminate the discrepancy, indicating that a change in cloud location is probably necessary also.

Table 28. Delayed gamma ray model exposure calculation to measurement ratios (nominal source location) for three NTS shots.

Shot	Time Interval sec	Range: (m)	457	914	1372	1829	2286	2779	3261
SHOB: 110m	0 - 1		1.08	1.34	1.26	1.16	.97	.93	1.05
	1 - 3		1.76	1.40	1.12	1.05	.87	.93	.91
	3 - 10		*	.74	.81	*	.95	1.04	1.07
	10 - 20		*	.38	.44	*	.61	.83	.83
	0 - 20		*	1.18	1.01	*	.90	.95	.99
SHOB: 73m	0 - 1		1.18	1.06	.89	1.00	1.02	.91	*
	1 - 3		.82	.88	.88	.97	.88	.95	*
	3 - 10		.46	.72	.77	.91	.85	.91	*
	10 - 20		.47	.63	.68	.83	.74	.73	*
	0 - 20		.84	.86	.83	.94	.88	.89	*
SHOB: 71m	0 - 1		.81	1.11	1.20	1.01	1.06	*	*
	1 - 3		.62	.91	.99	.88	.94	*	*
	3 - 10		.42	.63	.77	.74	.83	*	*
	10 - 20		.47	.40	.50	.58	.61	*	*
	0 - 20		.65	.82	.88	.81	.86	*	*

Table 29. Delayed gamma ray model exposure calculation to measurement ratios (moving source location) for three NTS shots.

Shot	Time Interval	Source Location	Range (m)	457	914	1372	1289	2286	2779	3261
SHOB: 110m	0 - 1	N		1.08	1.34	1.26	1.16	0.97	0.93	1.05
	1 - 3	NH		1.40	1.13	0.95	0.93	0.78	0.84	0.84
	3 - 10	NL		*	0.95	0.84	*	0.85	0.89	0.89
	10 - 20	L		*	1.10	0.90	*	0.76	0.85	0.75
	0 - 20			*	1.15	0.99	*	0.85	0.88	0.90
SHOB: 73m	0 - 1	N		1.18	1.06	0.89	1.00	1.02	0.91	*
	1 - 3	N		0.82	0.88	0.88	0.97	0.88	0.95	*
	3 - 10	NL		0.67	0.74	0.72	0.82	0.75	0.79	*
	10 - 20	L		1.30	1.18	0.95	0.95	0.75	0.68	*
	0 - 20			0.91	0.90	0.84	0.92	0.84	0.84	*
SHOB: 71m	0 - 1	N		0.81	1.11	1.20	1.01	1.06	*	*
	1 - 3	N		0.62	0.91	0.99	0.88	0.94	*	*
	3 - 10	NL		0.62	0.65	0.72	0.67	0.73	*	*
	10 - 20	L		1.31	0.76	0.71	0.67	0.63	*	*
	0 - 20			0.70	0.85	0.89	0.80	0.83	*	*

Lowering the sources at late times improves the agreement between measurement and calculation but, just as importantly, it reverses the nature of the discrepancy as it varies with range. The remaining discrepancy can be accounted for to a large extent on the basis of the radial displacement of the source as it moves down the outside of the fireball and eventually becomes incorporated in the torus.

At times between five and ten seconds the outer surface of the rising fireball begins to cool, the vapors are subject to drag from the surrounding atmosphere. The resulting downward flow around the outside of the fireball is matched by an upward flow at its center. This flow pattern produces a torus, within which reside the debris. The radius of the torus depends on yield. Thus, the torus for the 110m SHOB shot attains a radius approximately 325 meters by ten seconds, while those for 71 and 73m SHOB shots are approximately 200 meters in radius. The flow about the torus causes rapid mixing, cooling and return to the near ambient density. Under such conditions the radial displacement of the debris causes an increase in exposure which increases with range. In the case of the 110m SHOB shot that increase in terms of multiplicative factors has been estimated using simple point-kernal calculation techniques, as follows:

Radial Source Displacement Correction Factor, 110 SHOB

Time Period (sec)	Range: (m)	914	1372	2286	2779	3261
3-10		1.04	1.07	1.15	1.19	1.23
10-20		1.13	1.17	1.25	1.30	1.35

These factors have been applied to the 110m SHOB shot source height-adjusted calculation-measurement ratios and the results provided in Table 30. The data in Table 30 represent a definite improvement over the original calculation-measurement ratios, incorporating nominal source location data only, as found in Table 28.

OTHER MODEL COMPARISONS WITH WEAPON TESTS.

There are other comparisons which can be made with data from weapon tests in addition to those discussed previously. However, most involve total exposure rather than exposure rate.

Total gamma ray exposure data are available for device F, 22 Kt yield, air dropped and exploded at a height of 437m. Data are also available for device D, 21 Kt yield, air dropped and exploded at a height of 432m. Both devices were similar to Fat Man in design and high explosive thickness.

Calculated and measured (Refs. 36 and 37) gamma ray exposure intensities are provided for device F in Figures 59 and 60 and for device D in Figures 61 and 62. Each shot had two orthogonal lines of film dosimeters, one running west from the intended ground zero and one running south. The measured values have been revised as recommended by Ellery Storm, LANL (Ref. 52). Those revisions include corrections for betatron calibration energy (meas. * .885) and for energy-dependence of film sensitivity (sensitive films (exposure less than 10r) * .909, insensitive films (exposure greater than 10r) * .840).

The calculated exposure values are generally 10 to 20% below the revised measured values. However, agreement is somewhat better in the first 2000 meters than at greater ranges. Taking the source location into account is likely to improve the agreement, particularly at long ranges. However, for shorter ranges the effect is likely to be minimal given the high burst height.

In summary, comparisons of results of the best available model for delayed gamma ray calculation with results of gamma ray exposure rate measurements made at atmospheric tests indicate that the model has short comings which are mainly due to incorrect hydrodynamic data or inadequate modeling detail based on existing data.

The hydrodynamic model used in the ATR code suffers from deficiencies similar to those attributed to the more sophisticated model. It does not account for source motion relative to that of the fireball, nor does it account for the effect of torus formation. However, as described in the body of this report, the properties of the cloud rise and blast model incorporated in ATR do allow successful scaling based on scaled burst height to obtain a reasonable value for the time-integral delayed gamma ray dose, although the rate data may be significantly in error at any given time.

Table 30. Delayed gamma ray model exposure calculation to measurement ratios for the 110m SHOB shot (moving source with adjustment for Torus formation.

Time Interval	Source Location	Range: (m)	457	914	1372	1829	2286	2779	3261
0 - 1	N		1.08	1.34	1.26	1.16	0.97	0.93	1.05
1 - 3	NH		1.40	1.13	0.95	0.93	0.78	0.84	0.84
3 - 10	NL		*	0.99	0.90	*	0.98	1.06	1.09
10 - 20	L		*	1.24	1.05	*	0.95	1.11	1.01
0 - 20			*	1.16	1.02	*	.91	.97	1.00

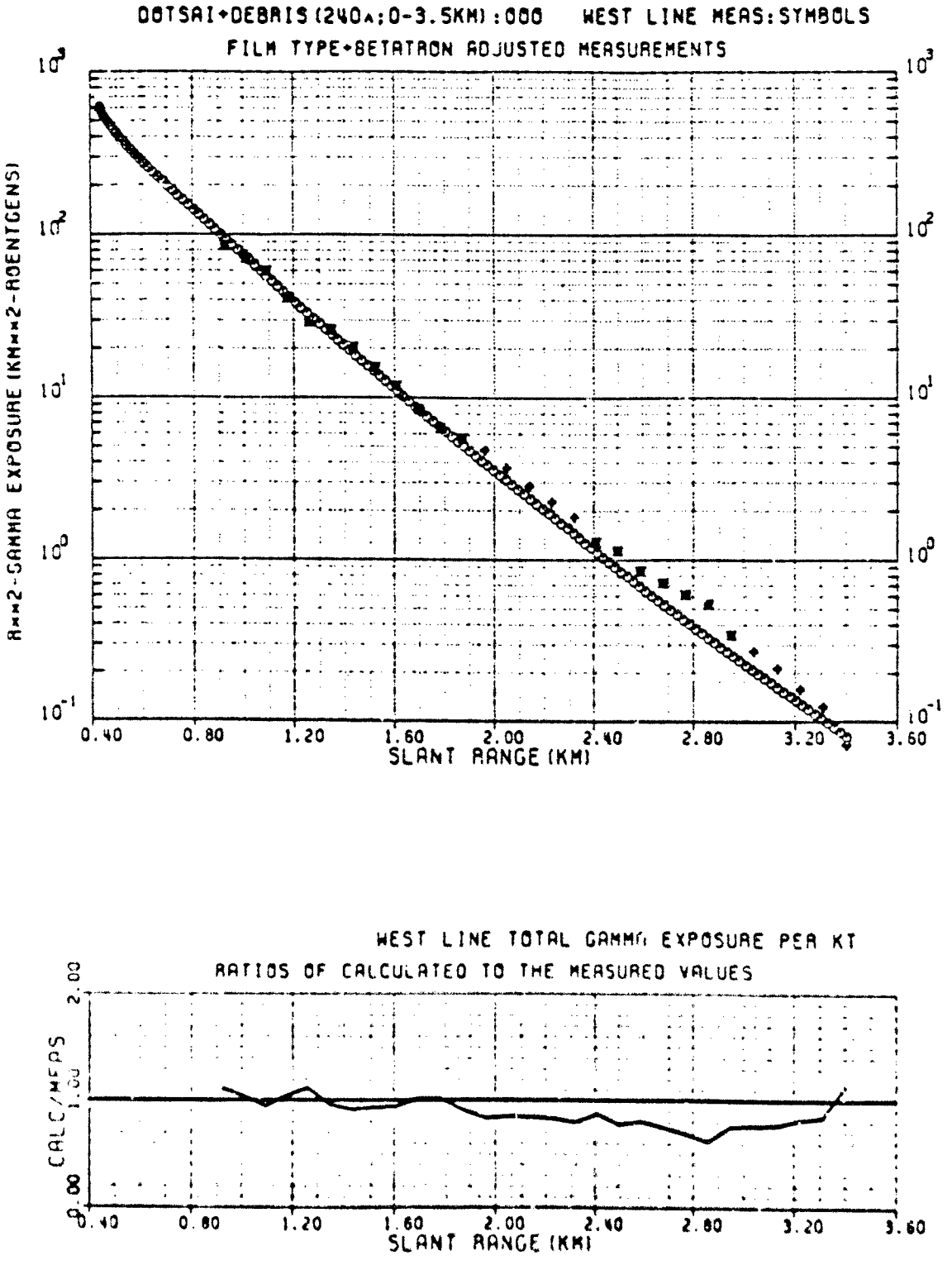

Figure 50. Device F gamma exposure per kt.

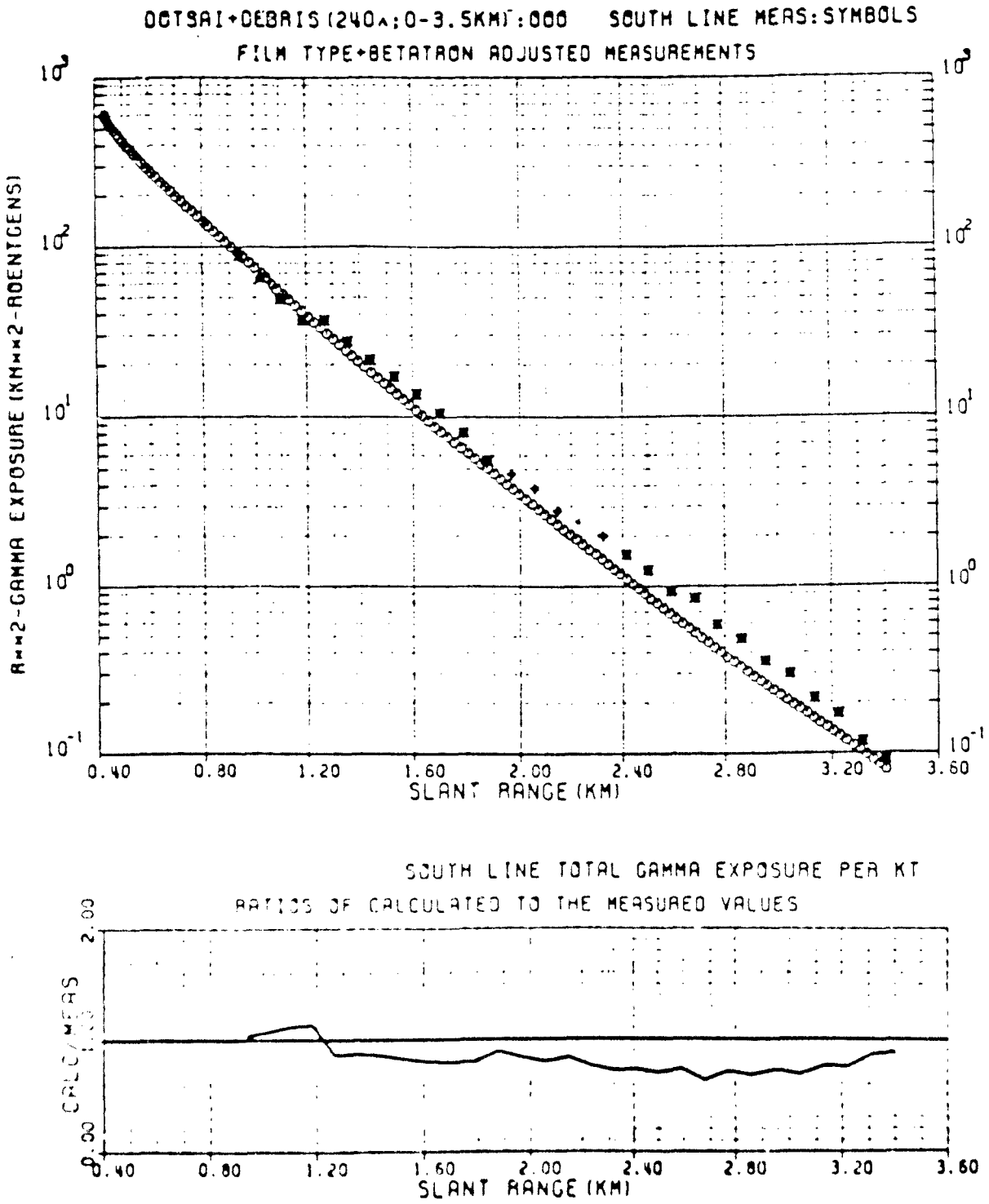

Figure 60. Device F total gamma exposure per kt.

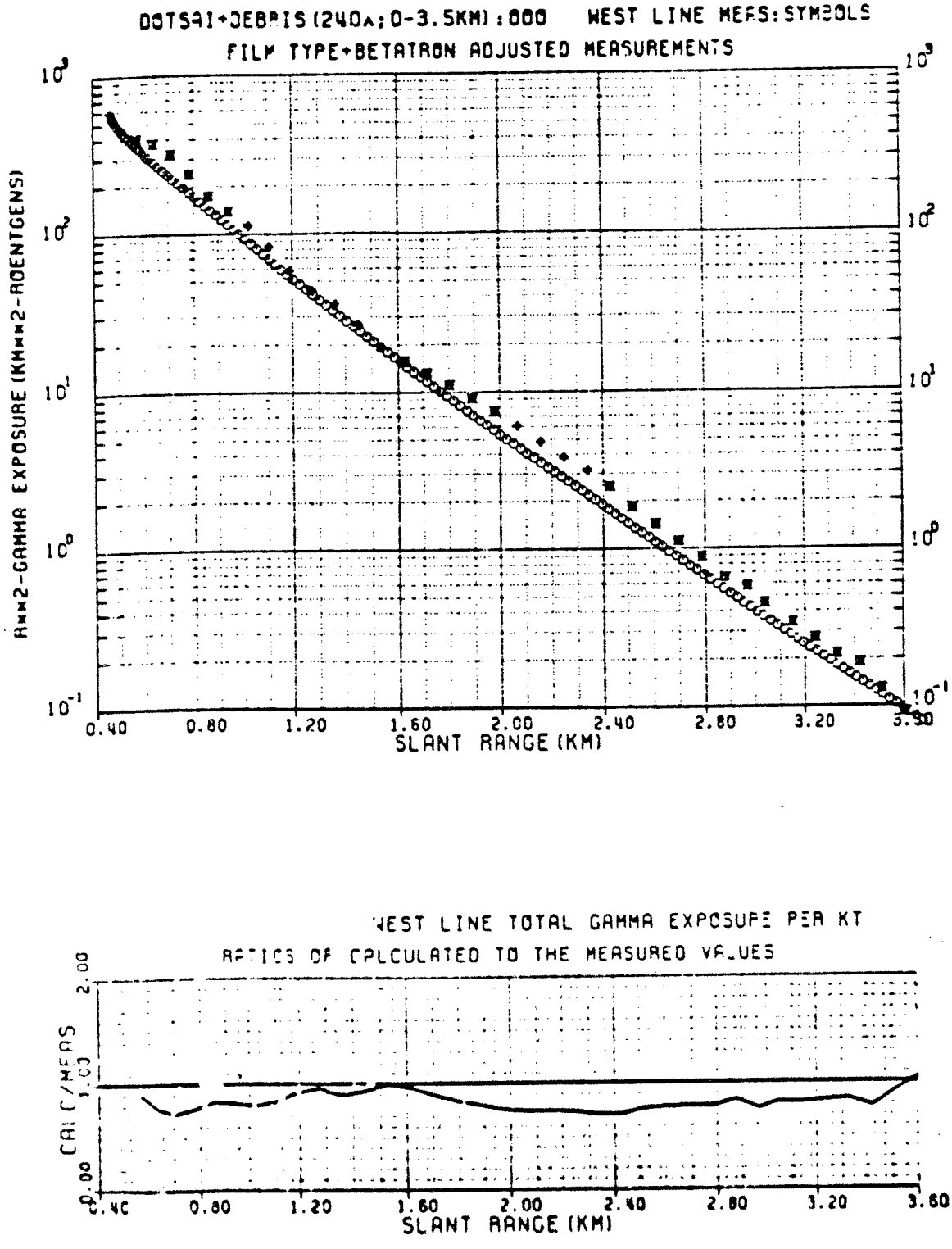

Figure 31. Device D total gamma exposure per kt.

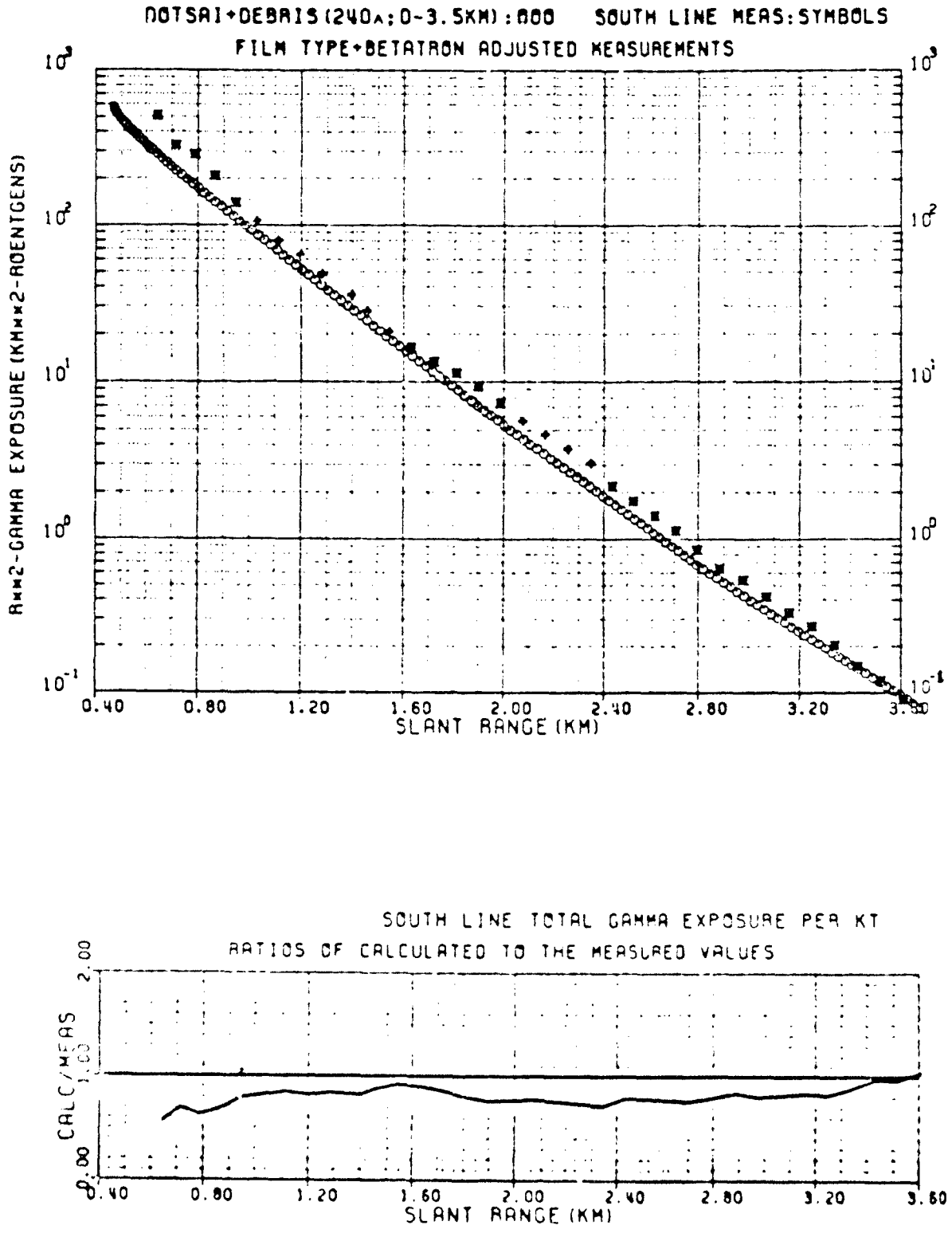

Figure 62. Device D total gamma exposure per kt.

DISTRIBUTION LIST

DNA-TR-89-14

DEPARTMENT OF DEFENSE

ARMED FORCES RADIOBIOLOGY RSCH INST
ATTN: BHS
ATTN: DIRECTOR
ATTN: EXH
ATTN: MRA
ATTN: PHY
ATTN: RBD
ATTN: RSD
ATTN: SCIENTIFIC DIRECTOR
ATTN: TECHNICAL LIBRARY

ARMED FORCES STAFF COLLEGE
ATTN: LIBRARY
ATTN: STRAT STUDIES

ASSISTANT SEC OF DEF (C3I)
ATTN: DIR (S&TNFC3)
ATTN: DIR TACTICAL INTELL SYSTEMS

ASSISTANT SECRETARY OF DEFENSE
INTERNATIONAL SECURITY POLICY
ATTN: NUC FORCES & ARMS CONTROL PLCY

ASSISTANT TO THE SECRETARY OF DEFENSE
ATTN: EXECUTIVE ASSISTANT
ATTN: MIL APPL
ATTN: MIL APPL, C FIELD

DEFENSE INTELLIGENCE AGENCY
ATTN: COUNTERTERRORIST THREAT BR
ATTN: DB
ATTN: DB-1 (G FERRELL)
5 CYS ATTN: DB-4, RSCH RESOURCES DIV
ATTN: DB-6 (R MANN)
ATTN: DE (ESTIMATES)
ATTN: DIA/VPA-2 (FED RES DIV)
ATTN: DN
ATTN: DT
ATTN: OFFICE OF SECURITY
ATTN: OS
ATTN: RTS-2B

DEFENSE INTELLIGENCE COLLEGE
ATTN: DIC/RTS-2
ATTN: DIC/2C

DEFENSE LOGISTICS AGENCY
ATTN: COMMAND SECURITY OFC

DEFENSE NUCLEAR AGENCY
ATTN: CID
ATTN: DFRA
ATTN: DFSP G ULLRICH
ATTN: NANF
ATTN: NASF
ATTN: OPNA
ATTN: OPNS
ATTN: RAEE
20 CYS ATTN: RARP
4 CYS ATTN: TITL

DEFENSE NUCLEAR AGENCY
ATTN: TDNM
2 CYS ATTN: TDTT W SUMMA

DEFENSE TECHNICAL INFORMATION CENTER
2 CYS ATTN: DTIC/FDAB

DIRECTOR
ATTN: DOCUMENT CONTROL

FIELD COMMAND DEFENSE NUCLEAR AGENCY
ATTN: FCPR
3 CYS ATTN: FCPRT
ATTN: NUC SECURITY

INTELLIGENCE CENTER, PACIFIC
ATTN: COMIPAC

INTERSERVICE NUCLEAR WEAPONS SCHOOL
ATTN: TTV
2 CYS ATTN: TTV 3416TH TTSQ

JOINT DATA SYSTEM SUPPORT CTR
ATTN: C-312
ATTN: C-332

JOINT STRAT TGT PLANNING STAFF
ATTN: JK (ATTN: DNA REP)
ATTN: JLKS
ATTN: JLT
ATTN: JP
ATTN: JPTP

NATIONAL DEFENSE UNIVERSITY
ATTN: ICAF, TECH LIB
ATTN: NWCLB-CR
ATTN: LIBRARY
ATTN: STRAT CONCEPTS DIV CTR

NATIONAL SECURITY AGENCY
ATTN: CHIEF A GROUP

OFFICE OF THE SEC OF DEFENSE
ATTN: NAVAL FORCES
ATTN: STRATEGIC PROGRAMS & TNF

STRATEGIC AND THEATER NUC FORCES
ATTN: DR E SEVIN
ATTN: DR SCHNEITER

THE JOINT STAFF
ATTN: ED30(J-3 STRATEGIC OPS DIV)
ATTN: J-3 SPECIAL OPERATIONS
ATTN: J-3/NUC OP BR STRAT OP BR
ATTN: J-5 STRAT DIV W MCCLAIN
ATTN: JAD/SFD
ATTN: JAD/SSD
ATTN: JSOA
ATTN: SAGA

U S EUROPEAN COMMAND/ECCS
ATTN: ECCS/SASM

U S EUROPEAN COMMAND/ECJ-LW
ATTN: ECJ-LW

U S EUROPEAN COMMAND/ECJ-3
ATTN: ECJ-3

U S EUROPEAN COMMAND/ECJ-5NPG
ATTN: ECJ-5

U S EUROPEAN COMMAND/ECJ-6-OJ
ATTN: ECJ-6

U S EUROPEAN COMMAND/ECJ-7/LW
ATTN: ECJ-7 LW

U S EUROPEAN COMMAND/ECJ2-T
ATTN: ECJ2-T (TGTS DIV)

U S EUROPEAN COMMAND/ECJ5-N
ATTN: ECJ5-N (NUC BRANCH)

UNDER SEC OF DEFENSE FOR POLICY
ATTN: DUSP/P
ATTN: USD/P

UNDER SECRETARY OF DEFENSE
ATTN: CHAIRMAN PSEAG
ATTN: CHAIRMAN, DEF SCIENCE BD
2 CYS ATTN: C3I
ATTN: DEP UND SEC, TAC WARFARE PROG

DEPARTMENT OF THE ARMY

ARMY RESEARCH INSTITUTE
ATTN: COMMANDER

COMBAT MATERIAL EVAL ELEMENT
ATTN: SECURITY ANALYST

DEP CH OF STAFF FOR OPS & PLANS
ATTN: DAMO-NCN RM 3B540
ATTN: DAMO-NCN(NUC CHEM DIR)
ATTN: DAMO-RQS
ATTN: DAMO-ZXA

DEPARTMENT OF THE ARMY
ATTN: DAMA-CSS-N
ATTN: DAMO-NCZ
ATTN: DAMO-OD
ATTN: DAMO ODSO
ATTN: DAPE-HRE

HARRY DIAMOND LABORATORIES
ATTN: SLCIS-IM-TL (TECH LIB)

JOINT STRATEGIC OPERATIONS CTR
ATTN: J 2
ATTN: J 5

U S ARMY AIR DEFENSE SCHOOL
ATTN: COMMANDANT

U S ARMY ARMAMENT RSCH & DEV CENTER
ATTN: DRDAR LCN F

U S ARMY ARMOR SCHOOL
ATTN: ATSB CTD
ATTN: TECH LIBRARY

U S ARMY BALLISTIC RESEARCH LAB
ATTN: AMXBR VLD R (DR RAINIS)
ATTN: AMXBR VLD DR KLOPCIC
ATTN: DRDAR-BL
ATTN: DRDAR-BLA-S TECH LIB
ATTN: DRDAR-BLT

U S ARMY CHEMICAL SCHOOL
ATTN: ATZN-CM-M

U S ARMY COMB ARMS COMBAT DEV ACTY
ATTN: ATZL-CAP

U S ARMY COMD & GENERAL STAFF COLLEGE
ATTN: ACQ LIBRARY DIV
ATTN: ATZL-SWJ-CA
ATTN: ATZL-SWS-L D DORRIS
ATTN: ATZL-SWT-A

U S ARMY CONCEPTS ANALYSIS AGENCY
ATTN: TECHNICAL LIBRARY

U S ARMY FIELD ARTILLERY SCHOOL
ATTN: ATSF-CD

U S ARMY FORCES COMMAND
ATTN: AF-OPTS

U S ARMY HUMAN ENGINEERING LAB
ATTN: DIRECTOR
ATTN: DR D HODGE

U S ARMY INFANTRY CTR & SCH
ATTN: ATSH-CD-CSO

U S ARMY INTEL THREAT ANALYSIS DET
ATTN: IAX-Z

U S ARMY MATERIEL COMMAND
ATTN: DRCDE-D
ATTN: DRCNC
ATTN: DRCSS

U S ARMY MATERIEL SYS ANALYSIS ACTVY
ATTN: DRXSY-DS
ATTN: DRXSY-S

U S ARMY NUCLEAR & CHEMICAL AGENCY
ATTN: DR DAVIDSON
ATTN: MONA NU

U S ARMY TRAINING AND DOCTRINE COMD
ATTN: ATCD AO
ATTN: ATCD FA
ATTN: ATCD N, CBT DEV, NUC DIR
ATTN: ATOO NCO

U S ARMY WAR COLLEGE
ATTN: LIBRARY
ATTN: STRATEGIC STUDIES

USA MILITARY ACADEMY
ATTN: DEPT OF BEHAVORIAL SCI & LDRSHIP
ATTN: DIR NATL SECURITY STUDIES

USA SURVIVABILITY MANAGMENT OFFICE
ATTN: SLCSM-SE J BRAND

DEPARTMENT OF THE NAVY

FLEET INTELLIGENCE CENTER
ATTN: FICPAC, CODE 21

MARINE CORPS
ATTN: CODE PPO
ATTN: PSI G/RASP

MARINE CORPS DEV & EDUCATION COMMAND
ATTN: LIBRARY, CODE WF15E/MCCDC

NAVAL OCEAN SYSTEMS CENTER
ATTN: CODE 4471, TECH LIB

NAVAL PERSONNEL RES & DEV CENTER
ATTN: CODE P302

NAVAL POSTGRADUATE SCHOOL
ATTN: CODE 1424 LIBRARY

NAVAL RESEARCH LABORATORY
ATTN: CODE 1240
ATTN: CODE 2627 (TECH LIB)

NAVAL SEA SYSTEMS COMMAND
ATTN: PMS-423
ATTN: SEA-09G53 (LIB)
ATTN: SEA-643

NAVAL SURFACE WARFARE CENTER
ATTN: CODE F-31
ATTN: G GOO

NAVAL TECHNICAL INTELLIGENCE CTR
ATTN: NISC-30

NAVAL WAR COLLEGE
ATTN: CODE E-11 TECH SVC
ATTN: CTR FOR NAV WARFARE STUDIES
ATTN: DOCUMENT CONTROL
ATTN: LIBRARY
ATTN: STRATEGY DEPT

NAVAL WEAPONS EVALUATION FACILITY
ATTN: CLASSIFIED LIBRARY

NUCLEAR WEAPONS TNG GROUP, ATLANTIC
ATTN: CODE 222
ATTN: DOCUMENT CONTROL

NUCLEAR WEAPONS TNG GROUP, PACIFIC
ATTN: CODE 32
ATTN: DOCUMENT CONTROL

OFC OF THE DEPUTY CHIEF OF NAVAL OPS
ATTN: NIS-22
ATTN: NOP 009D
ATTN: NOP 009D3
ATTN: NOP 06D
2 CYS ATTN: NOP 403
ATTN: NOP 50, AVN PLNS & RQMNTS DEV
ATTN: NOP 60
ATTN: NOP 60D
ATTN: NOP 603
ATTN: NOP 91
ATTN: OP 654(STRAT EVAL & ANAL BR)
ATTN: OP 981

OFFICE OF THE CHIEF OF NAVAL OPERATIONS
ATTN: CNO EXECUTIVE PANEL (OP 00K)

OPERATIONAL TEST & EVALUATION FORCE
ATTN: COMMANDER

PLANS, POLICY & OPERATIONS
ATTN: CODE-P
ATTN: CODE-POC-30

SPACE & NAVAL WARFARE SYSTEMS CMD
ATTN: PME 121-3

TACTICAL TRAINING GROUP, PACIFIC
ATTN: COMMANDER

DEPARTMENT OF THE AIR FORCE

AFIA
ATTN: AFIA/INKD, MAJ COOK

AFIS/INT
ATTN: INT

AIR UNIVERSITY
ATTN: AU/SP
ATTN: STRATEGIC STUDIES

AIR UNIVERSITY LIBRARY
ATTN: AUL-LSE
ATTN: LIBRARY

ASSISTANT CHIEF OF STAFF
2 CYS ATTN: AF/SAMI

ASSISTANT CHIEF OF THE AIR FORCE
ATTN: SAF/ALR

DEPUTY CHIEF OF STAFF/XOO
ATTN: AF/XOOIR

DEPUTY CHIEF OF STAFF/XOX
ATTN: AFXOXFM
ATTN: AFXOXFS

FOREIGN TECHNOLOGY DIVISION, AFSC
ATTN: CCN
ATTN: SDN
ATTN: TQTM

SECRETARY OF AF/AQQS
ATTN: AF/RDQI

SPACE DIVISION/YH
ATTN: YH

STRATEGIC AIR COMMAND/ADWN
ATTN: ADWN

STRATEGIC AIR COMMAND/SPD
ATTN: SPD

STRATEGIC AIR COMMAND/STIC
ATTN: STIC

STRATEGIC AIR COMMAND/XOXO
ATTN: XOXO

STRATEGIC AIR COMMAND/XPX
ATTN: XPZ

STRATEGIC AIR COMMAND/XRFS
ATTN: XRFS

TACTICAL AIR COMMAND/XPSC
ATTN: TAC/DOA

U S AIR FORCE ACADEMY
ATTN: LIBRARY
ATTN: USAFA/SP

USAF SCHOOL OF AEROSPACE MEDICINE
ATTN: RADIATION SCIENCES DIV

WEAPONS LABORATORY
ATTN: SUL

DEPARTMENT OF ENERGY

LAWRENCE LIVERMORE NATIONAL LAB
ATTN: D DIVISION
ATTN: Z DIVISION LIBRARY

LOS ALAMOS NATIONAL LABORATORY
ATTN: REPORT LIBRARY
ATTN: T DOWLER

SANDIA NATIONAL LABORATORIES
ATTN: TECH LIB 3141
ATTN: W LING

OTHER GOVERNMENT

CENTRAL INTELLIGENCE AGENCY
ATTN: COUNTER-TERRORIST GROUP
ATTN: DIRECTOR OF SECURITY
ATTN: MEDICAL SERVICES
ATTN: NIO-T
ATTN: N10 - STRATEGIC SYS
ATTN: R & D SUBCOMMITTEE
ATTN: TECH LIBRARY

FEDERAL BUREAU OF INVEST ACADEMY
ATTN: BEHAVIORAL RSCH UNIT
ATTN: LIBRARY

FEDERAL EMERGENCY MANAGEMENT AGENCY
ATTN: ASST. ASSOC. DIR FOR RSCH
ATTN: CIVIL SECURITY DIVISION
ATTN: G ORRELL NP-CP
ATTN: OFC OF CIVIL DEFENSE, J F JACOBS

U S DEPARTMENT OF STATE
ATTN: PM/STM

U S NUCLEAR REGULATORY COMMISSION
ATTN: DIR DIV OF SAFEGUARDS
ATTN: S YANIV

DEPARTMENT OF DEFENSE CONTRACTORS

ADVANCED RESEARCH & APPLICATIONS CORP
ATTN: DOCUMENT CONTROL

AEROSPACE CORP
ATTN: LIBRARY ACQUISITION

BDM INTERNATIONAL INC
ATTN: C SOMERS
ATTN: C WASAFF
ATTN: J BODE
ATTN: J BRADDOCK
ATTN: R BUCHANAN

DATA MEMORY SYSTEMS, INC
ATTN: T DUPUY

KAMAN SCIENCES CORP
ATTN: E CONRAD

KAMAN SCIENCES CORPORATION
ATTN: DASIAC

KAMAN SCIENCES CORPORATION
ATTN: DASIAC

PACIFIC-SIERRA RESEARCH CORP
2 CYS ATTN: G ANNO
ATTN: H BRODE

PACIFIC-SIERRA RESEARCH CORP
ATTN: D GORMLEY
2 CYS ATTN: G MCCLELLAN

R & D ASSOCIATES
ATTN: C MCDONALD
2 CYS ATTN: DOCUMENT CONTROL

R & D ASSOCIATES
ATTN: J THOMPSON
ATTN: K MORAN

SCIENCE APPLICATIONS INTL CORP
2 CYS ATTN: D C KAUL
ATTN: DOCUMENT CONTROL
ATTN: E SWICK
2 CYS ATTN: F DOLATSHAHI
2 CYS ATTN: J A ROBERTS
ATTN: J MARTIN
2 CYS ATTN: J PHILLIPS
ATTN: J WARNER
ATTN: M DRAKE
ATTN: R J BEYSTER

SCIENCE APPLICATIONS INTL CORP
ATTN: B BENNETT
ATTN: DOCUMENT CONTROL
ATTN: J FOSTER
ATTN: J PETERS
ATTN: J SHANNON
ATTN: L GOURE
ATTN: M FINEBURG
ATTN: W LAYSON

SCIENCE APPLICATIONS INTL CORP
ATTN: R CRAVER

SYSTEM RESEARCH & DEVELOPMENT CORPORATION
ATTN: A WAGNER

SYSTEMS RESEARCH & APPLICATION CORP
ATTN: R STEELE
ATTN: S GREENSTEIN